THE SOLAR WIND INTERACTION WITH PLUTO'S ESCAPING ATMOSPHERE

Fran Bagenal[1], [1]LASP & APS, University of Colorado, 3665 Discovery Drive, Boulder CO 80303

Introduction: Pluto's interaction with the solar wind is determined by the rate of photoionization of Pluto's escaping neutral atmosphere. If the escape flux from Pluto is very weak then we expect a Venus-like interaction with the solar wind being deflected by ionospheric currents. Recent models suggest that exobase of Pluto's atmosphere is high above the surface (at ~10 R_{Pluto}) and that the escape flux is as recently estimated to be 2-5 x 10^{27} N_2 molecules per second (Strobel 2008; Tucker et al. 2012; Erwin et al. 2013). This means that, from a plasma-interaction viewpoint, Pluto is effectively an enormous comet (Bagenal and McNutt 1989).

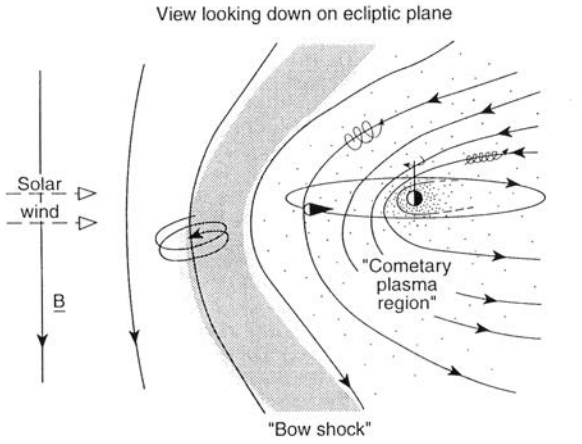

Sketch of the interaction from Bagenal & McNutt (1989).

Variability: In a cometary interaction, where the solar wind is slowed and deflected due to momentum-loading by fresh ionization, the spatial scale of the interaction is directly proportional to the atmospheric escape flux and inversely proportional to solar wind mass flux (ρ V) varies by factors of several over timescales of minutes to hours (John Richardson, private communication). This means that the scale of the interaction region encountered by New Horizons could be anywhere between 10 and 100 R_{Pluto} and that the scale of the interaction could vary during the few-hour encounter period.

Kinetic Effects: The weak magnetic field at >30AU means that ion kinetic effects play a crucial role at Pluto given both large ion gyro-radii and upstream ion inertial lengths that are comparable to the size of the obstacle (2–4 R_{Pluto}). The net results of including such kinetic effects are: strong asymmetry in the interaction, a weak and extended bowshock region, turbulent flows, a low-density wake (Cravens & Kecskemty 1993; Delamere & Bagenal 2004; Delamere 2009). Pickup ions move initially in the direction of the solar wind convection electric field (E) and the solar wind flow (V_{SW}) is deflected in the opposite direction, consistent with momentum conservation. The kinetic effects of Pluto's interaction with the solar wind are very dependent on the direction of the magnetic field in the solar wind, B_{SW}, resulting in opposite deflection of the mass-loaded solar wind and the large gyro motion of the new pick-up ions.

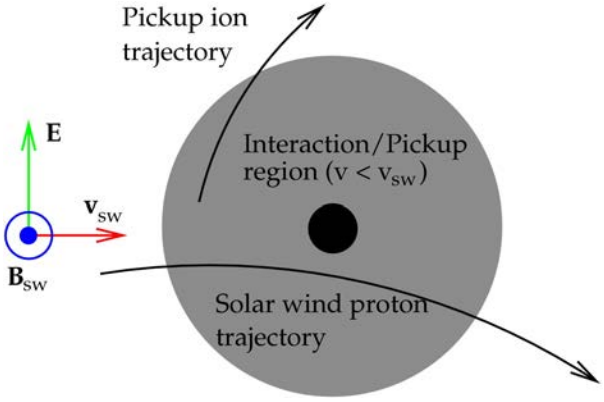

Schematic of ion motion near Pluto's interaction region.

Magnetic field: The Pioneer and Voyager spacecraft have provided average conditions of the interplanetary magnetic field at ~30 AU of a magnitude of ~0.2 nT and directed close to azimuthal in direction, flipping east-west a few times per solar rotation cycle of ~month (Charles Smith, private communication). But without local measurements of the magnetic field at the time of the New Horizons flyby of Pluto it will be hard to determine the sign of the magnetic field direction. The best method will likely be the measurement of the direction of pick-up ion motion just upstream of the interaction region.

Solar Wind: observations of the solar wind are extremely challenging because the flux, which falls off roughly with the square of heliocentric distance, is approximately three orders of magnitude lower at Pluto compared to typical solarwind fluxes observed near Earth's orbit. In addition, because the solar wind continues to cool as it propagates through the heliosphere, the solarwind beam becomes narrow in both angle and energy. Nevertheless, the large field of view of the new

Horizons SWAP instrument (McComas et al. 2008) allows it to measure the speed, density, and temperature of the solar wind and its interaction with Pluto. At the same time, the New Horizons PEPSSI instrument (McNutt et al. 2008) measures ions (with compositional information) and electrons from 10s of keVto ~1MeV. Between the low energy plasma measured by SWAP and the energetic particles detected by PEPSSI, the New Horizons will characterize the environment surrounding Pluto and quantify how the escaping atmosphere is picked up by the solar wind.

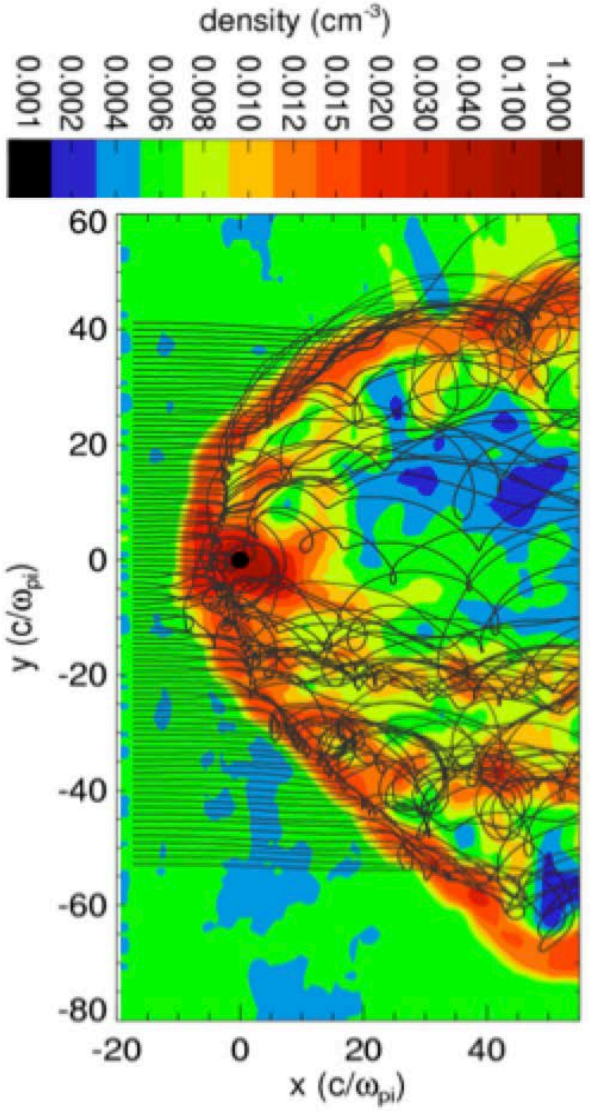

Hybrid simulation of the Pluto interaction where the color contours show density and the black lines show ion trajectories. From Delamere (2009).

Bagenal, F., R.L. McNutt (1989), *Geophys. Res. Lett.,16,* 1232; Biermann, L., B. Brosowski, and H.U. Schmidt (1967), *SolarPhys., 1*, 254; Delamere, P.A., F. Bagenal (2004), *Geophys. Res. Lett., 31,* L04807; Delamere, P.A. (2009), *J. Geophys. Res., 114,* A03220; Erwin et al. (2013), *Icarus, 218,* in press; Galeev, A.A., T.E. Cravens, T.I. Gombosi (1985), *Astrophys. J., 289,* 807; Kecskemety, K., T.E. Cravens (1993), *Geophys. Res. Lett., 20,* 543; McComas et al. (2008), *Space. Sci. Rev., 140,* 261; McNutt et al. (2008), *Space. Sci. Rev., 140,* 315; Strobel, D.F. (2008), *Icarus, 193,* 612; Tucker et al. (2012), *Icarus 217*, 408;

CHEMISTRY IN PLUTO'S ATMOSPHERE AND SURFACE: PREDICTIONS OF TRACE AEROSOL AND SURFACE COMPOSITION, AND A POTENTIAL GEOLOGIC CHRONOMETER

K. H. Baines[1] and M. L. Delitsky[2] , [1]SSEC, University of Wisconsin-Madison, 1225 West Dayton St., Madison, WI 53706, USA, blueskies4321@yahoo.com [2]California Specialty Engineering, PO Box 1522, Flintridge, CA, 91012, USA, cal_specialty@yahoo.com

Summary: The atmosphere and surface of Pluto contain mainly methane and nitrogen at low temperature (~38K), similar to Triton. Thus, the chemistry and aerosol content of Pluto is likely to bear great similarity to that of Neptune's largest moon. Previous studies [1] show that energy sources such as UV-photons and galactic cosmic rays (GCRs) will cause methane and nitrogen on the surface and in the atmosphere of Triton to be converted to higher hydrocarbons and C-N containing compounds. Some of these materials likely form hazes in Triton's atmosphere [2]. Similarly, Pluto's atmosphere and surface are likely to exhibit the same type of gas-phase and solid state ice reactions, producing higher-order hydrocarbon compounds and C-N materials, particularly during the harsh Pluto winter when the atmosphere is collapsed or nearly so. Indeed, evidence for hydrocarbons and nitriles on Pluto as well as albedo changes over time has been inferred from recent Hubble data [3].

Sputtering of both atmospheric and surface materials results in a loss of lighter gases to space, subsequent surface chemistry, and rainout of heavier molecules, resulting in a residue of refractory (higher molecular weight) materials on the surface of Pluto from cross-linking and polymerization of the hydrocarbon materials present. These materials may have color or be darkened, similar to cometary crusts. There will be some deposition of GCR energy into the atmosphere of Pluto but the majority of energy will be deposited in the surface. GCR deposition happens in the first 10 meters of the surface of Triton [1]. Therefore, on Pluto as well, it is likely that processed polymeric surface materials occur in the first 10 meters. However, the chemically processed layer may be significantly enhanced on Pluto, given the thicker atmosphere and enhanced hydrocarbon content compared to Triton, leading to a near-continuous rain of higher-mass hydrocarbons and perhaps nitriles, as the Cassini mission has found for Titan [4,5].

Given Pluto's high obliquity amd presumed lack of a global magnetic field, these UV- and GCR-produced darkened materals should occur nearly isotropically around the planet. Thus an inactive Pluto with no internally- or externally-induced geological processes would be uniformally darkened – assuming, in the long-term, that the surface is not significantly affected by seasonal effects due, for example, to the condensation and sublimation of surface frosts during the winter/summer cycle. Mean (seasonally-adjusted) variations in surface darkness may then be useable as a chronometer of surface processes. For example, water ice precipitating on the surface due to cometary collisions with either Pluto or its retinue of satellites could produce notably bright areas on the surface. As well, bolides impacting more than 10 meters deep into the dark surface would produce bright craters with associated ejecta as rays extending outward for perhaps thousands of miles superimposed on the dark surface. Due to the continual UV and GCR flux and near-continuous creation of higher-order dark materials in the atmosphere, such bright areas should darken over time as surface chemistry occurs and dark aerosols continue to rain down onto the surface. Thus, the observed brightness of various surface features on Pluto may be indicative of relative ages, with bright features being significantly younger than older ones.

References:

[1] Delitsky, M.L. and Thompson, W. R., (1987*). Icarus*, *70*, 354-365.

[2] Krasnopolsky, V.A., Sandel, B.R., Herbert, F., (1992) *J. Geophys Res*., *97*, 11695-11700.

[3] Stern, S.A. et al. (2012). *Astron. J., 143*, 22

[4] Griffith, C. A., *et al*., (2006). *Science*, *313*, 1620-1622.

[5] Lorenz, R. D., West, R. D., and Tomasko, W. T. K., (2008). *Icarus*, *195*, 812-816.

SURFACES PROCESSES ON THE MOONS OF PLUTO: INVESTIGATING THE EFFECTS OF GRAVITY O. S. Barnouin[1], A. F. Cheng[1], C. M. Ernst[1], and E.G. Kahn[1], [1]The Johns Hopkins University Applied Physics Laboratory, Laurel, MD 20723, USA (olivier.barnouin@jhuapl.edu).

Introduction: Surface processes that influence local and global geology of both regular and irregular asteroids, comets and satellites are sometimes dominated by local gravity. For example, gravity influences sedimentation and mass movements seen on the walls of many craters on Eros [e.g., 1], Lutetia [2], and Phoebe, the widespread presence of regolith at low potential on the surface of Itokawa [e.g., 3], the exposure of fresh material at higher elevation on Deimos (Fig. 1), and the location and orientation of a surface flow seen on the comet Temple 1 [e.g., 4]. In order to distinguish gravitational effects from other factors (e.g., surface strength, porosity, ejecta emplacement) on the surface geology of some of the irregular-shaped satellites of Pluto, numerical calculations of surface gravitational and centrifugal potential as well as surface effective gravity are essential. Such calculations are also important to determine where slow moving ejecta excavated by surface impact craters are likely to be deposited. In preparation for New Horizons' arrival in the Pluto system, this study presents an efficient method for undertaking these numerical computations of surface gravity and gravitational potential, and compares them to other approaches. In the approach presented, we assume the object can be modeled assuming a constant density, but the presented method could be adapted for variable density.

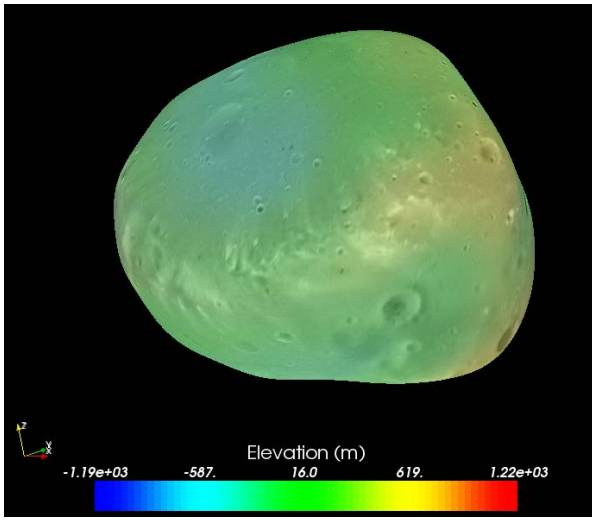

Figure 1. Bright streaks along a ridge of Martian satellite Deimos that indicate downslope motion from the high ridge to the lower basin.

Background: Werner and Scheeres [5] introduced an exact method for calculating the gravitational potential of constant density, polyhedral bodies using a sum over surface polygon faces and another sum over polygon edges. While this potential calculation is exact for polyhedral bodies, the polyhedral shape model is itself an approximation, as is the constant density assumption. For application to Eros and Itokawa, we have used a simpler, approximate method for calculating the effective potential and effective gravity of a small body, summing over faces of shape models in which the surface is tessellated into triangular plates. Here we use various high-resolution, polyhedral shape models of a spheroid, and oblate ellispsoidto make quantitative comparisons of the accuracy of the effective potential and gravity calculated from the exact polyhedral method [5], the approximate method [6], and a spherical harmonic method applied outside the body.

Calculation Method: The plate models are polyhedral shape models with triangular faces whose vertices are control points on the surface. The vertex vectors are $\boldsymbol{v_m}$, with $\mathrm{m} = 1, \ldots,$ vertex number.

The plate centroids, where plate *n* is made from vertices *i*, *j*, *k*, are defined by the vectors:

$$\boldsymbol{R_n} = \frac{\boldsymbol{v_i} + \boldsymbol{v_j} + \boldsymbol{v_k}}{3}, \qquad n = 1, \ldots, \text{plate number}.$$

Outward normal vectors are defined for each plate, such that each has length equal to twice the plate area,

$$\boldsymbol{N_n} = (\boldsymbol{v_j} - \boldsymbol{v_i}) \times (\boldsymbol{v_k} - \boldsymbol{v_i}),$$

where again *n* is the plate number index.

The gravitational potential is a sum over plates [6]:

$$\mathrm{U}(\boldsymbol{x}) = \frac{\mathrm{G}\rho}{4} \sum_{\mathrm{n}} \frac{(\boldsymbol{x} - \boldsymbol{R_n}) \cdot \boldsymbol{N_n}}{|\boldsymbol{x} - \boldsymbol{R_n}|}.$$

The gravitational acceleration is also a sum over plates:

$$\boldsymbol{g} = -\frac{\mathrm{G}\rho}{4} \sum_{n} \left[\frac{\boldsymbol{N_n}}{|\boldsymbol{x} - \boldsymbol{R_n}|} - \frac{(\boldsymbol{x} - \boldsymbol{R_n})(\boldsymbol{x} - \boldsymbol{R_n}) \cdot \boldsymbol{N_n}}{|\boldsymbol{x} - \boldsymbol{R_n}|^3} \right].$$

If the field point is at a plate centroid, $\boldsymbol{x} = \boldsymbol{R_n}$, then the contribution of that plate to the potential *U* is vanishing, but the contribution to the gravity is:

$$-\frac{\mathrm{G}\rho}{4} \boldsymbol{N_n} \left[\frac{3}{|2\boldsymbol{v_j} - \boldsymbol{v_i} - \boldsymbol{v_k}|} + \frac{3}{|2\boldsymbol{v_i} - \boldsymbol{v_j} - \boldsymbol{v_k}|} + \frac{3}{|2\boldsymbol{v_k} - \boldsymbol{v_i} - \boldsymbol{v_j}|} \right].$$

Conclusion: The error of our plate model calculations, when compared with exact analytic solutions, decreases as the number of faces increases (Fig. 2). and also decreases rapidly with distance above the surface. Similar behavior is found for the Werner and Scheeres polyhedral model, which is more complex and requires more computation time but is also slightly more accu-

rate. This increase in accuracy, however, is not warranted in most situations given the plate model approximation for topography, and the uniform density consideration. The plate model calculation yields a comparably accurate approximation to the actual potential of a small body (Fig. 3).

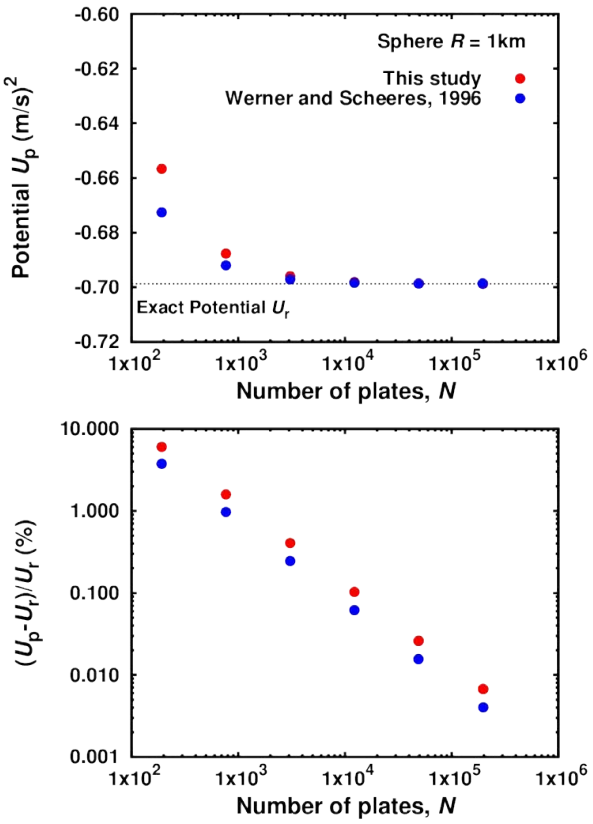

Figure 2 . Comparison of the gravitational potential U_p for a sphereical shape model to the the exact potential U_r.

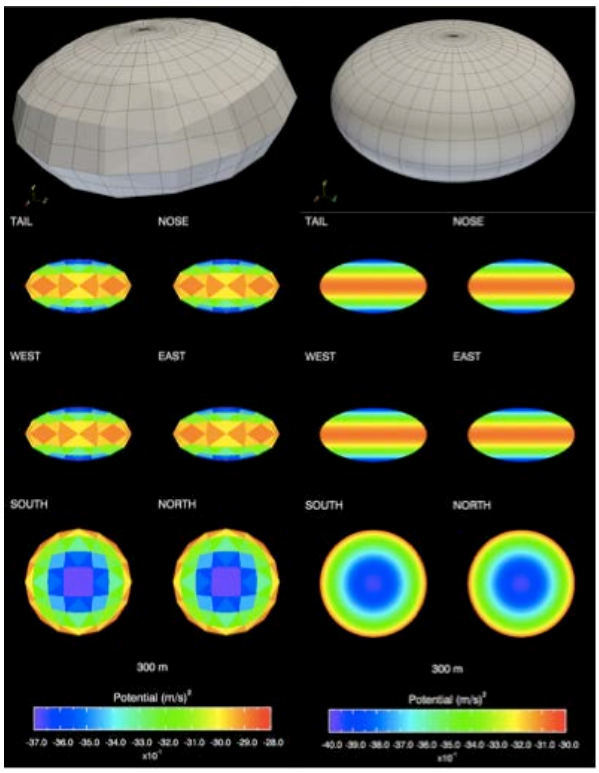

Figure 3. Plots showing improvements in gravitational potential for an oblate ellipsoid with increasing plate resolution from 192 plates on the left to 99000 on the right.

References: [1] Thomas, P.C. et al., 2002. Eros: Shape, Topography, and Slope Processes. *Icarus* 155, 18–37. [2] Thomas, N, et al. 2012. The geomorphology of (21) Lutetia: Results from the OSIRIS imaging system onboard ESA's Rosetta spacecraft. *Planet. Space Sci.* 66, 96–124. [3] Barnouin-Jha, O.S. et al., 2008. Small-scale topography of 25143 Itokawa from the Hayabusa laser altimeter. *Icarus* 198, 108–124. [4] Thomas, P.C. et al., 2007. The shape, topography, and geology of Tempel 1 from Deep Impact observations. *Icarus* 191, 4-15.. [5] Werner R. A. and D. J. Scheeres, 1997. Exterior gravitation of a polyhedron derived and compared with harmonic and mascon gravitation representations of asteroid 4769 Castalia. *CeMDA* 65, 313-344. [6] Cheng A.F. et al. 2002.. Small-scale topography of 433 Eros from laser altimetry and imaging. *Icarus* 155, 51-74.

ANALYZING THE PLUTO-CHARON SYSTEM USING THE SMALL BODY MAPPING TOOL.

Olivier S. Barnouin, Eliezer G. Kahn, and Carolyn M. Ernst, The Johns Hopkins University Applied Physics Laboratory, Laurel, MD 20723, USA (email: olivier.barnouin@jhuapl.edu).

Introduction: Visualizing and mapping the surfaces of irregular bodies is a difficult task. Determining spatial relationships between features can be nearly impossible in a two-dimensional map projection. The search for available data is also cumbersome. To address these difficulties and to facilitate the analysis of small body data from spacecraft, the Johns Hopkins Universith Applied Physics Laboratory has developed the Small Body Mapping Tool (SBMT). The SBMT is specialized for visualizing and mapping the surfaces of especially irregular bodies, but is a valuable tool for analysis of objects of any shape, even spheres.

The SBMT is an easy-to-use tool that is well suited for geologic analysis of the Pluto-Charon system from data that will be collected by the New Horizons spacecraft during its flyby in 2015, and may be a critical tool for analysis of Nix, Hydra, P4, and P5, which are likely to be irregularly shaped. We present here the capabilities of the SBMT, which has been used to analyze data missions including NEAR-Shoemaker, Hayabusa, MESSENGER, Dawn, and Rosetta. It is currently being adapted for use by the OSIRIS-REx mission, and an interface for the NASA Planetary Data System (PDS) Small Bodies Node is under development.

Architecture: The SBMT provides an intuitive user interface that makes use of modern interactive 3D graphics and visualization algorithms. It is written in the Java programming language and uses the Visualization Toolkit (VTK), an open source, cross-platform visualization library containing many advanced geometry algorithms, for 3D rendering and visualization, [1]. It therefore runs on all major operating systems including Mac, Linux, and Windows, and is designed to handle most data types delivered to the NASA PDS. Customization of SBMT is easy, and updates can be quickly pushed to the user.

A key advantage of the SBMT is that it does not require the user to store all of his or her data on the user's local machine, but instead communicates with a remote server over the internet to fetch data. Data files are only downloaded as needed and are then cached on the user's machine to avoid redundant downloads. In addition, the server hosts a structured query language(SQL) database backend for indexing the data and performing searches on the datasets as requested by the user. If internet access is lost, ongoing analyses still can continue using the data that have been cached.

Current capabilities: The SBMT has a wide array of capabilities that facilitate the search and analysis of PDS-formatted derived planetary datasets.

*Visualize Shape Models***:** The SBMT allows free rotation, zooming, and panning of custom or built-in shape models. Built-in shape models are available for those found at the NASA PDS (e.g., Eros, Itokawa). Custom shape models in several supported formats can be loaded directly by the user into the tool. Lighting can be simulated to custom coordinates or to match overlain images.

*Search and Display Spacecraft Data***:** The SBMT is capable of rapid identification of data available in a region of interest. Current searchable datasets include those from NEAR (MSI, NIS, NLR), Hayabusa (AMICA, LIDAR), Dawn (FC*), and Rosetta (OSIRIS*). Data can be overlain on shape models (Fig. 1). Resulting images can be easily downloaded in original file formats for subsequent analysis by a user's own tools. Multiple datasets can be viewed simultaneously, providing a means to compare various results.

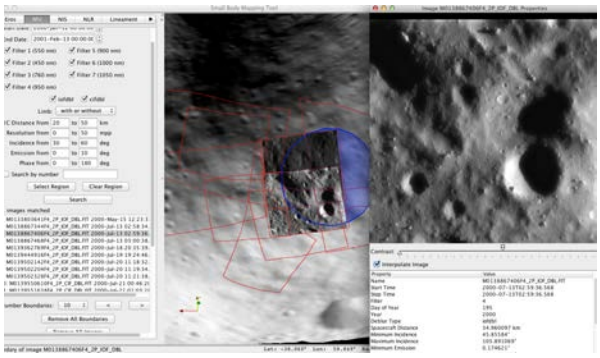

Figure 1. Search and display of MSI images on the surface of 433 Eros using the SBMT.

*Overlay Custom Images***:** Any image can be draped across a shape model (Fig. 2). These include, but are not limited to, basemaps, elevation maps, and slope maps. Spacecraft datasets can be overlayed on these custom images, creating an integrated research environment. All data can be easily output for presentations or further investigations.

*Map Surface Features***:** Paths, polygons, circles, ellipses, and points can be drawn directly onto shape models and images (Fig. 3). These structures are easily exportable as ascii files for additional analyses.

* Only data delivered to the PDS are available to users not on active mission teams.

As mentioned above, the SBMT can be used to map regularly shaped bodies. Fig. 4 provides an example of SBMT use with MESSENGER data of Mercury.

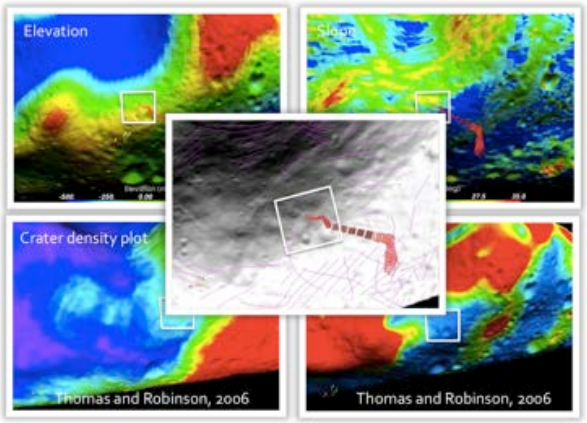

Figure 2. Common and customized SBMT data of surface elevation, crater size frequency distribution, ejecta distribution, and slopes and lineaments on 433 Eros at the NEAR landing site [2].

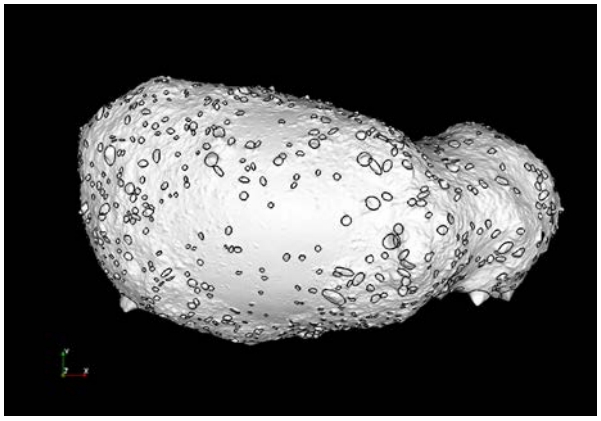

Figure 3. Distrubtion of over 1100 blocks on the surface of Itokawa [3] providing evidence for complex reaccretion of the asteroid following initial disruption of Itokawa's parent-body. The blocks were measured in the SBMT.

Under Development: New plantary objects are constantly being added to the SBMT. These include:

*Mathilde, Gaspra, and Ida***:** Shape models are being refined for these three flyby targets. Image data from NEAR (Mathilde) and Galileo (Gaspra and Ida) are being registered to these shape models and will be searchable and downloadable. This work is being supported by an active NASA PMDAP grant.

Phobos and Deimos: Updated and detailed shape and topography models are being developed. Data from multiple Mars missions (including Viking Orbiter, Phobos 2, Mars Pathfinder, Mars Global Surveyor, Mars Express, and Mars Reconnaissance Orbiter) are being integrated and incorporated into the SBMT. This work is supported by an active NASA MDAP grant.

Tethys, Mimas, Pheobe, Rhea and Iapetus: Updated and detailed shape and topography models have been developed by R. Gaskell from the Cassini flybys of these satellites. These are being incorporated into the SBMT, including registered images that were used to make the shape model. The icy satellittes of Saturn are good analogues for interpretting processes expected to affect the objects in the Pluto-Charon system, including Pluto and Charon themselves.

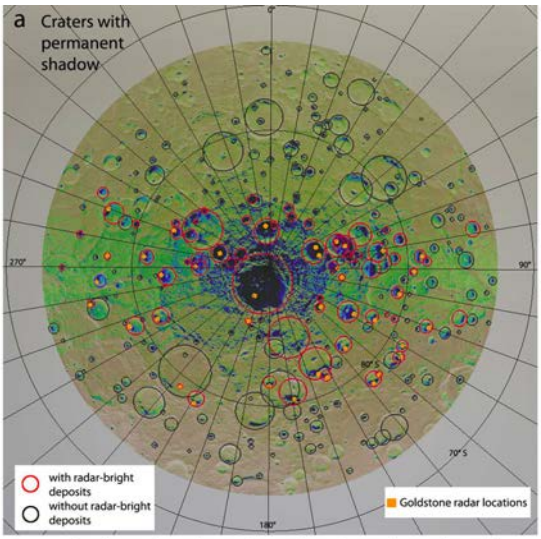

Figure 4. Distribution of permanently shadowed craters on Mercury, mapped in the SBMT. This analysis used a custom shape model and custom images and maps [from 4].

References: [1] Schroeder, W. et al. (2006). *The Visualization Toolkit* (4th ed.), Kitware, ISBN 978-1-930934-19-1 [2] Barnouin, O.S. et al. (2012). Revisiting the NEAR-Shoemaker landing site. Asteroids, Comets, Meteors #6419. [3] Mazrouei, S. et al. (2012). Distribution of boulders on asteroid 25143 Itokawa. *LPSC*, 43, #2404. [4] Chabot, N.L. et al. (2012). Areas of permanent shadow in Mercury's south polar region ascertained by MESSENGER orbital imaging. *GRL* 39, doi: 10.1029/2012GL051526.

Is methane supersaturation consistent with the presence of haze particles in Pluto's atmosphere?

E. L. Barth[1] and E. F. Young[2], [1]Southwest Research Institute, 1050 Walnut Street, Suite 300, Boulder, CO 80301, ebarth@boulder.swri.edu [2]Southwest Research Institute, efy@boulder.swri.edu.

Introduction: Recent observations have confirmed the presence of N_2, CO, and CH_4 gases in Pluto's atmosphere. The 2003 stellar occultation observations of [1] indicated that additionally, there may be a layer of haze particles present. These particles were thought to be fractal in structure with a radius of 0.2 μm. [2] modeled the production of photochemical haze particles by scaling the production function from their Titan model and concluded that the production rates required to explain the extinction would be unphysically high for Pluto's atmosphere. They further looked at condensation of Pluto's primary atmospheric constituents and concluded submicron-sized N_2 and CO ices may comprise this extinction layer.

Condensation implies that Pluto's atmosphere possess a troposphere. [3] postulate temperature profiles which include a troposphere of 17 km depth (surface pressure = 24 μm, surface radius ~1170 km). They also found that methane appears to be significanly supersaturated, given a mixing ratio of 0.5%, supersaturations up to a factor of 30 are possible for a ~38 K tropopause.

Model: We have developed a 1-D microphysics model based on the Community Aerosol and Radiation Model for Atmospheres (CARMA). CARMA has been used successfully many times to explore the vertical distribution, size, shape, and composition of particles in Titan's atmosphere, and in particular, to predict the appearance of methane condensate layers which were observed at the Huygens' landing site [4]. The Pluto version allows for the simulation of N_2, CO, and CH_4 cloud formation.

Nucleation of methane onto tholin (laboratory analogs to Titan's haze particles) has been measured in the lab at T~45 K [5]. Only a small supersaturation is required to initiate cloud formation, then growth will proceed as long as the atmosphere is above saturation.

Simulations: Initial simulations have shown methane cloud formation will proceed if aerosol particles are present to serve as cloud condensation nuclei (CCN). This serves to deplete the atmospheric reservoir of methane, limiting the amount of supersaturation. Figures 1 and 2 compare methane supersaturation between two cases (1) no haze particles to serve as CCN and (2) haze particles present. Both models start with the same initial amount of methane and were run out for 500 (terrestrial) years. There is about a factor of 10 decrease in the amount of supersaturation when cloud formation is included. The growth of methane ice particles was limited to a radius of ~1 μm. A plot of the size distribution shows a dramatic increase in the population of particles in the largest size-bin, indicating condensational growth would continue in the absense of this restriction. It is likely that methane ice particles would grow to radii of ~10 μm, which would further decrease the supersaturation from that shown in Fig. 2, as well as cause them to fall to the surface much more quickly.

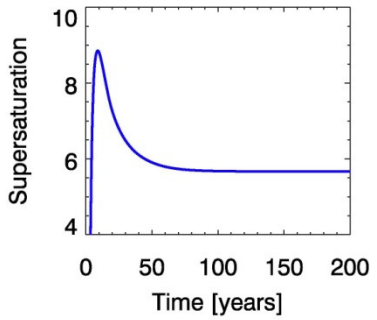

Figure1. Methane supersaturation as a function of time for a case without haze particles to serve as condensation nuclei for methane ice formation.

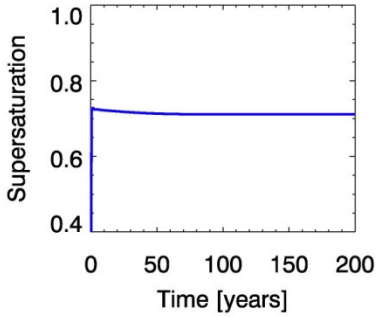

Figure2. Methane supersaturation as a function of time for a case with haze particles and methane ice formation.

These are two extreme cases. We will discuss a number of sensitivity tests which include varying the abundance, size, and shape of haze particles; evaluating the onset of homogeneous methane nucleation; exploring the size distribution of the resulting methane ice particles; and the effects of N_2 and CO condensation as well.

References: [1]Elliot J. B. et al. (2003) *Nature, 424,* 165-168. [2]Rannou P. and Durry G. (2009) *JGR., 114,* E11013. [3] Lellouch et al. (2009) *A&A, 495*, L17-L21. [4] Barth E.L. and Toon O.B. (2004) *GRL, 31*, L17S07. [5] Curtis et al. (2008) *Icarus, 195*, 792-801.

CYCLING OF VOLATILES IN TRITON'S ICY LITHOSPHERE WITH IMPLICATIONS FOR CANTALOUPE TERRAIN ON PLUTO'S SURFACE.

S. M. Battaglia[1], [1]Department of Geology and Environmental Geosciences, Northern Illinois University, Davis Hall 312, Normal Rd., DeKalb, IL, 60115. (Email: battagl1@niu.edu)

Introduction: Spectroscopic analyses indicate that volatile ices including N_2, CO, CH_4, and CO_2 cover Triton's surface [1,2]. Solid or liquid volatile compounds on the surface of a volcanically active planetary body suggest a magmatic-tectonic distillation process that concentrates the volatiles in surface reservoirs. On Earth, the hydro-tectonic cycle transfers water from the Earth's interior to its oceans. Volatiles that are solid or liquid in crustal reservoirs are transported into the subsurface as the crust recycles to the convecting mantle. As the slab penetrates the mantle, the interior thermal gradient melts the volatiles in the reservoir, distilling the compounds to shallow depths. Liquid volatiles are less dense than the bulk crust and remain in the lithosphere until a rising plume assimilates them, which aids the magma in erupting onto the surface [3]. Therefore, a planetary body suspected of active volcanism with solid or liquid volatiles on its surface may exhibit a similar self-sustaining process, where cycling of volatiles in the lithosphere aid in planetary resurfacing and crustal recycling. Here, I investigate this process by modeling the thermal gradient of Triton's solid ice lithosphere and speculate Pluto's surface may exhibit cryovolcanic features similar to the cantaloupe terrain found on Triton's surface.

Background: Triton is a differentiated Kuiper Belt object (KBO) captured by Neptune in the early solar system [4-6]. There are very few impact craters on Triton's surface, suggesting that it is likely geologically and tectonically active today [7-9]. This geological activity is interpreted to be cryovolcanic in origin. The current internal radiogenic heat is sufficient to partially melt Triton's lower water-ice crust and generate a convecting ice shell [10] with the possibility of a subsurface ocean also existing beneath the shell [11]. The resulting cryomagmas may ascend in the crust and erupt on the surface. Since Earth-like plate tectonic processes do not appear to operate on Triton, another process must be occurring to resurface and recycle the ice shell.

Pluto, also a differentiated KBO, has a similar surface composition to Triton [12,13] and likely retains a sufficient amount of internal heat to partially melt its lower water-ice crust, implying a possible convective ice shell and subsurface ocean [10,11]. Cryomagmas may also be erupting onto Pluto's surface due to the convecting ice shell, suggesting a process similar to the proposed cycling of volatiles in Triton's lithosphere.

Thermal Gradient Model for Triton's Shell: Triton's lithosphere is composed of Ice-I with an estimated thermal conductivity ($k(T)$) of $621/T$ W m^{-2} [10]. Estimated NH_3 concentrations (X) in water-ice shells of outer solar system icy planetary bodies range from 1-15% [11]. This X range in Triton's shell corresponds to melting temperatures (T_b) of 255 K (for X = 1%) and 187 K (for X = 15%) [11]. The estimated surface heat flux (q_s) from Triton's internal radiogenic heating is 3.3 – 6.6 mW m^{-2} [14].

The true shell thickness (D') for a planetary body encapsulated by a water-ice crust is given by [10]:

$$D' = \frac{k(T)\ln\left[\frac{T_b}{T_s}\right]}{q_s + \frac{k(T)\ln\left[\frac{T_b}{T_s}\right]}{R_s}} \quad (1)$$

where T_s is the mean surface temperature (38 K) and R_s is the planetary radius (1353 km). Using T_b values in Eq. 1, representing the base of Triton's shell, the minimum and maximum D' values are 135 km and 283 km, respectively (Fig. 1).

The D' variation is used for estimating the thermal gradient in Triton's shell. The temperature profile ($T(r)$) for a planetary body's crust that is undergoing surface heat loss due to thermal conduction is given by [15]:

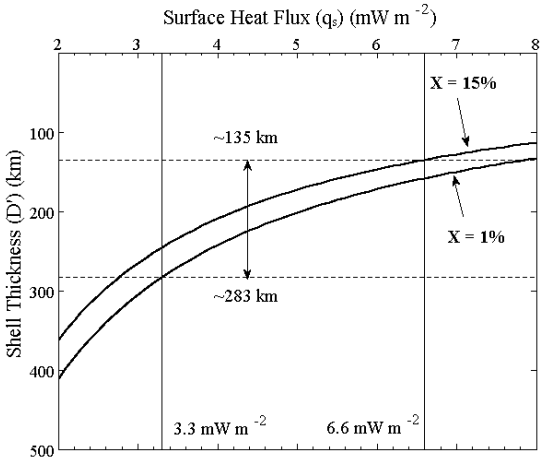

Fig. 1. True shell thickness (D') for Triton's crust using previously estimated surface heat fluxes (q_s) and NH_3 concentrations (X) of the water-ice lithosphere.

$$T(r) = T_s + \frac{T_b - T_s}{1 - R_b/R_s}\left(\frac{R_b}{r} - \frac{R_b}{R_s}\right) \quad (2)$$

where R_b is the distance from the planetary center to the bottom of the crust and r is the radial distance from the planetary center. Using the minimum and maximum D' in Eq. 2, the temperature profiles for Triton's shell have thermal gradients of ~1.05 K/km and ~0.65 K/km, respectively (Fig. 2).

Volatile Melting Depths in Triton's Lithosphere: For a minimum q_s (3.3 mW m^{-2}) and X (1%), the melting depths for N_2, CO, CH_4, and CO_2 are 40, 48, 82, and 217 km, respectively. These are likely the greatest depths the volatiles can remain solid before melting during vertical transport through the shell. Increasing the interior heat or X will melt the volatiles at shallower depths within the lithosphere.

For a maximum q_s (6.6 mW m^{-2}) and X (15%), the melting depths are 25, 29, 51, and 141 km, respectively. Since Triton's ice shell may be convecting, these depths are reasonable estimates for initial melting of the volatiles during vertical transport.

Volatile Cycling and Lithosphere Recycling: Volatile cycling in Triton's lithosphere is analogous to Earth's hydro-tectonic cycle, where volatiles extracted from the partially melted ice shell are transferred to the surface via cryovolcanism, while the ice shell is recycled to the lower crust (a "cryo-tectonic" cycle). Cryomagmas ascend through Triton's ice shell and assimilate volatiles, increasing the likelihood of eruption onto the surface. Fresh cryolavas are likely denser than older

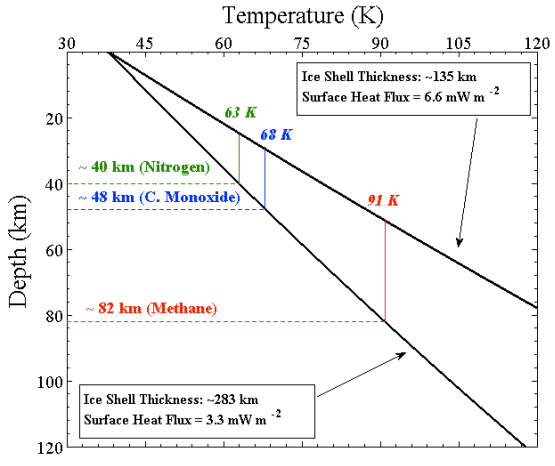

Fig. 2. Temperature profiles for Triton's ice shell using true shell thicknesses (D'). The melting temperatures and depths for N_2, CO, and CH_4 are shown in green, blue, and red, respectively. Melting of CO_2 occurs at a greater depth not shown on the figure.

surface material, resulting in a density inversion. Over time, this density inversion will form cantaloupe terrain [16]. Volatile ices on the surface are buried from cryovolcanic eruptions and interleaved within the shell. While the ice shell recycles to the partial-melt regime by vertical mass transport due to continuous surface burial, the volatiles N_2, CO, and CH_4 melt and are distilled. The liquid volatiles are less dense than the bulk water-ice crust, which implies the ice shell may be differentiated. Volatile CO_2 likely remains solid during vertical transport to the convecting layer of the ice shell, suggesting CO_2 concentrations and melting depths within the subsurface partial-melt zone may be important in recycling Triton's ice shell.

Cantaloupe Terrain on Pluto: The volume of radiogenic elements in Pluto is ~20% smaller than Triton [13], which implies q_s values of ~2.7 – 5.4 mW m^{-2}. Using the same model described above, D' for Pluto varies from ~140 to 298 km. The thermal gradients for Pluto's shell are ~1.02 K/km and ~0.63 K/km. The minimum melting depths for N_2, CO, CH_4, and CO_2 are 36, 45, 84, and 233 km, respectively. These melting depths are similar to those of Triton's lithosphere, implying Pluto's ice shell may also be differentiated.

If cryovolcanism is currently active on Pluto and the lithosphere is differentiated, then surface features should be similar to Triton's. Near-surface density inversions due to the cryovolcanic processes may be common, resulting in the formation of cantaloupe terrain. If cryovolcanism is inactive on Pluto, then it is still reasonable to predict that past cryovolcanic features may be currently present on the surface, assuming Pluto's seasonal atmospheric processes have not eroded its surface history.

References: [1] Cruikshank D. P. et al. (2000) *Icarus, 147,* 309-316. [2] Bauer J. M. et al. (2010) *Astro. Phys. J. Lett., 723,* 49-52. [3] Kargel J. S. et al. (1999) *Icarus, 142,* 249-280. [4] McKinnon W. B. et al. (1995) *Neptune and Triton,* 807-877. [5] Agnor C. B. and Hamilton D. P. (2006) *Nature, 441,* 192-194. [6] Taylor S. R. and McLennan S. M. (2007) *Planetary Crusts,* 343-344. [7] Croft S. K. et al. (1995) *Neptune and Triton,* 879-948. [8] Stern S. A. and McKinnon W. B. (2000) *Astro. J., 119,* 945-952. [9] Prockter L. M. et al. (2010) *Space Sci. Rev., 153,* 63-111. [10] McKinnon W. B. (2006) *Icarus, 183,* 435-450. [11] Hussmann H. et al. (2006) *Icarus, 185,* 258-273. [12] Owen T. C. et al. (1993) *Science, 261,* 745-748. [13] Robuchon G. and Nimmo F. (2011) *Icarus, 216,* 426-439. [14] Brown R. H. et al. (1991) *Science, 251,* 1465-1467. [15] Turcotte D. L. and Schubert G. (2001) *Geodynamics 2nd Ed.* [16] Schenk P. and Jackson M.P.A. (1993) *Geology, 21,* 299-302.

KBO Long-Range Candidate Observations with HST

S. D. Benecchi[1,2], K. S. Noll[3], S. S. Sheppard[1], H. A. Weaver[4], J. R. Spencer[5], S. A. Stern[5], and M. W. Buie[5]. [1]Carnegie Institution of Washington, Department of Terrestrial Magnetism, 5241 Broad Branch Road, NW, Washington, DC 20015; susank@alum.mit.edu, [2] Planetary Science Institute, 1700 East Fort Lowell, Suite 106, Tucson, AZ 85719, [3]NASA Goddard Space Fight Center, 8800 Greenbelt Rd. Code 693, Greenbelt, MD 20771, [4] Space Department, Johns Hopkins University Applied Physics Laboratory, 11100 Johns Hopkins Road, Laurel, MD 20723-6099, [5] Southwest Research Institute, 1050 Walnut St., Suite 300, Boulder, CO 80302.

Following the Pluto system fly-by in 2015 we hope to send the New Horizons spacecraft to fly-by one or more Kuiper Belt Objects (probably between 2017 and 2020). A substantial ground-based effort has been made to identify candidate objects for these observations. At the time of this abstract we have 26 discoveries of which five objects are long-range reconnaissance candidates (passing within 0.2 AU of NH and bright enough to image with ~150km resolution or ~10x Hubble resolution), two are pre-Pluto encounter observation candidates and two have current orbit predictions that require only about a factor of 2 more propellant than available for the targeting maneuver. Obtaining precise orbits for flyby candidates to determine whether NH can target them is critical to the success of the extended mission. HST excels in several aspects that challenge ground-based observing: instrument sensitivity, image resolution and PSF stability. Therefore, we followed up on our three best long-range candidates (2011 JW_{31}, 2011 JY_{31}, and 2011 HZ_{102}) in September 2012 WFC3 on HST. For each object 2 HST orbits were utilized. Observations for each orbit followed the sequence: F606W – F814W – F814W – F606W in order to obtain crude color information in addition to highly accurate astrometry. Using 2011 JY_{31} as an example of the success of our observations, we measure photometry to the accuracy of 0.05 magnitudes on this 25.5 magnitude object in the F606W waveband with color accuracy to 0.1 magnitudes. Even at the high angular resolution of our observations, 0.04 arcsec, this object is not obviously binary. We also confirm that our discovery ephemerides are sufficient for recovery by HST. Astrometry is measured to a fraction of a pixel (40 mas) and is currently accurate to 200 mas, limited by the accuracy of astrometric catalogs. We anticipate with future GAIA astrometry (promised to be at the level of 24 microacrseconds) we can improve a 3 year baseline orbit to the equivalent precision of a 34 year baseline.

ASTROMETRIC ANALYSIS OF 15 YEARS OF PLUTO OBSERVATION

Benedetti-Rossi, G.[1] (gustavorossi@on.br); Vieira-Martins, R.[1] (rvm@on.br); Camargo, J. I. B. [1] (camargo@on.br); Assafin, M.[2] (massaf@astro.ufrj.br)

[1] - Observatório Nacional – ON/MCTI
[2] - Observatório do Valongo – OV/UFRJ

Introduction: The New Horizons spacecraft is scheduled to reach Pluto's system in july 2015. Until then, stellar occultations are the most efficient method, from the ground, to provide the temperature and density profiles of its atmosphere and determine dimension of its sattelites with kilometric accuracy. From observations of stellar occultations it was evident a drift in declinations (about 30 mas/year) when compared to the DE418, as shown by Assafin et al. in 2010 [1]. This drift motivated us to re-reductions and re-analyse of a large set of our observations made at Pico dos Dias Observatory (OPD/LNA) and from 3 runs at the 2.2m telescope at ESO, in a total of 15 years. The ephemerides (DE421) and occultations results was then compared with the astrometric reductions of CCD images of Pluto (around 7100 images). The UCAC4 catalog was used as reference in the reductions.

Corrections: Two corrections were applied to the data set: diferential chromatic refraction and photocenter. The first comes from the fact that Pluto is, for an Earth-based observer, backgrounded by the Galactic plane so that the mean color of the field stars are redder than that of Pluto and may induce a difference of 0”.1 in the observed minus calculated (O-C) positions. The photocenter correction is based on two gaussian curves overlapped, with different maxima and non-coincident centers, corresponding to Pluto and Charon (since they have less than 1” of angular separation). The objective here is to properly separate Pluto's photocenter from the combined Pluto/charon one. The method is strongly dependent of the maxima of each of the gaussian curves, related to the ratio of albedos of Charon and Pluto.

Analysis and results: A detailed analysis of the astrometric results, as well a comparison with those from occultation was made. The 7131 images reduced showed a σ_α= 0,090 and a σ_β= 0,075 before the two corrections and σ_α= 0,049 and σ_β= 0,053 after (with 5854 images left after a 2σ and 3σ filter on the data set). We also confirmed the drift in declination positions in the period 2005-2012.

Reference:

[1] Assafin, M.; Camargo, J. I. B.; Vieira Martins, R.; Andrei, A. H.; Sicardy, B.; Young, L.; da Silva Neto, D. N.; Braga-Ribas, F.: Precise predictions of stellar occultations by Pluto, Charon, Nix, and Hydra for 2008–2015, A&A 515, A32 (2010).

The Ninth Planet's Third Dimension

Ross A. Beyer[1,2], Paul Schenk[3], and Jeff Moore[2] [1]Carl Sagan Center at the SETI Institute, [2]NASA Ames Research Center, Mail Stop 245-3, P.O. Box 1, Moffett Field, CA 94035 (Ross.A.Beyer@nasa.gov, Jeff.Moore@nasa.gov), and [3]The Lunar and Planetary Institute, Houston, TX, (schenk@lpi.usra.edu)

A quantitative understanding of Pluto's topography will enable a variety of scientific investigations [1], including understanding the magnitude of geologic processes and the origin of geologic features. In order to provide the topography of Pluto's surface at the best possible vertical and horizontal resolution with the New Horizons data set, we will perform stereo reconstruction from LORRI framing camera [2] and Ralph MVIC TDI pushbroom [3] images.

New Horizons will return the first high resolution images of Pluto's surface [4], and the New Horizons team has orchestrated some of those images to provide stereo pairs from which we will be able to extract terrain.

Planned Stereo Observations: The Pluto encounter geometry's single fly-by nature provides an interesting challenge for stereo reconstruction. Finding the best times to capture images for stereo data was a process of finding the times before closest approach which maximized coverage (and lighting), equalized ground scale, and optimized parallax, all while balancing the needs of other instruments and targets.

The five potential observations in the nominal plan that we can use to derive terrain models for Pluto are detailed in Table 1 and Figure 1. Parallax drives the expected vertical precision of a stereo-produced terrain model, and the difference in phase angle is a proxy for the convergence angle of the stereo pair. As you can see, in a little over three hours, New Horizons sweeps out over 40° in phase. Ideally, we'd use a single instrument for both halves of the stereo pair. However, in that time the ground scale and footprint size of the instruments have changed significantly (compare the cyan LORRI squares in Figure 1a to the one in Figure 1d). So terrain models will mostly be a combination of a LORRI mosaic and an MVIC scan later on.

Expected Terrain Models: Table 2 shows what different combinations of the observations in Table 1 would provide in terms of the characteristics of terrain models. From a resolution and vertical precision standpoint, the best possible combination is the BE terrain model which combines data from a LORRI mosaic (P_LORRI_STEREO_MOSAIC) with the latest MVIC pass (P_MVIC_LORRI_CA). Depending on the details of Pluto's surface, there is the possibility that the very large convergence angle will result in occlusions which might make automatic correlation difficult, but manual correlation should still be possible. Furthermore, the BD and CE combinations provide suitable backup observation geometries for reasonable terrain extraction if there are issues with the BE combination. In addition, the AD model will provide terrain information (although at worse resolution) for regions east of 240°E longitude that BE and BD cannot provide.

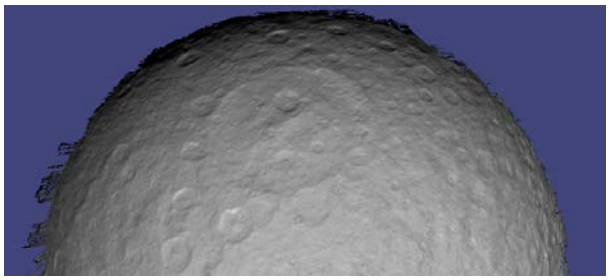

Figure 2: Example hillshaded terrain model made from Cassini ISS data of Rhea, comparable to what the BD model might provide.

Terrain Model	Convergence Angle (°)	Ground Scale (km/post)	Expected Vertical Precision (m)
AC	18	2.7	550
AD	26	2.7	360
BC	13	2.2	630
BD	21	1.6	370
BE	37	1.2	190
CE	24	2.2	330

Table 2: Characteristics of potential terrian models.

References

[1] L. A. Young, *et al.*, *Space Science Reviews* **140**, 93 (2008).
[2] A. F. Cheng, *et al.*, *Space Science Reviews* **140**, 189 (2008).
[3] D. C. Reuter, *et al.*, *Space Science Reviews* **140**, 129 (2008).
[4] S. A. Stern, *Space Science Reviews* **140**, 3 (2008).
[5] H. B. Throop, S. A. Stern, J. W. Parker, G. R. Gladstone, H. A. Weaver, *AAS/Division for Planetary Sciences Meeting* (2009), vol. 41.

	Observation Name	Start time on 2015-07-14	Instrument	Ground Scale (m/pixel)	Phase Angle (°)
A	P_LORRI	08:14:00	LORRI	895	19.5
B	P_LORRI_STEREO_MOSAIC	10:10:50	LORRI	415	24.6
C	P_COLOR_2	11:09:40	MVIC	720	37.4
D	P_MPAN_1	11:22:00	MVIC	537	45.7
E	P_MVIC_LORRI_CA	11:34:00	MVIC	380	61.1

Table 1: Planned (and subject to change) observations that could be used for stereo terrain reconstruction on Pluto.

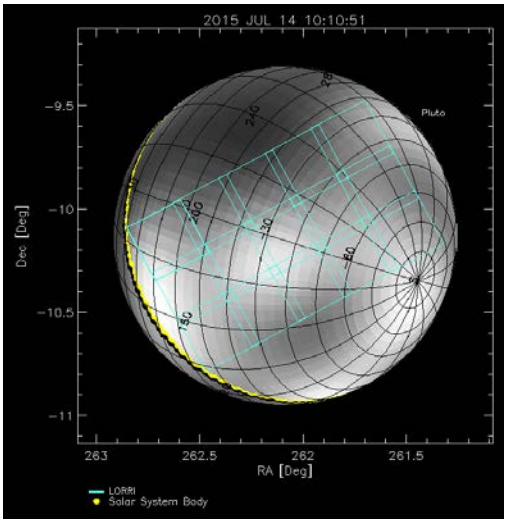

(a) P_LORRI_STEREO_MOSAIC

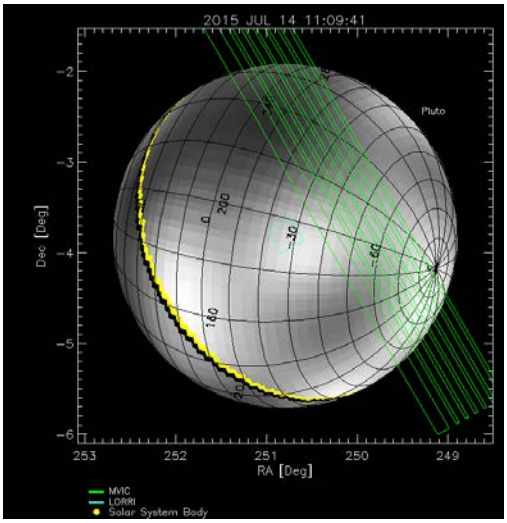

(b) P_COLOR_2

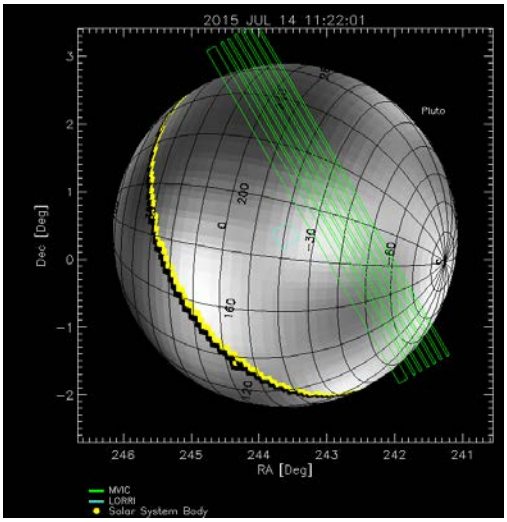

(c) P_MPAN_1

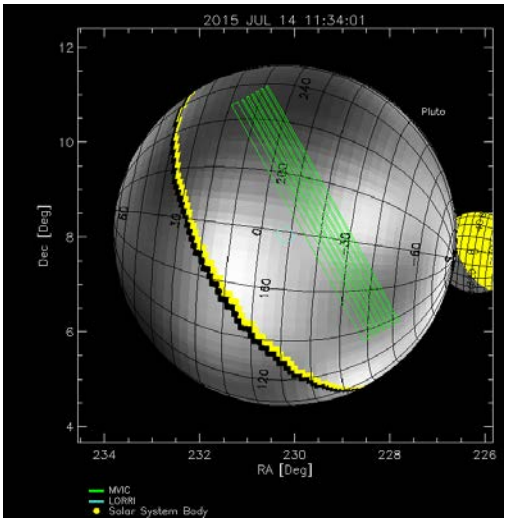

(d) P_MVIC_LORRI_CA

Figure 1: Visualizations [5] of the observations. Cyan boxes show the outline of LORRI frames, and the green outlines show the extent of the MVIC TDI CCDs. The MVIC TDI frames will sweep in the direction perpendicular to the long axis of the CCDs, such that the P_COLOR_2 and P_MPAN_1 observations will capture the full disk of Pluto.

CRATER AND EJECTA POPULATIONS ON PLUTO AND ITS ENTOURAGE

E. B. Bierhaus[1] , L. Dones[2], and D. Kaufmann[2], [1]Lockheed Martin Space Systems Company (edward.b.bierhaus@lmco.com), [2]Southwest Research Institute.

Introduction: The flyby of Pluto is our first opportunity to view the surface that is the gateway to the deep outer solar system. The lessons of Voyager, Galileo, and Cassini tell us that small icy worlds of the outer solar system are determined to confound our preconceived notions of what complexity is possible in small bodies. Ongoing ground- and space-based observations of Pluto have revealed an increasingly intricate multi-body system, demonstrating that the Pluto-Charon system continues the wondrous befuddlement imparted by the icy satellites of the giant planets.

To understand the Pluto system, we start by applying the familiar tools developed by examination of other planetary surfaces across the solar system. A key tool is the examination of impact craters, which are the most abundant landform in the solar system. Examining crater sizes, shapes, and spatial distributions enables a host of scientific explorations that are diagnostic of the surface and near sub-surface, while comparing craters between objects enables an extensive array of comparative planetology. The crater size-frequency distribution (SFD) tells us about the impacting population, and the variation of the crater SFD tells us about the relative ages of different surface units. Crater morphology (e.g. depth-to-diameter ratios, ejecta blanket styles) probes the structure of the surface and the near-surface; comparing morphology and degradation of similarly-sized craters provides information on erosional rates and/or relaxation rates. Ejecta from craters create secondary craters, and especially on low-mass, multi-body systems like Pluto and Charon, can lead to sesquinary craters (craters made by ejecta that initially escape a surface but ultimately re-impact), as well as potentially long-lived orbital debris that may affect spacecraft safety. We address the following topics:

- Small, distant objects are hard to see, but the craters they make on Pluto and Charon should be visible. Thus the primary crater populations on Pluto/Charon are the best opportunity to evaluate the SFD of small KBOs below current detection limits of ground- and space-based telescopes.
- Secondary and sesquinary crater populations can confound interpretation of the primary crater record, but we predict these populations will be significantly less dense on Pluto and Charon compared with the Galilean satellites
- Consequences of crater ejecta for small moon formation, and spacecraft safety
- uncertainties, and corresponding scientific opportunities, due to nitrogen ice and low impact speeds

Primary Crater and their Parent Impactor SFDs: Observations of primary craters on the young surface of Europa and of the Saturnian satellites generally show a -2 differential power-law slope for small craters (diameters < 10 km), suggesting that the comets (derived from the scattered disk) that makes these craters also have a -2 differential power-law slope [1]. Observations of craters on Pluto will be the purest test yet, since there may be dynamical or thermal effects that introduce changes to the impacting SFD as the objects migrate to Saturn and Jupiter.

Secondary and Sesquinary Crater Populations: We follow the strategy developed in [1] to estimate the magnitude of the secondary and sesquinary crater populations. Briefly, ejecta mass is divided into three velocity bins: 1) material moving faster than escape velocity (v_{esc}), which is mass available to make sesquinary craters; 2) material moving slower than v_{esc} but faster than v_{min} (the minimum velocity necessary to make a secondary crater rather than landing intact as a boulder or a part of the ejecta blanket), which is mass available to make secondaries; 3) material moving slower than v_{min}, which is mass that contributes to the ejecta blanket.

We calculate these masses for a crater formed by a 1 km comet. We use 1 km because (i) it is large enough to generate enough ejecta to make an observable population of secondary craters, (ii) impacts of such bodies are frequent on geologic time scales, (iii) its excavation depth may be deep enough that the crater characteristics are adequately described by water ice, rather than nitrogen ice. We use the scaling laws in [2] (with application to water ice as described in [1]), in conjunction with impact speeds given in [3].

Figure 1 shows the primary crater size for the impact of a 1 km comet on Pluto and Charon, as well as a number of the icy moons of the outer solar system. Notably, the estimated primary crater sizes for P/C are smaller than the other objects; this is due to the low impact speeds on P/C (1-2 km/s) relative to the other objects (> 10 km/s, except for Iapetus at 6 km/s). Thus we expect that the primary crater SFD will be shifted to smaller sizes relative to the Saturnian and Galilean satellites.

Secondary and Sesquinary Crater populations: The low primary impact speeds have two consequences for impact ejecta: 1) the smaller primary crater for a given impactor means that a smaller amount of ejecta

will be produced (reducing mass available for secondaries and sesquinaries); and 2) the ejecta itself will be moving slower. Figures 2 and 3 plot the amount of mass available to make secondaries (m_{sec}) and sesquinaries ($m_{1.5}$), respectively, while Table 1 summarizes these masses normalized to the impactor mass.

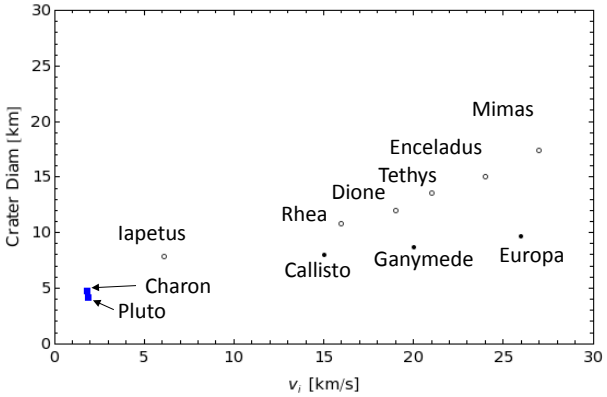

Figure 1: Estimated crater sizes for a 1 km comet striking Pluto, Charon, the Galilean satellites of Jupiter, and the mid-sized Saturnian satellites.

Secondary Craters. Clearly the Galilean satellites, Europa in particular, have the most mass available to make secondary craters (due to the combination of higher impact speeds, and a sufficiently high surface gravity to retain high-speed ejecta to make secondary craters). For these impact conditions, Pluto and Charon have over an order of magnitude less mass to make secondaries. While we expect an observable population of secondaries (given sufficient primary crater density), they will contribute to the crater SFDs at a lower-level than on the icy satellites of Jupiter and Saturn.

Sesquinary Craters. As with secondaries, we predict that the population of sesquinary craters is subdued on P/C relative to the icy satellites, although the presence of sesquinary craters is not well understood on any surface (see [1]).

Evolution of Escaped Crater Ejecta. We have used scaling relations from [2] to estimate the distribution of ejecta speeds, and are initiating analytical arguments [4] and numerical integrations to model the orbital evolution and sweep-up of crater ejecta. We initially estimate that the optical depth in dangerous, mm-sized or larger ejecta is likely to be small (also see [5]), unless one of the moons has suffered an unlikely large impact during the past million years.

Uncertainties and Scientific Opportunities. All of the calculations used here assume water ice as the target surface, and are derived on the assumption of hypervelocity impacts. The presence of a thick nitrogen icy layer could complicate both assumptions, but that in itself would be a scientific bonanza.

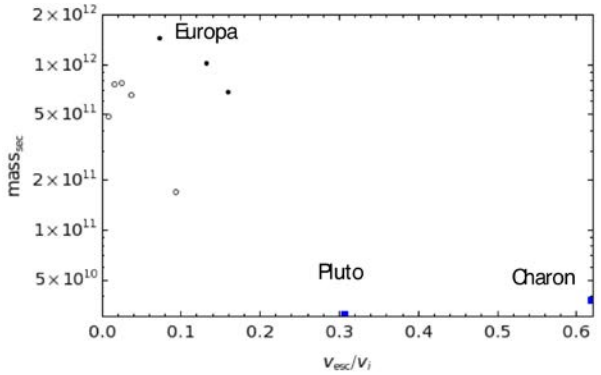

Figure 2: Estimated mass available to make secondary craters due to a 1 km cometary impact. Open circles are the Saturnian satellites, filled circles are the Galilean satellites.

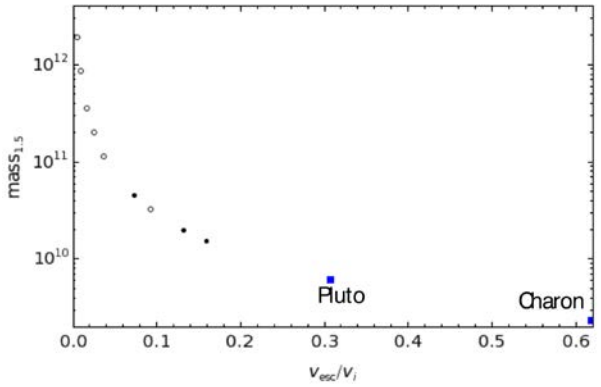

Figure 3: Estimated mass available to make sesquinary craters due to a 1 km cometary impact. Symbols are the same as in Figure 2.

Object	m_{sec}/m_i	$m_{1.5}/m_i$
Pluto	0.1	< 0.01
Charon	0.1	0.02
Mimas	0.0	6.1
Enceladus	1.5	2.7
Tethys	2.4	1.1
Dione	2.4	0.6
Rhea	2.0	0.4
Iapetus	0.5	0.1
Europa	4.6	0.1
Ganymede	3.2	0.1
Callisto	2.2	<0.1

References: [1] Bierhaus E. B. et al. (2012) *Icarus, 218*, 602-621. [2] Housen K. R. and Holsapple K. A. (2011) *Icarus, 211*, 856-875. [3] Zahnle K. et al. (2003) *Icarus 163*, 263-289. [4] Burns, J. A. and Gladman, B. J. (1998) Planet. Space Sci. 46, 1401-1407. [5] Kenyon, S. J. and Bromley, B. C. (2013) http://arxiv.org/abs/1303.0280.

EARTH-BASED OBSERVING CAMPAIGN FOR THE NEW HORIZONS ENCOUNTER

R. P. Binzel[1], L. A. Young[2] and F. E. DeMeo[1], [1]Dept. Earth, Atmospheric, Planetary Sciences, Massachusetts Institute of Technology, Cambridge, MA, rpb@mit.edu; [2]Southwest Research Institute, 1050 Walnut St., Suite 300, Boulder, CO, layoung@boulder.swri.edu

---

Introduction: The New Horizons encounter in 2015 presents a once-in-a-lifetime opportunity to measure *in situ* the state of the Pluto-Charon system. We know the system is dynamic through decades of measurements from Earth-based telescopes. Thus we must realize that New Horizons is providing a "snapshot" in time that establishes a single "moment" of ground truth in the Pluto-Charon system. Our understanding of the temporal variation of the system *requires* that we anchor the ground truth of New Horizons to the Earth-based view through simultaneous telescopic observations before, during, and after the New Horizons encounter.

Campaign Organization: The first author (RPB) is taking the lead for the campaign organization on behalf of the New Horizons science team. Wide international participation is most especially welcome! The concept moving forward is one of broadly sharing ideas for observing plans and perceived needs from the project. While some observing programs may be specifically recommended by the project and seek observers, largely the campaign will rely upon individual investigators responding to calls for observations. We will especially seek to identify how the plans of one program may be complemented by the plans of another.

Observatory Support: Specific requests to allocate blocks of time for mission support will be made by New Horizons to specific Telescope Allocation Committees (TACs), such as the NASA IRTF. While the time surrounding the July 2015 encounter is obvious for mission support, we are seeking ideas and justification for observations (and time block allocations) that might begin as early as 2014 and continue through 2016.

Getting Involved: This Pluto System 2013 Conference is the official kick-off for the organization of the observing campaign. Please indicate your interest by contacting: rpb@mit.edu A web page will be set up where ideas and plans can be shared, including progress on securing New Horizons mission support time blocks at major observatories.

Acknowledgement: This work is supported by NASA's New Horizons mission to the Pluto system.

New Horizons Earth-Based Campaign: Calibration and Context of the Pluto System

Campaign Phase	Date Range (MM/YY)	Pluto Coordinates	Measurements Required	Relative Priority *High - - - - - - - - - - > Highest*
Phase I: Pre-Encounter	4/14 - 10/14	18:50 -20 V14.4	Stellar Occultations: Atmospheric profiles.	
			Spectral / Thermal: Atmospheric composition & Surface mapping. Full rotational coverage.	
			Photometry: Rotation lightcurve & phase function.	
Phase II: Immediate Approach	4/15 - 5/15	19:05 -20 V14.5	Stellar Occultations: Atmospheric profiles.	
			Spectral / Thermal: Atmospheric composition & Surface mapping. Longitude of closest approach.	
			Spectral / Thermal: Atmospheric composition & Surface mapping. Full rotational coverage.	
			Photometry: Rotation lightcurve & phase function.	
Phase III: Encounter	6/15 - 8/15 (encounter date 7/14/15)	19:07 -21 V14.4	Stellar Occultations: Atmospheric profiles.	
			Spectral / Thermal: Atmospheric composition & Surface mapping. Longitude of closest approach.	
			Spectral / Thermal: Atmospheric composition & Surface mapping. Full rotational coverage.	
			Photometry: Rotation lightcurve & phase function.	
Phase IV: Immediate Post-Encounter	9/15 - 10/15	18:54 -21 V14.6	Same as Phase II	
Phase V: Post-Encounter	4/16 - 10/16	19:09 -21 V14.5	Same as Phase I	

SELECTED STELLAR OCCULTATION BY PLUTO SYSTEM UP TO 2015.

F. Braga-Ribas[1], B. Sicardy[2], M. Assafin[3], J. I. B. Camargo[1] and R. Vieira-Martins[1], [1]Observatório Nacional/MCTI – Rua Gal. José Cristino 77, 20921-400 Rio de Janeiro RJ Brazil – ribas@on.br, [2]Observatoire de Paris-Meudon/LESIA – 5 place Jules Janssen, Meudon, France – bruno.sicardy@obspm.fr, [3]Observatório do Valongo/UFRJ – Ladeira do Pedro Antônio 43, 20080-090 Rio de Janeiro RJ Brazil – massaf@astro.ufrj.br.

Introduction: Pluto is one of the most know dwarf-planets and is the target of the NASA's New Horizons space mission. Until now, it is the only object of its kind to have a tenuous global atmosphere detected.

The stellar occultation is the only ground based technique capable of providing the temperature and density profiles of its atmosphere. It is also a powerful technique to determine shape and dimensions with kilometric accuracies for atmosphereless objects like Pluto's satellites (Charon, Hydra, Nix, P4 and P5).

We present a selection of predicted stellar occultations by the Pluto system up to 2015, that will allow, for example, the continuous study of Pluto's atmosphere evolution.

Predictions: The occulted star candidates come from the observation of Pluto's sky path from 2009 to 2015, held at the ESO/Max-Planck 2.2m telescope with the Wide Field Imager (WFI) [1].

The predictions are made considering an offset to the JPL-DE413 ephemeris, and using a satellite solution obtained with Hubble Space Telescope images [2]. The applied offset was determined from a linear fit to the offset measurements in positive stellar occultations from 2005 to 2012 (Figure 1).

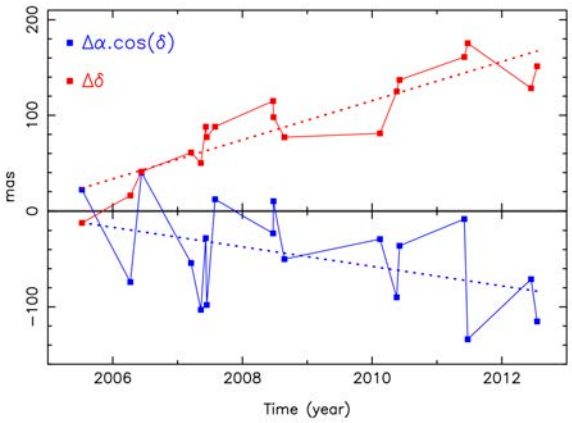

Figure 1. Positional offsets for Pluto from observed stellar occultations (observation minus DE413 ephemeris). Blue: right ascension. Red: declination. Dashed lines are the linear fit used to extrapolate the offset to the future occultation date.

Selection: The selected events involve the brightest stars to be occulted during the period with a shadow track, going over regions of the Earth with large availability of telescopes. They were also selected aiming three scientific objectives: continuous monitoring of Pluto's atmosphere; astrometry of the satellite system; and measurement of the size of Pluto's small satellites.

Events: hereafter we present the list of the selected events by date, object, UT time of the closest approach, R magnitude and location:

Date	Object	UT	R	Location
2013/07/20	Pluto	08:02	16.5	CHL, ARG, NZL
2014/03/07	Nix	17:32	13.3	AUS
2014/07/05	Pluto	23:26	15.7	FRA, DEU, ESP
2014/07/05	Charon	23:36	15.7	BRA, RSA, NAM
2014/07/05	Nix	23:53	15.7	BRA, NAM
2014/08/13	Pluto	06:20	16.5	EUA, CAN
2014/08/13	Charon	06:20	16.5	PER, NZL, CHL
2014/09/23	Hydra	18:48	14.6	ISR, MDG, TUR
2015/06/29	Pluto	16:54	12.2	AUS, PNG, MDG
2015/07/18	Pluto	06:46	14.1	ARG, URY, NZL

From the listed events we highlight the Nix occultation on March 2014 by a bright star, with good observation conditions to the australian observatories. We also highlight the multiple event by Pluto, Charon and Nix.

The best event will happen few days before the New Horizons rendezvouz with Pluto system, on the 29th June 2015, and involves one of the brightest star ever occulted by Pluto with R magnitude 12.2 (Figure 2). A big observation campaign with many detections will bring invaluable information of Pluto atmosphere. If it is linked to the New Horizons discoveries, it will allow an unprecedented study of Pluto's atmosphere temperature, pressure and density profiles.

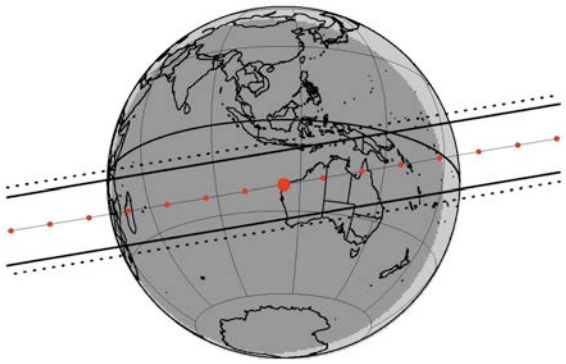

Figure 2. The prediction map for the 29th June 2015 occultation. It is the best of the selected events, involving a 12.2 R magnitude star.

Considerations: The presented events will allow the continuous monitoring of Pluto atmosphere, before and after the New Horizons rendezvous with the system. It will also permits to obtain precise astrometry of Pluto's satellites and maybe even the measurement of the small moons size.

It is estimated an error of about one Pluto radius for the predictions, so the tracks may shift of about a thousand kilometer. To reduce this error, careful astrometry of the target stars and last minute prediction updates will be done and made available on-line at our occultation campaigns site:

http://devel2.linea.gov.br/~braga.ribas/campaigns/

References:

[1] Assafin, M., et al. (2010), A&A, 515, A32.

[2] Buie, Marc W., et al. (2012), AJ, 144, 15.

IMPACT CRATER MORPHOLOGY ON PLUTO

V. J. Bray[1], [1]Lunar and Planetary Laboratory, University of Arizona, Sonett Space Sciences, 1541 E University Blvd. Tucson, Arizona, 85721, USA. vjbray@lpl.arizona.edu

Introduction: Impact cratering is a fundamental process that affects the surfaces of all solid bodies in the solar system. It is a complex process that depends upon the size, velocity and composition of the impacting body, as well as the gravity and near-surface properties of the target. As a result of the latter, the study of impact craters offers a tool for investigating the subsurface structure and composition of solar system bodies. This abstract combines previous cratering studies on icy bodies and numerical modeling of the impact process to predict crater morphology on Pluto.

General Crater Characteristics: As an icy body, we would expect craters on Pluto to be shallower and with lower rim heights and gentler wall slopes than for a rocky body of similar mass [e.g., 1, 2]. However, experimental work has shown that lower impact velocities produce deeper transient craters [e.g., 3]. The low impact velocity calculated for the Pluto system (~ 1.9 km/s. c.f. [4]) may lead to anomalously deep simple craters.

The Simple to Complex (s-c) Transition: The morphology of an impact crater, and the crater diameters at which morphological transitions (such as the simple to complex transition) occur should be similar on bodies with similar gravity [5]. Figure 1 shows the relationship between s-c transition diameter and planetary gravity for rocky and icy bodies. Although the Moon and the Galilean satellites have similar gravity, the difference in surface composition influences the crater diameter at which the simple-to-complex transition occurs: central peaks are noted in smaller craters on icy bodies relative to rocky bodies with similar gravity. Based on Pluto's gravity of ~0.65 ms^{-1} and its icy surface a predicted transition diameter of ~6 km has been marked on Figure 1. The complication of a relatively low impact velocity may act to delay the formation of central peaks until larger crater diameters. An s-c transition diameter of 6km is therefore considered a lower bound.

Rim Collapse and Central Uplift Formation – New insights from New Horizons: On the Moon (g~1.64ms^{-2}) rim collapse occurs prior to central peak formation at crater diameters of ~15 and ~20 km respectively. Conversely, on Ganymede (g ~ 1.43 ms^{-2}), peak formation is noted in craters of ~ 2 km diameter, followed by a decrease in rim height (indicating rim collapse) at D ~ 9 km [e.g., 1, 2]. This is either a fundamental difference in the crater modification process between rocky and icy bodies, or might be the result of measurement bias when assessing craters below 2 km with imagery of ~ 0.4 km/pix resolution. The 0.6 – 0.1 km/pix resolution of the Multicolor Visible Imaging Camera (MVIC) and the Long Range Reconnaissance Imager (LORRI) on board New Horizons [e.g., 6], combined with the larger predicted s-c transition diameter on Pluto (Figure 1) might provide an opportunity for this unanswered question of the cratering process to be investigated.

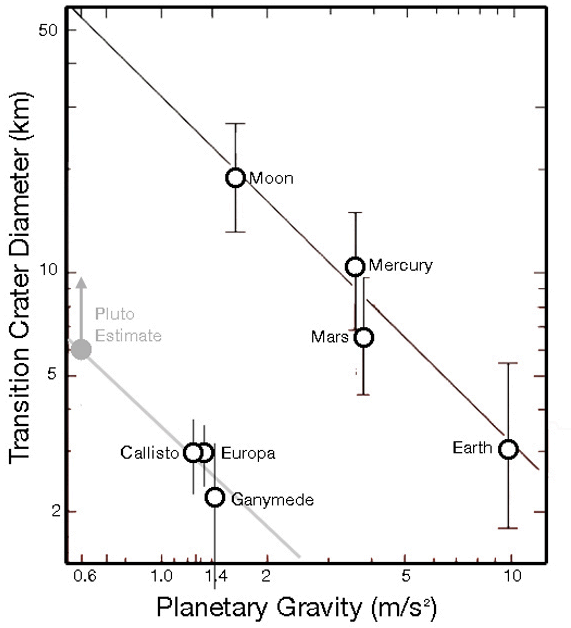

Figure 1: Diameter at which craters transition from simple bowl-shaped to complex as a function of gravity for the Moon Mercury, Mars, Earth, Europa, Ganymede, and Callisto. Predicted Pluto transition diameter is marked, assuming that data from the icy Galilean satellites can be extrapolated to Pluto.

The Peak to Peak-Ring/Pit Transition: In craters of increasing diameter on rocky bodies the internal morphology changes from central peak to peak-ring. On ice-rich crusts like those of Mars or the Galilean satellites, the transition is instead from peaks to central pits. However, pit formation is not only due to the presence of ice in the crust.

The peak to peak-ring transition is not noted on most small icy satellites. Central pit craters are likewise absent [e.g., 1].

One suggested formation theory for these central pits and their absence on small icy bodies involves the formation of a peak-ring which acts to confine impact melt water to the crater centre. The melt then drains, or is lost as vapor, leaving a central pit and over-printing peak-ring morphology [e.g., 2, 7]. The formation of large 'floor pits' therefore require: 1) enough impact melt to be produced and 2) the transition from peak to peak-ring craters to occur.

The transition from peak to central pit morphology occurs at crater diameters of ~ 60 km on Ganymede [e.g., 8, 9]. Scaling for gravity, the transition from peak morphology to either peak-rings or central pit morphology on Pluto would occur above crater diameters of ~ 150 km. Calculations of melt drainage on Pluto by [7] suggest that central pit craters are theoretically plausible for large impactor sizes. However, the low impact velocity in the Pluto system (~1.9 km/s c.f. [4]) will produce low volumes of impact melt. The formation of central pits on Pluto is therefore considered unlikely. Some small-scale pitting of the crater floor might be expected rather than a notable central pit.

Using crater morphology to probe sub-surface structure and heat flow: Current bulk density estimates for Pluto range from 1.83 to 2.05 g/cc implying rock/ice mass ratios of 1.27 to 3.35 [e.g., 10]. This mass is thought to be differentiated into an ice crust above a silicate mantle. Modeling by [11] has shown that a sub-surface ocean is possible beneath a convective ice shell. Such internal layering would have implications for crater morphology, perhaps allowing features such as the multi-ringed Tyre on Europa to form as a result of a large enough impact. A sub-surface ocean at a shallow enough depth to form Tyre-like features is unlikely without notable heat flow from the interior.

The morphology of impact craters on Europa have been used to infer its crustal thickness and heat flow through both analysis of fresh crater morphology, and relaxation of topography after crater formation [e.g., 12, 13, 14]. Methods that use analysis of a single crater can gain a snap-shot of the crustal conditions at the time of impact, in that specific location. Studies that use the full cratering record of Europa can alternatively provide an assessment of spatially and temporally averaged conditions.

Figure 2 presents example results of numerical modeling of impact into an ice target with various heat flows and associated sub-surface layering (see [13] and [14] for more details). The depth and diameter of the simulated impact craters were measured and compared with depth-diameter measurements of craters on Europa from [15]. With increasing heat flow, a 'turn over' in the depth-diameter trend occurs at lower crater diameters. Once surface observations of Pluto exist, similar depth-diameter plots of fresh craters can be constructed and the same modeling methods used to investigate layering and/or crustal heat flow.

References:[1] Schenk, P. M. (1991) JGR 96:15635-15664. [2] Bray V. J. et al. (2012) *Icarus, 217*, 115-129. [3] Schultz, P. H. (1988) in *Mercury*, Univ. Arizona Press, pp. 274–335 [4] Zahnle et al. (2003) Icarus 163 (2003) 263–289. [5] Melosh, H. J. (1982). JGR 87:371-380. [6] Weaver, H.A. et al., (2008) Space Sci. Rev. 140:75–91 (2008). [7] Elder C. M. et al. (2012) *Icarus, 221*, 831-843. [8] Passey, Q. R. and Shoemaker, E. M. (1982), Univ. of Arizona Press. pp. 340-378. [9] Schenk (1993) J. Geophys. Res. 98:7475-7498. [10] Olkin, C.B. et al. (2003) Icarus, 164, 254-259. [11] Robuchon and Nimmo (2011), Icarus 216:426-439 [12] Nimmo *et al*., (2003) LPSC Abs. 1296. [13] Bray (2009), PhD Thesis, Imperial College London. [14] Bray et al., in prep (2013) [15] Schenk (2002), Nature 417:419-421.

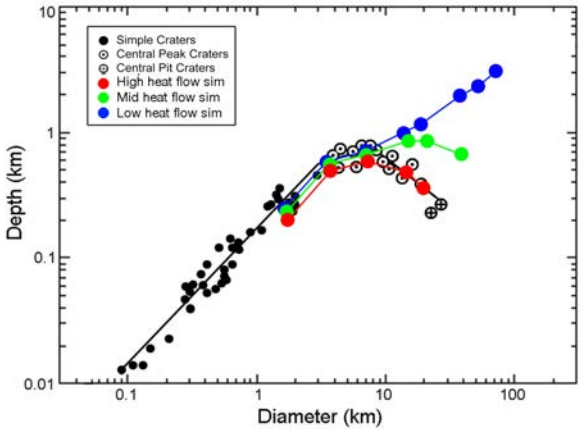

Figure 2: Depth diameter measurements for impact craters on Europa [15]. Hydrocode simulation of different sized impacts into ice with high, moderate and low (see [13, 14]) heat flow were performed and the dimensions of the simulated craters measured. High heat flow leads to 'turn over' of the depth-diameter trend at smaller crater diameters. A similar analysis of Pluto craters would yield information on globally averaged crustal heat flow over recorded geologic time.

THE ORBITS AND MASSES OF PLUTO'S SATELLITES

M. Brozović[1] and R. A. Jacobson[1], [1]Jet Propulsion Laboratory, California Institute of Technology (4800 Oak Grove Drive, Pasadena, CA 91109-8099, marina.brozovic@jpl.nasa.gov, robert.a.jacobson@jpl.nasa.gov)

Introduction: Dwarf-planet Pluto and its five currently known satellites (Charon, Nix, Hydra, S/2011 (134340) 1, and S/2012 (134340) 1) are the highly anticipated targets of NASA's New Horizons mission in 2015. New Horizons will be able to obtain unprecedented science data on the Pluto system that are likely to surprise and excite astronomers. Good-quality orbital solutions for Pluto and its satellites are the important prerequisites that will assure the success of the mission. Here, we provide the latest orbital elements and mass estimates for Pluto's satellites based on the most complete dataset to date.

Methods: We report on the numerically integrated orbital fits of Pluto's satellites. Our dataset consist of an extensive set of astrometric, mutual event, and stellar occultation observations obtained between 1980 and 2012. All relative observations of the satellites with respect to Pluto have been corrected for the Pluto center-of-figure center-of-light (COF) offset due to the Pluto albedo variations [1], [2]. In some instances, we also used the relative measurements of the satellites with respect to each other. We used bounded-least squares algorithm [3] in order to constrain the masses of the small satellites.

Results: The Pluto system mass is well determined with current data. However, the Charon's mass still carries a considerable amount of the uncertainty due to the fact that the primary source of information for the Charon mass is a small quantity of absolute position measurements [4], [5], [6] that are sensitive to the independent motions of Pluto and Charon about the system barycenter. The long-term dynamical interaction among the satellites does yield a weak determination of their masses. Hydra is the most massive of the satellites and also has the best constrained mass. The astrometric data for the most recently discovered satellite S/2012 (134340) 1 not only allowed its orbital determination, but they also contributed some valuable sensitivity for the mass of Nix. It is important to note that the differences between the orbits for the case of small satellites with zero masses and the case when the masses are non-zero are on the order of few hundred km at best. It will be necessary to have at least 5-10 years of observations with few miliarcseconds measurement precision in order to detect such differences. We are just now gaining the sufficient data quantity and quality to improve the estimates on the masses of the small satellites.

Acknowledgements: The research described in this paper was carried out at the Jet Propulsion Laboratory, California Institute of Technology, under a contract with the National Aeronautics and Space Administration.

References:

[1] Buie et al. (1992) Icarus 97, 211-227
[2] Buie et al. (2010) AJ 139, 1128-1143
[3] Lawson and Hanson (1995)
Solving Least Squares Problems, SIAM
[4] Null et al. (1993) AJ 105, 2319-2335
[5] Null and Owen (1996) AJ 111, 1368-1381
[6] Olkin et al. (2003) Icarus 164, 254-259

The Surface of Charon

M. W. Buie[1], [1]Southwest Research Institute, 1050 Walnut St., Suite 300, Boulder, CO 80302, buie@boulder.swri.edu.

Introduction: The surface of Charon has been very difficult to observed directly largely because it never gets more than an arc-second from Pluto and is usually lost in the confusing glare from Pluto.

Mutual Events: The first technique to be used successfully was to use the mutual events in the late 1980's to obtain data with Pluto+Charon and for a brief time Pluto alone while Charon was hidden from view. By subtracting these two results the properties of Charon were revealed. Optical spectra showed a neutral colored surface with no spectral features from 0.5-1.0 microns[1]. Near infrared spectra showed a surface dominated by water frost[2,3]. Albedo measurements indicate a moderately reflective surface, similar to that of Uranian satellites[4].

Directly Resolved Observations: With advancing technology, it became possible to directly resolve Charon from Pluto. The Hubble Space Telescope is easily able to separate the two as well as adaptive optics systems on ground-based observatories.

Hubble Space Telescope. The global photometric properties of Charon have come from HST observations[5,6,7]. Here we see that Charon has a small (~8% amplitude) lightcurve that is symmetric with the Pluto direction. It clearly does not show a more typical leading/trailing asymmetry such as is seen on other large satellites. The darkest longitude is on the Pluto-facing hemisphere. Charon has a larger photometric variation due to the solar phase angle than due to surface variegation.

Near-infrared observations with NICMOS were able to get well calibrated albedo spectra of Charon[8,9]. These spectra show the familiar water frost spectrum and a frost temperature. These data are also useful for subtracting Charon from ground-based spectra where Pluto and Charon are observed together.

Ground-based Observatories. Using adaptive optics systems it is possible to separate Pluto and Charon and permit direct observations of Charon. Most of this work has concentrated on spectroscopic investigations in the near-infrared region. The most intriguing of this work had led to an assertion that there are nitrogen-bearing compounds on the surface[10]. This signature is very weak and appears to be non-uniform. There are suggestions that this is endogenic but keeping in mind the stream of nitrogen that is being lost from Pluto there could be an exogenic explanation as well.

Presentation: This presentation will summarize our state of knowledge and layout the current mysteries that face us in our understanding of Charon. It is quite clear that the data to be returned from the New Horizons mission will forever alter our understanding of this interesting satellite (or double-planet member).

References: [1] Fink, U. and M. A. DiSanti (1988) *AJ, 95*, 229-236. [2] Buie, M. W., D. P. Cruikshank, L. A. Lebofsky, and E. F. Tedesco (1987) *Nature, 329*, 522-523. [3] Marcialis, R. L., G. H. Rieke, and L. A. Lebofsky (1987) *Science 237*, 1349-1351. [4] Buie, M. W., E. F. Young, and R. P. Binzel (1997) In *Pluto and Charon*, (D. J. Tholen and S. A. Stern, eds.) UA Press, Tucson, AZ. [5] Buie, M. W., D. J. Tholen, and L. H. Wasserman (1997) *Icarus, 125*, 233-244. [6] M. W. Buie, W. M. Grundy, E. F. Young, L. A. Young, and S. A. Stern (2010) *AJ, 139*, 1128-1143. [7] M. W. Buie, W. M. Grundy, E. F. Young, L. A. Young, and S. A. Stern. (2010) *AJ, 139*, 1117-1127. [8] M. W. Buie and W. M. Grundy (2000) *Icarus, 148*, 324-339. [9] Dumas, C., R. J. Terrile, R. H. Brown, G. Schneider, B. A. Smith (2001) *AJ, 121*, 1163-1170. [10] Cook, J. C.; S. J. Desch, T. L. Roush, C. A. Trujillo, T. R. Geballe (2007) *ApJ, 663*, 1406-1419.

Seasonal Variations on the Surface of Pluto.

M. W. Buie[1] and E. R. George[2], [1]Southwest Research Institute, 1050 Walnut St., Suite 300, Boulder, CO 80302, buie@boulder.swri.edu, [2]University of Colorado, Boulder, CO.

Introduction: The photometric record for Pluto spans 1930 to the present day and contains clues regarding how the surface changes in response to the seasons. There is a complex interplay between the time from perihelion and the sub-solar latitude that is coupled with surface properties. The changes induced are expected to large in some locations while perhaps smaller in others. These changes also couple to the atmosphere through the vapor pressure from the surface frosts. The scope of this presentation is to collect the clues provided from the photometric record and point to how this information connects to other observable phenomena. New Horizons will undoubtedly contribute to understanding the seasonal cycle but will unfortunately only provide one epoch. Full understanding of these processes that shape and sculpt the surface will require integrating remote photometry and the detailed views of the surface from the flyby.

Datasets: Photometric data comes in three basic groups. Photographic magnitudes that span the time from discovery (near 1930) up to the mid 1950's when photoelectric photometry superseded this technique. Such data are intrinsically low in precision but sufficient observations exist to permit constraining the mean lightcurve properties[1].

Ground-based data since 1954 has either been based on photoelectric photometers or CCD imaging devices. In these datasets, as with photographic data, the photometry collected is of the combined light from the Pluto system which is clearly dominated by Pluto but Charon contributes ~20% of the observed flux. The best published data are still from photoelectric systems but this option is no longer possible due to the low galactic latitude of Pluto starting around the year 2000[2]. Progress on the data during this recent period has been slow and has required the development of new techniques that can compete with the intrinsic quality of photoelectric observations.

The Hubble Space Telescope, with its stable PSF and high spatial resolution, has been used to collect separate photometric properties[3]. With these data is is now possible to provide reasonably accurate corrections for all combined-light photometry to extract the individual photometric properties of Pluto from 1930 onward where we have suitable data.

Lightcurve Evolution: This presentation will show the historical and new data on a common footing with a systematic removal of the photometric signature of Charon. Basically, we saw a very slight decrease (few percent) in mean brightness from 1930 to 1954. From 1954 to 2000 the surface can be very effectively described as static. The global color was constant with rotation, aspect, and time to a small fraction of a percent. By 2002 the situation had changed dramatically with a global reddening and now a slight modulation in color with rotation. This sharp onset of changes is consistent with some models of volatile migration [4,5] and can be used as very good diagnostics to sort out the most plausible cases.

Further observations will continue to be valuable both for tying in the historical dataset to the New Horizons encounter but also in continuing to monitor Pluto in the post-encounter era as it continues to move to aphelion and the seasonal cycle continues.

References: [1] B. E. Schaefer, M. W. Buie, and L. T. Smith. (2008) *Icarus, 197*, 590-598. [2] .M. W. Buie and W. M. Grundy (2000) *BAAS, 32*, 1083. [3] M. W. Buie, W. M. Grundy, E. F. Young, L. A. Young, and S. A. Stern. (2010) *AJ, 139*, 1117-1127. [4] Hansen, C. J. and D. A. Paige (1996) *Icarus, 120*, 247-265. [5] L. A. Young (2013) *ApJL, 766*, L22.

THE DISTRIBUTION OF HYDROCARBONS ON PLUTO'S SURFACE: DEPENDENCE ON SEASONAL BEHAVIOR OF THE ATMOSPHERE.

M. A. Bullock[1], L. A. Young[1], A. M. Zalucha[2], X. Zhu[3], and D. F. Strobel[4], [1]Department of Space Studies, Southwest Research Institute, bullock@boulder.swri.edu, [2]SETI Institute, [3]The Johns Hopkins Applied Physics Laboratory. [4]Departments of Earth and Planetary Sciences and Physics and Astronomy, Johns Hopkins University

Introduction: Products from the photolysis of the primary gaseous constituents of Pluto's atmosphere, N_2, CH_4, and CO react to form hydrocarbons and nitriles. N_2 is disassociated starting at about 900 km, while CH_4 and CO are photochemically destroyed starting at about 140 km. Since Ly-α from the interplanetary medium is about as intense as solar Ly-α at 40 AU, day time photochemistry is only about twice as fast as on the night side. Hydrocarbons such as C_2H_2 and C_2H_4 and nitriles such as HCN and HC_3N are produced largely by thermochemical reactions much deeper in the atmosphere. These species also condense out of the current atmosphere at altitudes between 5 and 15 km, probably producing low hazes and precipitating onto the surface.

Photochemical models have calculated global mean production rates for hydrocarbons and nitriles with up to 4 carbons (Krasnopolsky and Cruikshank, 1999; Lara et al., 1997; Summers et al., 1997). To date, all published models agree that ethane (C_2H_6), acetylene (C_2H_2), hydrogen cyanide (HCN), and ethylene (C_2H_4) form in Pluto's atmosphere and are probably deposited on the surface. Summers et al., (1997) and Krasnopolsky and Cruikshank, (1999) also predicted that diacetylene (C_4H_2) will be produced and deposited on the surface. Krasnopolsky and Cruikshank (1999) argued that cyanoacetylene (HC_3N) is produced from acetylene and the CN radical, and from hydrogen cyanide and the C_2H radical. That cyanoacetylene is produced through these pathways in Pluto's atmosphere is bolstered by the *ab initio* calculations of Fukuzawa and Osamura (1997). Table 1 below compares the masses of the major organics predicted by these authors to form in 1 Gy on the surface of Pluto, in g/cm^2 (assuming the present-day atmosphere). SSG 97 is Summers et al. (1997), LIR 97 is Lara et al. (1997) and KC 99 is Krasnopolsky and Cruikshank (1999).

Persistent frost-free regions probably exist at subtropical latitudes, as evidenced by low albedo features and possibly the low brightness temperature at mm wavelengths. Seasonal frost migration from the edges of the caps poleward leaves the lower latitudes frost-free for at least half an obliquity cycle, or 1.5 My. Long term migration of volatiles to one pole, driven by obliquity (3 My) and longitude of perihelion cycles (3.7 My) may also have left bands of latitude at ±20° mostly frost-free for up to 1 Gy.

Tropical bands that are persistently free of frost will accumulate a layer of hydrocarbons and nitriles 20 μm - 2 mm thick in 1 My, from the present atmosphere. Precipitating continuously, the layer builds up as a mixture of ethane, acetylene, hydrogen cyanide, ethylene, and diacetylene ices. Higher order hydrocarbons are also produced, although at least at an order of magnitude lower rate. On the remainder of the planet, the hydrocarbon rain is swamped by frost migration, in whose surface deposits it is mixed to an average concentration of no more than one part in a million. High energy particles from galactic cosmic rays and solar events cook the hydrocarbon-ice brew into a dark organic crust. If the atmosphere collapses seasonally, however, the hydrocarbon and nitrile deposits would be covered every year, precluding their build up. We would have to look elsewhere to explain the low albedo features in the Pluto tropics.

Table 1. Production Rates of Organics on Pluto

Molecule g/cm^2 - Gy	SSG 97	LIR 97	KC 99
C_2H_6	0.42	25.7	9.0
C_2H_2	0.27	9.2	65.0
HCN	0.54	7.6	14.0
C_2H_4	0.54	0.06	6.0
C_4H_2	0.34	--	58.0
HC_3N	--	--	23.0
Totals	2.11	42.56	175.0

Method: We examine two different models of the seasonal behavior of Pluto's atmosphere for the distribution of hydrocarbon and nitrile deposits on the surface. These are specific cases of the VT3D volatile transport model (Young, 2013); one is a Permanent Northern Volatiles (PNV) scenario and the other is an Exchange with Pressure Plateau (EPP) model (Young, 2013). PNV solutions require high surface thermal inertias and a large inventory of surface volatiles, and result in a permanent northern cap and a substantial atmosphere year-round (Fig. 1a). EPP solutions result from low thermal inertias and smaller volatile inventories (Fig. 1b). Volatiles are shuttled across hemispheres, and the atmosphere retains approximately its current mass past 2015. The 9th PNV case, PNV9,

used a thermal inertia of 3.162 x 10^3 J m^{-2} $s^{-1/2}$ K^{-1} and N_2 column mass of 16 g/cm^2. Frost albedo was 0.6; non-frost regions had an albedo of 0.2. Frost emissivity was assumed to be 0.8, and non-frost region emissivity was 1.0. The surface pressure never goes below 9 mbar and reaches a maximum of 44 mbar in 2030. EPP7 used a thermal inertia of 10 J m^{-2} $s^{-1/2}$ K^{-1} and the same volatile inventory as PNV9, 16 g/cm^2 of N_2. However, the frost albedo was assumed to be 0.7 in EPP7, rather than 0.6.

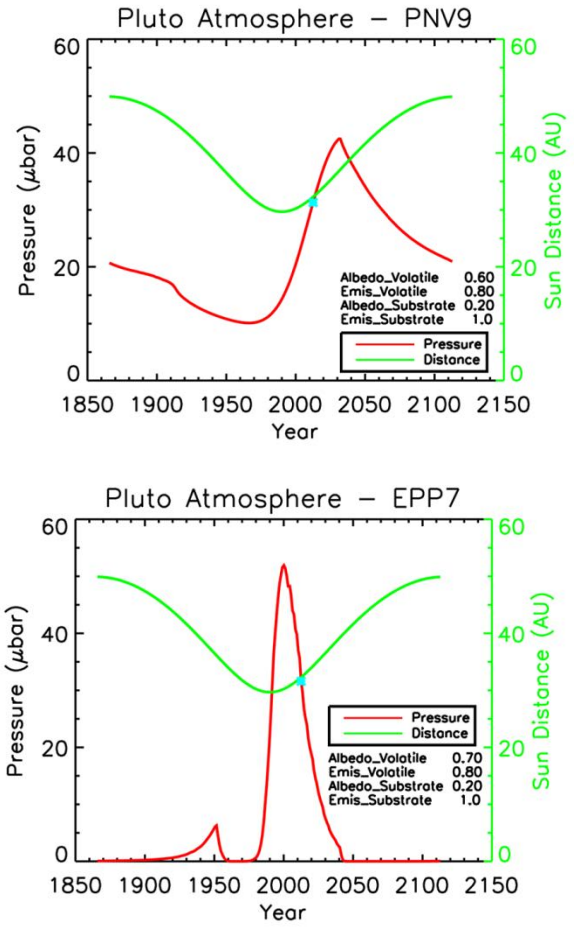

Fig. 1a (top) Sun distance (green) and surface pressure (red) for the PNV9 frost transport model. **Fig. 1b** (bottom) The same parameters plotted for the EPP7 case (Young, 2013).

The albedo and emissivity of non-frost regions were the same as used in PNV9, 0.2 and 1.0, respectively. Frost emissivity was also the same, at 0.8. EPP7 describes an atmosphere that briefly inflates for only a quarter of the year around perihelion, and will collapse by 2040. Frost transport in each model is quite different, as are the regions in which hydrocarbons and nitriles are likely to collect. PNV9 describes an atmosphere that rains hydrocarbons and nitriles continually and may have permanent non-frost regions where they collect circling the maximum perimeter of the permanent northern cap. In EPP7, photochemistry only occurs during a quarter of the year, and the tiny quantity of organics produced are probably mixed with the collapsed atmosphere.

We use the atmospheric radiative-conductive model of Strobel et al. (1996) with enhancements described in Zalucha et al. (2011) to calculate the temperature profile at 24 points equally spaced over a Pluto year. The VT3D volatile transport code is used to track the deposition of frost on the surface over each of these intervals. We will use a new photochemical-thermochemical code to calculate the deposition of hydrocarbons and nitriles for both cases over 1 My and, more speculatively, over 1 Gy. In our poster, we will also discuss the observable consequences for the deposition of organics in frost-free regions for each case.

References: Fukuzawa, K., Osamura, Y., 1997. The Astrophysical Journal. 489**,** 113. Krasnopolsky, V. A., Cruikshank, D. P., 1999. Journal of Geophysical Research. 104**,** 21979-21996. Lara, L. M., Ip, W. H., Rodrigo, R., 1997. Icarus. 130**,** 16-35. Strobel, D. F., Zhu, X., Summers, M. E., Stevens, M. H., 1996. Icarus. 120**,** 266-289. Summers, M. E., Strobel, D. F., Gladstone, G. R., In Pluto and Charon. University of Arizona Press, Tucson, 1997. Young, L. A., 2013. The Astrophysical Journal Letters. 766**,** L22. Zalucha, A. M., Gulbis, A. A. S., Zhu, X., Strobel, D. F., Elliot, J. L., 2011. Icarus. 211**,** 804-818.

PLUTO'S LIGHT CURVE OVER TIME AS AN INDICATION OF SEASONAL VOLATILE TRANSPORT.

B. J. Buratti[1], M. D. Hicks[1], P. A. Dalba[1], J. K. Hillier[2], S. Banholzer[1], D. S. Chu[1], A. O'Neill[1]; [1]Jet Propulsion Laboratory, California Inst. Technology (4800 Oak Grove Dr. 183-401, Pasadena, CA 91109; Bonnie.Burattti @jpl.nasa.gov); [2]Grays Harbor College

Introduction: The rotational light curve is a first-order description of the distribution of albedo patterns on the surface of an airless body. Changes in the rotational light curve through time provide a direct measurement of volatile transport, once all corrections to changes in viewing geometry have been modeled. Changes in the color of the light curve are also significant, because frosts tend to be blue in the visual part of the spectrum. Because of their substantial obliquity, Pluto and Triton should exhibit seasonal volatile transport on their surfaces [1]. This transport is associated with the sublimation of gasses into the atmosphere, leading to substantial changes in the vapor pressures of methane and nitrogen. Rotational light curves of Pluto have been obtained since 1950 and can be compared to a static frost model constructed from HST maps [2]. For five decades, between 1950 and 2000, Pluto's light curve was consistent with a stable albedo pattern [3]; see Figure 1. In 2007, there were indications that volatile transport was occurring [4]. New HST maps of Pluto also suggest recent volatile transport [5].

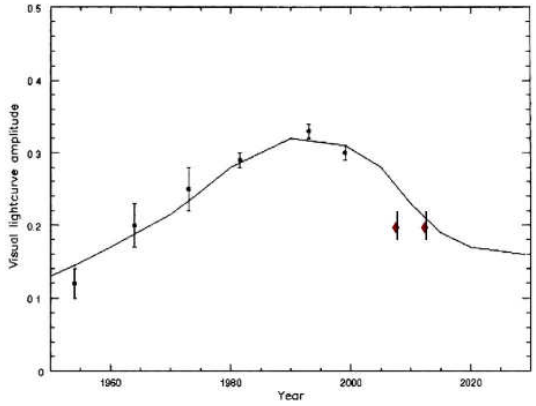

Figure 1. The amplitude of Pluto's light curve through time, based on historical observations. The solid line is a static frost model, based on HST maps. The last two points are recent measurements from Table Mountain Observatory (TMO) showing seemingly contradictory results. Based on [3], with recent data added in.

Observations 2012-2013: Rudimentary measurements from JPL's Table Mountain Observatory (TMO), obtained during 2012 at the expected maximum and minimum of the light curve, surprisingly suggest a static model. It is critical to get a complete light curve prior to the New Horizons encounter to understand whether volatile transport is now occurring, to expand the timeline of observations from the fast, single flyby, and to correlate surface volatile transport with changes in atmospheric pressure. As Pluto moves out of the densest part of the Milky Way, observing circumstances are becoming more favorable (see Figure 2)

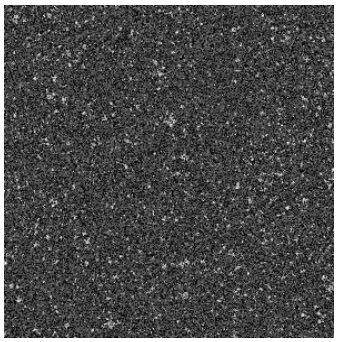

Figure 2. Pluto's star field in late July 2012.

During the summer of 2013, while Pluto is at opposition, a team of students will be obtaining a current light curve of Pluto on the 24-inch telescope at JPL's Table Mountain Observatory with the BVR filter system. Data analysis procedures will be implemented with standard routines from IRAF, with absolute photometry being accomplished by frequent measurements of Landolt standard stars each night. Twelve nights have been assigned for June 2013, and an additional 9 nights will be requested in July. If these observations are all successfully obtained, a dense three-color rotational light curve of Pluto will be the result. In addition, we should be able to detect any opposition surge on Pluto (although the minimum solar phase angle does not occur for another few years). Color and albedo changes will also be measured.

References: [1] Stern, S. A. and L. Trafton (1984). *Icarus* **57**, 231. [2] Stern, S. A., et al. (1997) *Astron. J.* **113**, 827. [3] Buratti B. J. et al. (2003) *Icarus* **162**, 171. [4] Hicks, M. D. et al. (2008) *B.A.A.S.* **40**, 460. [5] Buie, M. W. et al. (2010) *Astron. J.*, **139**, 1128.

Acknowledgments: This research was carried out at the Jet Propulsion Laboratory, California Institute of Technology under contract to the National Aeronautics and Space Administration.

Deep Non-linear Search for Additional Satellites around the Dwarf Planet Haumea

Luke D. Burkhart[1], Darin Ragozzine[2] and Michael E. Brown[3], [1]Harvard University (burkhart@college.harvard.edu), [2]University of Florida, [3]California Institute of Technology.

The dwarf planet Haumea, its two moons, and associated collisional family provide a unique Kupier Belt system of study for comparison to the Pluto system. Haumea exhibits many interesting properties, is the only known KBO aside from Pluto with multiple moons, and is the only other KBO that has been observed deeply enough to detect moons of a size comparable to P4 and P5. We present a deep, non-linear shift-and-stack satellite search in the Haumean system. We find no third satellite and place firm constraints on the presence of satellites above a size of ~10 km at distances above ~8000 km (near the stability limit). The absence of a cohort of small satellites in the Haumean system suggests that the collisional family formed in a manner quite different from the Pluto, although both systems are believed to have resulted from low velocity impact events. Moreover, we show that such a non-linear search, where shift rates are usually assumed to be quadratic in time, is made much more tractable by sampling only unique quadric rates that correspond to physical orbital parameter space, as suggested by Parker and Kavelaars 2010. This incarnation of the shift-and-stack search method can be applied to search for and characterize small moons around other KBOs. It can be fruitfully applied in the Pluto system to both search for even smaller satellites and to improve astrometric constraints on the small satellites even when they are not detected in individual images. We acknowledge funding from NASA through grant HST-GO-12243 from the Space Telescope Science Institute.

References: [1] Parker, A. H. and Kavelaars J.J. (2010) *Publications of the Astronomical Society of the Pacific* 122.891 (2010): 549-559.

Observations of Pluto, Charon and Other TNOs at Long Wavelengths

B. J. Butler[1], A. Moullet[2], and M. A. Gurwell[3], [1]National Radio Astronomy Observatory (Socorro, NM; bbutler@nrao.edu), [2]National Radio Astronomy Observatory (Charlottesville, VA; amoullet@nrao.edu), [3]Harvard-Smithsonian Center for Astrophysics (Cambridge, MA; mgurwell@cfa.harvard.edu).

Introduction: Observations of Pluto, Charon, and other TNOs at long wavelengths offer a unique method of determining not only surface, but also subsurface temperatures and properties. For Pluto and Charon, determining the distribution of temperature across their surfaces is important in trying to understand which volatiles are dominant in different locations. Since Pluto's atmosphere is in vapor-pressure equilibrium with surface frosts, understanding the volatile distribution is also key in understanding the atmosphere [1]. For all such icy bodies, the temperature at depth yields clues as to subsurface composition and physical state (amount of cracks and voids in the ice, for instance). And for those TNOs without an accurate diameter determination, the method of thermal radiometry can be used with such observations to determine their diameters (and hence density for the ~60 with companions that have known masses) [2-4].

Temperature of Pluto and Charon: The expected equilibrium temperature for an icy body at the distance of Pluto is ~53 K. IRAS observations indicated that the surfaces of Pluto and Charon were indeed at 55-60 K [5,6]. This was later confirmed by ISO and Spitzer [7,8], though the ISO and Spitzer observations showed that there must be different surface types on Pluto. Early millimeter wavelength observations showed colder temperatures, near 40 K [9-11]. It was suggested that these low temperatures, at least on Pluto, could be caused by the surface being in vapor-pressure equilibrium with N_2 gas in a tenuous atmosphere, and this was later confirmed by observation [12]. The combined observations were thus understood in the context of a Pluto with parts of its surface in N_2 vapor-pressure equilibrium, but not entirely, and a Charon covered mostly with water ice and having no atmosphere.

None of these previous observations resolved Pluto from Charon, however, so modeling was required to determine the relative contributions of the two bodies to the combined emission. In 2005 we obtained the first such observations of the separated thermal emission from Pluto and Charon, using the SubMillimeter Array (SMA), shown in Figure 1 [13]. We have since observed similarly with the SMA on two more occasions. These observations confirm the different surface temperatures on Pluto and Charon. We have also since observed with the Very Large Array (VLA) at even longer wavelengths, as shown in Figure 2 [14].

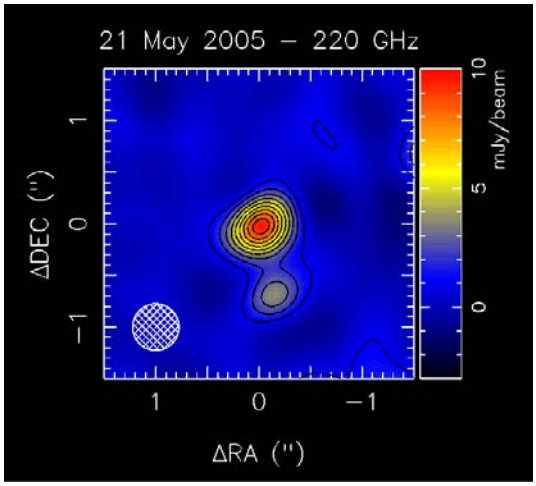

Figure 1. The emission from Pluto and Charon at 1.4 mm from the SMA. The separation of the two bodies is clear.

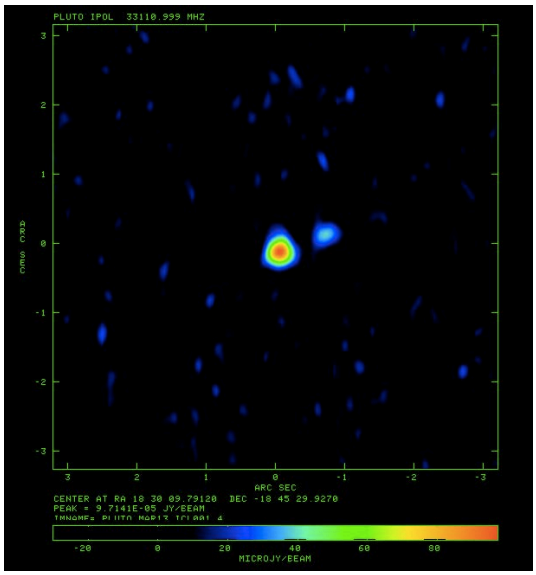

Figure 2. The emission from Pluto and Charon at 1 cm from the VLA.

Temperatures of Other TNOs: A number of TNOs have had their emission measured at thermal wavelengths, especially with the recent Spitzer and Herschel programs [3,4], but very few at wavelengths of millimeters or longer. Only the largest have had such observations [15-19]. We have carried out observations of the TNOs Makemake, Quaoar, and 2002 TC_{302} with the VLA, with detections for the first two and a non-detection for the third [14].

Modeling Long Wavelength Emission: Given an equilibrium physical temperature T_e for a body, the expected flux density is simply the product of the Planck function (using a brightness temperature of $T_b=\varepsilon T_e$ for thermal emissivity ε), and the solid angle subtended by the source (equal to $\pi R^2/D^2$ for source radius R and distance D). The main uncertainties in the equilibrium temperature are the values of the optical albedo, the rotation state (which determines heat penetration into the subsurface), and the surface macroscopic roughness (which determines the so-called "beaming parameter" if one uses one of the standard thermal models). For the flux density, the diameter of the body is the main uncertainty. In addition, one must recall that we are sensitive only to the *difference* of emission between the body and the background temperature at the current location of the body, which includes mostly galactic and Cosmic Microwave Background (CMB) emission. Using information on the physical properties of Pluto, Charon, and the larger TNOs [3], along with an estimate of the background emission at the location of the body during the observation (obtained from either WMAP or Planck observations depending on the wavelength [20,21]), it is straightforward to calculate the predicted flux density from any of these targets, or, conversely, given an observation of the flux density to derive the brightness temperature and hence other physical characteristics. Note that observations of Pluto and Charon were particularly difficult in the late 2000's as its path crossed the galactic plane multiple times, making the estimate of the background emission particularly important (Figure 3). We will present all of our previous observations of these bodies, along with their interpretation, within this framework.

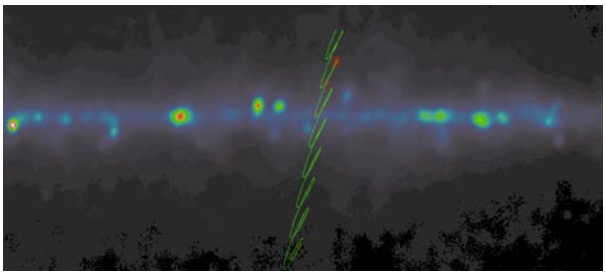

Figure 3. The path of Pluto and Charon, plotted in galactic coordinates over the 1 cm background emission measured by WMAP. The times of our observations are shown as the red circles. The bodies spent significant time in or near the galactic plane, where there is significant background emission even at millimeter and centimeter wavelengths.

References: [1] L.A. Young (2013) *ApJL, 766:*L22. [2] Spencer, J.R. et al. (1989) *Icarus, 78:337*. [3] Stansberry, J. et al. (2008) in *The Solar System Beyond Neptune, 161*. [4] Muller, T.G. et al. (2010) *A&A, 518:L146*. [5] Sykes, M.V. et al. (1987) *Science, 237:1336*. [6] Aumann, H.H., and R.G. Walker (1987) *AJ, 94:1088*. [7] Lellouch, E. et al. (2000) *Icarus, 147:220*. [8] Lellouch, E. et al. (2011) *Icarus, 214:701*. [9] Altenhoff, W.J. et al. (1988) *A&A, 190:L15*. [10] Stern, S.A. et al. (1993) *Science, 261:1713*. [11] Jewitt, D.C. (1994) *AJ, 107:372*. [12] Tryka, K.A. et al. (1994) *Icarus, 112:513*. [13] Gurwell, M.A. and B.J. Butler (2005) *BAAS, 37:743*. [14] Butler, B.J. et al. (2011) *EPSC-DPS, 2011:1670B.* [15] Jewitt, D.C. et al. (2001) *Nature, 411:446*. [16] Lellouch, E. et al. (2002) *A&A, 391:1133*. [17] Margot J.-L. et al. (2002) *BAAS, 34:871*. [18] Altenhoff, W.J. et al. (2004) *A&A, 415:771*. [19] Bertoldi, F. et al. (2006) *Nature, 439:563.* [20] Jarosik, N. et al. (2011) *ApJS, 192:14*. [21] http://tinyurl.com/cdm8n8p.

STELLAR OCCULTATIONS AND THE HELIOCENTRIC DISTANCE OF PLUTO

J. I. B. Camargo[1] and R. Vieira–Martins[1] and M. Assafin[2] and F. Braga–Ribas[1] and B. Sicardy[3] and A. H. Andrei[1] and G. Benedetti–Rossi[1] and D. N. da Silva Neto[4], [1]Observatório Nacional/MCTI – Rua Gal. José Cristino 77, 20921–400 Rio de Janeiro RJ Brazil – camargo@on.br, [2]Observatório do Valongo/UFRJ – Ladeira do Pedro Antônio 43, 20080–090 Rio de Janeiro RJ Brazil – massaf@astro.ufrj.br, [3]Observatoire de Paris-Meudon/LESIA – 5 place Jules Janssen, Meudon, France – bruno.sicardy@obspm.fr, [4]Centro Universitário Estadual da Zona Oeste – Av. Manuel Caldeira de Alvarenga 1203, 23070–200, Rio de Janeiro RJ Brazil – darionneto@gmail.com

Introduction: Transneptunian objects (TNOs) are relics, relatively unaltered, of the Solar System formation so that they provide invaluable information about the history and evolution of the outer Solar System. Pluto is, by far, the best studied TNO and is on the spot with NASA's New Horizons space mission.

When ground based observational techniques are considered, those based on stellar occultations are the only ones capable of providing the determination of dimensions with kilometric accuracies [1][2] and the detection of atmospheres as tenuous as few nanobars [3][4] to those objects. By their nature, stellar occultations also provide relative positions between the occulting and occulted bodies with milliarcsecond accuracy so that a careful astrometry of the occulted star results in an accurate position of the occulting body. In this work, we profit from a number of stellar occultations by Pluto to derive accurate offsets between its observed and ephemeris positions. From these offsets, we show that an underestimation of the heliocentric ephemeris distance of Pluto is a possible explanation to the offsets we find in right ascension.

Astrometry of Pluto: Observations of Pluto, in most cases, do not possess enough angular resolution to resolve it from Charon so that Pluto's photocenter is not directly accessed: one has to correct it for the nearby presence of Charon. In addition, since 2005, Pluto is seen from Earth in a region of the sky that is backgrounded by the Galactic plane. As a consequence, we have: the average colour of the reference stars is redder than Pluto's colour – so that chromatic differential refraction should be taken into consideration – and the high density of stars frequently makes it difficult to disentangle Pluto from faint objects in the background. Corrections for the effects of the photocenter displacements due to the presence of Charon and from the chromatic differential refraction can be found in the work by Benedetti-Rossi *et al.* [5], where positions of Pluto are obtained from fifteen years of optical observations. All these effects, however, contribute to increase the uncertainty on the observed Pluto's position. From stellar occultations, however, better accuracies are possible. When Pluto – or any other TNO – occults a star, the relative positions of both bodies can be obtained with milliarcsecond precision. Then, a careful astrometry of the occulted star, inlcluding its proper motion determination when necessary, may result in a final accuracy of about 20 milliarcseconds to the position of Pluto.

In Fig.1, the blue and green curves show $\Delta\alpha\cos\delta$ in the sense observation, as obtained from stellar occultations, minus ephemeris (DE418). For the blue curve, ephemeris right ascensions are taken without modifications. For the green curve, the heliocentric distance of Pluto is changed by Δh so that the respective ephemeris right ascensions are geometrically corrected accordingly. The red curve shows $\Delta\delta$ in the sense observation, as obtained from stellar occultations, minus ephemeris (DE418). This curve is fully used in our predictions of stellar occultations by Pluto.

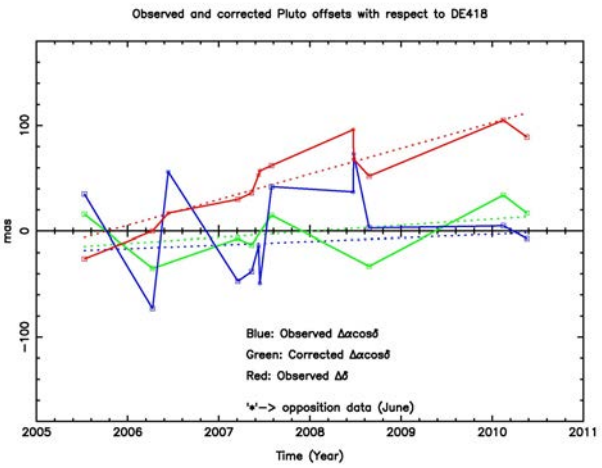

Figure 1. Positional offsets in the sense observation, as obtained from stellar occultation, minus ephemeris for Pluto. Blue: observed offsets in right ascension. Green: observed offsets in right ascension as obtained by changing the ephemeris heliocentric distance of Pluto by Δh and geometrically correcting the respective right ascensions accordingly. Red curve: observed offsets in declination. The planetary ephemeris used here is DE418.

The model we developed to relate the observable with the error in distance is given by

$$\frac{\Delta h}{d_g}\cos\delta_h \sin(\alpha_h - \alpha_g) = \Delta\alpha\cos\delta_g\,, \quad \text{(Eq.1)}$$

where the right part of the equation is the observable (the points linked by the blue lines in Fig.1). The quantities d_g, α_h, δ_h, α_g, and δ_g are all given by the ephemeris (DE418) and represent, respectively, Pluto's geocentric distance, heliocentric right ascension, heliocentric declination, geocentric right ascencion and geocentric declination. Δh is the error on heliocentric distance we want to determine. With this model, we find that Pluto is further from the Sun by 28.500 km (+/– 10.300 km, 1σ) as compared to the distance given by DE418. When the obtained Δh is replaced in Eq.1, we can derive the corrected offsets shown in Fig.1 (green curve).

The dotted lines in Fig.1 are determined by least–squares. For the red curve, all Δδ are used in that determination. For the blue and green curves, only those Δαcosδ not obtained (identified by small squares) close to Pluto's opposition were used in the least–squares. In fact, those Δαcosδ close to Pluto's opposition (identified by asterisks) are not well fit by Eq.1. We labled as opposition data all those from observations made in June.

It is interesting to notice that, with respect to the respective dotted lines, the dispersion of the Δαcosδ in the blue curve (small squares only) is 40 milliarcseconds whereas the dispersion of the Δαcosδ in the green curve (small squares only) is 23 milliarcseconds. For reference, the dispersion of the Δδ in the red curve is 16 milliarcseconds. These results support the existence of a measurable Δh.

Considerations: Any model that takes into account the shape of the blue curve would provide a green one where the smaller dispersion presented above is verified. However, given a position of the Earth in its orbit, the observed right ascension of Pluto will be greater or less than that given by the ephemeris under the hypothesis of an heliocentric distance underestimation and it is interesting to notice that the signs of the respective offsets in Fig.1 are compatible with such scenario.

We also notice that the ratio $\sigma_{\Delta h}/\Delta h$ is large. It is not to be expected that Δh in Eq.1 is the only effect to contribute to the observed offsets in right ascension shown in Fig.1. This supports the assumption that the heliocentric distance is not the only source of positional error. In addition, the reference catalogue for astrometry used in this work was the UCAC2 so that migration to UCAC4 should contribute (perhaps only marginally) to a smaller $\sigma_{\Delta h}/\Delta h$. Also, considering the DE413, the DE418, and the DE421, the more recent the ephemeris the further Pluto is placed from the Sun. Therefore, new Pluto positions – including those from occultations – are an important contribution to future planetary ephemerides as far as Pluto is concerned.

References:

[1]Elliot *et al*., "Size and albedo of Kuiper belt object 55636 from a stellar occultation", Nature 465, 897 (2010).

[2]Sicardy *et al*., "Charon's size and atmospheric upper limit", Nature 439, 52 (2006).

[3]Sicardy *et al*., "A Pluto-like radius and a high albedo for the dwarf planet Eris from an occultation", Nature, 478, 493 (2011).

[4]Widemann *et al*., "Titania's size and atmospheric upper limit", Icarus 199, 458 (2009).

[5]Benedetti-Rossi *et al*., "Detailed astrometric analysis of Pluto" (2013), in preparation.

ORIGIN OF PLUTO'S SATELLITES.

R. M. Canup, Southwest Research Institute (1050 Walnut Street, Suite 300; Boulder, CO 80302; robin@boulder.swri.edu) .

Introduction: Pluto and its massive satellite, Charon, are thought to have formed as a result of a giant impact (e.g., [1]). The most successful impacts form Charon as an intact object on an initially eccentric orbit, and imply that Pluto and Charon should have broadly similar compositions [2]. The origin of Pluto's four small satellites remains less well understood and they may represent either debris from the Charon-forming impact or captured material.

Giant Impact Origin of Pluto-Charon: A collision origin for Pluto-Charon is favored because of the pair's high angular momentum, which can be most readily explained by a large, grazing collision. While such collisions are improbable in the current Kuiper Belt, they would have been more common in a more massive, less dynamically excited primordial Kuiper Belt.

Smooth particle hydrodynamics (SPH) simulations of potential Pluto-Charon forming impacts have considered a range of impactor and target masses and compositions, impact velocities, pre-impact spin states, and impact angles [2]. Two types of impacts were shown capable of producing a satellite as massive as Charon (*i.e.*, having a satellite-to-planet mass ratio $q \approx 0.12$). In the first, a grazing, low-velocity collision involving similarly sized, differentiated objects (with ice mantles and rock or rock-metal cores) produces an orbiting disk of ice, with the rocky cores of both of the colliding objects absorbed by the final planet. The disk produced by this type of collision would yield a predominantly icy satellite whose density is substantially lower than that of the planet. Although such a "graze and merge" collision has been advocated for the origin of the large KBO Haumea and its ice-rich collisional family [3], both Charon's sizeable rock fraction and its large mass relative to Pluto are rather difficult to explain through such a scenario [2].

The more probable impact scenario involves an oblique, low-velocity collision by a largely undifferentiated impactor containing $\geq 0.3M_{PC}$, where M_{PC} is the total mass of Pluto and Charon. With an undifferentiated impactor, the binary forms directly as a result of the collision, with the satellite arising from an intact portion of the impactor. The final satellite's composition is in this case similar to that of the impactor (*i.e.*, a mixture of rock and ice), and its initial orbit is quite eccentric. Several dozen cases displaying this behavior produced binary pairs with $0.03 < q < 0.36$ and system angular momenta similar to that in the Pluto-Charon pair [2].

A Pluto-Charon forming impact leads to little ice vaporization. The energy deposited in Pluto by the impact, in combination with prior accretional and later radiogenic heating, seems most consistent with ice melting and a differentiated state. In constrast, an undifferentiatied state for Charon appears probable.

Origin of Small Satellites: Tiny Nix, Hydra, P4 and P5 occupy essentially co-planar orbits with Charon and are located near the 3:1 (P5), 4:1 (Nix), 5:1 (P4), and 6:1 (Hydra) mean-motion commensurabilities with Charon. The small moons' orbital properties suggest that they formed within a dissipative disk. One way to create a low-mass disk is from debris leftover from the Charon-forming impact. If the impactor is partially differentiated with a thin ice shell overlying a mixed ice-rock interior, a single collision can generate an intact Charon together with a dispersed disk whose mass is comparable to or larger than the combined masses of the small moons [4]. In these cases, the composition of the disk varies from a mixture of rock and ice to pure ice. However the debris disk typically extends out to only 20 Pluto radii or less, well interior to the current orbits of Pluto's small moons that orbit exterior to 35 Pluto radii.

It was proposed [5] that Nix and Hydra were trapped into corotation resonances with an initially eccentric Charon, and were resonantly driven outward to their current locations as Charon's orbit tidally expanded. However later works found that Nix and Hydra cannot simultaneously be transported in this manner [6-7]. Recent work [8] suggests that the small moons may either be captured or that they formed due to collisions among debris from the Charon-forming impact that was perturbed by the binary onto escaping orbits.

References: [1] McKinnon, W. B. *ApJ* 344,41 (1989); [2] Canup, R. M. *Science* 307, 546 (2005); [3] Leinhardt et al., ApJ 714, 1789 (2010); [4] Canup, R. M. *Astron. J.* 141, 35 (2011); [5] Ward, W. R. and R. M. Canup *Science*, 313, 1107 (2006); [6] Lithwick, Y. and Y. Wu arXiv:0802.2951 (2008); [7] Cheng, W. H., M. H. Lee and S. J. Peale, submitted (2013); [8] Kenyon, S. J. and B. C. Bromley arXiv: 1303.0280 (2013).

.

LONG-RANGE RECONNAISSANCE IMAGER ON NEW HORIZONS

A. F. Cheng[1], H. A. Weaver[1], S. J. Conard[1], J. R. Hayes[1], M. F. Morgan[1], M. Noble[1], H. W. Taylor[1], O. Barnouin[1], J. D. Boldt[1], E. H. Darlington[1], M. P. Grey[1], T. Magee[1], E. Rossano[1], C. Schlemm[1], K. E. Kosakowski[2], and D. Sampath[2], [1]The Johns Hopkins University Applied Physics Laboratory, 11100 Johns Hopkins Road, Laurel, MD 20723 (andrew.cheng@jhuapl.edu), [2]L-3 Communications SSGTinsley, 65 Jonspin Road, Wilmington, MA 01887.

Introduction: The LOng-Range Reconnaissance Imager (LORRI) is the highest resolution imaging instrument on NASA's New Horizons mission to Pluto and the Kuiper Belt. New Horizons is the first mission in NASA's New Frontiers program and was successfully launched on 2006-Jan-19 [1]. After a 9.5 year interplanetary journey, the New Horizons spacecraft will fly ~12,500 km above the surface of Pluto in July 2012, providing the first in situ investigation of this fascinating system comprised of the dwarf planet Pluto, its large moon Charon, and at least four small satellites (Nix, Hydra, P4, and P5). LORRI has the sensitivity and dynamic range required to image these multiple targets at illumination levels only 1/900th of those on Earth, and with a resolution of ~100 m during closest approach to Pluto.

Design: LORRI is a narrow angle (field of view=0.29°), high resolution (4.96 μrad pixels), Ritchey-Chrétien telescope with a 20.8 cm diameter primary mirror, a focal length of 263 cm, and a three lens field-flattening assembly (Fig. 1). LORRI's total mass and power draw are 9.0 kg and 4.6 W, respectively. A 1024 × 1024 pixel (optically active region), thinned, backside-illuminated charge-coupled device (CCD) detector from E2V is used in the focal plane unit and is operated in frame transfer mode. The design and fabrication of LORRI are described in Conard et al. [2].

LORRI provides panchromatic imaging over a bandpass that extends from about 350 nm to 850 nm. LORRI operates in an extreme thermal environment, situated inside the warm spacecraft with a large, open aperture viewing cold space. LORRI has a silicon carbide optical system, designed to maintain focus over the operating temperature range without a focus adjustment mechanism. Moreover, the spacecraft is thruster-stabilized without reaction wheels, placing stringent limits on the exposure time and the optical throughput needed to satisfy measurement requirements.

LORRI has flexible exposure control. Exposure times can be set either *manually*, using values between 0 and 30 s at 1 ms increments, or via *autoexposure*, in which the integration time is determined autonomously from the observed brightness of the target. During observations in the Jovian system, excellent imaging was obtained with exposure times of only a few milliseconds. Typical exposure times during the Pluto encounter are 100-150 ms. In 2012 the LORRI flight software was modified to enable *trigger mode* operation, in which LORRI saves images during a pointing scan only when the target is within the field of view, reducing data volume requirements. LORRI images can be taken at a maximum rate of once per second. LORRI images are digitized to 12 bits and can be stored and downlinked using either lossless or lossy compression.

Performance: LORRI underwent extensive ground testing and calibration prior to launch [3]. After launch, LORRI was commissioned for operations during the summer and fall of 2006, followed by annual performance monitoring [4]. The measurement requirements and scientific objectives of LORRI, and the processing steps required to calibrate LORRI data, are described by Cheng et al. [5].

LORRI has not shown any evidence of performance degradation since launch. The point spread function varies over the field of view but is stable over time (the best fit gaussian FWHM is 1.8−2.4 pixels in the row direction and 2.5−3.1 pixels in the column direction, depending on the location; the CCD's charge transfer efficiency is better in the row direction). The flat field and photometric sensitivity are stable over time to within a few per cent. The read noise is ~24 e, as it has been since pre-launch testing. There is no evidence of radiation damage to the CCD (New Horizons is powered by a radioisotope thermoelectric generator), and only a handful of cosmic ray events are detected during typical exposures.

Some examples of LORRI's in-flight imaging performance are shown in the figures. Remarkably, LORRI produced superb images of objects in the Jovian system (Figs 2 & 3) even though those bodies are ~35 times brighter than the targets LORRI was *designed* to observe in the Pluto system. LORRI's exceptional sensitivity is demonstrated by the long exposure of the Pluto approach field, where stars as faint as V≈18 are detected (Fig. 4). LORRI's optical design is not optimized for scattered light rejection, but LORRI produced exciting scientific results during high solar phase angle observations in the Jovian system.

References: [1] Stern, S. A. (2008) Space Sci Rev, 140, 3–21, DOI: 10.1007/s11214-007-9295-y. [2] Conard, S. et al. (2005) Proc. SPIE 5906, 407–420, DOI: 10.1117/12.616632. [3] Morgan, F. et al. (2005) Proc. SPIE 5906, 421–432, DOI: 10.1117/12.616880. [4] Noble, M. W. et al. (2009) Proc. SPIE 7441, DOI: 10.1117/12.826484. [5] Cheng, A. F. et al. (2008) Space Sci Rev, 140, 189–215, DOI: 10.1007/s11214-007-9271-6.

Fig. 1: Photograph of LORRI during laboratory testing prior to integration into the New Horizons spacecraft.

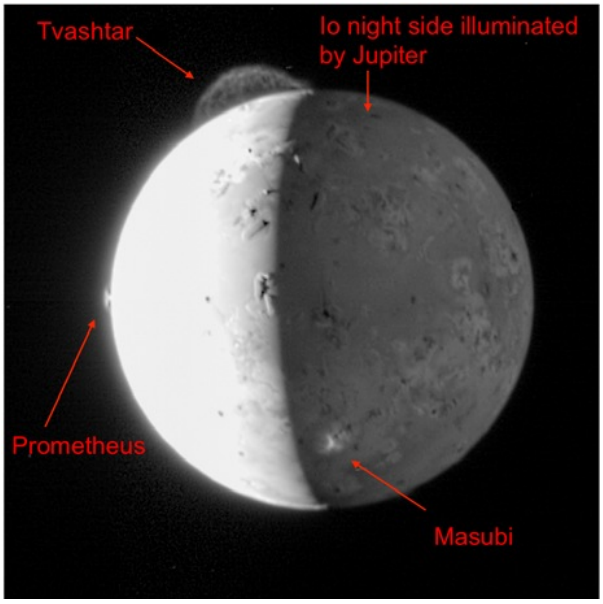

Fig. 2: During the New Horizons flyby of Jupiter, LORRI captured many spectacular images of active volcanos on Io. The above LORRI image was taken on UT 2007-Feb-28 11:04 at a range of 2.4 million km, a phase angle of 102°, and a resolution of 12 km. LORRI captured a 5-frame sequence of a Tvashtar eruption over an 8-min period, providing the most detailed view ever obtained of the dynamics of an extraterrestrial volcano.

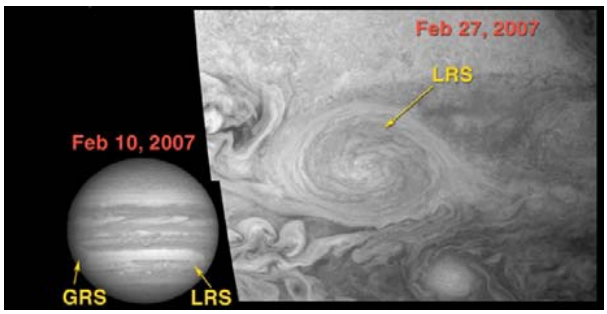

Fig. 3: LORRI made the highest resolution observations of the Little Red Spot on Jupiter, allowing a detailed mapping of the winds in this giant hurricane.

Fig. 4: Composite of five LORRI images taken on 2012 June 1 during a New Horizons annual checkout. Each LORRI image had an exposure time of 10 sec and was obtained in 4x4 format (i.e., on-chip binning over 16 pixels during CCD readout). This star field is centered near the expected location of Pluto during the entire period from January 2015 until approximately 1 month prior to closest approach. In fact, Pluto is already seen within the LORRI field of view during this observation 3 years before closest approach (Pluto is circled in red). This deep exposure reaches down to V≈18. The black tails to the right of the bright, saturated stars are caused by amplifier undershoot.

PREDICTIONS ABOUT TECTONICS ON PLUTO AND CHARON

G. C. Collins[1] and A. C. Barr[2], [1]Physics and Astronomy Dept., Wheaton College, Norton, Massachusetts 02766, gcollins@wheatoncollege.edu, [2]Dept. of Geological Sciences, Brown University, Providence, Rhode Island 02912.

Introduction:

The majority of Pluto- and Charon-sized icy satellites that we have visited with spacecraft show evidence of past, or even current tectonic activity on their surfaces. Tectonic activity is particularly intense and widespread on bodies that have experienced significant tidal flexing during their dynamical evolution. Possible driving forces for tectonic activity include: changes in the rotational and tidal equilibrium figure of the body; diurnal tidal deformation; volume changes due to freezing/thawing of an interior ocean; thermal or compositional overturn within the ice crust; and/or lateral flow due to variations in ice shell thickness.

Observations of Pluto's tectonics by *New Horizons* may give us insight into the orbital evolution of the binary system [1-3]. At first glance, Pluto and Charon would seem to be exempt from tidally driven tectonics because they do not orbit a giant planet. However, their proximity and the associated tidal forces on each other, particularly in the immediate aftermath of the Charon-forming impact, raises the question of whether tides could generate significant stresses to deform their surfaces.

Tidal Stresses During Early Dynamical Evolution:

In successful Pluto/Charon-forming simulations, Charon's initial orbital semi-major axis after the impact a_o ranges from 3.7 to 21 R_p (where R_P is Pluto's radius; Canup, personal communication). Immediately following the Charon-forming impact, we assume that Charon is launched into a highly eccentric, co-planar orbit around a rapidly spinning Pluto [*cf.* 4]. After the impact, Charon de-spins until it is in a synchronous orbit where its spin frequency $\omega_{o,}$ is equal to its orbital frequency, n_o, over a time scale τ_{sync}~$0.35Q_c$ yr [4]. For a nominal quality factor for Charon, Q_c~100 [5], this gives τ_{sync}~35 yr [4].

Through subsequent orbital evolution, Pluto's spin angular momentum is transferred to Charon's orbit, allowing Charon to recede from (or in some cases, come closer to) Pluto until they reach their current mutually tidally locked state. Pluto's initially rapid spin and Charon's proximity to Pluto result in the raising and lowering of a large tidal bulge on a frequency ω_p-n. It is this bulge that exerts a torque on Charon and drives its orbital evolution.

A crude estimate of the tidal distortion of Pluto during its early period of rapid rotation can shed light on the stresses exerted on its lithosphere during this early phase of orbital evolution. The magnitude of the strain (ε) on Pluto's lithosphere due to the tidal deformation is also related to the degree-2 Love number of Pluto ($k_{2,p}$) and the system properties [4,6],

$$\varepsilon = \frac{\delta r}{R_P} \sim \frac{5}{3} k_{2,p} \frac{m_c}{m_p} \left(\frac{R_p}{a_o} \right)^3 \sim 3\% \left(\frac{k_{2,p}}{0.001} \right)$$

for a_o~$3.7R_p$ and a nominal $k_{2,p}$~ O(10^{-3}). This implies stresses of order σ~$2\mu\varepsilon$ ~ 100 MPa, where μ=$3.6\text{x}10^9$ Pa is the shear modulus for water ice. These values of stress are significantly higher than the ~2 MPa tensile strength of polycrystalline water ice at outer solar system temperatures [7], or the ~0.1 MPa yield stress of temperate polycrystalline water ice inferred from terrestrial ice sheets [8], or the lower yield stress of the lithosphere of Europa inferred from models of the formation of its tectonic features [e.g., 9-12]. This suggests that the tidal stresses may be sufficient to fracture Pluto's surface and create tectonic features.

Model:

Here, we calculate the stresses built up in the lithospheres of both Pluto and Charon during post-impact tidal evolution. The time scale over which Charon's orbit evolves depends sensitively on the tidal quality factor, Q, of Pluto, which prior studies assume is a constant, nominal value Q~100. We use the *SatStress* software package [13] to estimate Q for layered, viscoelastic plutos to provide more realistic constraints on the orbital evolution time scale of the system. The calculated distortions to the figure of Pluto are transformed into stresses using the thin elastic shell approximation [14].

Results:

The value of Q depends strongly on the internal density structure of Pluto. We find only two options for self-consistent models:

Option A – Cold and Dead: Undifferentiated plutos with even a modest near-surface layer of highly viscous cold ice and no internal ocean experience essentially no tidal bulging, and have orbital evolution time scales longer than the age of the solar system, unless the effective viscosity within Pluto can be lowered below ~10^{15} Pa s, close to the viscosity of pure water ice at its melting point, and with a small grain size, d<1 mm [15]. Such low viscosity values would not be consistent with

a realistic interior structure of an ice/rock Pluto warmed from within by radiogenic heating.

Option B – Warm and Vigorous: A second self-consistent interior model is differentiated, with an internal liquid water ocean separating the ice shell from the rocky interior. Such an ocean may be formed through radiogenic heat flow into a conductive lid [16], and/or by tidal heating after the Charon-forming impact. Pluto ice shells that have a *uniform* viscosity less than ~ 10^{19} Pa s (corresponding to a temperature of 190 K assuming a melting point viscosity of 10^{14} Pa s and flow by Newtonian volume diffusion) that do not have a cold near-surface layer (as may be the case in Pluto immediately after the P/C-forming impact) can be strongly heated by their tidal evolution, which in this case, is rapid, lasting only tens of Ma. We find that the presence of a high-viscosity surface ice layer does not inhibit tidal flexing of the satellite because the ocean de-couples the ice shell from the interior and allows it to deform. This situation leads to the most rapid orbital evolution time scales for the Pluto-Charon system. In this case, hundreds of MPa of stress due to de-spinning can be built up in Pluto's lithosphere, which could drive global tectonics. Despinning reduces the oblateness of the spheroid along the polar axis, causing east-west-oriented extensional features (e.g., normal faults) near the poles and north-south-oriented contractional features (e.g., thrust faults) near the equator. A similar distribution of features was predicted for Mercury [14], but only contractional featurs are observed in that case, suggesting that the overall tectonic regime may have been modified by global cooling and contraction [17]. Pluto's tectonics may be similarly modified by interior volume changes [e.g., 16], but the sign depends on whether the ocean is melting or freezing at the time of despinning.

Predictions for *New Horizons* observations: The presence of lithospheric fractures on Pluto and the present-day dynamical state of the system would be consistent with a Pluto that at one time in its history harbored a liquid water ocean. An ocean seems to be required to permit large ice shell deformations through tidal mechanisms. A thick lid of cold near-surface ice (as would be expected on Pluto given its cold surface temperatures) is required to "store" stress over the dynamical evolution time scale of the system. The ratio between the viscosity of the surface ice and the lower, warmer ice shell must be greater than 10^{7} for stresses to be maintained over the orbital evolution time scale. In the absence of a near-surface cold ice layer (i.e., if the near-surface ice has a low viscosity), lithospheric stresses would relax over the time scale of orbital evolution, and no fractures would be observed. If we do observe tectonic features on Pluto, they will give us insight into changes in the interior state of Pluto immediately following the Charon-forming impact; estimates of the thermal energy deposited by the impact can elucidate the early (pre-impact) thermal state of Pluto.

References:

[1] Collins and Pappalardo, LPSC 31 #1035, 2000; [2] Collins and Barr, Fall AGU P51C-1425, 2008; [3] Collins and Barr, in prep; [4] Dobrovolskis et al., in *Pluto and Charon*, p. 159, 1997; [5] Murray and Dermott, *Solar System Dynamics*, 1999; [6] Love, *A Treatise on the Mathematical Theory of Elasticity*, 4th ed., 1944; [7] Litwin et al., *JGR*, 117, E08013, 2012; [8] Kehle, *GSA Bull.*, 75, 259–286, 1964; [9] Hoppa et al., *Science*, 285, 1899–1902, 1999; [10] Stempel et al., *Icarus*, 177, 297–304, 2005; [11] Hurford et al., *Nature*, 447, 292–294, 2007; [12] Hurford et al., *Icarus*, 186, 218–233, 2007; [13] Wahr et al., *Icarus*, 200, 188-206, 2009; [14] Melosh, *Icarus*, 31, 221-243, 1977; [15] Barr and McKinnon, *JGR*, 112, E02012, 2007; [16] Robuchon and Nimmo, *Icarus*, 216, 426-439, 2011; [17] Watters and Nimmo, in *Planetary Tectonics*, 2010,

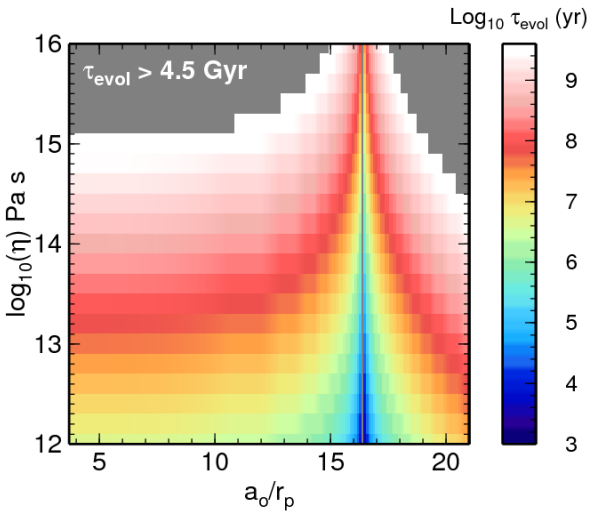

Figure 1: Orbital evolution timescale of the Pluto-Charon system from formation to present state, assuming a differentiated Pluto with an internal ocean. The horizontal axis plots Charon's initial orbital radius (a_o) in units of Pluto radii (r_p). The vertical axis plots the effective viscosity of the ice shell, below a stiff upper lid, assuming constant viscosity over the timescale of orbital evolution. Gray areas at the top of the plot show inaccessible regions in parameter space in which the Pluto-Charon system never reaches its current state within solar system history.

OBSERVATIONS OF PLUTO'S SURFACE AND ATMOSPHERE AT LOW RESOLUTION.

Jason C. Cook[1], Dale P. Cruikshank[2], Leslie A. Young[1], [1]Southwest Research Institute, 1050 Walnut St., Suite 300, Boulder CO 80302, [2]NASA Ames Research Center, MS 245-6, Moffett Field, CA, 94035, (jccook@boulder.swri.edu)

Introduction: With temperatures $\lesssim 40$ K, the surfaces of both Triton and Pluto are composed of complex combinations of various ices. On Triton, six different ices have been confirmed on its surface: N_2, CH_4, CO, and CO_2 [1, 2], H_2O [3], and HCN [4]. On Pluto, however, only solid N_2, CH_4, and CO have been clearly detected in prior studied in its near-infrared spectrum [5, 6].

Photochemical modeling of the atmospheres of Pluto and Triton and laboratory experiments of irradiated ices predict the formation of a number of molecules, including hydrocarbons and nitriles, that should contribute to the formation of atmospheric hazes and surface deposits [7, 8, 9]. Given these avenues for production, C_2H_6 is thought to be the most abundant photo product. Its presence has been established on Triton [10, 11] and suspected on Makemake [12]. However, the detection of C_2H_6 on Pluto has remained to some degree ambiguous [11, 13].

The investigation by [11] analyzed several spectra in the H and K-bands (1.4-2.5 μm). In consideration of all the available C_2H_6 bands in the H and K bands, [11] concluded that four bands of pure ethane from laboratory data match the Pluto spectrum reasonably well, suggesting that a few percent of this molecular ice is present on the surface. However, they noted discrepancies between the observations and models near 2.317 μm.

We bring new infrared spectroscopic data to bear on this problem. With these data, we establish that to describe the spectrum of Pluto at moderate resolving powers ($\lambda/\Delta\lambda \sim 1600$) such as our data and those analyzed by [11], models must address the contribution of Pluto's atmosphere. By including an atmospheric component, the discrepancies seen by [11] near 2.317 μm can be explained.

Observations: We present K-band observations of Pluto obtained using Gemini North 8-m telescope on June 27, 2004. The 2 pixel (narrowest) slit on the NIRI (Near InfraRed Imager) instrument was used. This slit gives a resolving power ($\lambda/\Delta\lambda$) of $\sim$1550 at these wavelengths. The slit was oriented along the Pluto-Charon axis to obtain simultaneous spectra. The seeing, for most of the observations, was 0.8-1.0$''$ and Pluto and Charon were not resolved.

Data Reduction: The data were reduced using in-house IDL programs. Prior to extracting the 1-D spectrum, the data were pretreated to remove several electronic patterns. These patterns become more apparent when the data are read-noise limited. We remove three patterns: (i) bias offsets, (ii) banding and (iii) striping. The bias differences are estimated by taking the median of the non-illuminated portion of each quadrant. The four median values are averaged and a constant is added to each quadrant so the median background equals the average value. Banding is a 16-pixel wide pattern seen in the spectral images that runs perpendicular to the spectrum. The pattern is measured in each quadrant and removed. Striping is an alternating pattern that is parallel to the spectrum. The intensity of the alteration is sensitive to the flux incident on a given pixel. This striping pattern is measured in each quadrant and removed.

The extraction of the 1-D spectrum generally follows the method of optimal extraction by [14]. This method is most useful in the extraction of low signal-to-noise (SNR) data and can result in a final SNR that is equivalent to a 70% increase in the exposure time.

We determine the wavelength calibration by identifying night sky lines. We estimate that the wavelength calibration is good to 0.03 and 0.10 pixels (with a wavelength dispersion of 7.09 Å/pix), depending on the spectrum and wavelength. The standard star observations, which range in airmasses similar to the observations of Pluto, are used to model the telluric and solar absorption spectrum at the airmass of the Pluto observations. These models are used to convert the Pluto spectra to albedo, correct for telluric and solar absorption and correct for instrument response by dividing Pluto by the model. A weighted average spectrum of Pluto is then obtained.

Data Analysis: Analysis of the observations is performed by fitting spectral models which combine absorption from the surface using Hapke theory, and absorption from the atmosphere using line data from the 2008 HITRAN [15] database. We analyze the spectrum over the range 2.215 to 2.415 μm. We show the spectrum over this wavelength range in Fig. 1. Apparent in the spectrum are two CH_4 bands at 2.32 and 2.38 μm and a CO band at 2.35 μm. This wavelength range also covers several C_2H_6 bands, denoted in Fig. 1 by the inclined lines. The strongest C_2H_6 bands are near 2.27 and 2.31 μm. A third possible band is at 2.405 μm, however, it has been suggested that C_2H_6 alone can not produce the absorption band at 2.405 μm. Instead, this band may be a blended with ^{13}CO [11]. In addition to C_2H_6, our models also show a slight preference for C_2H_4 and HCN. For our analysis and discussion here, we focus on the wavelength range 2.30 to 2.33 μm.

To model the surface components, we use optical constants for pure CH_4 ice, diluted and pure CO ice and a variety of other hydrocarbons and nitriles ices which

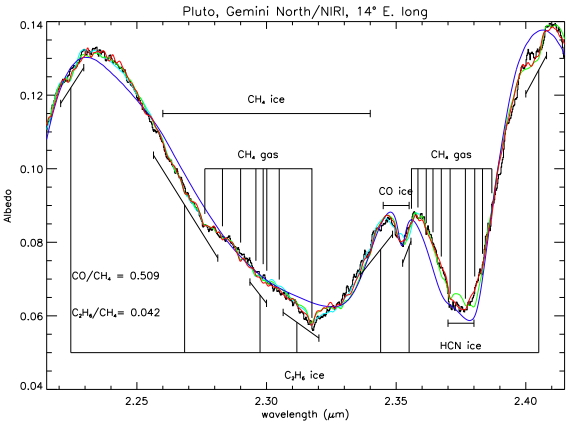

Figure 1: The spectrum of Pluto (black) from 2.230 to 2.345 μm shown with Hapke models (red, green and blue). The blue curve assumes only a mix of pure and "diluted" CH_4 are present on the surface as described in the text. The green curve includes pure and "diluted" CH_4, pure $C_2H_6$and an isothermal layer of gaseous CH_4. The red curve, which best fits the data, shows the addition of HCN ice improves the fit near 2.37 μm.

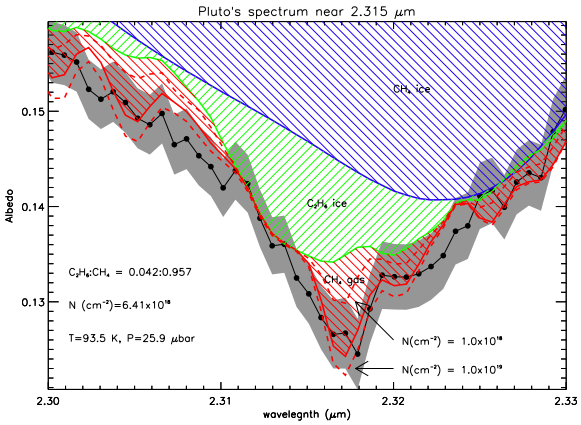

Figure 2: Pluto's spectrum near 2.315 μm showing the contributions of each identified species to the observed spectrum. The gray region represents the 1σ errors.

may be present on Pluto. It is well established that CH_4 on Pluto's surface is found in the pure state and diluted in N_2. Spectra of diluted N_2 show that many of the CH_4 bands shift to shorter wavelengths. To synthesize the optical constants for diluted CH_4, we shift the optical constants in 1 Å increments and find the χ^2 which best fits the observations. Using a combination of pure, "diluted" CH_4, and CO, we fit the blue model shown in Fig. 1 to the observations. We improve the fit further (green curve in Fig. 1) when we include C_2H_6 ice and an isothermal layer of gaseous CH_4. The addition of gaseous CH_4 is best seen in Fig. 2 with the gaseous CH_4 fitting the absorption feature near 2.317 μm. Our trials with other hydrocarbons and nitriles suggest HCN and C_2H_4 may also be present. The red curve in Fig. 1 shows the addition of HCN improves the fit near 2.37 μm.

Discussion & Conclusion: We have computed many models using a variety of ices and gaseous CH_4. We can conclude from these models that (i) C_2H_6 ice is present on the surface of Pluto at the 1-4% level, relative to CH_4 ice. Models also showed favorability to the addition of C_2H_4 and HCN even with the presence of C_2H_6 ice. Because C_2H_4 and HCN lack strong spectroscopic features, we treat our measurements of these mass fractions like upper limits. Therefore, we can conclude (ii) C_2H_4 and HCN ices may also be present at the 1-5% and 0.5-1.0% level, relative to CH_4 ice; both molecules are predicted in photochemical models of Pluto's surface [8].

Our best fit models include an atmospheric layer suggest a column abundance of $\sim 6 \times 10^{18}$ molecules cm^{-2}. We are currently treating this value as preliminary because this abundance is much lower than measured at high resolution. We are aware of an error in the modeling code that would lead it to underestimate the abundance. We anticipate correcting this error in time for the meeting. Despite this error, our analysis shows that when examining high SNR spectra even at low resolutions ($\lambda/\Delta\lambda \sim 1000$) we should include an atmospheric component. It may also be possible, if other datasets exist, to examine Pluto's atmosphere in years between its noted change from the 1988 occultation to the 2002 occultation.

References: [1] Cruikshank, D. P., et al. (1993) *Science* 261:742. [2] Quirico, E., et al. (1999) *Icarus* 139:159. [3] Cruikshank, D. P., et al. (2000) *Icarus* 147:309. [4] Burgdorf, M., et al. (2010) *ApJL* 718:L53. [5] Owen, T. C., et al. (1993) *Science* 261:745. [6] Douté, S., et al. (1999) *Icarus* 142:421. [7] Krasnopolsky, V. A., et al. (1995) *J. Geophys. Rev.* 1001:11271. [8] Krasnopolsky, V. A., et al. (1999) *J. Geophys. Rev.* 104:21979. [9] Hudson, R. L., et al. (2009) *Icarus* 203:677. [10] Cruikshank, D. P., et al. (2006) BAAS 38, #21.03. [11] DeMeo, F. E., et al. (2010) *Icarus* 208:412. [12] Brown, M. E., et al. (2007) *Astron. J.* 133:284. [13] Merlin, F., et al. (2010) *Icarus* 210:930. [14] Horne, K. (1986) *PASP* 98:609. [15] Rothman, L. S., et al. (2009) *JQSRT* 110:533.

ANALYSIS OF HIGH-RESOLUTION SPECTRA OF PLUTO: A SEARCH FOR COLD GASEOUS CH_4 LAYER AND SPATIAL VARIATION IN CH_4 COLUMN ABUNDANCE

Jason C. Cook[1], Leslie A. Young[1], Henry G. Roe[2], Elliot F. Young[1], S. Alan Stern[1], [1]Southwest Research Institute, 1050 Walnut St., Suite 300, Boulder CO 80302, [2]Lowell Observatory, 1400 West Mars Hill Road, Flagstaff, AZ 86001 (jccook@boulder.swri.edu)

Introduction: Pluto's atmosphere is responsible for the transport of mass and latent heat, maintaining a near constant global frost temperature. Since Pluto's atmosphere is in vapor pressure equilibrium with the N_2 frost on the surface, the surface pressure is equal to the equilibrium vapor pressure at that temperature. Similar conditions exist on Triton and Mars, and probably several Kuiper Belt Objects capable of retaining N_2 over the age of the solar system. Thus understanding how Pluto's atmosphere interacts with its surface is important to our understanding of this classification of atmospheres. A common characteristic among equilibrium atmospheres is the large changes in the atmospheric bulk over a season. Models by [1] and [2] show that Pluto's pressure may vary by more than a factor of 100 over its season. Occultations of Pluto in 1988 and 2002 show that the pressure has doubled over this period. Since 2002, occultations have shown the pressure has remained nearly constant [*i.e.* 3]. This behavior is consistent with models in [1, 2] that predict a decrease in pressure by 7-20% between now and the arrival of New Horizons at Pluto in 2015. Methane is a trace gas that dominates the chemistry and energy balance in Pluto's atmosphere. How the trace gases vary with changing surface pressure is unknown.

Our current understanding of the vertical structure of Pluto's atmosphere is of a warm upper atmosphere, where radiative heating by CH_4 keeps the atmosphere near 100 K for many scale heights, and a cold lower atmosphere near 40 K, dominated by conduction and turbulence. It is unclear how deep the cold layer is because stellar occultations can not probe Pluto's atmosphere at such high pressures. Models suggest this layer may be as thin as 1 km [4], and probably no thicker than 17 km [5]. The only way to determine the depth of Pluto's cold atmospheric layer from Earth is through high resolution spectroscopy [6].

On Pluto's analog, Triton, [7] report a factor of 10 difference in CH_4 atmospheric number densities between ingress and egress of UV occultations. We could expect similar longitudinal variations at Pluto. On Pluto, we might expect more gaseous CH_4 over areas with more CH_4 frost (either nearly pure or diluted in N_2), or higher levels only over regions with nearly pure CH_4 [8]. It is likely that any longitudinal variation is connected with a planetary boundary layer, and so longitudinal changes may be particularly evident in the column abundance of the cold CH_4 in the lower atmosphere.

Observations: We obtained new observations of Pluto on 2011 August 12, 14-16 using the NIRSPEC instrument on the Keck telescope. At a resolving power ($\lambda/\Delta\lambda$) of 35,000 (2 pixel slit), our observations cover orders 43 through 50 (1.51-1.79 μm). Because these orders do not obtain continuous wavelength coverage, we select wavelength regions which contain CH_4 absorption lines that are highly sensitive to (i) column abundance and (ii) atmospheric temperature. Besides the observations of Pluto, we also observed several asteroids and HR 7390 (A0V standard) to obtain a reflected solar spectrum and telluric spectrum.

Our observations target 4 sub-observer longitudes to (i) establish a baseline for temporal change, (ii) search for spatial variability in gaseous CH_4, and (iii) refine the vertical distribution of gaseous CH_4. Three of the observed longitudes correspond to regions of minimum CH_4 frost, maximum CH_4 frost, and maximum ratio of near pure to highly diluted CH_4 frost. We expect that these three terrains produce detectable differences in the gaseous CH_4. These observations will provide a temporal and spatial context in which to place the New Horizons encounter with Pluto in 2015.

Data Reduction: We reduce the data using several in-house programs written in IDL. Each 2-D spectral image is first pre-cleaned for instrument effects. To obtain the 1-D spectrum from each image, we used an algorithm that follows the prescription of [9] for the optimal extraction of spectra. Following extraction, each spectrum is wavelength calibrated using the OH sky lines [10].

Preliminary Data Analysis: In Figs. 1 and 2 we show the results of some preliminary analysis. Here we have fit a gaseous CH_4 model spectrum to the Q-branch and the $R(5)$ line. We choose these lines because they are the most sensitive lines to the presence of a cold layer of CH_4 gas. We show in the figures the case of pure cold CH_4 gas (blue, 40 K at 2×10^{19} molecules cm^{-2}) and pure hot CH_4 gas (red, 100 K at 2×10^{19} molecules cm^{-2}; orange, 100 K at 4×10^{19} molecules cm^{-2}). We then make models where the total CH_4 abundance is fixed at 2×10^{19} molecules cm^{-2} but we vary the ratio of hot-to-cold from 0 to 1 and we calculate χ^2 between the observations and the model. We find that χ^2 is minimized at 43% 100 K and 57% 40 K. This model is shown as the green curve in both figures.

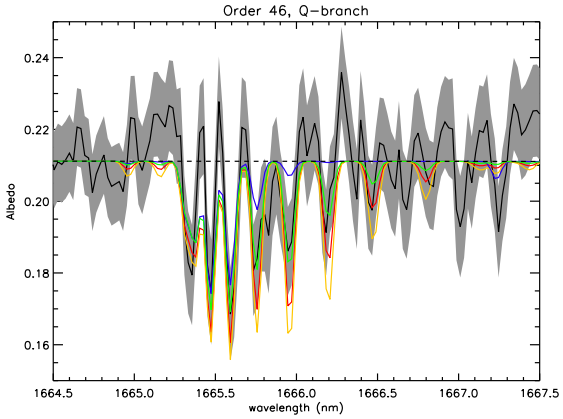

Figure 1: An example of the 1665.5 nm Q-branch of CH_4., showing the sensitivity of the model to CH_4 mixing ratio and the depth of the tropopause. Preliminary reduction of the data show that the Q-branch was easily detected, despite residual noise from the removal of the telluric spectrum. The average observed spectrum from the four nights is shown in black with 3σ error range shown in gray. We compare these observations with a model spectrum of CH_4. The blue, green and red curves all have a total column abundance of 2×10^{19} molecules cm^{-2}, while orange has double. The blue curve is set to 40 K, the red and orange curves are at 100 K. The green curve is a mixture of 43% at 100 K gas and 57% at 40 K. This mixture minimizes χ^2 between the observations and models for the Q-branch and the $R(5)$ line in Fig. 2. We estimate the continuum level by averaging the points before and after the Q-branch and fitting a line through the points. The dashed line represents the estimated continuum level.

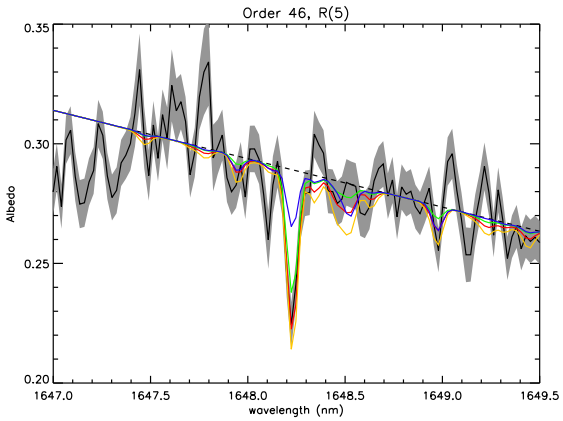

Figure 2: The $R(5)$ line of CH_4. See Fig. 1 for description of the lines.

Future Work: We plan to refine our preliminary work beginning with improving our telluric model spectra. We will use atmospheric models from ATRAN [11] to determine the abundance of water vapor ($\sim$2-3 mm) and CH_4 gas ($\sim$1.9-2.2 ppm) in the Earth's atmosphere near the time of the Pluto observations. We expect that this will eliminate the lines which are over- or under-corrected in the data. This step will also allow us to better measure the reflected solar spectrum from our solar analogs (asteroids).

After the removal of telluric and solar lines from the Pluto spectra, we will combine the data to make nightly average spectra and a run average spectrum. We will model these spectra using a combination of Hapke reflectance to account for Pluto's surface ice and an atmospheric component using CH_4 lines from HITRAN [12]. Once we have a better idea of the surface reflectance (effectively defining the continuum level for the atmospheric lines) we will be able to improve our estimates of hot to cold CH_4. We will also determine the CH_4 abundance for each night to see if there are any significant longitudinal differences. We will present our findings at the Pluto Science Conference.

References: [1] Hansen, C. J., et al. (1996) *Icarus* 120:247. [2] Young, L. A. *ApJL*. [3] Young, E. F., et al. (2008) *Astron. J.* 136:1757. [4] Zalucha, A. M., et al. (2011) *Icarus* 211:804. [5] Lellouch, E., et al. (2009) *A&A* 495:L17. [6] Roe, H. G., et al. (2008) BAAS 40, #36.04. [7] Broadfoot, A. L., et al. (1989) *Science* 246:1459. [8] Vangvichith, M., et al. (2012) Presented at Pluto Atmospheres Workshop. [9] Horne, K. (1986) *PASP* 98:609. [10] Rousselot, P., et al. (2000) *A&A* 354:1134. [11] Lord, S. D. (1992) *NASA Technical Memorandum*. [12] Rothman, L. S., et al. (2009) *JQSRT* 110:533.

HELIOSPHERIC IRRADIATION IN THE DOMAINS OF PLUTO SYSTEM AND KUIPER BELT

J. F. Cooper[1], M. E. Hill[2], N. Lal[1], and S. J. Sturner[3], [1]Heliospheric Physics Laboratory, Code 672, NASA Goddard Space Flight Center, Greenbelt, MD 20771 (E-mail: John.F.Cooper@nasa.gov), [2]Johns Hopkins University Applied Physics Laboratory, MP3-E128, 11100 Johns Hopkins Rd., Laurel, MD 20723-6005 (E-mail: matt.hill@jhuapl.edu), [3]CRESST/Astroparticle Physics Laboratory, Code 661, NASA Goddard Space Flight Center, Greenbelt, MD 20771.

Introduction: Pluto's orbit and the Kuiper Belt at 30 – 50 AU are located within an intermediate region of the heliosphere far removed from the two major sources of energetic particles inwards near the Sun and outwards at the solar wind termination shock and beyond. This region has previously been traversed at various time in 1983 – 1996 by the Pioneer 10&11 and Voyager 1&2 spacecraft with full sets of energetic particle instrumentation providing particle flux spectra. New measurements into this region are being provided also by New Horizons.

Over millions to billions of years the structural and chemical effects of irradiation can observably modify icy body surfaces. These effects are layered with respect to the penetration depths and ionizing power of different spectral components of the incident radiation. Topmost layers to millimeters or more can be heavily modified into radiation crusts while deeper layers to meters are only moderately processed. The topmost thin layer may also be removed by erosive sputtering from low-energy particles. The end states of irradiated surfaces depend on these relative effects of low and higher energy particles as characterized in intensity by spectral flux measurements. Modeling of these layered effects depends on definition of time-averaged flux spectra from the sparse measurements.

Spectral Flus Data: The Virtual Energetic Particle Observatory (http://vepo.gsfc.nasa.gov) supports public access to multi-sensor Pioneer and Voyager flux data in spectra form. New Horizons spectral flux data in the relevant region is becoming available on approach to the Pluto system and the Kuiper Belt. We consider the spectra from these multiple sources in the 1983 – 1996 and present time frame to determine the most representative time-averaged spectral forms appropriate for modeling of long-term irradiation effects.

Irradiation Effects: The spectral form of incident particles determines the relative weighting of low and high energy particle effects. Low and high energy particles separated in energy by a deep spectral minimum can produce different effects from a strongly mixed suprathermal population with no spectral minimum. These differences might for example account for color diversity or uniformity of certain populations of Kuiper Belt Objects, e.g. the red colors of dynamically cold Classicals. In any case it is necessary to consider a multi-layer view of the radiation effects.

THE PLASMA ENVIRONMENT OF PLUTO AND X-RAY EMISSION: PREDICTIONS FOR NEW HORIZONS.

T. E. Cravens[1] and C. M. Lisse[2], [1]Dept. of Physics and Astronomy, University of Kansas, Lawrence, KS 66047, cravens@ku.edu, [2]Planetary Exploration Group, Space Dept., Johns Hopkins Applied Physics Lab, 11100 Johns Hopkins Rd, Laurel, MD 20723, carey.lisse@jhuapl.edu.

Introduction: Exospheric neutral atoms and molecules (primarily N_2 and CH_4 according to our current understanding of Pluto's atmosphere) escape from Pluto and travel into interplanetary space for millions of kilometers. Eventually, the neutrals are ionized by photoionization by solar EUV photons and/or by collisions with solar wind electrons. The mass loading associated with this ion pick-up is thought to produce a comet-like interaction of the solar wind with Pluto as discussed by Bagenal and McNutt [1]. Note that heavy ion gyroradii far upstream of Pluto should be about a half million kilometers due to the weak interplanetary magnetic field at 30 AU, and this results in a very extensive region of ion pick-up [2]. Closer to Pluto the solar wind interaction should lead to a magnetic field pile-up and draping, as it does around other "non-magnetic" bodies such as Venus and comets. And a weak ionosphere should be present within a few thousand kilometers of the planet with a composition that is determined both by the primary ion production and ion-neutral chemistry. For example, primary N_2^+ ions will rapidly be converted to $C_2H_5^+$ ions via reaction with methane. Eventually, dissociative recombination of electrons and ions will balance ion production in the main ionosphere.

Plasma Structures: The structure of plasma regions and boundaries will be greatly affected by large gyroradii effects and the extensive exosphere. For example, comets are known to have weak and very broad bow shocks associated caused by mass-loading of the upstream solar wind. Will this type of shock be found at Pluto? And Venus has a sharply defined ionopause boundary separating hot magnetized solar wind plasma and cold ionospheric plasma, whereas comets do not have a Venus-like ionopause. Instruments onboard the Giotto spacecraft observed a field-free region, or diamagnetic cavity, surrounding the nucleus of comet Halley in the inner coma. This cavity was explained as being due to the outward force on magnetized plasma by ion-neutral collisions associated with the outflowing neutral gas. In this talk we will discuss the types of plasma structures that New Horizons is likely to find at Pluto.

X-Ray Emission: X-ray emission from a comet was first discovered in 1996 (Lisse et al, 1996) and was explained as being due to the charge exchange of heavy solar wind ions with cometary neutrals (Cravens, 1997). Subsequently, x-ray emission has been observed from a large number of comets and from other objects with extensive neutral exospheres (e.g., Mars). Pluto should also produce x-rays via this solar wind charge exchange mechanism. We will present some predictions for a Pluto x-ray source and assess its observability by the Chandra X-ray observatory or by XMM-Newton. Our preliminary estimate is that the x-ray luminosity of Pluto is only about 1 MW, which will make Pluto's x-ray detection difficult but not impossible.

References:

[1] Bagenal F. and McNutt R. (1989) *GRL, 16*, 1129.

[2] Kecskemety K. and Cravens T. E. (1993) *GRL, 20*, 543.

[3] Lisse C.M. et al. (1996) *Science, 274*, 205.

[4] Cravens T. (1997), *GRL, 24*, 105.

COMPOSITIONS OF THE SURFACES OF PLUTO AND ITS SATELLITES

Dale P. Cruikshank[1], [1]NASA Ames Research Center, Moffett Field, CA 94035 Dale.P.Cruikshank@nasa.gov

The information we have on the chemical compositions of the surfaces of Pluto and Charon has been obtained from Earth-based near-infrared spectroscopy. These bodies are seen in diffusely scattered sunlight upon which absorption bands diagnostic of specific ices are superimposed. Identified so far on Pluto are molecular nitrogen (N_2), methane (CH_4), carbon monoxide (CO), and ethane (C_2H_6), all in the frozen state. Charon has the clear spectral signature of H_2O ice in the crystalline phase, plus an absorption band near 2.2 μm identified as a hydrated form of NH_3. No diagnostic spectra of Pluto's other satellites are currently available. A fraction of Pluto's CH_4 is dissolved in solid N_2, which is in the hexagonal beta-phase. When a small concentration of CH_4 exists in a N_2 crystalline matrix, its absorption bands are shifted in wavelength by a small but detectable amount. Indeed the shifting of the CH_4 bands is diagnostic of a host matrix. In the case of Pluto, the N_2 band (2.148 μm) itself is detected, but for other transneptunian objects where the N_2 band cannot be seen, the shifted CH_4 bands demonstrate the presence of N_2 or (less likely) some other spectrally neutral and transparent matrix material (e.g., Ar). The absence of detectable CO_2 and H_2O ices on Pluto, while they are clearly present on the otherwise very similar Triton, is noteworthy.

The ices of Pluto distributed non-uniformly across its surface, and the distribution shows long-term (decadal) changes. Both seasonal and secular changes may be occurring through transport across the surface as a result of changing temperature, and by seasonal changes in the vapor pressure equilibrium of the ice with the tenuous and variable atmosphere.

Models of the photochemistry of the surface ices and the atmosphere of Pluto predict the presence of several materials not yet detected; the most abundant photoproducts are expected to be C_2H_2, C_4H_2, HCN, C_2H_6; HCN has been detected on Triton.

Both Pluto and Charon have surface components in addition to the detected ices. These materials of presently unknown composition serve to reduce the albedos of both bodies below that expected for pure ices, and in the case of Pluto impart a yellow-brown coloration; the color of Charon is more nearly neutral. It is generally thought that the non-ice components are more refractory than the ices and that they may be complex carbonaceous materials derived from the ultraviolet and charged particle processing of the surface ices. Minerals are also plausible candidates for the non-ice fraction. The refractory colored components may constitute bedrock upon which variable amounts of the ices are alternately deposited and evaporated as the seasons change. Water ice is expected to be a component of the bedrock, although it has not yet been reliably identified.

THE ATMOSPHERE-PLASMA INTERACTION: HYBRID SIMULATIONS

P. A. Delamere[1] and F. Bagenal[2], [1]University of Alaska Fairbanks (Geophysical Institute, 903 Koyukuk Drive, PO Box 757320, Fairbanks, AK 99775, Peter.Delamere@gi.alaska.edu) , [2]LASP & APS, University of Colorado (3665 Discovery Drive, Boulder CO 80303).

Introduction: Pluto's low gravity implies that the atmosphere is only weakly bound and significant hydrodynamic outflow can exist. Though surface spectroscopy of Pluto has revealed methane frost, the dominant escaping neutral gas is thought to be N_2. These escaping neutrals are photoionized and the heavy ions (N_2^+) move away from Pluto in the direction perpendicular to the solar wind flow (i.e. nearly unmagnetized relative to the length scales of the plasma interaction region). The turning distance of the solar wind protons at the magnetic pileup boundary is large compared to the interaction region. As a result, large ion gyroradius effects determine Pluto's highly asymmetric interaction with the solar wind. We use a three-dimensional hybrid code (fluid electrons, kinetic ions) to investigate the geometry of the interaction region for a variety of possible atmospheric escape rates in anticipation of the New Horizons encounter with Pluto. From our previous studies [*Delamere*, 2009], we found considerable structuring in the wake region due to bi-ion waves and Kelvin-Helmholtz waves. The shock structures vary from a simple Mach cone for low escape rates (~2×10^{26} s^{-1}) to a full detached bow shock for large escape rates (~2×10^{28} s^{-1}).

Pluto's asymmetric solar wind interaction: A significant challenge in interpreting particle data from the New Horizons Solar Wind Around Pluto (SWAP) [*McComas et al*., 2008] and Pluto Energetic Particle Spectrometer Science Investigation (PEPSSI) [*McNutt et al*., 2008] instruments is the inherent asymmetry of the solar wind interaction with Pluto. The asymmetry is caused by large ion gyroradius effects in a very weak magnetic field (0.2 nT). Figure 1 is taken from *Delamere* [2009] and illustrates the solar wind proton motion through the shocked flow. The pickup ion motion (N_2^+) is on a scale much larger than the region shown (gyroradius ~ 650,000 km). As a result, symmetry is broken in the plane containing the solar wind flow and the convection electric. Figure 2 shows isosurfaces of proton density (blue), proton temperature (red) and magnetic field (green) to illustrate the degree of asymmetry in the direction perpedicular to the solar wind flow and interplanetary metnic field (IMF) direction. That is, if the IMF were reversed, then the proton density (blue) and temperature (red) isosurfaces would mirror. We will present our most recent simulations using current models for atmospheric escape (e.g. *Strobel, personal communication*, 2012).

Data/model comparison: Without knowledge of the IMF direction, interpretation of the SWAP and PEPSSI data will be dependent on a careful comparison of particle data with output from our simulations for different atmospheric escape profiles and IMF conditions. The hybrid simulations provide the full ion velocity distribution functions (Figure 3) and synthetic energy spectrograms (Figure 4) can be generated and compared directly with the spacecraft data. We will show model/data comparisions of simulations of pickup ions in the solar wind. These results are a part of an ongoing study of the SWAP solar wind data and will serve as an excellent callibration of our model/data comparison tools (see *Elliot et al*., presentation).

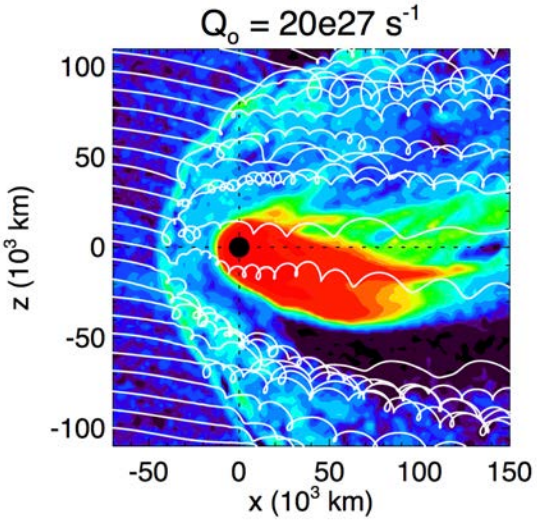

Figure 1: Hybrid simulation of the solar wind interaction with Pluto's escaping atmosphere. The color scale indicates ion density, and sample solar wind proton trajectories are indicated.

References:

[1] Delamere, P. A., (2009) Hybrid code simulations of the plasma interaction at Pluto, J. Geophys. Res., 114, A03220,doi:10.1029/2008JA013756.

[2] McComas et al. (2008), The Solar Wind Around Pluto (SWAP) Instrument Aboard New Horizons Space. Sci. Rev., 140, 261.

[3] McNutt et al. (2008), The Pluto Energetic Particle Spectrometer Science Investigation (PEPSSI) on the New Horizons Mission, Space. Sci. Rev., 140, 315.

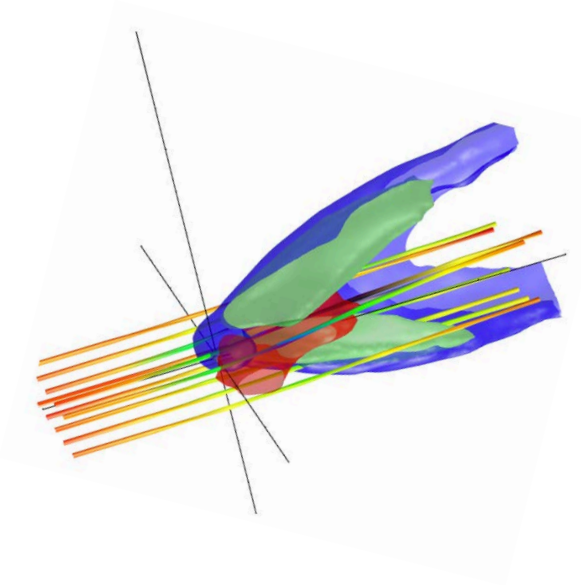

Figure 2: Sample output *from hybrid simulations showing the asymmetry of the plasma environment near Pluto. The isosurfaces show proton density (blue), proton temperature (red), the magnetic field component in the solar wind flow direction (green), and sample flow lines that are color coded according to flow speed.*

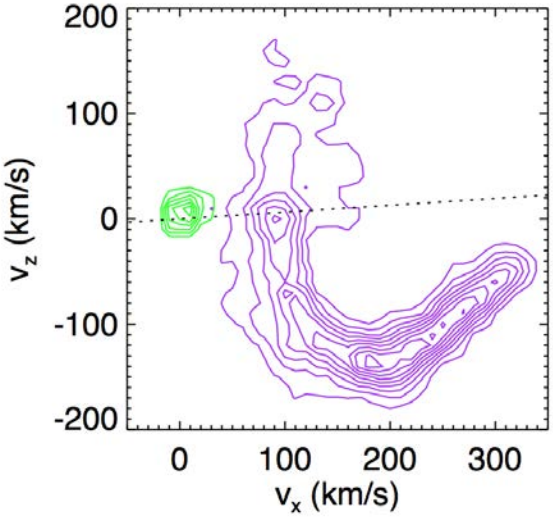

Figure 3: The ion velocity distributions from *a hybrid simulation in the shock region. The partial ring beam (purple) corresponds to solar wind protons that are partially thermalized behind the shock. The cold pickup ions (green) are essentially at rest near Pluto since pickup gyromotion occurs on a spatial scale that is much larger then characteristic scales of the interaction region seen in Figure 1.*

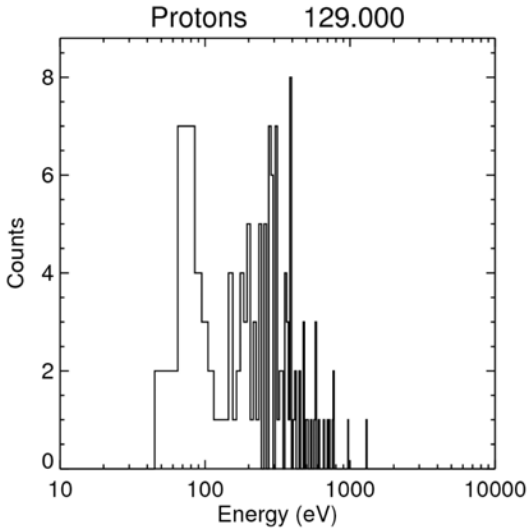

Figure 4: Sample energy spectrogram generated from the ion velocity distribution in the hybrid simulation.

Near-Infrared Spectroscopic Measurements of Charon with the VLT

F. E. DeMeo[1], C. Dumas[2], and R. P. Binzel[1] Department of Earth, Atmospheric, and Planetary Sciences, Massachusetts Institute of Technology, Cambridge, MA 02139 fdemeo@mit.edu, [2]European Southern Observatory, Vitacura, Santiago, Chile.

Introduction: Water ice is abundant in the Kuiper Belt [1],[2]. A few bodies with sufficiently high quality data have spectral signatures showing the 1.65-micron feature characteristic of crystalline H_2O ice, such as seen on Charon [3], [4], Haumea [5], and Orcus [6]. Charon and Orcus also have a feature at 2.21 microns attributed to ammonia hydrates e.g. [7]. Here we present unpublished data for Charon.

Observations: Near-infrared spectral measurements from 1.4-2.5 microns were taken for Charon using the SINFONI instrument (Spectrograph for INtegral Field Observations in the Near Infrared), installed at the 8.2-m ESO Very Large Telescope, Unit 4 at Paranal Observatory. Data were taken on May 13, June 9, and August 9, 2005 (see Table 1). Total exposure times for each night were 25 minutes. Observational circumstances are given in Table 1. Pluto data that were taken on the same dates have been published in [8].

Results: The spectra of Charon on each of the three observation dates are plotted in Fig. 1. Charon shows H_2O ice features at 1.5 and 2.0 microns and a clear crystalline H_2O ice feature at 1.65 microns. The May and August spectra have a slightly lower continuum beyond 2 microns than for June. We find variation in the shape and depth of the feature located at 2.21 microns (Fig 2). [9] attribute this feature to ammonia hydrates which are not expected to be stable on the surface over the age of the body, and argue that cryovolcanism is the most plausible mechanism of refreshing this material on Charon's surface. We will present this spectral data of Charon and in context with previous work [3-4],[9-11].

References: [1] Barkume, K. M. et al. (2008) *AJ*, 135, 55-67. [2] Guilbert, A. et al., (2009) *Icarus*, 201, 272-283. [3] Buie, M. W. & Grundy, W. M. (2000) *Icarus*, 148, 324-339. [4] Brown, M. E., & Calvin, W. M. (2000) *Science*, 5450, 107-109. [5] Trujillo, C. A., et al. (2007) *ApJ* 655, 1172-1178. [6] de Bergh, C. et al. (2005) *A&A*, 437, 1115-1120. [7] Barucci, M. A. et al. (2008) *A&A*, 479, L13-L16. [8] DeMeo, F. E., Dumas, C. et al., (2010) *Icarus, 208,* 412-424. [9] Cook, J. C. et al. (2007) *ApJ, 663,* 1406-1419. [10] Dumas, C. et al., (2001) *AJ*, 121, 1163-1170. [11] Merlin, F. et al., (2010) *Icarus*, 210, 930-943.

Table 1: Observational Circumstances

Date	Sub-Earth Longitude*	Sub-Earth Lattitude*	Pluto-Charon Separation
2005 May 13	201	-36	0.59
2005 Jun 09	273	-35	0.9
2005 Aug 09	158	-34	0.58

*Sub-Earth Longitudes and Latitudes are from JPL Horizons

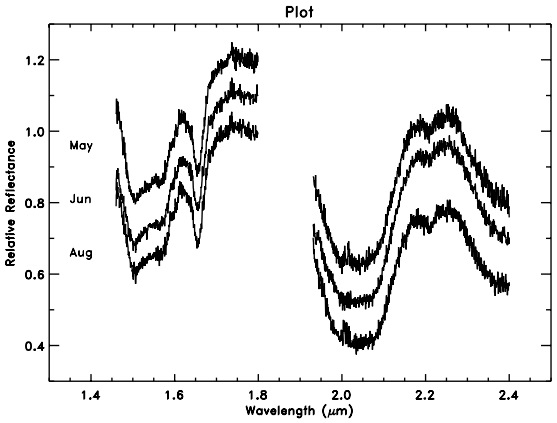

Figure 1: Near-infrared spectra of Charon on three different dates at three positions on the surface.

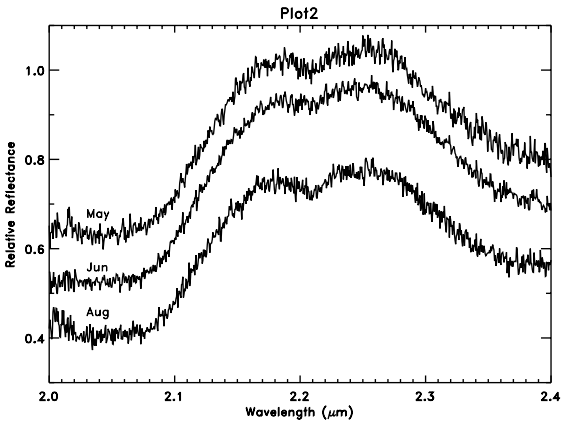

Figure 2: Detail of Charon's spectrum near 2.2 microns.

DISTINGUISHING PLUTO-CHARON FORMATION SCENARIOS USING THE PARTIAL DIFFERENTIATION OF THEIR IMPACTORS. **S. J. Desch**[1]. [1]School of Earth and Space Exploration, Arizona State University, Tempe, AZ 85287. (steve.desch@asu.edu).

The unique Pluto-Charon system has been modeled as arising from the impact of two large Kuiper Belt Objects (KBOs) [1]. Two scenarios are considered. In the first, an impactor with relatively low mass (30% of the Pluto-Charon total mass) collides with the larger body; after losing substantial mass, the impactor separates from the larger body and enters into orbit around it. In the second, the impactor and the target have essentially identical mass (50% of the Pluto-Charon total mass). The collision sends material into orbit around the pair as their cores merge to form Pluto. Charon forms from some of the material in the disk, the rest of which is reaccreted by Pluto, except for some escape. The intact impactor scenario was considered by [1] to be somewhat more probable with regard to the resultant angular momentum, but both scenarios were considered viable. Here I discuss how predictions of the internal structure before the impact can be used to distinguish between these scenarios and constrain the origin of Pluto and Charon.

According to [1], the collision of the two objects had to happen with low relative velocity ($\leq 0.9\,\mathrm{km\,s^{-1}}$). For this to occur with high probability, [1] considered it likely that the collision took place after the two bodies were caught in the 3:2 resonance with Neptune. This requires the collision to take place after Neptune started its outward migration, which [2] have associated with the Late Heavy Bombardment 3.9 Gyr ago. Accordingly, we consider it likely the collision took place ≈ 1 Gyr after solar system formation. This is sufficiently long that heating by long-lived radionuclides should have caused the separation of a rocky core from an ice mantle, even for an impactor as small as 30% of the Pluto-Charon mass [3]. An object with this mass and a mean density $2\,\mathrm{g\,cm^{-3}}$ would have radius 800 km, a mass almost triple that of Charon, and would have been large enough to differentiate.

The fact that the impactor would have differentiated casts doubt immediately on the formation of Charon by the intact impactor scenario. In this scenario the impactor must lose $\approx 70\%$ of its mass before emerging as the intact Charon. Because its outer icy layers would have been preferentially lost, Charon would have a density *greater* than that of the impactor. This is difficult to reconcile with the low density of Charon, $\approx 1.65\,\mathrm{g\,cm^{-3}}$, lower than that of Pluto, $\approx 2.03\,\mathrm{g\,cm^{-3}}$, which is itself comparable to other KBOs. We consider the formation of Charon from a disk to be more likely.

In the disk scenario, Charon forms from some fraction of the disk material that is ejected from the outer layers of the two impactors. Allowing both objects to have masses of 53% of the Pluto-Charon total mass, and mean densities $2\,\mathrm{g\,cm^{-3}}$, they would each have radii 975 km. This is again more than large enough for both bodies to differentiate and form rocky cores [3]. Now the question is why Charon has as *high* a density as it does, since it should form preferentially from the outer icy layers of the bodies. This conundrum, pointed out by [1], is resolved by the recognition that for the surface temperatures characteristic of the Kuiper Belt, the viscosity of the ice is too high to allow for complete differentiation; an undifferentiated crust is predicted to remain [3,4]. This is despite the gravitationally unstable nature of the resultant structure, with a rock/ice layer atop an ice mantle; the structure is stable against Rayleigh-Taylor instabilities on geologic timescales [4]. Because of this undifferentiated crust, the resultant disk will contain some rocky material as well as ice.

To estimate the fraction of rock in the disk, we have run the thermal evolution code of [3] for a KBO with radius 975 km and mean density $2\,\mathrm{g\,cm^{-3}}$. We have allowed for differentiation to occur wherever the temperature exceeded $T_{\mathrm{diff}} = 145\,\mathrm{K}$. This is a conservative estimate of the temperature required to allow for Rayleigh-Taylor instabilities [4]. Including only heating from long-lived radionuclides, we find that differentiation should proceed out to a radius of 935 km, leaving a crust 40 km thick that does not differentiate. The structure of the body includes: a rocky core of radius 717 km and mass $5.088 \times 10^{24}\,\mathrm{g}$ at the center (assuming olivine rock with density $3.3\,\mathrm{g\,cm^{-3}}$); an ice mantle extending from 717 km to 935 km, with mass $1.759 \times 10^{24}\,\mathrm{g}$ (with density $0.935\,\mathrm{g\,cm^{-3}}$); and an undifferentiated ice/rock layer with mass $0.917 \times 10^{24}\,\mathrm{g}$, of which $0.681 \times 10^{24}\,\mathrm{g}$ is rock and $0.245 \times 10^{24}\,\mathrm{g}$ is ice. This is the structure of the two bodies when they collide.

Following the collision, we assume that Pluto forms from the merger of the two rocky cores, plus whatever ice is needed to accrete to yield Pluto's

mass and density. Exactly one half of Pluto's mass is found within a radius of 903 km within each impactor. Forming Pluto from this material in each impactor ensures it has the required mass and a rock fraction ≈ 0.78, yielding a mean density only slightly higher than the mean densities of the impactors. As for Charon, it must form from whatever material does not escape and does not form Pluto. Because the undifferentiated crusts on both impactors add up to more than the mass of Charon, the rock fraction in Charon could be as high as that in the impactors themselves, ≈ 0.74. We note that the exterior material is most likely to escape, so that Charon probably formed from some mixture of undifferentiated crust plus ice. There is insufficient ice in the layers between 903 km and 935 km for Charon to be composed entirely of these shells from the two impactors. The total mass of ice from both bodies is only 0.636×10^{24} g, meaning that some of the rock-ice crust must be mixed in as well. We therefore calculate a *minimum* rock fraction of 0.55. Thus, depending on the composition of escaping material, it seems likely that Charon must have a rock fraction between 0.55 and 0.74, which nicely brackets the observationally inferred rock fraction on Charon, 0.61.

Both the impactor and target objects that formed Pluto and Charon must have been large enough to differentiate before the impact. Because the mean density of Charon would be greater than the starting bodies in the intact moon scenario, yet Charon is less dense than Pluto and most KBOs, we consider this scenario unlikely. The alternative scenario, formation of Charon from a disk, was considered less likely because Charon was predicted to form mostly from ice [1]. This conclusion is based on the impactor and target being fully differentiated. Thermal evolution models [3,4] indicate that such bodies will retain undifferentiated crusts of thickness ≈ 40 km. In the disk scenario, Charon would form from a mix of ice and this undifferentiated crust material, explaining why its density is somewhat lower than Pluto's but not close to that of ice alone.

References: [1] Canup, R. 2005, *Science* **307**, 546. [2] Gomes, R., Levison, H. F., Tsiganis, K. & Morbidelli, A. 2005, *Nature* **435**, 466. [3] Desch, S. J., Cook, J. C., Doggett, T. C. & Porter, S. B. 2009, *Icarus* **202**, 694. [4] Rubin, M. E., Desch, S. J. & Neveu, M. 2013, *LPSC 44*, 2559.

PLUTO'S ATMOSPHERE FROM 18 JULY 2012 STELLAR OCCULTATION

Alex Dias de Oliveira[1,2], B. Sicardy[1], J. I. B. Camargo[2], R. Vieira-Martins[2], M. Assafin[3], F. Braga-Ribas[1,2], A. H. Andrei[2], D. N. da Silva Neto[4], A. Doressoundiram[1], E. Lellouch[1], F. Roques[1], T. Widemann[1], F. Colas[5], C. Dumas[6], V. D. Ivanov[6], J. H. Girard[6] and J.L. Ortiz, R. Andres[8], L. Espinoza[8], L. Vanzi[8], E. Meza[9]

[1]Observatoire de Paris-Meudon/LESIA – 5 place Jules Janssen, 92195 Meudon cedex, France, « aoliveira@obspm.fr »,

[2]Observatório Nacional/MCTI – Rua Gal. José Cristino 77, 20921-400 Rio de Janeiro RJ Brazil,

[3]Observatório do Valongo/UFRJ – Ladeira do Pedro Antônio 43, 20080-090 Rio de Janeiro RJ Brazil,

[4]Centro Universitário Estadual da Zona Oeste – Av. Manuel Caldeira de Alvarenga 1203, 23070-200, Rio de Janeiro RJ Brazil,

[5]Observatoire de Paris-Meudon/IMCCE – 77 Av. Denfert-Rochereau, 75014 Paris, France,

[6]European Southern Observatory, Alonso de Córdova 3107, Vitacura, Casilla 19001, Santiago 19, Chile,

[7]Instituto de Astrofísica de Andalucía, CSIC, Apartado 3004, 18080 Granada, Spain

[8]Pontificia Universidad Católica de Chile (PUC), Vicuña Mackenna 4860, 7820436 Macul, Santiago, Chile

[9]Facultad de Ciencias, Universidad Nacional de Ingeniería, UNI. Lima 25 - Peru

Introduction: With the soon arrival of NASA's probe New Horizons the demand for physical and dynamic information about the Pluto system became even greater. As far as ground-based observations are concerned, stellar occultations constitute the only technique capable of providing the temperature and density profiles of Pluto's tenuous nitrogen atmosphere.

Observation and partial results: On July 18, 2012, a multi-chord occultation by Pluto was observed from three stations in Chile: European Southern Observatory ESO/Paranal*, San Pedro de Atacama and Santa Martina (near Santiago). It was also recorded at Cerro Burek (Argentina) and Huancayo (Peru). Due to the brightness of the star in the IR (H magnitude=11.1), the event was recorded with high signal-to-noise ratio at the ESO 8.2-m Very Large Telescope equipped with the NACO instrument [1][2], at a rate of 5 frames per second, without adaptative optics. This event provides one of the best data set ever obtained during a Pluto stellar occultation. It allows to build an accurate profile of Pluto's atmosphere and reveal local fluctuations possibly caused by gravity waves (Fig. 1). These features are comparable, both in size and location, to those observed during a previous occultation recorded in June 2006 [3].

Using images taken 20 minutes before the occultations, we can measure the separate fluxes of the star and the Pluto-Charon system. This provides measurement of the residual stellar flux Φ_{resid} during the occultation. A preliminary analysis shows that Φ_{resid} lies in the range 0.008-0.018, relative to the full unocculted stellar flux (Fig 1). This flux is related to the temperature gradient in the lower part of the atmosphere that connects Pluto's surface (at 35-40 K) to the isothermal upper part (at about 105 K). Our value of Φ_{resid} indicates a temperature gradient in the range 8-15 K km^{-1} for that atmospheric region.

Improved values of Φ_{resid} will be given and constraints to Pluto's radius will be presented, as well as temperature profiles derived from inversions of the ingress and egress light curves.

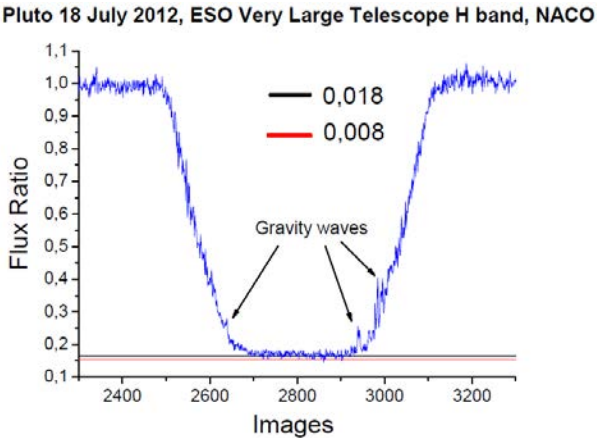

Figure: 1 – The occultation light curve obtained with VLT (5 frames per second) during the 18 July 2012 stellar occultation.

References:

[1] Lezen,R. *et al*., "NAOS-CONICA first on sky results in a variety of observing modes", SPIE 4841, 944 (2003).

*Program ID : 089.C-0314

[2] Rousset, G. *et al*., "NAOS, the first AO system of the VLT: on-sky performance", SPIE 4839, 140 (2003).

[3] Young *et al*., "Vertical structure in Pluto's atmosphere from the 2006 June 12 stellar occultation", Astron. J. 136, 1757 (2008).

Probing outer solar system small bodies with stellar occultations.

A. Doressoundiram[1], F. Roques[2], C-Y. liu, L. Maquet and the MIOSOTYS team
[1]Observatoire de Paris, 92195 Meudo cedex, France alain.doressoundiram@obspm.fr
[2]Institute of Astronomy, National Tsing Hua University, Hsinchu, Taiwan

---

MIOSOTYS (Multi-object Instrument for Occultations in the SOlar system and TransitorY Systems) is a multi-fiber positioner coupled with a fast photometry camera. This is a visitor instrument mounted on the 193 cm telescope at the Observatoire de Haute-Provence, France. Our immediate goal is to characterize the spatial distribution and extension of the Kuiper Belt, and the physical size distribution of TNOs.

We present the observation campaigns during 2010-2012, objectives and observing strategy. We report the detection of potential candidates for occultation events of TNOs. We will discuss more specifically the method used to process the data and the modelling of diffraction patterns.

Analysis Techniques and Tools for the New Horizons Solar Wind Around Pluto Measurements

H. A. Elliott[1], D. J. McComas[1], J. Mukherjee[1], P. Valek[1], P. A. Delamere[2], F. Bagenal[3], and G. Nicolaou[4], [1] Southwest Research Institute, San Antonio, TX (helliott@swri.edu), [2]University of Alaska, Fairbanks, AK, [3]University of Colorado, Boulder, CO, [4]University of Texas, San Antonio, TX.

Introduction: The Solar Wind Around Pluto (SWAP) instrument on the New Horizons (NH) spacecraft has collected and received solar wind measurements from 5 to 23 AU, and another 230 days of hibernation data are scheduled to be downlinked this April. In this presentation we show many examples of SWAP solar wind observations from the cruise phase of the mission in order to illustrate the types of data planned in the Pluto sequence. Although the SWAP instrument is simple in design, this simplicity adds complexity to the analysis of the measurements. We describe key aspects of the instrument calibration necessary to obtain accurate solar wind parameters. Most of the solar wind observations are collected while spinning (12 sec period). The SWAP instrument performs a 64 step coarse scan over the full energy range followed by another 64 step fine scan centered on the step with the peak rate during the coarse scan. The pair of scans takes 64 seconds, and each step has a 390 msec accumulation time. At every step ions from the full field-of-view (10 by 276°) are focused onto a pair of coincidence Channel Electron Multipliers (CEMs). The instrument sensitivity varies across the FOV, and the energy and range of energies observed depends on the entrance angle of the ions. We developed a simple analytic expression for the count rates, which neglects such angle dependences, but runs quickly. Recently, we developed a more comprehensive method that models the spin variation due to the angle dependences in the instrument response. In the process of developing this new method, we have assembled an instrument model applicable to any analytic or simulated particle distribution. For the new method, we show 3 examples at 11.22, 18.31 and 23.21 AU. Additionally, we examine recent measurements at 23.8 AU where a clear rarefaction with a decreasing speed profile is followed by an increase in the speed forming a wave or shock. We will examine the solar wind and pickup ions to determine if the solar wind temperature speed relationship for this compression is different than what is observed in the inner heliosphere. To indicate the utility of the instrument model, we also apply the instrument model to a hybrid simulation, which includes both solar wind and interstellar pickup ions.

NEAR-INFRARED (3.6 AND 4.5 μm) SPECTROPHOTOMETRY OF LARGE KBOs

J.P. Emery[1], N. Pinilla-Alonso[1], D.P. Cruikshank[2], D.E. Trilling[3], C.M. Dalle Ore[4], J.A. Stansberry[5], Y.R. Fernández[6]; [1]University of Tennessee (jemery2@utk.edu), [2]NASA Ames Research Center, [3]Northern Arizona University, [4]SETI Institute, [5]University of Arizona, [6]University of Central Florida.

Introduction: The largest KBOs (some of which are now characterized as dwarf planets) comprise a distinct class of Solar System body. By virture of their size and low surface temperatures, these bodies have the potential to retain otherwise volatile materials and, particularly in the case of the dwarf planets, even support atmospheres [1]. Furthermore, accretional heating combined with heating from radioactive decay likely led to interior melting, which in turn could have intitiated episodes of cryo-volcanism [2]. Surface compositions of these bodies therfore provides an important marker of past geology and present atmospheric (or exospheric) properties.

Because the largest KBOs also tend to be the brightest, most have been observed extensively in the visible and near-infrared (VNIR; 0.4 – 2.5 μm). These observations have revealed major surface compositions, the state (pure or diluted) and distribution of CH_4, the phase (amorphous or crystalline) of H_2O, the presence of minor surface consitutents, and the presence of low-albedo, in some cases spectrally very red, material that is likely comprosed of complex organic molecules. Relevant ices and organics exhibit strong fundamental vibrational bands in the 2.5 to 5 μm region. Extending reflectance spectrophotometry to this wavelength range therefore provides additional leverage for uraveling the composition and state of the surfaces of large KBOs.

Observations: We have measured broad-band reflectances of KBOs at 3.6 and 4.5 μm (and in a few cases 5.8 and 8.0 μm) with the InfraRed Array Camera (IRAC) on the Spitzer space telescope. IRAC contains four detectors and two fields of view (FOV). A beamsplitter in each FOV separates light by wavelength, such that the 3.6 and 5.8 μm channels are paired for simultaneous observations, as are the 4.5 and 8.0 μm channels. In all observations presented here, the 3.6/5.8 μm FOV was observed, after which the object was observed throught he 4.5/8.0 μm FOV. Each object was observed twice. The second observation for each object was timed so that the object moved ~1 to 2 arcmin across the 5.1 arcmin FOV and, if the rotation period was known at the time of observation, was phased to observe the opposite hemisphere from the first observation. The second observation enables accurate subtraction of background objects and diffuse flux, identification of the object by its motion, and a search for surface heterogeneity. Data are calibrated by the Spitzer Science Center, and we performed aperature photometry to determine fluxes.

Results: The Spitzer IRAC data for each object provide new insight into surface compositions and structures. For instance, the data of Sedna are consistent with inferences of organics from the red VNIR spectral slope and of CH_4 from a weak absorption near 2.3 μm [3,4]. Furthermore, the full VNIR+IRAC spectral reflectance is fit by models that include H_2O, a molecule not previously detected on Sedna [5]. Similarly, analysis of VNIR+IRAC reflectances of Quaoar indicates that the surface may contain a substantial fraction of amorphous H_2O or very small grains [6]. VNIR+IRAC data of the dwarf planet Haumea are consistent with a surface that is almost pure H_2O.

We will present IRAC reflectances of the following Kuiper Belt objects: Eris, Makemake, Haumea, Sedna, 2007 OR_{10}, Quaoar, and Orcus. For each object, we will also present analyses of the spectral reflectance across the VNIR+IRAC spectral range.

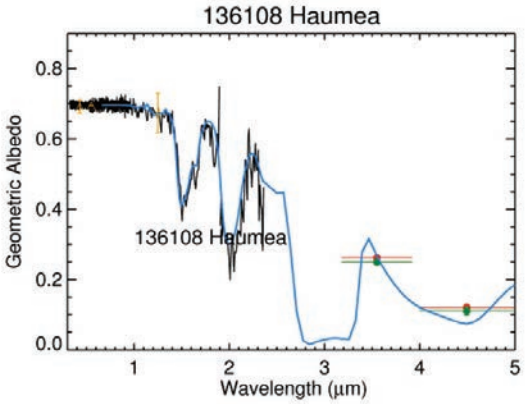

Figure 1. VNIR spectrum and IRAC geometric albedos for the dwarf planet Haumea. The green and red symbols represent the two observations of Haumea, and the horizontal lines illustrate the IRAC bandwidths.

References: [1] Stern, S.A. & L.M. Trafton (2008) In *Solar System Beyond Neptune*, 365-380. [2] McKinnon, W.B. et al. (2008) In *Solar System Beyond Neptune*, 213-241. [3] Barucci et al. (2005), *A&A, 439*, L1-L4. [4] Barucci et al. (2010), *AJ, 140*, 2095-2100. [5] Emery et al. (2007), *A&A, 466*, 395-398. [6] Dalle Ore et al. (2009), *A&A, 501*, 349-357.

CRATERING IN THE PLUTO-CHARON SYSTEM:
INSIGHTS FROM LOW-VELOCITY EXPERIMENTS.

C. M. Ernst and O. S. Barnouin, Johns Hopkins University Applied Physics Laboratory (carolyn.ernst@jhuapl.edu)

Introduction: The images taken by NASA's New Horizons spacecraft will be the first high-resolution images ever taken of in-situ Kuiper Belt Objects, allowing for the first geomorphological analyses of these bodies. Mean impact velocity at Pluto is ~1.9 km/s [1], slower than at any other environment thus far observed by spacecraft. At such low speeds, early coupling between the projectile and the target plays a critical role in the cratering process, whereas at higher velocities this coupling become less important [2, 3]. This early coupling has effects on crater formation, the fate of the projectile, and crater shape.

The impact velocities experienced at Pluto are easily attained at laboratory facilities. Therefore, not only can experimental studies be used to assess the nature of craters on the surfaces of Pluto, Charon, and the smaller satellites, but also New Horizons observations can be used to evaluate extrapolations from experimental to planetary scales. Here, we discuss insights from low-velocity experimental studies and explore the possible consequences for crater and surface morphologies in the Pluto-Charon system.

Crater Growth: At low velocities, the projectile interacts with the target primarily through friction and stress waves. If the impact speed is lower than the sound speed of the material, shock processes are not involved. If the impact speed is close to the sound speed in the materials, shocks do form but are commensurate in effect with friction and stress waves. Only when velocities are well above the sound speed and into the hypervelocity regime do shock processes control crater growth.

At the lower velocities, frictional deceleration of projectiles makes for long interaction times between the projectiles and the targets, as projectiles take longer to fail. As a consequence, the energy and momentum of the projectiles couple over significant distances with the targets, projectiles penetrate further into the targets, and the transient crater depths become larger relative to their diameters (see Figures 1,2).

These results indicate that impacts in the Pluto-Charon system should form deep transient craters relative to their diameters when compared to hypervelocity impacts. Dependent on the strength of target material, however, the steeper walls of the crater may lead to greater collapse during the modification stage, which could result in shallower final craters. Slight warming by the impact of the volatile rich surface is likely to enhance this collapse.

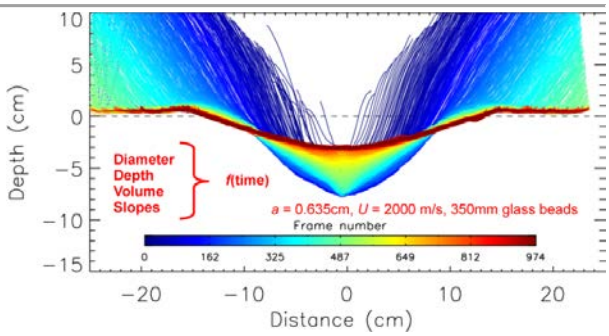

Figure 1. Crater growth through time (frame number) for a 6.35-mm projectile launched into 350 μs glass beads at 1.32km/s at NASA Ames.

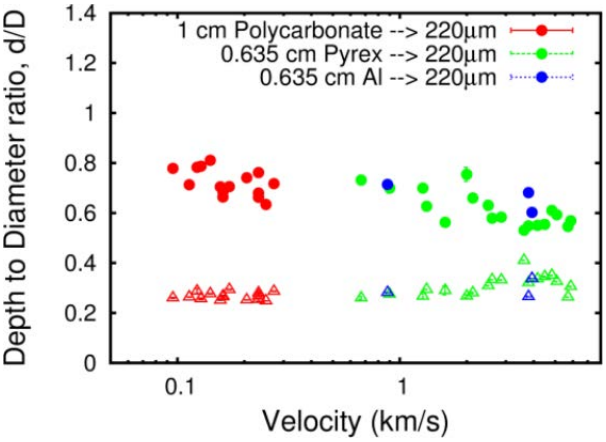

Figure 2. Preliminary results showing changes in the transient and final diameter-to-depth ratio of craters versus impact velocity.

Fate of the Projectile: For low velocities, melt and vaporization of the projectile and target will be minimal. Whereas during high-speed impacts the impactor is typically completely destroyed, at low speeds, significant projectile material is likely to survive relatively in tact. In experiments performed at the NASA Ames Vertical Gun Range designed to investigate light the flash generated at the moment of impact [4-6], a transition in behavior between low- (1-2 km/s) and high-speed (4-5 km/s) impacts is observed (Figures 3,4) for impacts of Pyrex projectiles into pumice powder targets. The changes exhibited in the early-time behavior of the impact flash are indicative of changes in the interaction and coupling between the projectile and target. As impact velocity decreases, the projectile is less damaged, the projectile and target interact for a longer length of time [2], and friction becomes more important [3, 7].

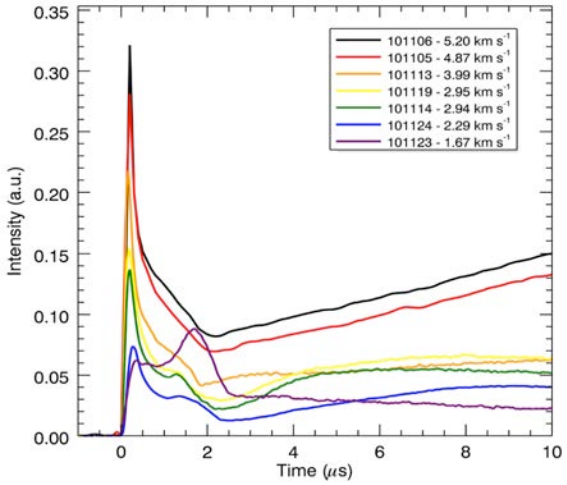

Figure 3. Impact flash intensity through the first 10 μs of time for impacts of 6.35-mm-diameter Pyrex projectiles into pumice powder targets at 90º. By 1.68 km/s, the flash no longer exhibits the delayed intensity peak in the visible wavelength range that is so characteristic of the faster impacts [6].

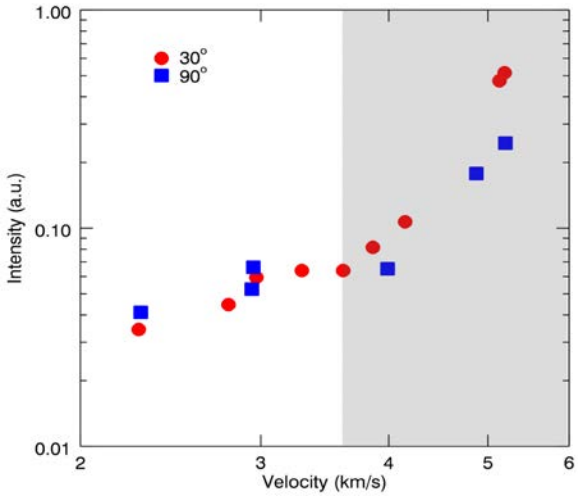

Figure 4. Peak intensity of the delayed thermal signal versus velocity for 90º and 30º impacts. The relationship changes between 3-4 km/s.

In the case of the lowest velocities tested (~1.7 km/s), which are comparable to the mean impact velocity at Pluto) the Pyrex projectiles did not fail completely at any impact angle, resulting in a different flash evolution. At these lower velocities, projectiles ablate and are not dispersed into the target (i.e., little or no fragmentation). In fact, nearly intact projectiles were pulled from just beneath the crater floor (in the 90º, or vertical, case) or were found on the surface in or around the crater (for more oblique angles). At such low impact velocities, even icy projectiles will not be completely vaporized on impact.

These results indicate that for impacts in the Pluto-Charon system, large pieces of projectile material may be found inside or near craters.

Possibilities for the Pluto-Charon System: Due to the low impact velocities, craters may look different than expected based on our experience looking at other planetary surfaces. Factors not discussed here (e.g., relaxation of craters in icy targets, modification of Pluto's craters by atmospheric fallout) will further affect the appearance of the craters. Based on the experimental results described above, however, here are some things to look for once New Horizons images are returned. Craters are likely to have formed with deeper transient craters relative to their diameters. Whether the final craters end up shallower or deeper than 'normal' will depend on the strength of the target material and the extent of crater cavity collapse.

Exogenic material from non-destroyed impactors may be seen on the surface for cases where the projectile pieces were not buried by the subsequent crater modification; perhaps large pieces of projectiles will be seen. Whether these materials will be identifiable as exogenic is unknown. Because large portions of projectiles may remain in tact, multiple impacts may be formed by the primary impactor for sufficiently oblique impacts.

Ejecta extent and distribution are also likely to differ from those of typical craters observed in the inner solar system. Little or no melting will occur during these impacts, so ponds of melt are not likely to be found.

Due to the high eccentricity of the Pluto-Charon system's orbit, mean impact speeds will vary from as low as ~0.5 km/s to as high as ~2.5 km/s [8], likely spanning impact velocities under, at, and over the sound speed in the target material; therefore, it's possible we may observe craters of differing characteristics on the same surfaces. For the small satellites Hydra, Nix, P4, and P5, it is highly likely that craters will be produced on slopes, which further complicate their appearances.

Regardless of expectations and predictions, craters on Pluto, Charon, and the smaller satellites will be the first of their kind observed on planetary surfaces, and are guaranteed to reveal new insights as well as surprises.

References: [1] Zahnle, K. et al. (2003) *Icarus*, *163*, 263–289. [2] Schultz, P.H. (1988) In: Mercury. 274–335. [3] Barnouin-Jha, O.S. et al. (2007) *Icarus*, *188*, 506–521. [4] Ernst, C.M. and Schultz, P.H. (2002) *LPS 33*, 1782. [5] Ernst, C.M. and Schultz, P.H. (2003) *LPS*, *34*, 2020. [6] Ernst, C.M. et al. (2011) *LPS*, *42*, 2299. [7] Barnouin, O.S. et al. (2011) *LPS*, *42*, 2258. [8] Dobrovolskis, A.R. et al. (1997) In: *Pluto and Charon*. 159-190.

ONE-DIMENSIONAL DSMC MODEL OF PLUTONIAN ATMOSPHERE.

T. J. Fleming (thadeus.j.fleming@utexas.edu)[1], D. B. Goldstein (david@cfdlab.ae.utexas.edu)[1], L. M. Trafton (lmt@astro.as.utexas.edu)[1], P. L. Varghese (varghese@mail.utexas.edu)[1], A. T. Hawkins (athawk2@utexas.edu)[1].
[1]University of Texas at Austin

Introduction: The Plutonian atmosphere is poorly understood due to its distance from Earth. However, as the New Horizons spacecraft will arrive in 2015, a prediction of atmospheric behavior is desired. We will present early results using Direct Simulation Monte Carlo (DSMC) modeling in one dimension with spherical symmetry.

Background: Current knowledge of the Plutonian atmosphere suggests that it is a sublimation-supported, primarily N_2 atmosphere with a small component of CH_4. The atmosphere exists in vapor pressure equilibrium with ices on the surface, and its density should vary with Pluto's proximity to the Sun. The atmosphere is believed to escape, although the rate at which this occurs is a subject of debate. Because the barycenter of Pluto and Charon is outside of both bodies, the atmosphere is suspected to behave in an unusual manner.

Simulation: While Johnson [1][2] utilized a hybrid fluid-DSMC approach, our method currently consists of DSMC exclusively. The DSMC method simulates a dilute gas by moving and colliding a set of representative molecules, each of which corresponds to a large number of physical molecules. The molecules are then sampled, and flow properties are determined.

Density Gradients: Although DSMC is primarily useful for simulating dilute gases, it can simulate a variety of different densities. However, flows with significant density variation present an issue. In standard DSMC, the ratio of real and simulated molecules is constant throughout the domain; a density difference must be accompanied by a proportional difference in the number of simulated molecules. For Pluto, the density gradient over the domain poses a challenge.

Molecule Weighting: One solution involves cell weighting, with molecules in lower cells representing many physical molecules, and those further away representing fewer. As molecules cross the cell boundaries, the difference in weight results in molecule destruction or duplication. Particles moving downward are destroyed, resulting in few particles reaching the surface from high altitude, and particles moving upward are duplicated, amplifying noise. For these reasons, cell weighting has been avoided.

Domain Restriction: When the domain of the simulation is restricted to a region beginning somewhat below the exobase and ending at the closest approach of New Horizons, the density difference is reduced to only a few orders of magnitude. This is tractable using unweighted molecules.

Initial Conditions: For the sake of simplicity, an isothermal atmosphere is initialized, with gravitational acceleration varying with altitude. Since the initial atmosphere is too dense at high altitudes, the atmosphere collapses onto itself and rebounds off the lower simulation boundary, forming a shockwave. After some oscillation, the atmosphere settles into an approximate equilibrium.

Considerations in cell sizing: While the molecules can translate between cells during the move phase, they can only collide with other molecules within the same cell. There are two primary limiting factors on cell size: the scale height of the gas, and the mean free path. While scale height varies only with temperature, mean free path increases to infinity as density drops. Mean free path initially dominates cell sizing considerations, with scale height dominating at higher altitudes.

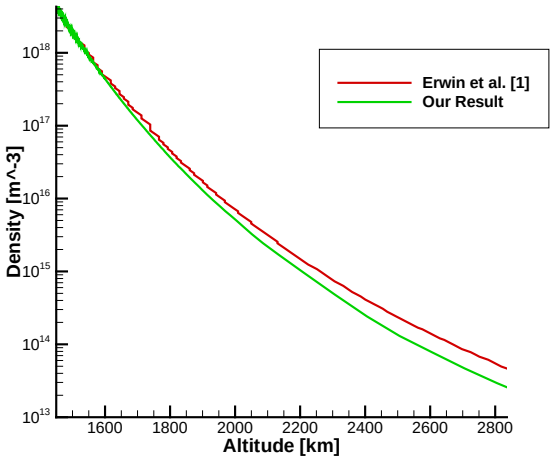

Comparison in the low-altitude continuum regime of Erwin et. al. with present DSMC results. Difference is likely due to a centrifugal effect in the rotating Pluto frame.

Results: Initial results include verification of the fluid regime results from Johnson et al. We will present full one-dimensional density, velocity, and temperature results in the poster.

References: [1] J. Erwin, O. J. Tucker, and R. E. Johnson (2012), arXiv, 1211.3994. [2] O. J. Tucker, J. T. Erwin, J. I. Deighan, A. N. Volkov, R. E. Johnson (2012), Icarus, 217, 408-415.

3D MODELLING OF THE METHANE CYCLE ON PLUTO.

F. Forget[1] and M. Vangvichith[1], [1]Laboratoire de Météorologie Dynamique (LMD), Paris, France (forget@lmd.jussieu;fr)

Introduction: We have developed two complementary models to predict and understand the New Horizons observations of the Pluto atmosphere and surface ice distribution. The main model is a complete 3D General Circulation Model (GCM) adapted to Pluto [1] which includes the methane cycle. The second model is derived from the GCM, but is designed to simulate the evolution of the distribution of nitrogen and methane surface ice for thousands of years.

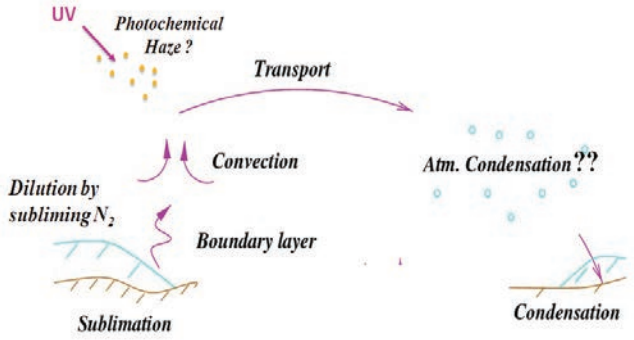

Figure 1: *The different components included in the methane cycle model.*

Global Climate Modelling of the methane cycle on Pluto: On the basis of our experience gained at LMD by modeling the other planetary atmosphere in the solar system, and in particular Mars [2] and Triton, we have developed a new general circulation model (GCM) for Pluto [1]. In addition to a 3D dynamical core which solves the primitive equation of meteorology, the model takes into account the N_2 condensation and sublimation, the vertical turbulent mixing, the radiative transfer through methane and carbon monoxide (using the correlated k method), molecular thermal conduction, and a detailed surface thermal model.

Within this context, we have incorporated in the GCM a detailed model of the methane cycle, including its sublimation and condensation on the surface and in the atmosphere, mixing by turbulence in the planetary boundary layer, transport by the atmospheric circulation. Surface methane ice can be mixed with nitrogen frost, but in our baseline simulations we assume that the vapor pressure of solid methane is not affected by the possible diluation in methane ice. This assumption will be discussed. This model enable us to consistently predict the 3D methane abundance in the atmosphere which is used as an input for our radiative transfer calculations.

The key assumption in Pluto GCM simulations is the initial distribution of surface ices. In our baseline simulation, we have taken the "Modified Grundy and Fink" surface map from [3] which assumes three kind of surfaces (N_2 ice, CH_4 ice, Tholins) and which is derived from observations taken in the 80s and 90s. With such a nitrogen and methane frost distribution, and without any adhoc tuning The methane mixing ratio predicted by the model significantly varies in space and time, and reach a few tenth of percent in the summer hemisphere in 2008-2010, consistently with the value reported by [4-5]. Sensitivity studies reveal that such values are only possible if a subliming source of methane ice is assumed to be present at high latitude in the summer hemisphere. In fact, our simulations predict that the methane gas column is maximum at high summer latitude, with values reaching twice the equatorial column. The polar methane volume mixing may increase up to about one percent in 2015, but only if methane frost remains available on the polar surface. Assuming no supersaturation, methane ice is predicted to condensate in the first hundreds of meters above the summer surface, but the clouds optical depths remain very low.

Could Titan-like hazes be present in the atmosphere of Pluto in 2015 ? To address this question, we are including a simple parametrization of the formation of organic aerosols resulting from the interaction of methane with the solar UV radiation, and we compute their sedimentation and transport by the general circulation.

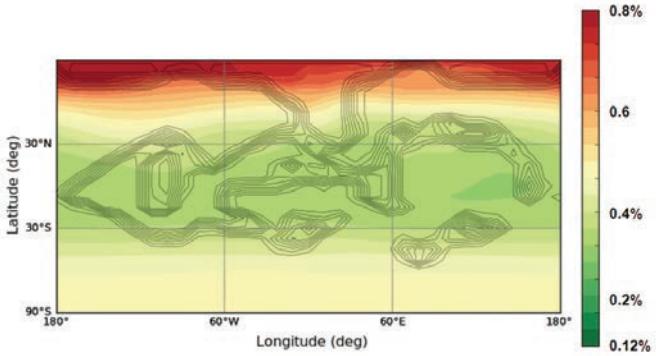

Figure 2: *A prediction of the column-averaged methane volume mixing ratio in 2015, assuming that methane ice is still available on the surface at high summer latitude*

Long term evolution of N_2 and CH_4 surface ices. A model of the surface of Pluto (in which the atmospheric transport of volatiles is simply parametrized rather than fully calculated) has been derived from the GCM. We can run it for thousands of years and explore the repartition of ices with seasons and the variation of pressure and atmospheric methane abundance. As expected, the evolution of nitrogen is similar than in [6]. For methane, a similar seasonal cycle is predicted, but interestingly the model predict the formation of permanent CH4 ice deposits at low latitudes, consistently with maps retrieved from the observations . We also investigate the process which could create methane ice deposits near the summer pole as suggested by the abundance of methane gas in the atmosphere.

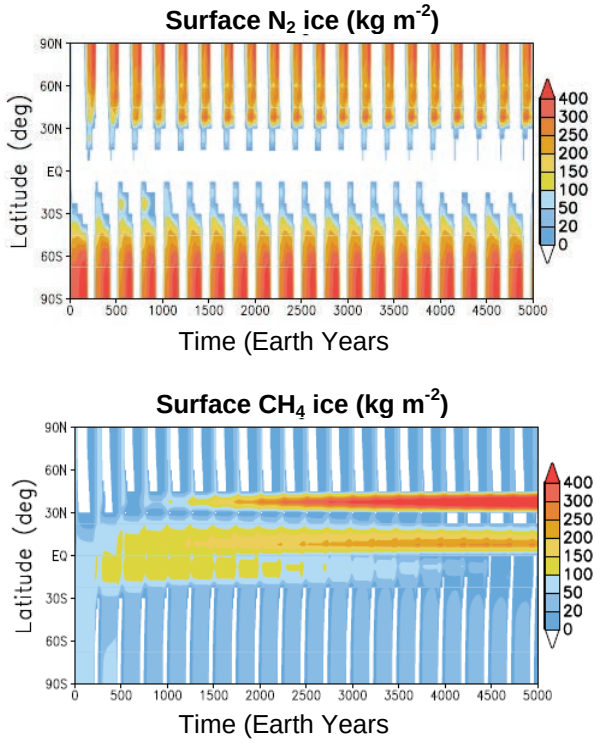

Figure 3. *An example of simulations using the long term surface frost model derived from the GCM. Results obtained assuming a initial inventory of 50 kg m^{-2} for both ices, albedo of 0.65 and 0.45 for N_2 and CH_4 respectively, emissivity of 0.9, and surface thermal inertia of 400 SI.*

References.

[1] see companion abstract by Vangvichith and Forget.
[2] Forget et al. *JGR* 104 E10 p.24,155-24,176 (1999)
[3] Lellouch et al. *Icarus* 147, 220–250 (2000)
[4] Lellouch et al. *A&A* 495, L17–L21 (2009)
[5] Lellouch et al. *A&A* 530, L4 (2011)
[6] Hansen and Paige *Icarus* 120, 247–265 (1996)

A Comparison of Models of Tides in Pluto's Atmosphere and Stellar Occultation Observations

Richard G. French[1], Anthony D. Toigo[2], and Peter J. Gierasch[3], [1]Wellesley College (rfrench@wellesley.edu), [2]Johns Hopkins University APL, [3]Cornell University.

Stellar occultation observations have provided strong evidence for the presence of atmospheric waves in Pluto's atmosphere, including inertia-gravity waves with vertical wavelengths from a few km to tens of km [1,2]. Here, we search for evidence in the stellar occultation observations of atmospheric tides, predicted to be driven by sublimation and freezing of N_2 on Pluto's surface. *Toigo et al.* [3] developed a classical tidal model, based on the assumption that the high-albedo areas on Pluto are regions of frost deposition and sublimation. While the actual situation may be more complex, this provides a reasonable starting point, as well as testable predictions about the amplitudes, wavelengths, and regional variability of temperature perturbations associated with the vertically propagating waves.

The most direct comparison between the tidal predictions and the occultation observations is provided by constructing synthetic occultation light curves, using a ray-tracing code to model the refraction of starlight as it passes through the tidally-perturbed atmosphere.

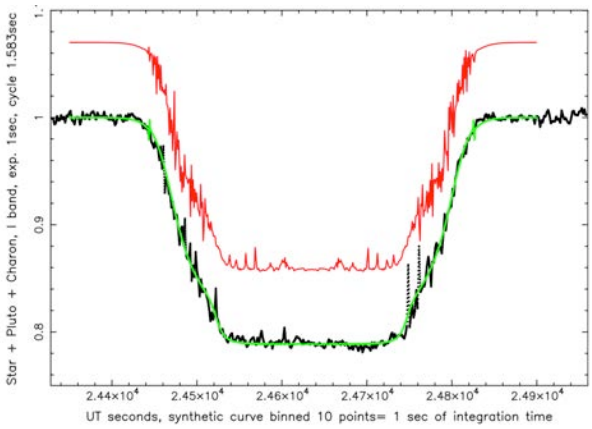

Figure 1: Synthetic light curves compared to the observed light curve (black) from the August 21, 2002 stellar occultation by Pluto, observed from the 3.55-m Canada-France-Hawaii Telescope (CFHT) in Hawaii [4]. A synthetic light curve derived from a smoothed model temperature profile is shown in green, and the results from tidal calculations [3] are shown in red. Here, the atmospheric temperature oscillation amplitudes from the tidal models have been reduced by a factor of 4, resulting in a reasonable qualitative match to the observations.

Figure 1 shows such a comparison, from *Toigo et al.* [3]. Here, the sharp spikes, or scintillations, in the model light curve result from the strong focusing of starlight by vertical temperature variations of about 1 K and vertical wavelengths of a few km. Although the nominal tidal amplitudes result in spikes that are larger then those observed, a fair match is obtained by reducing the tidal amplitudes by a factor of 3 or 4, as shown. The resulting qualitative similarity between the model and the observations is suggestive that sublimation-driven tides may be responsible for the spikes in the observed light curve, but a more detailed assessment is required before we can say that the tidal model has been substantiated.

We have improved on this exploratory comparison of tidal theory with observations in the followowing ways:

1. *Two-dimensional wave structure.* The ray-tracing results shown above assume that the atmosphere is radially symmetric (one-dimensional), but the tidally-driven waves have horizontal as well as vertical structure that should be taken into account. The effective horizontal path length of a ray through the atmosphere is of order $\lambda = (2\pi RH)^{1/2} \sim 600$ km for Pluto, where R is the planetary radius and H is the atmospheric scale height. When the horizontal wavelength $\lambda_h << \lambda$, the resultant scintillation spikes in the model light curve are substantially suppressed by horizontal averaging, compared to a one-dimensional calculation.

2. *Accounting for convection.* A vertically propagating wave of constant energy will increase in amplitude with height as it moves into lower density regions of the atmosphere. Eventually, the wave can become unstable against convection when its thermal perturbation exceeds the adiabatic lapse rate. Using a wavelength-dependent scaling, we modify the tidal results of [3] by damping the growth of vertically propagating waves to ensure that they remain subadiabatic. This also has the effect of reducing the strength of the scintillation spikes, bringing the predictions more in line with the observations.

3. *Detailed comparison of atmospheric vertical structure.* We compare the predicted tidally-induced vertical temperature perturbations, modified as described above, with the observed vertical thermal structure in Pluto's atmosphere, determined from numerical inversion of occultation light curves. Although this approach is limited to the highest SNR data sets, it enables us to make

direct comparisons between physical quantities of interest, such as the variation in tidal amplitude and wavelength with altitude. We employ both traditional Fourier techniques to derive the spectral density of the temperature variations, as well as wavelet decomposition, which has the advantage of more accurately characterizing waves whose amplitude varies with height, as expected for vertically propagating tidal modes.

The results of this ongoing analysis will provide a critical test of the atmospheric tidal model of *Toigo et al.* [3], and lay the groundwork for additional detailed comparisons of GCM predictions of atmospheric structure with high-SNR stellar occultation probes of Pluto's atmosphere. These, in turn, will help to lay the groudwork for the interpretation of upcoming observations of Pluto's atmospheric structure during the New Horizons encounter in 2015.

This work is supported by NASA Planetary Atmospheres Grant PATM NNX11AD83G.

References:

[1] McCarthy, D. W. et al. (2008) *Astron. J., 136,* 1519-1522. [2] Person, M. J. (2008) *Astron. J., 136,* 1510-1518. [3] Toigo, A. D. et al. (2010) *Icarus 208,* 402-411.

THE SIZE DISTRIBUTION OF THE KUIPER BELT.

C. I. Fuentesr[1], [1]Northern Arizona University (cesar.i.fuentes@nau.edu).

Introduction: The remnants of the protoplanetary disk, now in the form of trans-Neptunian objects (TNOs), provide a testing ground for the collitional and dynamical processes that formed and shaped the Solar System. In particular, the current TNO size distribution is defined by its initial properties, collisional history, and the formation and evolution of the giant planets [1,2,3]. The luminosity function of TNOs has been used extensively as a proxy for their size distribution. Besides the TNO size distribution, the luminosity function also depends on other TNO properties, such as surface albedos and orbital distribution. A systematic accounting of all these effects will be possible with the coming new synoptic observatoris and much larger ultradeep surveys.

Observations: TNOs shine in reflected light, which makes observing small and distant TNOs very challenging. Hence, knowledge of the trans- Neptunian region is based predominantly on the study of only the brightest objects, with typical diameters 100–300 km [4]. These objects, usually discovered in shallow surveys that cover a significant fraction of the available sky [5,6], are followed up extensively and become spectroscopic targets. Several 'Deep' surveys have been completed from the ground, using the largest telescopes available and reaching limiting magnitudes as faint as R~27 when digitally combining several hours of observation [7]. Space based searches have proven extremely efficient at finding TNOs with D<50km. HST's ACS/WFC TNO search by Bernstein et al. (2004) [8] yielded three new objects, discovered with a limiting magnitude of R=28.5. This result implied a break in the size distribution of TNOs and hinted at a different size distribution for high (i>5◦) and low (i<5◦) inclination objects. Since then a handful of single detection searches has been completed with HST data, yielding tens of TNOs with D>30km [9,10,11]. Occultation surveys rely on the indirect detection of small TNOs on background star's lightcurves to constrain the size distribution of km sized to sub-km sized TNOs [12,13,14,15,16] The report of the first TNO occultation event in 2009 [13] has allowed us to extend the TNO size distribution to km sizes objects.

Open Questions: We have now reached the point in this field that testable predictions about the history of the outer Solar System can be made from a collection of evidence: (1) There is an observed break in the TNO size distribution at R~25.2. This break exists for all dynamical classes of TNOs. This break may either be due to collisional evolution or primordial formation processes. (2) Cold classical TNOs (i<5◦) formed in the vicinity of their current location (~42–45 AU, with low eccentricities). Cold classical TNOs have not experienced significant dynamical mixing over the age of the Solar System. (3) Large cold classical TNOs have uniformly red surfaces [17,18]. The colors of small cold classical TNOs are not known. (4) Old surfaces in the outer Solar System become red through billions of years of radiolysis. Blue/neutral surfaces must be fresh(er) and young(er). (5) There is a hint that small TNOs in other dynamical classes may be bluer than their large counterparts, but the signal is weak and difficult to interpret dynamically. Filling in more completely the TNO size distribution with objects between the capabilities of current direct detection and occultation surveys, and characterizing the size distribution of different dynamical classes will allow us to distinguish between the collisional and dynamical processes that shaped the outer solar system.

Conclusions: The current size distribution of TNOs provides a direct comparison with the expectations from different Solar System evolution theories. This is one of the most appealing aspects motivating surveys that aim at measuring the TNO size distribution. I will review what we think are some open questions regarding the conclusions that can be supported with the current size distribution and the observational evidence that would help us answer those questions. I will focus on the new generation of wide-field facilities and the contribution that we expect from New Horizons.

References:

[1] Kenyon & Bromley 2004
[2] Pan & Sari 2005
[3] Kenyon et al. 2007
[4] Brown 2001
[5] Brown 2011
[6] Schwamb et al. 2009
[7] Fuentes et al. 2009
[8] Bernstein et al. 2004
[9] Fuentes et al. 2010
[10] Fuentes et al. 2011
[11] Trilling et al. 2012
[12] Liu et al. 2008
[13] Schlichting et al. 2009
[14] Bianco et al. 2010
[15] Schlichting et al. 2012
[16] Zhang et al. 2013

[17] Gulbis et al. 2006
[18] Fraser & Brown 2012
[19] Murray-Clay et al. 2010

Segregation on Pluto's moons? Paying Charon (and Nix and Hydra) closer attention.

G. G. Galuba[1] and S. van Gasselt[1], [1]Freie Universität Berlin, Planetologie und Fernerkundung, Malteserstr. 74-100, 12249 Berlin, Germany. (*goetz.galuba@fu-berlin.de*)

Introduction: While all planets and moons in the solar system have well-known surfaces Pluto's moons remain an open mystery. Charon seems to have no atmosphere and the details of the surfaces of Nix, Hydra and at least two further moons are unknown. What forms of interactions could dominate those surfaces? Segregation processes on Saturnian satellites are well known. Could we find these on Charon, too?

Segregation: On the surface of Saturn's moon Iapetus (see fig. 1) we find a global albedo dichotomy and also local craters and troughs with dark floors *[1]*. The thermal-feedback process is explained in *[2]*: An area is overheated compared to the average surface, water ice migration away from this area gets more effective. A mixture of ice with dark material therefore increases the percentage of dark material as the white ice migrates away. Albedo decreases and absorption increases. The absorbed sun irradiation leads to even more overheating. A runaway feedback occurs.

Fig 1: Cassini ISS image of Iapetus, showing the trailing side. The diameter of Iapetus is 1470 km. The image was taken on the only targeted flyby in September 2007.

In the Pluto-system: Due to the elliptic orbit of Pluto the surface temperatures of airless bodies in the Pluto system can vary significantly. The tilted axis of the Pluto system in regard to the solar ecliptic adds significant annual variation. After these considerations segregation driven by temperature/albedo gradients are probable.

However water can be excluded as migrating material as the vapour pressure of H_2O does not rise enough to get a migration dominating the global or local surface composition. Other chemical substances would have to fill that gap acting as migrating bright material.

For the dark material needed the situation looks better: The Pluto system is known to home hydrocarbons that are destroyed by photolysis and recombine making tholins a ressource present in Pluto's system. A small amount of intermixture with water ice or any light-scattering embedding matrix creates an effective tint; i. e., lowering the albedo.

The method: We propose, that the interpretation of possible segregation processes in the Plutonian system is done in a very modular way. As we still don't know which processes form interdependencies in this temperature and insolation regimes an approach with modular descriptions for solar flux, local surface temperature and sublimation has been built. Global migration rate networks for volatiles on planetary surfaces can be taken from our work on Iapetus (see. Fig. 2). However the exact mixture of the volatiles can not be anticipated with the precision needed for the description of surface chemistry and its interdependency with absorption of solar irradiation. In case the surface and gas temperatures deviate from each other not only *within* the atmosphere of Pluto but also on other surfaces we are interested in, a monte-carlo radiative-transfer block has been already prepared.

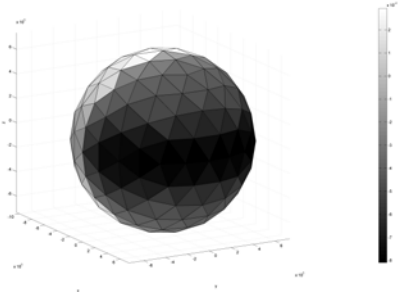

Figure 2: Model of global segregation on the surface of Iapetus

This modular approach has been illustrated in fig. 3. The input into the numerical process is data derived from the New Horizons experiments and the known solar flux. Building blocks in the procession of these inputs are

1. the calculation of the Bond surface albedo (A)
2. the derivation of constraints on relevant chemical compositions and their extinction coefficients $\kappa_{i,S}$
3. the thermodynamics of the respective surfaces including Temperature (T_S) and vapour pressures of volatiles (p_S)

If the gas phase above the respective surfaces is not negligible and local thermal equilibrium is not achieved on the surface, gas chemistry and the radiative-transfer model have to be taken into account for the gas phase extinctions $\kappa_{i,G}$ and the kinetic gas temperature T_G.

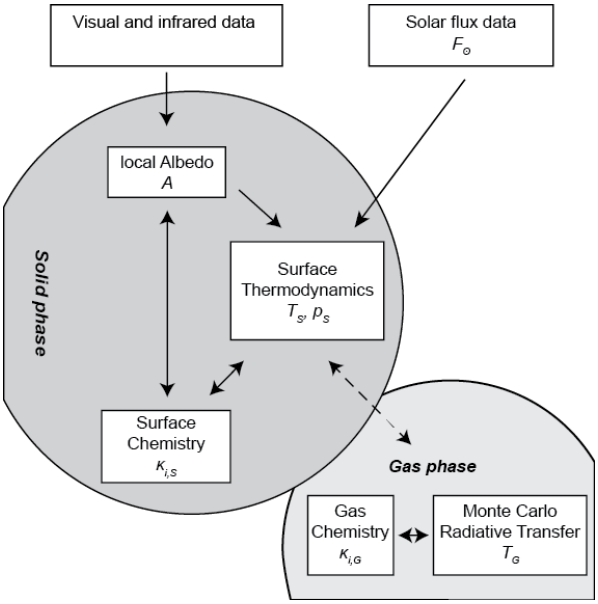

Illustration 3: Blocks of a modular approach to possible surface segregation on Pluto's moons

Aknowledgement: We gratefully acknowledge funding of this work by the German Space Agency (DLR) Bonn through grant no. 50OH1102.

References:

[1] T. Denk and 10 colleagues.
Iapetus: Unique Surface Properties and a Global Color Dichotomy from Cassini Imaging
Science, 327:435 – 439, February, 22th 2010

[2] J. R. Spencer and T. Denk
Formation of Iapetus' Extreme Albedo Dichotomy by Exogenically Triggered Thermal Ice Migration.
Science, 327:432 – 435, February, 22th 2010

Pluto Lightcurve in 2010

E. R. George[1] and M. W. Buie[2], [1]University of Colorado, Boulder, erin.george@colorado.edu, [2]Southwest Research Institute

Introduction: Our research is part of an ongoing project to monitor the long-term photometric behavior of Pluto to provide constraints on volatile surface migraiton. As Pluto passes near the center of the galaxy, the fields are too crowded with stars for normal aperture photometry. We approached this problem with a combination of point-spread function (PSF) photometry and optimal image subtraction (OIS). Our data are from the 0.8m robotic telescope at Lowell Observatory, the 1m robotic telescope at New Mexico State University, and the Faulkes 2m robotic telescope at Siding Spring (part of Las Cumbres Observatory). The main focus of our efforts is the data from 2010.

Background Catalog: The catalog is generated from non-Pluto images of the 13 fields observed on 3 photometric nights each. It is in two parts—Stage 1 and Stage 2. The Stage 1 catalog contains sufficiently isolated stars calibrated by Landolt standards with a full, computed transformation. The Stage 2 catalog contains field stars fit by a PSF. Together, these sources form the final catalog used to calibrate the Pluto frames.

Image Subtraction: We use OIS to remove contaminating sources from around Pluto in order to extract good photometry. We use a package for IDL described in [2] that has been optimized to run quickly. Using data from nights with overlapping fields, we stack the images into a template that is subtracted from each Pluto image after matching PSFs between frames. This process removes the stars from the image, leaving a differenced image containing only Pluto.

Pluto Extraction: We use the calibrated stars from the catalog and apply those sources to the Pluto images. We start with the images before the template subtraction and extract instrumental magnitudes for Pluto as well as the background sources. We then locate the standards contained in the image and compute the transformation. We apply the transformation to the differenced Pluto image to obtain our final results for the magnitude and color. After completing this process for the nights from 2010, we obtain a lightcurve for that year.

This presentation will cover the calibration techniques used to process the data, as well as aspects of the 2010 lightcurve.

References:

[1] C. J. Hansen and D. A. Paige. (1996) *Icarus, 120,* 247.

[2] J. P. Miller, C. R. Pennypacker, and G. L. White. (2008) *PASP, 120,* 49.

[3] M. W. Buie, D. J. Tholen, L. H. Wasserman. (1997) *Icarus, 125,* 233.

[4] M. W. Buie, W. M. Grundy, E. F. Young, L. A. Young, and S. A. Stern. (2010) *AJ, 139,* 1117.

[5] M. W. Buie, D. E. Trilling, L. H. Wasserman, and R. A. Crudo. (2011) *AJ, 194,* 40.

The dynamics of dust particles in the Pluto-Charon system

S.M. Giuliatti Winter[1] , P.M. Pires dos Santos[2] and R. Sfair[3], [1]UNESP (Univ. Estadual Paulista – UNESP- Av. Ariberto P. da Cunha, 333, Guaratinguetá, São Paulo, Brasil, CEP 12516410, silvia@feg.unesp.br), [2]UNESP (Univ. Estadual Paulista – UNESP- Av. Ariberto P. da Cunha, 333, Guaratinguetá, São Paulo, Brasil, CEP 12516410, pos09032@feg.unesp.br), [3]UNESP (Univ. Estadual Paulista – UNESP- Av. Ariberto P. da Cunha, 333, Guaratinguetá, São Paulo, Brasil, CEP 12516410, rsfair@feg.unesp.br).

Introduction: At least four satellites are in orbit around the barycentre of the Pluto-Charon binary system. These satellites, P5, Nix, P4 and Hydra are smaller than Pluto and Charon and are located further from the binary. In this work we investigate the mass production rate of micron-sized dust particles generated by micro-meteoroids hitting Nix and Hydra. Numerical simulations taking into account the gravitational effects of the massive bodies and the solar radiation pressure were performed to derive the lifetime of the ejecta particles. This information allow us to estimate the optical depth of a putative ring extending from the orbits of Nix to Hydra [1].

Numerical Simulations: The typical size distribution of dust rings follows a power law ([2], eqn. 3); here we adopted the index q = 3.5. Thus, in our numerical simulations we assumed particles of 1, 5 and 10 μm in radius as a representative set of this distribution. For each size we simulated 360 particles for the time span of 6500yrs. The sample of 1 μm-sized particles was completely scattered in a very short time-scale (less than 1 yr), considerable quantity of these tiny particles cross the orbit of Charon and can collide with one of the members of the binary. Those particles which remain longer in the system are mostly removed by ejection. For a couple of years larger particles (5 and 10 μm) are distributed in a region encompassing the orbits of Nix and Hydra. The loss of ejecta due to escape from the system reaches 70 per cent of the initial set of the 1 μm-sized grains. The transfer of material between the moons depends on the particle size, for the 10 μm-sized particles the rate of ejecta exchange between the moons is less than 1 per cent.

Mass Production: First, we calculate the mass production of the ejected dust particles by analysing the mass flux of impactors at Pluto's region and the parameter known as ejecta yield (Y). This analytical model follows the approach summarized in [3]. For a steady-state ring its mass is directly proportional to the lifetime (T) of its particles, $m = M+ T$. In order to obtain m we compute how long the ejected particles stay in the region limited by the orbits of Nix and Hydra. This mechanism of dust production is able to generate an accumulated mass of $m\sim1000$kg which, for a radial width of 16000km (the average distance between Nix and Hydra) at $R \sim 57000$km, corresponds to an optical depth of 4×10^{-11}.

Discussion: The ejected particles, between the orbits of Nix and Hydra, form a wide ring of about 16000km. Collisions with the massive bodies and escape from the system are mainly determined by the effects of the solar radiation pressure. This is an important loss mechanism which removes 30 per cent of the initial set of 1 μm-sized particles in 1yr. The surviving particles form a ring too faint to be detectable. Preliminary results on the fate of the dust particles after being ejected from the recent discovered satellite, P4 and P5, will be presented.

References:

[1] Pires dos Santos, P.M., Giuliatti Winter, S.M. and Sfair, R. (2013). *MNRAS*, in press.

[2] Burns, J., Hamilton, D. & Showalter, M. (2001) Interplanetary Dust: Dusty Rings and Circumplanetary, 641.

[3] Sfair, R. and Giuliatti Winter, S.M. (2012). A&A, 543, A17.

The Dynamical Context of Pluto

Brett Gladman
University of British Columbia
Dept. of Physics and Astronomy

Pluto's orbital configuration generated many historical surprises as its complexities were gradually uncovered. As a showcase of bound chaos in the Solar System, Pluto is the lord of the 3:2 resonance but participates in other complicated dynamical interactions. We now understand that Pluto is one of a large number of resonant Kuiper Belt objects and the most important question is how it came to reside in its current dynamical state. For this Pluto needs to be viewed in its context relative to:

(a) the other trans-neptunian resonant objects,
(b) the hot classical Kuiper Belt,
(c) the current Centaur and scattering population,
(d) the detached population, and
(e) the cold classical Kuiper Belt's sub-components.

I will review what we know about these populations, with particular emphasis on what comparisons with calibrated observational surveys tell us about constraints on past histories of Pluto, which certainly did not form on its current orbit.

LYα@PLUTO

G. R. Gladstone[1],W. R. Pryor[2], and S. A. Stern[3] [1]Southwest Research Institute, 6220 Culebra Road, San Antonio, TX 78238 (rgladstone@swri.edu), [2]Central Arizona College, 8470 North Overfield Road, Coolidge, AZ 85128 (Wayne.Pryor@centralaz.edu), [3]Southwest Research Institute, 1050 Walnut St., Suite 300, Boulder, CO 80302.

Introduction: The Alice instrument on New Horizons will perform many observations of Pluto's far-ultraviolet (FUV) airglow emissions during the 2015 flyby. While Pluto's atmosphere is dominated by N_2, simulations suggest that the brightest airglow signal at Pluto will actually be due to Lyman alpha (Lyα) emission of atomic hydrogen. This is because H atoms, produced at lower altitudes during photolysis of CH_4, rise up to become an important constituent of the atmosphere at high altitudes, and are able to scatter the very bright Lyα lines from the Sun and the interplanetary medium (IPM). The IPM Lyα signal at Earth is very much less than direct solar Lyα, but IPM Lyα falls off much more slowly than r^{-2}, so that at Pluto's distance from the Sun the two sources are of comparable strength [1,2].

Resonantly Scattered Solar Lyα: At 32.9 AU from the Sun during the New Horizons flyby on July 14, 2015, Pluto is far enough away that the solar Lyα line undergoes considerable extinction due to scattering by H atoms in the interplanetary medium [3]. However, since Pluto is currently situated almost directly upstream in the interstellar wind, this extinction is shifted from line center by about 20 km/s, or ~15 Doppler widths from line center for 100-K H atoms in Pluto's upper atmosphere, and thus has very little affect on the corona, as seen in Fig. 1. The sub-solar brightness of Lyα due to resonant scattered sunlight is ~50 Rayleighs.

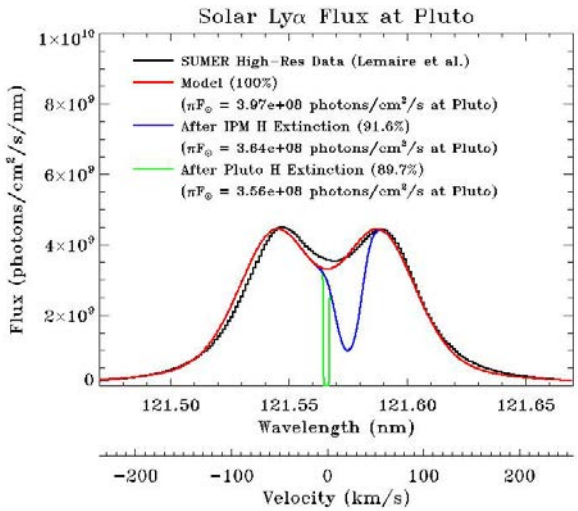

Fig. 1. The estimated solar line profile at the top of Pluto's atmosphere, and at the top of the methane layer.

Resonantly Scattered IPM Lyα: Models of IPM Lyα indicate that the IPM brightness at Pluto during the New Horizons flyby will be ~100 Rayleighs over most of the sky, increasing to ~500 Rayleighs within ~30° of the Sun (located downstream), as shown in Fig. 2. Although relatively bright, the IPM (like the extinction of the solar Lyα line) has a large Doppler shift at most directions on the sky, and can only really interact with Pluto's atmosphere when incident from a band around the terminator (i.e., incident from a solar zenith angle near 90°).

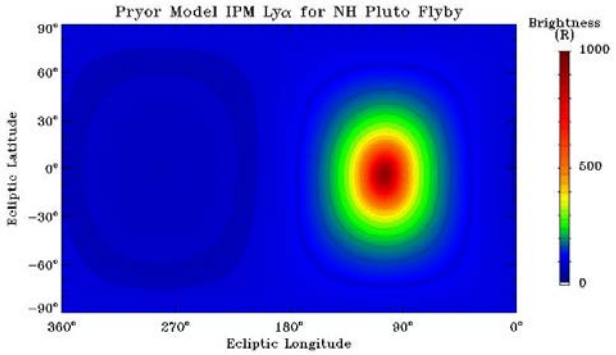

Fig. 2. Model IPM brightness (in ecliptic coordinates) expected for the New Horizons flyby of Pluto.

In this talk we will further discuss how Lyα emissions are formed at Pluto, and will show predictions for Pluto's Lyα corona as seen from New Horizons.

References:

[1] Broadfoot A. L. et al.. (1989) *Science, 246,* 1459–1466. [2] Gladstone G. R. et al. (2013) in *Calibration of Far UV Spectra of Solar System Objects and the Heliosphere,* E. Quemerais, M. Snow, R. M. Bonnet, Eds., ISSI Sci. Report Series, 13, 275 pp, Springer, New York. [3] Wu F. M., Judge D. L. *Astrophys. J., 231*, 594–605, 1979.

A Search for Predicted Photochemical Products on Pluto and Triton.

J. D. Goguen[1], R. Hodyss[1], P. V. Johnson[1], K. J. Lawrence[1], M. D. Hicks[1], [1] Jet Propulsion Laboratory, MS 183-401, 4800 Oak Grove, Dr., Pasadena, CA 91109
Jay.D.Goguen@jpl.nasa.gov

Introduction: We report observations of Pluto and Triton with the Double Beam Spectrometer and Photopolarimeter (DBSP) using the Palomar 5 meter telescope on July 20 and 21, 2010 UT.

Background: Laboratory photochemical studies of thin cryogenic ice films composed of N_2, CH_4 and CO in ratios analogous to those on the surfaces of Neptune's largest satellite, Triton, and on Pluto suggest that C_2^-, CN, HCO, and CNN may be found in significant quantities on the surfaces of Pluto and Triton [1]. Several absorption bands of these photochemical products occur towards the blue end of the visible spectrum and many of these products have no significant spectral absorption bands in the well-studied near infrared region. Our objective was to use the Palomar DBSP spectra to search for evidence of these products through their predicted visible wavelength absorptions as well as to provide new high signal-to-noise spectra of Pluto and Triton at wavelengths from 340 to 950 nm prior to the New Horizons Pluto encounter.

Observations:
We used the Double Beam Spectrometer Photopolarimeter (DBSP) facility instrument on the Palomar 5-meter telescope to acquire ~Å resolution spectra with SNR > 100 on both Triton and Pluto. The DBSP [2] is still a workhorse instrument at Palomar that has been significantly upgraded in both hardware and software (see http://www.astro.caltech.edu/palomar/200inch/dbl_spec/dbsphome.html). It is widely used to measure red shifts of faint galaxies and other astrophysical sources. It has independent blue and red channels, each with its own CCD camera, and a selectable dichroic filter to choose the dividing wavelength between the 2 channels. We used the 680 nm dichroic and the 600 lines/mm grating (400 nm blaze) to focus the blue channel on the 340 to 650 nm wavelength window containing the predicted absorption features targeted in this research. The red channel used the 316 lines/mm grating (750 nm blaze) and spanned wavelengths from 700 to 950 nm. The spectral features of C_2^- (474, 523 nm), HCO (400-700 nm), CNN (397, 420 nm) and CH_2N_2 (400 nm) have not been detected in prior studies of Pluto and Triton, but high SNR spectra at the critical blue end of the visible wavelength window are sparse. Due to the large and model dependent uncertainties in the spatial distribution and compositions of the Triton's and Pluto's ices, it is not possible to make a useful quantitative prediction of the expected strengths of these bands. Either detection or non-detection and strict upper limits in the Pluto and Triton spectra provide constraints on the importance of the photochemical processes observed in the laboratory spectra of analog ices. The observed spectra of Pluto and Triton will be compared to the laboratory spectra of the photochemical products in ices in this presentation.

References:
[1] Robert Hodyss, R., et al (2011). Formation of radical species in photolyzed CH_4:N_2 ices. Icarus ***214*** (2011) 748–753.
[2] Oke, J.B., J.E. Gunn, (1982). An efficient low and moderate resolution spectrograph for the Hale telescope. Publ. Astron. Soc. Pacific ***94***, 586-594.

EXPLORING THE DYNAMICAL CONSEQUENCES OF THE COLLISIONAL ENVIRONMENT OF THE KUIPER BELT ON THE ORBITS OF PLUTO'S SMALL SATELLITES.

A. J. Gonring[1] and D. A. Minton[2], [1]Purdue University (alex.gonring@gmail.com), [2]Purdue University.

Introduction: Nix, Hydra, P4, and P5 have presented problems to those wishing to determine how these four small satellites entered into their currently observed orbits about Pluto. It is largely believed that these satellites were formed through the Charon-generating impact on Pluto, but how could these satellites have ended up in their current orbits? And, why are the satellites' orbits very close to, but not exactly within, mean motion resonances [1, 2]?

We used new information about the Kuiper belt size distribution to make our own investigation into the orbital and collisional history of the satellites of Pluto over the age of the Solar System. With this new information, we generated a new model of the collisional evolution of Kuiper belt objects. These time histories were used to help determine whether collisions between these satellites and other objects within the Kuiper belt, and its various dynamical subpopulations, could have been important over their lifetimes.

Simulations: To estimate the importance of collisions in the Plutonian system, a total number of large impacts was estimated over the past 4 billion years. Simulations were performed with each of the four small satellites beginning in a circularized, resonant orbit. Each satellite was then inelastically collided with an impactor, factoring in effects from ejecta [3], to determine a new resulting orbit. If an impact was great enough to move the satellite from the initial resonant orbit to an orbit similar to its current one, the impact was flagged as significant.

Impactors were considered from four subpopulations of the Kuiper belt: the Scattered Disk, Plutinos, cold classical Kuiper belt, and hot classical Kuiper belt [4]. Subpopulation size distributions were modeled from newly identified Kuiper belt size distributions. From these distributions, collisional rates were created for each satellite from each subpopulation [5]. Collisional rates of impactors of significant size were then identified for each satellite, and then integrated to produce a total number of significant collisions for each satellite over 4 billion years. Care was taken to consider effects of mass loss over time within certain subpopulations of interest during the integrations as well [6, 7].

Over this 4 billion year period, we found that each of the four small satellites have rates of impact greater than or equal to one with significantly sized impactors, implying that collisions have played a non-negligible role in the dynamical evolution of the Plutonian system. Effects from even larger impactors, with impact rates greater than or near one, were looked into as well, providing insight into other methods for analyzing the collisional history of the satellites of Pluto. New simulations were then developed using Monte Carlo techniques to better analyze the dynamical evolution of the four smaller satellites of Pluto due to collisions from Kuiper belt objects.

References: [1] Buie M. W. and Grundy W. M. (2006) *AJ, 132,* 290-298. [2] Showalter M. R. et al. (2012) *AAS DPS Meeting #44, #304.07*. [3] Melosh H. J. et al. (1994) *Hazards due to Comets and Asteroids*, 1111-1132. [4] Gladman B. et al. (2008) *The Solar System Beyond Neptune,* 43-57. [5] Cheng A. F. (2004) *Icarus, 169,* 357-372. [6] Tiscareno M. S. and Malhotra R. (2009) *AJ, 138,* 827-837. [7] Volk K. and Malhotra R. (2008) *ApJ, 687,* 714-725.

Distribution and Evolution of Pluto's Volatile Ices from 0.8-2.4 μm Spectral Monitoring

W.M. Grundy[1,2], C.B. Olkin[2,3], L.A. Young[2,3], M.W. Buie[2,3], and E.F. Young[2,3]. [1]Lowell Observatory, 1400 W. Mars Hill Rd., Flagstaff AZ 86001. [2]Visiting or remote observer at the Infrared Telescope Facility, which is operated by the University of Hawaii under Cooperative Agreement no. NNX-08AE38A with the National Aeronautics and Space Administration, Science Mission Directorate, Planetary Astronomy Program. [3]Southwest Research Institute, 1050 Walnut St. #300, Boulder CO 80302.

We report observations of Pluto's 0.8 to 2.4 μm reflectance spectrum with IRTF/SpeX on 65 nights over the dozen years from 2001 to 2012 (Grundy et al. 2013). The spectra show vibrational absorption features of simple molecules CH_4, CO, and N_2 condensed as ices on Pluto's surface. These absorptions are modulated by the planet's 6.39 day rotation period, enabling us to constrain the ices' longitudinal distributions. Absorptions of both CO and N_2 ices are considerably stronger on Pluto's anti-Charon hemisphere. This longitudinal distribution is unlike that of CH_4 ice, which has its maximum absorption offset by roughly 90° from the longitude of maximum CO and N_2 absorption. The CH_4 absorptions are also less strongly modulated as Pluto spins on its axis. However, wavelength shifts in the CH_4 ice absorption bands caused by its dilution in N_2 ice are seen to be greatest on the anti-Charon hemisphere where N_2 and CO absorptions are strongest. CH_4 ice is much less volatile than N_2 and CO, with a vapor pressure at 40 K roughly three orders of magnitude below those of CO and N_2 (Fray & Schmitt 2009). The volatility contrast between CH_4 and the other two ices suggests that their distinct distributions could represent the product of sorting by volatility. The striking inhomogeneities in the distribution of Pluto's volatile ices and especially the Charon-oriented symmetry of Pluto's N_2 and CO ice distributions are especially intriguing. Such a pattern could perhaps be controlled by elevation if Pluto has a fossil tidal bulge or a displacement of its center of mass relative to its center of body, leading to a near-side/far-side dichotomy like Earth's Moon has. Large-scale patterns in Pluto's internal heat flow offer another possible explanation. The remarkably unbalanced volatile ice distribution is reminiscent of the Moore & Spencer (1990) "Koyaanismuuyaw" hypothesis of a perennially dichotomous Triton. Triton's volatile N_2 and CO ices are similar in exhibiting a longitudinal distribution corresponding to the tidal axis of symmetry, except that in Triton's case, both ices are strongly concentrated on the Neptune-facing rather than the anti-Neptune hemisphere (Grundy et al. 2010).

In addition to diurnal variations, the spectra show longer term trends. On decadal timescales, Pluto's stronger CH_4 absorption bands have been getting stronger, while the amplitude of their diurnal variation diminishes, consistent with additional CH_4 absorption at high northern latitudes rotating into view as the sub-Earth latitude moves north (as defined by the system's angular momentum vector). Unlike the CH_4 absorptions, Pluto's CO and N_2 absorptions appear to be declining over time, suggesting more equatorial or southerly distributions of those species. To get an idea of whether the observed trends are due to changing spatial distributions of the ices caused by seasonal volatile transport or simply from the changing observing geometry, we did observations on three pairs of nights selected to be separated in time by a little over a year, but with very little difference in observing geometry, thanks to parallax from Earth's motion. Comparisons of these geometrically-matched pairs of spectra favor geometric explanations for the observed secular changes in CO and N_2 absorption, although seasonal volatile transport could still be at least partly responsible. The case for a volatile transport contribution to the secular evolution looks strongest for CH_4 ice, despite it being the least volatile of the three ices. Both long-term and matched-pair CH_4 behaviors can be explained if volatile transport is reducing the strengths of the CH_4 bands at the same time as geometric effects are increasing them. Averaged over the past decade, the two effects combine to produce an overall increase in CH_4 band strengths, but if geometry is held constant, only the volatile transport weakening effect is seen.

Fray & Schmitt 2009. Sublimation of ices of astrophysical interest: A bibliographic review. *Planet. Space Sci.* **57,** 2053-2080.

Grundy et al. 2010. Near-infrared spectral monitoring of Triton with IRTF/SpeX II: Spatial distribution and evolution of ices. *Icarus* **205,** 594-604.

Grundy et al. 2013. Near-infrared spectral monitoring of Pluto's ices: Spatial distribution and secular evolution. *Icarus* **223,** 710-721.

Moore & Spencer 1990. Koyaanismuuyaw: The hypothesis of a perennially dichotomous Triton. *Geophys. Res. Lett.* **17,** 1757-1760.

Observations of a successive stellar occultation by Charon and graze by Pluto in 2011

A. A. S. Gulbis[1,2], J. P. Emery[3], M. J. Person[2], A. S. Bosh[2], C. A. Zuluaga[2], J. M. Pasachoff[4], and B. A. Babcock[4], [1]Southern African Large Telescope, P.O. Box 9, Observatory, Cape Town, 7935, South Africa; amanda@salt.ac.za, [2]Massachusetts Institute of Technology, Cambridge, MA, [3]University of Tennessee, Knoxville, TN, [4]Williams College, Williamstown, MA

Introduction: Since the late 1980s, stellar occultations have provided snapshots of the Pluto system and specifically of Pluto's atmospheric evolution. The lower atmosphere, below roughly half-light level in an occultation light curve, has changed distinctly over time (e.g. [1, 2]). Theorized explanations for the lower atmospheric structure include a steep thermal gradient and/or extinction, the latter of which can be characterized as a dependence between occultation flux and wavelength. Pluto's upper atmosphere has remained consistent. However, in 2007, a grazing occultation revealed waves in the upper atmosphere [3-5].

Data: Observations were made at NASA's 3-m Infrared Telescope Facility (IRTF) on Mauna Kea, Hawaii, for a predicted occultation of a UCAC2 14.43 magnitude star by Pluto on 23 June 2011. The stellar magnitude is 11.0, 10.1, and 9.7 in *J*, *H*, and *K*, respectively. The star was observed simultaneously with and SpeX [6] and MORIS (the MIT Optical Rapid Imaging System [7]). MORIS recorded visible images of a 1-arcmin by 1-arcmin field of view, with an effective central wavelength of 0.74 microns, at a cadence of 0.3 seconds and negligible deadtime. Low-resolution spectral IR data of the occultation star and a comparison were taken with SpeX, using the 1.6-arcsecond slit, at a cadence of 1.5 seconds including approximately 0.75 seconds of deadtime. The SpeX data cover the range of 0.9-2.5 microns over 474 wavelength channels. Data from both instruments show a full occultation of the star by Charon followed approximately 620 seconds later by an atmospheric graze by Pluto (Figure 1).

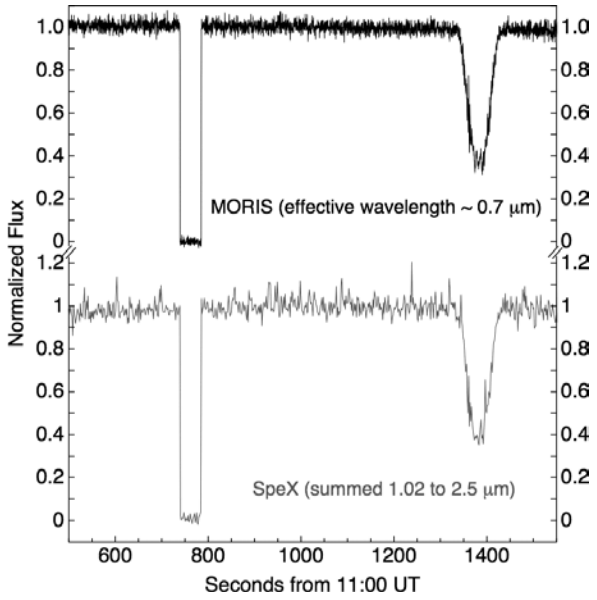

Figure 1. IRTF lightcurves of the 23 June 2011 occultation by Charon (*left*) and Pluto (*right*). The data are visible-wavelength images with MORIS and low-resolution spectra with SpeX. The signal-to-noise ratios of the lightcurves are approximately 125 (MORIS) and 80 (SpeX) per Pluto scale height of 60 km.

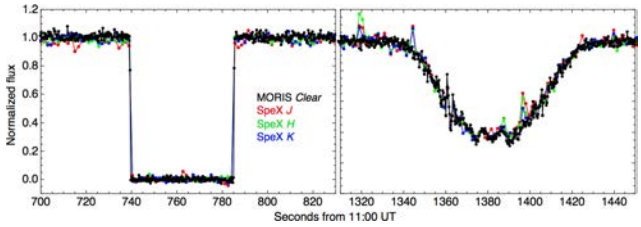

Figure 2. Expanded views of the occultation lightcurve for Charon (*left)* and Pluto (*right)*. The SpeX data have been summed into standard filter bandpasses: *H* is 1.164–1.326 μm, *J* is 1.483–1.779 μm, and *K* is 2.027–2.363 μm. The SpeX data are plotted as 2% trimmed means because *H* band is noisy. This trimming drops only 1-2 data points from each filter and does not affect the general characteristics of the lightcurve. No significant variation with color is apparent, except for slight differences in the spikes of the Pluto graze.

Conclusions: Based on model fitting to the MORIS data for light diffraction by an edge, the Charon occultation lasted 45.73 ± 0.01 s, corresponding to a chord length of 1111.70 ± 0.11 km. Assuming Charon's radius is 606.0 ± 1.5 km [8], the impact parameter for the IRTF was 241.4 ± 3.7 km. No diffraction spikes were seen and there is no difference in the flux level as a function of observational wavelength over the entire range of ~ 0.7–2.5 μm (see Figure 2).

The impact parameter in Pluto's shadow was 1138 ± 3 km as determined by a fit to six lightcurves from four stations that observed the event, including SOFIA (the Stratospheric Airborne Observatory for Infrared Astronomy, [9]). From the IRTF, the graze reached a minimum normalized flux level of roughly 0.35 and probed as deep as 1255 km from Pluto's center. As shown in Figure 2, there is no obvious difference in flux over the observed wavelength range. Atmospheric

model fits to a nearly central chord from SOFIA suggest that if a haze layer were present it would start at 1244 km from Pluto's center (~1103 km in the shadow) [9]; therefore, this graze did not probe deeply enough in the atmosphere to detect a trend between flux and wavelength.

There are multiple features in the Pluto graze that deviate more than 2σ from a smooth, atmospheric model fit. These bumps and spikes are due to atmospheric density variations. Unlike the graze in 2007 in which waves were detected [3-5], the 2011 data are asymmetric from immersion to emersion, excluding the bump at the very bottom (Figure 3). The flux variations are the strongest between ~ 1200–1300 km in the shadow (~ 1280–1335 km from Pluto's center). The features vary with observed wavelength: in particular, a spike was detected during emersion in the SpeX data, but not with MORIS (Figure 2).

We will present a detailed analysis of the SpeX and MORIS occultation data, taking into consideration how this dataset fits into our overall understanding of Pluto's atmospheric evolution.

References: [1] Elliot J.L. et al. (2007) *AJ, 134, 1-13.* [2] Young E.F. et al. (2008) *AJ, 136, 1757-1769.* [3] Person M.J. et al. (2008) *AJ, 136, 1510-1518.* [4] McCarthy D. et al. (2008) *AJ, 136, 1519-1522.* [5] Hubbard W. et al. (2009) *Icarus, 204, 284-289.* [6] Rayner J.T. et al. (2003) *PASP, 115, 362-382.* [7] Gulbis A.A.S. et al. (2011) *PASP, 123, 461-469.* [8] Person M.J. (2006) *AJ, 132, 1575-1580.* [9] Person M.J. et al. (2013) *AJ, submitted.*

Acknowledgements: Funding for this work was provided in part by the South African National Research Foundation and NASA grants NNX08AO50G & NNX12AJ29G (Williams), NNX10AB27G (MIT), and NNX10AB23G (UT). AASG and JPE were visiting astronomers at the IRTF, which is operated by the University of Hawaii under Cooperative Agreement no. NNX-08AE38A with the National Aeronautics and Space Administration, Science Mission Directorate, Planetary Astronomy Program.

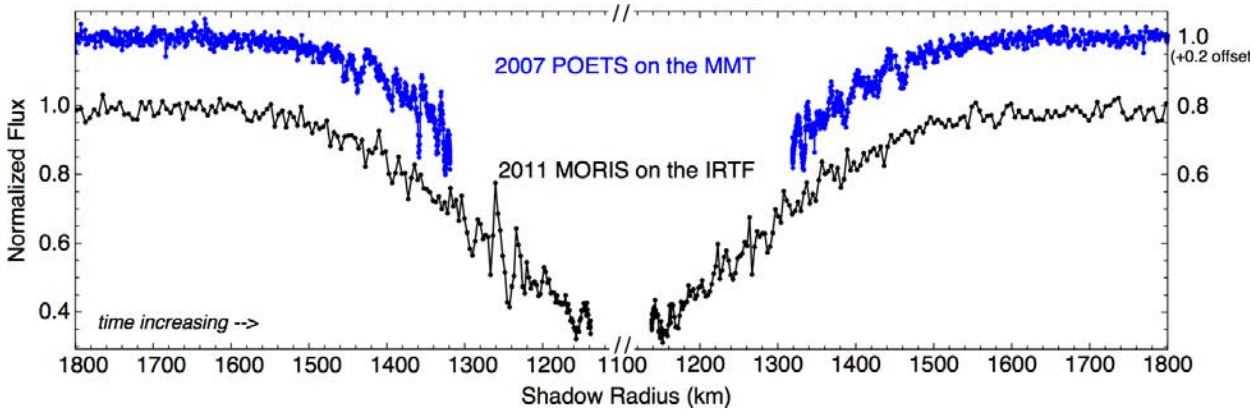

Figure 3. The 2011 Pluto occultation graze as a function of radius in the shadow, compared with an occultation graze in 2007 [3] observed on the 6.5-m MMT with a Portable Occultation Eclipse and Transit System (POETS, which is a similar instrument to MORIS). The calculated shadow radius at half-light level is comparable for these two events [9]. The 2011 graze goes significantly deeper into the atmosphere, but is at lower resolution: the occultation velocity in 2007 was 6.8 km/sec versus 24.3 km/sec in 2011. Other than the bump at the lowest flux level, the 2011 lightcurve does not display symmetric features like those determined in the 2007 data to be internal gravity waves [3-5].

ATMOSPHERIC CO ON PLUTO: LIMITS FROM MILLIMETER-WAVE SPECTROSCOPY

M.A. Gurwell[1], B.J. Butler,[2] and A. Moullet[3], [1]Harvard-Smithsonian Center for Astrophysics (Cambridge, MA; mgurwell@cfa.harvard.edu), [2]National Radio Astronomy Observatory (Socorro, NM; bbutler@nrao.edu), [3]National Radio Astronomy Observatory (Charlottesville, VA; amoullet@nrao.edu)

Introduction: Once considered an anomaly, Pluto and its moons are now recognized as benchmarks for studies of the Kuiper Belt. The Pluto system is the primary objective for the New Horizons mission (July 2015 flyby; [1]). Pluto and its primary moon Charon are two of the largest bodies of the Kuiper Belt (diameters ~ 2350 and 1200 km, respectively) yet, despite similar size and co-location, differ in key aspects. Charon's homogeneous surface is dominated by water ice, while Pluto's heterogenous surface has methane and CO/N_2 ices ([2], [3]) and supports a thin atmosphere. The atmosphere was discovered in 1988 (e.g. [4]) but many essential features are still poorly known. Stellar occultations reveal the middle atmosphere is relatively warm (near 100 K) and that the atmospheric pressure approximately doubled from 1988 to 2002, remaining roughly constant since (e.g. [5], [6]). The atmosphere must be dominated by N_2, with significant CH_4 and CO, and is likely similar to Triton's atmosphere (also nitrogen-dominated). Atmospheric CH_4 is detected in the near-IR ([7], [8]) indicating ~0.5% CH_4/N_2 and a total surface pressure of 7–24 μbar. The N_2-dominated atmosphere, in vapor-pressure equilibrium with N_2 ice, depends critically on the surface temperature, which at around 42 K is significantly below the radiative equilibrium temperature for 31 AU due to this vapor-pressure maintenance. Minor species (CH_4, CO) and photochemical products (particularly HCN) control the atmospheric temperature structure, and thus the escape rate. As described in [9], the escape rates of volatiles N_2, CO and CH_4 are powerful tools for understanding evolution of the surfaces of Triton, Pluto, Charon, Eris, Orcus and other KBOs. And while only Pluto and Triton have known atmospheres, some larger KBOs may still retain enough volatiles to develop sublimation atmospheres near perihelion; Pluto serves as an important reference point for the study of these possible atmospheres.

The CO Conundrum. Well-detected as an ice on Pluto's surface, carbon monoxide should also be present in the atmosphere; its vapor pressure at Pluto temperatures is only a factor of 8 lower than for N_2. CO should also be well-mixed in the atmosphere given its long lifetime and molecular weight identical to N_2. Initial non-detections of atmospheric CO (near-IR: [10]; mm CO(2-1): [11]) have more recently been followed by reported detections.

The first was in the near-IR by Lellouch and colleagues [12] (hereafter designated L2011), found by stacking spectra covering several absorption lines of CO to obtain a 6-σ detection of the gas. Nearly simultaneously, a detection in the 1.3 millimeter band was reported by Greaves and colleagues [13] (hereafter G2011). With several observations spread over 2009 and 2010 using the JCMT, G2011 present a combined spectrum with 5.5-σ feature they identify as the CO(2-1) rotational transition at 230.538 GHz. The near-IR method is sensitive to CO in the lowest scale height, while the millimeter line to much higher altitudes (nominally 300-500 km), and if CO is well mixed they should agree. Instead, they are strikingly inconsistent.

L2011 find CO at ~500 ppm assuming T=100 K. This abundance is somewhat higher than expected from equilibrium in an ideal mixture based upon the observed CO/N_2 ice ratio, and the authors favor a situation ("detailed chemical balance") in which a CO-enriched thin surface layer controls the atmosphere abundance. Still the low SNR of the detection (~6) did not allow a firm conclusion on the nature of surface-atmosphere interactions. By assuming a 'standard' atmospheric model with a constant CO abundance of 500 ppm, we can model the expected millimeter-wave CO(2-1) emission. Such calculations result in a line around 60 mJy peak (about 50 mJy above the 10.5 mJy continuum of Pluto).

G2011, in contrast, found the CO(2-1) line to be 27±5 mK (T_{mb}), equivalent to 591±110 mJy, an order of magnitude stronger than expected from the results of L2011. In order for this feature to be due to CO requires it must be extraordinarily abundant (with the τ=1 surface extending to ~5-6 apparent Pluto radii on the sky). However, since the line is also found to be extremely narrow (about 200 kHz FWHM) the CO must be at a significantly colder temperature (~50 K) than expected, at least for the lower to middle atmosphere.

To simultaneously fit both the reported detections of L2011 and G2011, our understanding of the atmospheric processes at work on Pluto must be seriously deficient. For example, the G2011 line exceeds the limits found for the same CO transition found in [11] by a factor of about 4, implying that the CO abundance increased by an immense amount and through an unknown process over just 10 years. Similarly, given the ratio of CO/N_2 ice on the surface and our knowledge of vapor pressure equilibrium physics, it is extremely difficult to imagine a process which would allow for CO to be more abundant than N_2 in the upper atmosphere

which is a necessary consequence of the G2011 result (E. Lellouch, private communication).

Submillimeter Array Observations. In order to examine the millimeter-band CO(2-1) detection reported in G2011, we have reanalyzed our observations of the Pluto system obtained in 2005 [14], and 2010 [15]. The observations were obtained in order to measure the separated mm-wave surface continuum brightness temperatures of Pluto and Charon, at 0.5" resolution, using the Submillimeter Array (SMA) located just below the summit of Mauna Kea in Hawaii. Fortuitously, both data sets also cover the CO(2-1) transition frequency at 230.538 GHz and can be used to investigate the CO abundance in the atmosphere of Pluto.

The 2005 observations were obtained at 203 kHz resolution, comparable to the FWHM of the spectral feature shown in G2011. The 2010 observations, while obtained under superior conditions, unfortunately were obtained at 812 kHz resolution. This is significantly broader than the G2011 line width, limiting our sensitivity to a narrow feature. Neither data set shows evidence for CO emission. The combined observations (binned at the 2010 resolution) also do not show evidence for CO emission, and we find that our lack of detection is inconsistent with the reported G2011 CO line, though only at the 3-σ level.

In order to further investigate the presence of atmospheric CO on Pluto, we have obtained several short observations of Pluto using the SMA, tuned to the CO(2-1) transition. The spectral resolution covering the line frequency is 101 kHz, a much better match to the narrow emission feature presented in G2011. As of June 1, we have obtained 12.4 hours on Pluto over six separate observations, with subarrays ranging from 5 to 7 antennas. Further, we have an approved project to obtain even more data, which we are hopeful may provide another 10-15 hours on source.

In all the interferometric SMA observations, the continuum (thermal) emission from Pluto and Charon are well-detected. For the new 2013 observations the spatial resolution is such that the pair remain unresolved. Nonetheless, the high SNR detections of the continuum in every single observation assure that the SMA was observing the Pluto system and that the flux scale is set appropriately. Additionally, observations of Titan and/or Neptune obtained for calibration with each data set show characteristic CO lines from their atmospheres (at appropreate frequency offsets due to their relative velocities with respect to Earth at the time of the observations), which verify that the tuning frequency was correctly set for all observations.

At this meeting we will present our initial analysis of all the SMA observations and discuss their implication in the context of the L2011 and G2011 observations of CO in Pluto's atmosphere.

[1] Stern (2008), *Space Sci. Rev. 140*, 3–21. [2] Douté et al. (1999), *Icarus 142*, 421-444. [3] Merlin et al. (2010), *Icarus 210*, 930-943. [4] Yelle & Elliot (1997), in "Pluto and Charon", U.Arizona, 347–390. [5] Sicardy et al. (2003), *Nature 424*, 168-170. [6] Elliot et al. (2007), *AJ 134*, 1-13. [7] Young et al. (1997), *Icarus 127*, 258. [8] Lellouch et al. (2009), *A&A 495*, L17-L21. [9] Schaller & Brown (2007), *ApJ 659*, L61-L64. [10] Young et al. (2001), *Icarus 153*, 148-156. [11] Bockelée-Morvan et al. (2001), *A&A 377*, 343-353. [12] Lellouch et al. (2011) *A&A 530*, L4-L7. [13] Greaves, Helling, & Friberg (2011), *MNRAS 414*, 36-40. [14] Gurwell & Butler 2005, *BAAS, 37*, 743. [15] Gurwell, Butler & Moullet 2010, *BAAS, 42*, 1014.

PLUTO'S CLIMATE MODELED WITH NEW OBSERVATIONAL CONSTRAINTS

C. J. Hansen[1], D. A. Paige[2], [1]Planetary Science Institute, 1700 E. Fort Lowell, Tucson, AZ 85719, cjhansen@psi.edu, [2]University of California, Los Angeles, CA 80024, dap@mars.ucla.edu.

Climate Model Overview: In the cold outer solar system Pluto and Triton have nitrogen atmospheres in vapor pressure equilibrium with surface frosts [1, 2, 3]. Nitrogen sublimes from the pole experiencing spring and condenses on the pole in autumn. This seasonal transport affects the pressure of the atmosphere, the location of polar cap boundaries (thus the albedo seen from the earth), and the surface temperatures. New earth-based observations constrain what we know about the climate and motivate updates to old models in anticipation of the New Horizons flyby.

Hansen and Paige [4, 5] developed a finite-element parameterized thermal model (HP96) that balances and conserves energy across Pluto while tracking locations and quantities of N_2 sublimation and condensation in and out of the atmosphere, maintaining the requirement of vapor pressure equilibrium. As shown in Figure 1 the energy balance equation consists of 5 components:

- solar energy absorbed by the frost and surface: $S_0(1\text{-}A)$, where S_0 is incident solar energy and A is the Bond albedo
- energy emitted from the surface and frost: $\varepsilon\sigma T^4$, where ε is the emissivity of the frost or surface, σ is the Stefan-Boltzmann constant, and T is the temperature
- energy conducted to and from the subsurface: $k\,dT/dz$, where k is the conductivity of the substrate and dT/dz is the thermal gradient
- latent heat of sublimation and condensation: $L\,dm/dt$, where L is the latent heat and dm/dt is the amount of N_2 condensed or sublimed in the time step
- the change in temperature of the frost layer $mC\,dT/dt$, where m is the mass of the frost in kg/m^2, C is the specific heat.

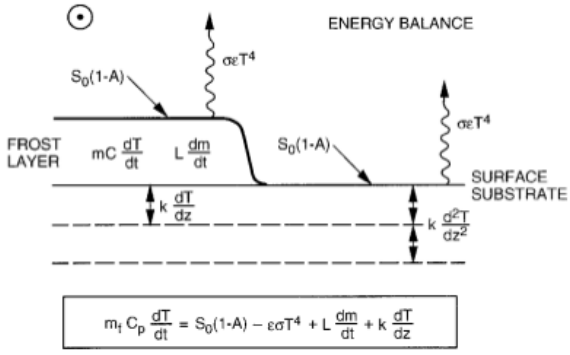

Figure 1. Conservation of energy is modeled for the surface and seasonal layer of frost. Mass is conserved.

New Observational Constraints: When the HP96 model was developed Pluto observations were sparse: a single occultation in 1988, and the albedo map derived from the mutual events provided the primary constraints. In the years since the original results were published many more observations of Pluto have been acquired - most significantly a number of stellar occultations between 2002 and 2011, plus resolved albedo maps from Hubble Space Telescope (HST).

Pluto's obliquity and albedo markings: Planets with obliquities greater than ~54^0 deg have annual insolation greater at the poles than at the equator [6]. Pluto's obliquity is effectively 60^0, which means that a permanent cold trap will be in a zonal band of ice, not polar caps. HST images [7] show NO zonal band which immediately a) eliminates a high thermal inertia surface - on a seasonal time scale higher thermal inertia surfaces require longer to cool or to warm, thus remain closer to their annual average temperatures; b) eliminates cold frost (high albedo with high frost emissivity); and c) eliminates a large abundance of N_2 (more than can be moved around seasonally).

Albedo patterns observed by HST which model output should reproduce include: a bright south pole in 1988 [8, 9]); bright north and south poles in 1994 [7, 10]; and a bright north pole in 2003 (the south pole has rotated out of view) [7].

Occultations. The original HP96 model had only the 1988 stellar occultation for comparison. We now have data from occultations in 2002, 2006, 2007, 2008, 2009, and 2010 [11]. Although the pressures are reported for an altitude of 1275 km, surface pressures can be bracketed as in Young, 2013 [11]. Another constraint to apply is that the atmospheric pressure detected in 2006 was 1.5 to 3 times the pressure in 1988 [12].

Model Runs: The HP96 effort tested a vast expanse of parameter space. This space was narrowed considerably by Young [11], which guided the efforts reported here. Starting with the promising set of conditions identified in Young [11] over 70 runs have been compared to the occultation pressure values to find conditions which reproduce the observations. The next criteria applied was to reproduce the observations of polar caps. The observation of a bright south polar region in 1988 is far more discriminative after the pressue constraints are met than the observations of caps in 1994 and a north polar cap in 2003. Other tests included matching the temperatures derived from IRTF spectra [13] and disk-integrated albedo trends.

Model Results: We now find a rather narrow range of frost albedo / emissivity values that produce atmospheric pressures in the range of the occultations. High albedo coupled with high emissivity produces cold frost and atmospheric pressures that are too low. Lower albedo (e.g. 0.6) combined with low emissivity yield warm frost and temperatures that are too high. The combination of frost albedo/emissivity that gives frost temperatures that produce the right pressure to match the occultations is just (0.8/0.55-0.6) or (0.7/0.7-0.8), for thermal inertias in the range of 18 to 32 J/m^2-sec$^{1/2}$ -K. When the thermal inertia is as low as 10 the frost albedo / emissivity range is further narrowed to (0.8/0.55) or (0.7/0.7). All runs are executed with the surface albedo set to 0.2, surface emissivity set to 1.0, and most have an N_2 inventory of 50 kg/m^2. If the N_2 inventory is too high the frost winds up sequestered in zonal bands; if the N_2 inventory is too low the pressure is too low.

Five cases yielded very good matches to observables. These five had thermal inertias in the 18 to 32 J/m^2-sec$^{1/2}$ -K range. The best match of all to observables however had a thermal inertia = 10 J/m^2-sec$^{1/2}$ -K, and frost albedo = 0.7, frost emissivity = 0.7, shown in Figure 2.

Atmospheric pressure in 2015. It does not appear that the atmosphere will collapse prior to the arrival of New Horizons although pressure is dropping as snow condenses on the south polar cap. The range of pressures predicted for 2015 for the 5 very good cases is 0.3 to 2.5 Pa. The best match predicts 0.14 Pa.

References: [1] Stern A. and Trafton L. (1984) *Icarus, 57, 231.* [2] Elliott J. et al. (1989) *Icarus 77, 148.* [3] Owen et al. (1993) *Science, 261, 745.* [4] Hansen C. and Paige D. (1992) *Icarus, 99, 273.* [5] Hansen C. and Paige D. (1996) *Icarus, 120, 247.* [6] Ward W. (1974) *JGR, 79, 3375.* [7] Buie M. et al (2010) *Ast J, 139, 1128.* [8] Buie M. et al. (1992) *Icarus, 97, 211.* [9] Young E. and Binzel R. (1993) *Icarus, 102, 134* [10] Stern S. A. et al. (1997) *Astron. J., 113, 827.* [11] Young L. A. (2013) *Astroph. J., 766, L22.* [12] Elliot J. L. et al. (2007) *Astron. J., 134, 1.* [13] Olkin, C. et al. (2007) *Astron J., 133, 420.*

Acknowledgements: We thank Leslie Young for preprints of her 2013 paper and numerous insightful discussions of volatile properties vs occultation results.

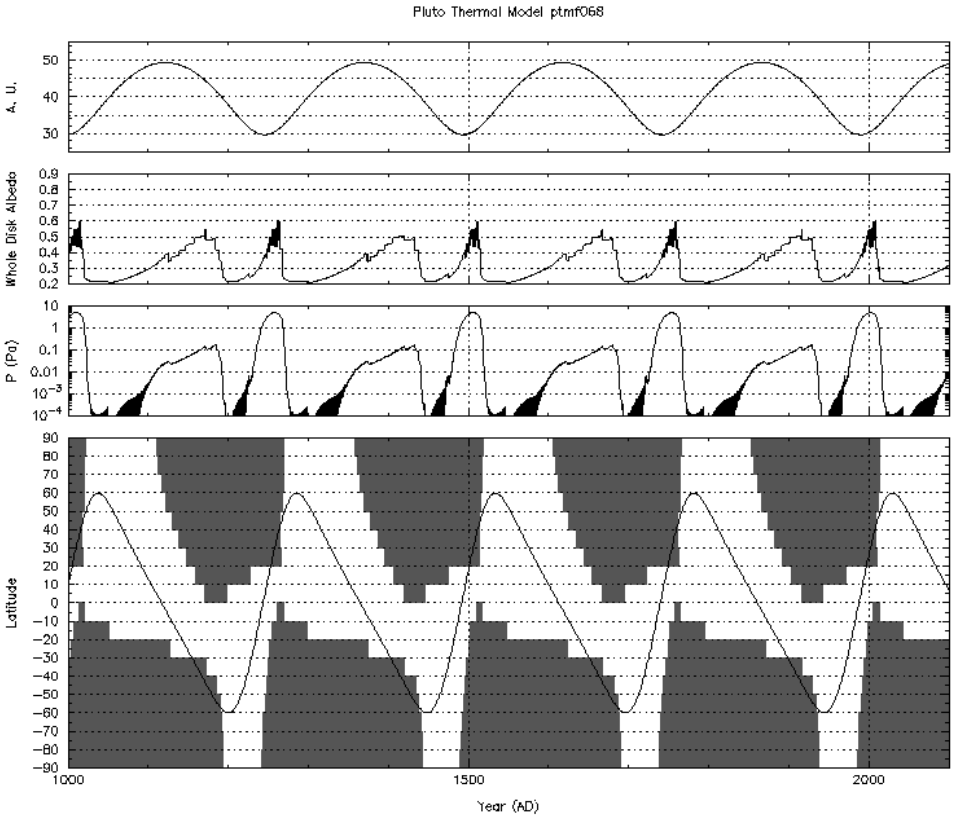

Figure 2. Model output which best matched constraints from observables. The line on the bottom panel shows the latitude of the subsolar point. Stippled areas in this panel are covered in N_2 frost.

THE VENETIA BURNEY STUDENT DUST COUNTER ONBOARD NEW HORIZONS TO PLUTO

M. Horányi, J. Szalay, M. Piquette (Laboratory for Atmospheric and Space Physics, Unoversity of Colorado, 1234 Innovation Drive, Boulder, CO 80303-7814, e-mails: horanyi@colorado.edu; jamey.szalay@lasp.colorado.edu; marcus.piquette@lasp.colorado.edu).

Introduction: The Venetia Burney Student Dust Counter (SDC) is an impact dust detector onboard the New Horizons mission to Pluto (Figure 1). It is designed to map the spatial and size distributions of interplanetary dust particles in order to verify the existence of the predicted structures in the dust disk of our own solar system. To date, six spacecraft have carried dust detectors beyond the asteroid belt: Pioneers 10 and 11 [1], Galileo [2] Ulysses [3], Cassini [4], and New Horizons [4]. SDC provides the first dust measurements beyond 18 AU. Figure 2 shows our data as of April 2012. After the Pluto-Charon fly-by, SDC will continue to measure dust as it transits through the Edgeworth - Kuiper belt. These observations advance our understanding of the origin and evolution of our own solar system and allow for comparative studies of planet formation in dust disks around other stars. SDC is the only experiment to date that was designed, built, and is now operated by students on a deep space mission. It has provided an unparalleled opportunity for about 25 students to learn about space instrumentation. SDC continues to involve an ever changing smaller group of 3 students who operate the instrument and analyze the data, handing over their responsibility to the next 'generation' every few years. SDC could not have been built without the support of the late Dr. Tony Tuzzolino who first designed these types of instruments.

In this talk we will review the scientific motivation, SDC and report on the observations to date. The talk will address our new approach to the analysis and interpretation of the data. We will conclude with a summary of our expectations for the SDC observations during the Pluto encounter, and for the years to follow ecploring the Edgeworth - Kuiper belt.

References: [1] Humes D.H. (1980) *J. Geophys. Res.*, 85:5841–5852. [2] Grün E., *et al.*, (1992) *Space Sci. Rev.*, 60:317–340. [3] Grün E., *et al.*, (1992) *A&AS*, 92:411–423. [3] Srama R., *et al.*, (2004), *Space Sci. Rev.*, 114:465–518. [4] Horányi M., *et al.*, (2008) *Space Sci. Rev.*, 140:387–402. [5] Han D., *et al.* (2011), *Geophys. Res. Lett.*, 38:L24102. [6] Szalay J. *et al.*, (2013) *Earth, Planets and Space*, in press.

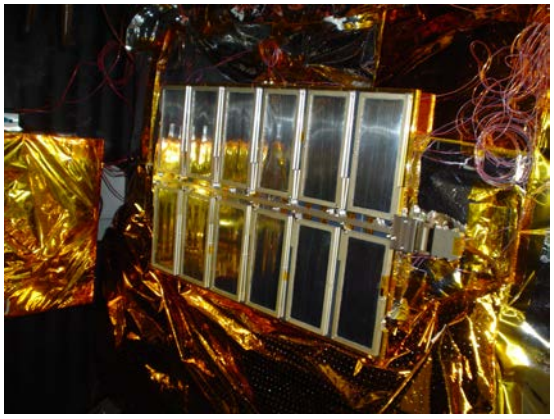

Figure 1. SDC during thermal testing. The detectors have a total of 0.1 m^2 of sensitive area. There are two additional sensors attached to the back to monitor noise events. SDC was designed to measure the mass of interplanetary dust particles in the range of 10^{-12} to 10^{-9} g. Impacts of bigger dust particles are registered without the ability to determine their mass. SDC weighs 1.6 kg and consumes 5.1 watts of average power.

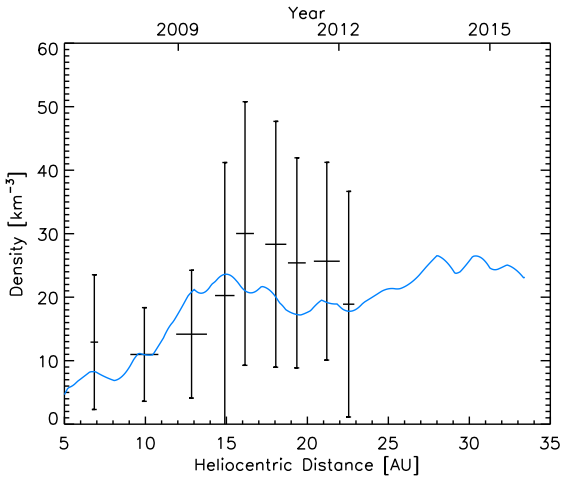

Figure 2. SDC measurements of the dust flux (m >10^{-12} g) through April 2012. The continuous line represents a model prediction out to the Pluto encounter at 33 AU based on SDC and Pioneer 10 data taken between approximately 5 and 18 AU [5,6].

LANDFORMS AND SURFACE PROCESSESES ON PLUTO AND CHARON.

A. D. Howard[1] and J. M. Moore[2], [1]Department of Environmental Sciences, University of Virginia, Charlottesville, VA 22904-4123 (ah6p@virginia.edu), [2]NASA Ames Research Center, MS 245-, Moffett Field, CA 94035-1000.

Introduction: A central axiom of planetary exploration is that you will be surprised by what you see when you get there, particularly with respect to surface landforms and processes. This will likely be doubly true for the Pluto system given its unique orbital configuration and multiple satellites. Nonetheless, our observations of other Solar System objects and known properties of surface components suggests a variety of possible exogenic and endogenic processes. This presentation presents several related quantitative and semi-empirical relationship and expressions for various geological processes under various scenarios of the major surface modifying processes. Processes that can be modeled include impact cratering, lava flow emplacement, aeolian erosion and deposition, weathering, mass wasting, volatile sublimation and precipitation, and fluvial erosion and sedimentation (which at this point cannot be completely ruled out). These processes are quantitatively incorporated in a spatially explicit simulation modeling framework that can be extended to landforms observed within the Pluto system [*1-4*]

Volatile Sublimation and Precipitation: The extreme eccentricity of Pluto's orbit, coupled with the high obliquity, a thin atmosphere, and ices of nitrogen, methane and carbon monoxide indicate that volatile transfer between atmosphere and surface is an important process. Indeed, Pluto has been observed to have brightened in the North Polar region and darken in the southern hemisphere on decadal timescales. Pluto has recently completed its closest approach to the Sun, so that we should observe the waning stages of strong volatile exchanges. A wide variety of landforms are produced by sublimation and precipitation in response to solar heating on Solar System objects [*5*]. During sublimation initially flat surfaces often become pitted by sunlight focusing into depressions producing penitentes [*6*] and accumulation of released dust accumulating in pits or on ridges producing suncups [*5, 7*], although rapid movement of the subsolar point may preclude their development. At high latitudes sublimation under oblique lighting can cause backwasting of volatile-rich equator-facing slopes and less ablation or ice accumulation on flat or pole-facing slopes. This process can be accentuated by accumulation of dust within the ice on the surface, lowering the albedo. The Martian polar troughs in the perrennial ice cap, the swiss-cheese terrain of the south polar CO_2 cap, and the scalloped terrain are examples [*8-13*]. However, given the high obliquity of Pluto, the absence of consistent illumination may disallow formation of large scarps.

Seasonal accumulations of ices may be largely transparent, allowing solar light to warm underlying, lower albedo materials, permitting volatilization of the ice cover from below, a solid-state greenhouse. The released gasses can locally break through the ice cover, producing gas geysers. The subsurface velocities converging to the vent can erode the subsurface and venting particulates that can form surface streaks. The "spiders" on the Martian south polar cap from CO_2 outgassing are an example [*14-16*] as are the N_2 geysers on Triton [*17*].

Sublimation and volatile deposition can be combined with additional processes to produce distinctive landforms. The distinctive "honeycomb" terrain on Hyperion appears to result a modification of an initially cratered surface due to sublimation of dust-rich bedrock coupled with downslope mass wasting [*18*]. A slightly more complicated scenario occurs on Callisto in that H_2O ice liberated from dust-rich bedrock exposed on crater walls by thermal radiation from dark dust accumulations subsequently accumulates on high points (e.g., crater rims) as thick deposits of ice [*3, 19*] (Fig. 1).

A characteristic of several of these sublimation processes is the threshold behavior induced by dust incorporated in ices. The high albedo of pure ices discourages sublimation and encourages deposition. A thin dark-albedo dust cover liberated during sublimation enhances sublimation rates and discourages deposition. This leads to the strong albedo contrasts, e.g., on Iapetus [*20*]. However, accumulated dust will eventually become an insulating cover if not removed by mass wasting or, on Mars, by aeolian erosion.

Mass Wasting: Mass wasting is downslope bulk transport under the influence of gravity. Slow downslope movement produced by the cumulative effect of small near-surface disturbances on loose debris occurs nearly ubiquitously on planetary surfaces, including asteroids. On small objects the diminished force of gravity is compensated by the smaller forces needed to move particles. The disturbing forces can include the direct influence of large to micrometeoritec impacts, indirect effect of impacts due to seismic energy, thermal cycling, and possibly electrostatic forces [*21, 22*]**.** Creep is a diffusive process, reducing relief and rounding sharp surfaces. Larger mass

wasting events include slumps, landslides, and avalanches, and mostly require steep slopes and strong relief. Interior rims of larger impact craters nearly universally exhibit slumping and occasionally larger landslides.

Aeolian Processes: If Pluto (or Charon) ever had a transient dense atmosphere, aeolian bedforms may have been created. Even with a thin atmosphere, as at present, dust ejected into the atmosphere by gas geysers or impacts may be atmospherically transported and preferentially deposited, e.g., in association with volatile precipitation.

Impact cratering: The default planetary surface unaffected by subsequent endogenic or exogenic processes is one saturated by impacts. The presence of Charon and several smaller satellites in orbit around Pluto suggests that impact cratering has likely strongly affected Pluto, possibly generating the addendant satellites by a major collision of proto-Pluto by a similar sized-object (e.g. [*23*]).

Endogenic Processes: Pluto, like Triton, could possibly have been resurfaced at least locally by endogenic processes**.** In addition tensional (graben) and compressional (wrinkle-ridge) deformation, cryogenic volcanism might have modified the surface, as in Fig. 2.

References: [1]. C. J. Barnhart *et al*., (2009), *JGR* **114**, E01003, doi:10.1029/2008JE003122; [2]. A. D. Howard, (2007), *Geomorphol.* **91**, 332-63; [3]. A. D. Howard, J. M. Moore, (2008), *GRL* **35**, L03203, doi:10.1029/2007GL032618; [4]. A. D. Howard, J. M. Moore, (2011), *JGR* **116**, E05003, doi:10.1029/2010JE003782; [5]. N. Mangold, (2011), *Geomorph.* **126**, 1-17; [6]. D. E. J. Hobley *et al.*, (2013), *LPSC 44*, Abstr 2432; [7]. M. C. Malin, K. S. Edgett, (2001), *JGR* **106**, 23429-570; [8]. A. D. Howard, (1978), *Icarus* **34**, 581-99; [9]. A. D. Howard *et al.*, (1982), *Icarus* **50**, 161-215; [10]. S. W. Squyres, (1979), *Icarus* **40**, 244-61; [11]. S. Byrne, A. P. Ingersoll, (2003), *Science* **299**, 1051-53; [12]. P. C. Thomas *et al.*, (2005), *Icarus* **174**, 535-59; [13]. A. Lefort *et al.*, (2010), *Icarus* **205**, 259-68; [14]. H. H. Kieffer, (2007), *JGR* **112**, Article Number E08005; [15]. H. H. Kieffer *et al.*, (2006), *Nature* **442**, 793-96; [16]. S. Piqueux, P. R. Christensen, (2008), *JGR* **113, doi:**. 10.1029/2007je003009; [17]. R. L. Kirk *et al.*, in *Neptune and Triton*, D. P. Cruikshank, Ed. (Univ. of Ariz. Pr., Tucson, 1992); [18]. A. D. Howard *et al.*, (2012), *Icarus* **220**, 268-76; [19]. J. Moore, M., e. al., (1999), *Icarus* **140**, 294-312; [20]. J. R. Spencer, T. Denk, (2010), *Science* **327**, 432-5; [21]. A. Mantz *et al.*, (1984), *Icarus* **167**, 197-203; [22]. P. Thomas, J. Veverka, (1980), *Icarus* **42**, 234-50; [23]. R. M. Canup, (2011), *Astr. J.* **141**, art. 35.

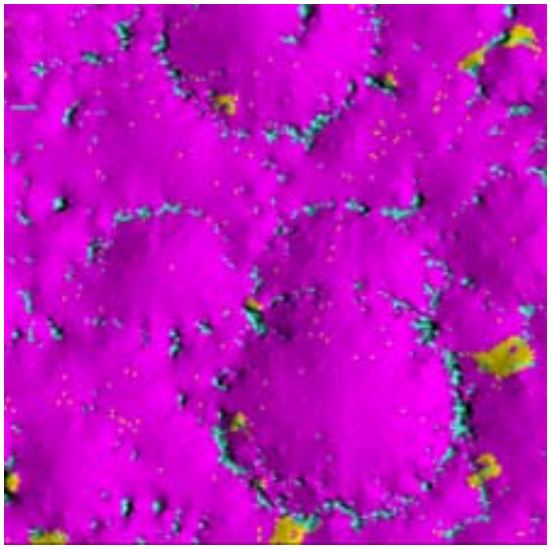

Fig. 1. Simulated landscape on Callisto [3]. Purple is dust-covered surface, yellow is exposure of dusty ice bedrock, blue is deposits of water ice on upland areas, mostly crater rims.

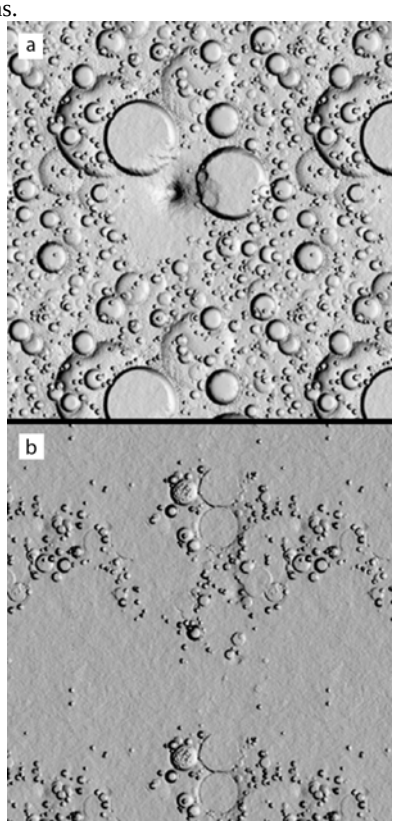

Fig. 2. Simulated cryovolcanic inundation of a cratered landscape. (a) by viscous flows producing edifice; (b) by less viscous flows from multiple sources.

Calibration of the Ralph/MVIC Camera

C.J.A. Howett[1], C. Olkin[1] and K. Ennico[2], [1]Southwest Research Institute, 1050 Walnut Street, Boulder, CO, USA, howett@boulder.swri.edu. [2] NASA Ames Research Center, Moffett Field, CA, USA.

Introduction: The Ralph instrument on the Pluto-bound New Horizons spacecraft is a spectral imager with a single telescope and two focal planes: MVIC (Multi-spectral Visible Imaging Camera) and LEISA (Linear Etalon Imaging Spectral Array) [1]. MVIC uses seven separate CCD arrays, with a resolution of 19.8 μrad/pixel, to cover from near-infrared to visible wavelengths. Three of the detectors are panchromatic (400 to 975 nm), whilst the remaining four have filters to narrow down the wavelengths detected: blue (400 to 550 nm), red (540 to 700 nm), near-infrared (780 to 975) and a methane band filter (860 to 910 nm). All of the filtered and two of the panchromatic CCDs are 5024x32 pixel array operated in a Time Delay and Integrate (TDI) mode. In this mode the total signal to noise of an image is increased by coadding the signal as the image moves across each of the 32 pixels in the scan direction. The final detector array is a 5024x128 pixel panchromatic Frame Transfer (FT Pan) detector, which takes a single image but prior to readout transfers the whole image to a shielded CCD. This FT Pan, due to its larger field of view and simpler operational mode, is the focus of this preliminary study into the calibration of the image quality (PSF/Point Spread Function) calibration of the MVIC instrument.

Calibration Process: To minimize smearing short exposure images are used in this calibration (0.5 – 1 s). Twenty five short exposure MVIC FT Pan image cubes, corrected for flat field and geometric distortion, are currently available; of these five images have stars above the sky noise level observed in consecutive images (stars that fulfill this criteria are henceforth known as confirmed stars). Details of the calibration images are given in Table 1.

Image cube identifier (mpf_filename_0x539)	Date and mid-observation time (UTC)	Exposure Time (s)	# Images	Image Ra/Dec (°)	# Stars
0086353134	15 Oct 2008 05:07:07	1.0	3	267/-33	7
0086420815	15 Oct 2008 23:55:11	0.5	6	346/-7	6
0139570615	23 June 2010 03:45:10	0.5	6	2/-1	8
0139808935	25 June 2010 21:57:10	1.0	5	2/-1	55
0200906425	2 June 2012 01:28:34	1.0	2	270/-15	125

Table 1 – MVIC FT Pan images used for calibration.

The center location of each confirmed star was determined by fitting them to a 2-D Gaussian, whose center was assumed to be the star location. For each confirmed star the FWHM was determined using M. Buie's IDL basphote routine [2]. The background sky value was set to 25±3 DN/pixel and a range of reasonable aperture radii (0.5 to 3 pixels) were iterated over to provide the FWHM error estimate.

Preliminary Results: Figure 1 shows how the FWHM is observed to vary with position on the detector array, for all confirmed stars in all of the images. It shows no discrete area on the detector has notably higher FWHMs. Figure 2 shows the FWHM of each confirmed star, in each image, along with its associated error value. The mean FWHM is 1.36±0.61 pixels, which agrees with pre-launch values [1]. Next steps are to repeat this exercise for the other six MVIC channels

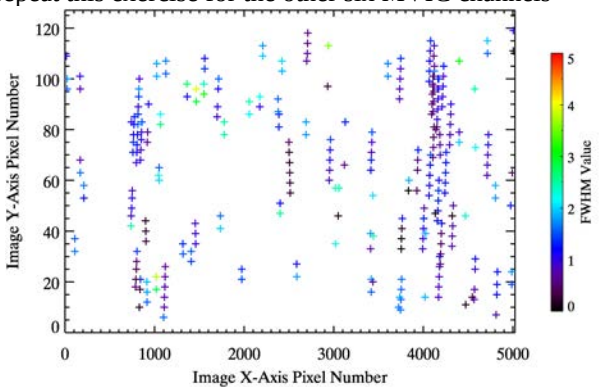

Figure 1 – FWHM of all confirmed stars as a function of location in the detector array.

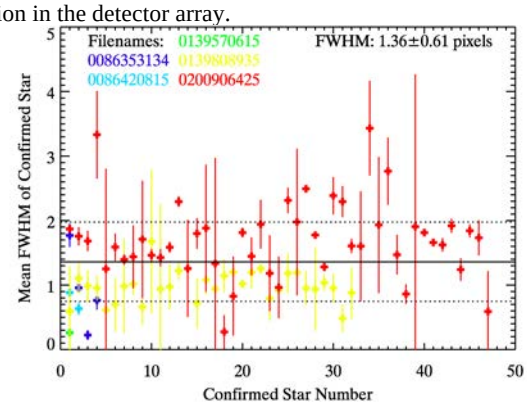

Figure 2 – FWHM and associated error of all confirmed stars in all images.

References:

[1] Reuter, D.C., et al. (2008) *Space Sci. Rev*, *140*:*129-154*.

[2] Buie, M. (2013) http://www.boulder.swri.edu /~buie/

THREE NEW STUDIES OF THE SPECTRA AND CHEMISTRY OF PLUTO ICES

R. L. Hudson[1], P. A. Gerakines[1], and M. J. Loeffler[1], [1]Astrochemistry Laboratory, NASA Goddard Space Flight Center, Greenbelt, MD 20771 USA (reggie.hudson@nasa.gov).

Introduction: The data returned by New Horizons instruments will reveal new details of chemical composition for the Pluto system. Laboratory measurements will play an important role in the interpretation of such data, just as they have going back to at least the original detections of solid methane (CH_4) by Pilcher et al. [1]. Since ionizing radiation will influence the composition of Pluto's surface, laboratory studies of radiation chemical effects also are of interest [2,3].

New Work: Our research group recently has initiated three separate projects related to frozen CH_4 and other ices relevant to Pluto, and in the process we have uncovered a few surprises. Here we highlight three areas, all concerning frozen CH_4.

1. Infrared spectroscopy of low-temperature ices. New mid- and near-IR spectra are being recorded at temperatures under 50 K. As an example of our new data, the figure below shows near-IR spectral changes of CH_4 that have been described in the literature, but seldom shown with this clarity. All such spectra may be important for understanding Kuiper-Belt chemistry, yet much less is known about the data for frozen CH_4 at the lower temperatures as compared to the spectra for higher-temperature ices [4]. In most cases, peak absorptivities and optical constants (n, k) are either unknown or available only in selected regions, and not in an electronic format, a situation we intend to remedy. Interestingly, and in contrast to the usual trend, we find that some our newest IR measurements agree best with some of the oldest work in the literature and somewhat less so with work published during the past 20 years.

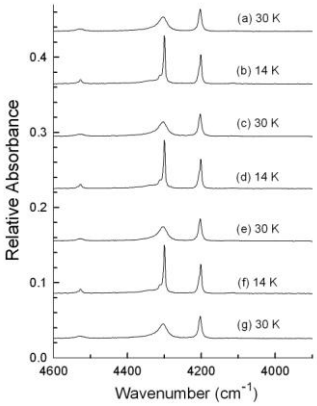

Figure 1. A sequence of near-IR spectra showing the reversibility of solid-phase conversions of crystalline CH_4 with temperature. The sample shown was prepared by slowly freezing CH_4 gas at 30 K.

2. Radiation effects on low-temperature ices. We also have reinvestigated the influence of ionizing radiation on the physical state (phase) and chemistry of methane ices. Nearly all such measurements in the past have been made with the goal of understanding interstellar ices, which are much lower in temperature than Pluto's surface. Accordingly, in our new work we have focused on chemical and physical changes of frozen CH_4 at temperatures more applicable to the Pluto system.

3. Vacuum-uv spectroscopy of ices. Our third new project concerns a spectral region often neglected by laboratory astrochemists, the vacuum ultraviolet. New measurements are in progress for CH_4 and other Pluto ices with a focus on the 115 – 240 nm region. Spectra are recorded as a function of temperature and ice composition, and optical constants are calculated.

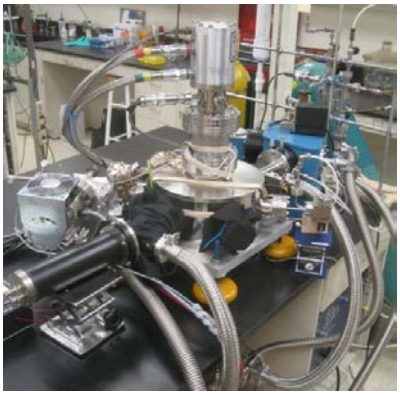

Figure 2. Equipment used in our laboratory for studying the far-uv spectra and optical constants of CH_4 and other ices.

References: [1] Cruikshank D. P., Pilcher C. B., and Morrison D. (1976) *Science, 194*, 835–837. [2] Stern S. A., Trafton L. M., and Gladstone G. R. (1988) *Icarus, 75*, 485–498. [3] Hudson R. L.. (2008). Chapter in *The Solar System Beyond Neptune*, University of Arizona Press. [4] de Bergh C. et al. (2008). Chapter in *The Solar System Beyond Neptune*, University of Arizona Press.

Acknowledgements: NASA funding through the Outer Planets Research and Cassini Data Analysis programs is acknowledged. RLH and PAG received partial support from the NASA Astrobiology Institute through the Goddard Center for Astrobiology.

$^{14}N^{15}N$ DETECTABILTY IN PLUTO'S ATMOSPHERE

Kandis Lea Jessup[1,*4] ([1]Southwest Research Institute, Boulder CO 80302, email: jessup@boulder.swri.edu) G. R. Gladstone[2] [2]Southwest Research Institute, San Antonio TX 80302, email: RGladstone@swri.edu), A. N. Heays[3,4] ([3] Leiden Observatory, Leiden University, P.O. Box 9513, 2300 RA Leiden, The Netherlands, email: heays@strw.leidenuniv.nl), S. T. Gibson[4] ([4]Research School of Physics and Engineering, The Australian National University, Canberra, ACT 0200, Australia, email: Stephen.Gibson@anu.edu.au), B. R. Lewis[4] (email: Brenton.Lewis@anu.edu.au), G. Stark[5] ([5]Department of Physics, Wellesley College, 106 Central Street, Wellesley, MA 02481, email: gstark@wellesley.edu).

Introduction: The study of the evolution of Pluto's atmosphere is tantalizing because it has the potential to inform our understanding of the formation and evolution of the solar nebula and other solar system atmospheres. Pluto's atmosphere is known to be predominantly composed of N_2 gas, and the measurement of the $^{15}N/^{14}N$ ratio within Pluto's atmosphere is a critical parameter needed for investigating Pluto's atmospheric evolution.

Absorption Cross-section Data: The most straightforward way of determining the $^{15}N/^{14}N$ ratio in Pluto's atmosphere is via spectroscopic observation of the $^{14}N^{15}N$ gas species. Recently, the 85-90 nm absorption behavior of the $^{14}N_2$ and $^{14}N^{15}N$ isotopologues has been calculated [1-4] Though the peak magnitudes of the $^{14}N_2$ and $^{14}N^{15}N$ absorption bandheads are similar, the wavelength of the peak $^{14}N^{15}N$ and $^{14}N_2$ bandheads are offset. Thus, there are multiple wavelengths where the magnitude of the $^{14}N^{15}N$ absorption cross-section is significantly larger than that of the $^{14}N_2$ species (Fig. 1). Consequently, the depth of absorption achievable at these wavelengths is higher for an atmospheric model that includes both the $^{14}N_2$ and $^{14}N^{15}N$ species than one that does not— and detection of the $^{14}N^{15}N$ species should be possible for a specific range of $^{14}N^{15}N$ concentrations, provided the spectral resolution of the observations is smaller than the 4.5-5Å wide N_2 isotopologue absorption bands.

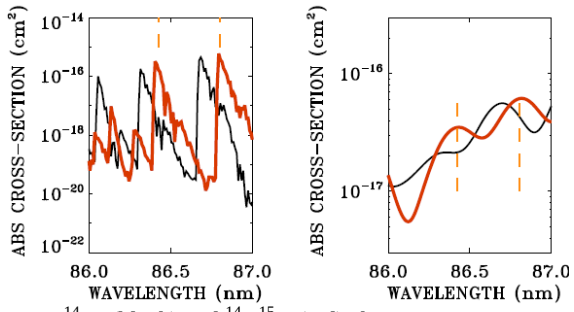

Fig. 1 $^{14}N_2$ (black) and $^{14}N^{15}N$ (red) absorption crossection calculated at 0.1 Å sampling (left) and convolved to 3.0 FWHM spectral resolution (right).

Atmospheric Model: We use the most recent N_2 isotopologue calculations [1] and the atmospheric density profiles resulting from photochemical models developed by Krasnopolsky and Cruikshank [5] to predict Pluto's transmission signature per altitude. We characterize the detectability of the isotopic absorption signature per altitude assuming $^{14}N^{15}N$ concentrations ranging from 0.1 to 2% of the $^{14}N_2$ density and instrumental spectral resolutions ranging from 0.5 to 3 Å.

Predictions: The New Horizons Mission will be able to obtain high S/N, 2.7-3.5 Å FWHM 84-100 nm spectral observations of Pluto using the ALICE spectrograph [6]. Our calculations indicate that for an observation with 3 Å spectral resolution, optical depth of unity is attained at ~1100-1300 km for most of the key $^{14}N^{15}N$ absorption bands. Based on our model of the atmospheric transmittance per altitude and the specifications of the NH/ALICE instrument we predict that the S/N obtainable by ALICE at 1100-1300 km within the key $^{14}N^{15}N$ bands is ~18-22. We presume the percent error in the observed spectrum per wavelength must be a minimum of 25% lower than the increase in absorption expected at the wavelength of the isotope bands. In this case, NH will be able to successfully detect $^{14}N^{15}N$ in Pluto's atmosphere if the $^{14}N^{15}N$ gas density is sufficient to produce an absorption depth ~7% or more greater than the absorption depth attainable if $^{14}N_2$ is the only N_2 isotopologue present in the atmosphere. Our calculations indicate that this level of absorption should be recorded in 3 Å spectral observations of Pluto's atmosphere at the τ =1 level of the atmosphere if the $^{15}N^{14}N$ concentration is ~ 0.65% or greater. Thus, even the lack of $^{14}N^{15}N$ detection would place a firm upper limit on the $^{15}N/^{14}N$ ratio within Pluto's atmosphere.

References:

[1] Heays, A. N., Lewis, B. R., Stark, G., Yoshino, K., Smith, P. L., Huber, K. P. and K. Ito,2009. *J. Chem. Phys*. **131**, 194308. [2] Lewis, B. R., Gibson, S. T., Zhang, W., Lefebvre-Brion, H., & Robbe, J.-M., 2005. *J. Chem. Phys*. **122**, 144302. [3] Lewis, B. R., Heays, A. N., Gibson, S. T., Lefebvre-Brion, H., & Lefebvre, R., A 2008. *J. Chem. Phys*. **129**, 164306 [4] Haverd, V. E., Lewis, B. R., Gibson, S. T., & Stark, G., 2005. *J. Chem. Phys*. **123**, 214304 [5] Krasnopolsky, V. A. and D. P. Cruickshank 1999. *JGR* **104**, 21979-21996. [6] Stern, S.A., Slater, D. C., Scherrer, J., Stone, J., Dirks, G., Versteeg, M. Davis, M. Gladstone, G. R., Parker, J. W., Young, L.A. and Siegmund, O.H.W, 2008. *Space Science Reviews* **140**, 155-187.

ACCRETION OF KUIPER BELT OBJECTS

A. Johansen[1], [1]Lund University, Box 43, 22100 Lund, Sweden (e-mail anders@astro.lu.se).

The formation of km-sized planetesimals from smaller cm-dm sized pebbles faces major difficulties in the traditional coagulation scenario [1]. Such particles do not stick well and very quickly drift towards the star to sublimate in the inner nebula [2]. I will present an alternative scenario where overdense regions of particles collapse under their own gravity to form massive 1000-km-scale planetesimals [3,4]. The overdensities are seeded by hydrodynamical streaming instabilities arising in the coupled motion of gas and particles. New computer simulations that include particle collisions show the perseverance of planetesimal formation by this route [5]. Planetesimal masses are relatively independent of the computational resolution and the simulations reveal a characteristic planetesimal size that increases with distance from the sun. The resulting planetesimal sizes agree well with the observed largest bodies residing in the asteroid and Kuiper belts. The time-scale for forming even the largest Kuiper belt objects by this route is dominated by the formation time of the pebbles; the concentration and contraction phases take less than 1000 years.

I will critically compare the streaming instability scenario with the traditional coagulation scenario for the formation of Kuiper belt objects [6].

[1] Blum J. and Wurm G. (2008), Annual Review of Astronomy and Astrophysics, 46, 21-56. [2] Weidenschilling S. J. (1977), MNRAS, 180, 57-70. [3] Johansen A., Oishi J. S., Mac Low M.-M., Klahr H., Henning Th. and Youdin A. N. (2007), Nature, 448, 1022-1025. [4] Johansen A., Youdin A. N. and Mac Low M.-M. (2009), ApJ, 704, L75-L79. [5] Johansen A., Youdin A. N. and Lithwick Y. (2012), A&A, 537, A125 (17 p). [6] Kenyon S. and Bromley B. (2004), ApJ, 128, 1916-1926

Formation of High Mass Hydrocarbons on Kuiper Belt Objects

Brant Jones[1,2] and Ralf I. Kaiser[1,2], [1]Department of Chemistry, University of Hawaii at Manoa, 2545 McCarthy Mall, Bilger 301 Honolulu, HI 96822, [2] W. M. Keck Research Laboratory in Astrochemsitry, University of Hawaii, Honolulu, HI, 96822.

Introduction: We present recent results from the newly established W.M. Keck Research Laboratory in Astrochemistry regarding the formation of high molecular weight (~ C_{22}) hydrocarbons starting from pure simple hydrocarbons ices upon interaction of these ices with ionizing radiation; methane (CH_4), ethane (C_2H_6), propane (C_3H_8) and *n*-butane (C_4H_{10}). Specifically, we have utilized for the very first time a novel application of reflection time-of-flight mass spectrometry (ReTOF) coupled with soft vacuum ultraviolet photoionization to observe the nature of high mass hydrocarbons as a function of their respective sublimation temperature. The Kuiper Belt is estimated to consist of over 70,000 icy bodies which extend beyond the orbit of Neptune at 30 AU. Furthermore, simple hydrocarbons such as methane and ethane have been detected on the surfaces of these icy bodies. In particular, evidence of pure methane has been detected on the surfaces of Eris[1], Quaoar[2], and Pluto[3] along with ethane being tentatively assigned on Quaoar, Pluto, and Orcus[2]. The surfaces of these bodies have undergone 4.5 Gyr of chemical processing due to ionizing radiation from the solar wind and Galactic Cosmic Radiation. Our research has been focused on trying to understand how these ices have evolved over the age of our solar system by simulating the chemical processing via ionizing radiation (keV H^+, He^{++} and Lyman-α photons) in an ultrahigh vacuum chamber coupled with a variety of optical analytical spectroscopies (FT-IR, Raman, and UV-Vis) along with gas phase mass spectroscopy. In particular, results from ReTOF spectroscopy of the subliming products synthesized from the energetic processing of amorphous methane ice indicate that over 50 molecules with distinct m/z ratios and sublimation temperatures are formed easily under conditions relevant to the outer solar system environment. Despite, the numerous previous experimental investigations probing the effect of ionizing radiation on simple hydrocarbon astrophysical ice analogs, our results suggest that there is still a vast unknown molecular composition formed upon exposure of these ices to ionizing radiation.

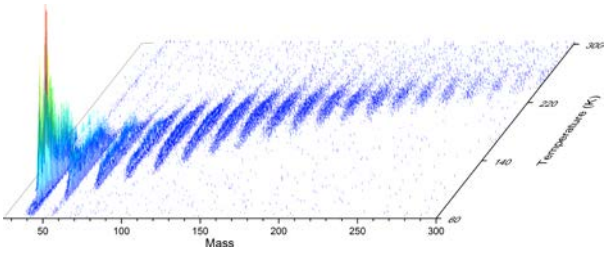

Reflection Time-of-Flight spectrum as a function of temperature of the newly formed hydrocarbon species from the energetic processing of a pure amorphous methane ice taken at a photoionization energy of 10.5 eV.

References:

[1.] Merlin, F., A. Alvarez-Candal, A. Delsanti, S. Fornasier, M.A. Barucci, F.E. DeMeo, C.d. Bergh, A. Doressoundiram, E. Quirico, and B. Schmitt, The Astronomical Journal, 2009. 137(1): p. 315.

[2.] Brown, M.E., Annual Review of Earth and Planetary Sciences, 2012. 40(1): p. 467-494.

[3.] Douté, S., B. Schmitt, E. Quirico, T.C. Owen, D.P. Cruikshank, C. de Bergh, T.R. Geballe, and T.L. Roush, Icarus, 1999. 142(2): p. 421-444.

DYNAMICAL SIMULATIONS OF THE DEBRIS DUST ENVIRONMENT OF THE PLUTO SYSTEM

D. E. Kaufmann, S. A. Stern
Southwest Research Institute, Boulder, CO, USA

Introduction: On January 19, 2006, the New Horizons spacecraft was launched from Cape Canaveral Air Force Station in Florida towards its rendezvous with the Pluto system. Its closest approach to Pluto is projected to occur on July 14, 2015. In addition to Charon, four smaller moons of Pluto have been discovered to date: Nix, Hydra, P4 and P5. The presence of these additional small moons has raised concern about the possibility of rings or other debris structures that can pose impact hazards to New Horizons.

Synopsis: In this report we describe numerical simulations of the dynamical structure of the debris dust environment of the Pluto system as one part of efforts to understand where hazards may lie at Pluto. We model the dust as particles of mass $3x10^{-4}$ g and density 1 g/cm^3 (the smallest, but likely most prevalent, particle that would be lethal to New Horizons). We dynamically evolve the Pluto system members and dust particle ensembles using the RMVS3 integrator [1], modified to include radiation pressure and P-R drag, and remove particles from the integrations if they escape the system or are accreted by a system member. The Sun is explicitly included in the simulations in order to model the effects of solar tides. We report the results of two classes of simulations: (a) systematic explorations of the full orbital element parameter space available to the dust particles, and (b) models of dust particle ensembles ejected from the smaller moons of the Pluto system.

References:

[1] Levison, H. F. and Duncan, M. J. (1994) *Icarus*, *108*, 18

FORMATION OF PLUTO'S LOW MASS SATELLITES.

S. J. Kenyon[1] and B. C. Bromley[2], [1]Smithsonian Astrophysical Observatory, 60 Garden Street, Cambridge, MA 02138 (skenyon@cfa.harvard.edu), [2]Physics Department, University of Utah, 201 JFB, Salt Lake City, UT 84112 (bromley@physics.utah.edu).

Abstract: Motivated by the New Horizons mission, we consider how Pluto's small satellites - currently P5, Nix, P4, and Hydra - grow in debris from the giant impact that forms the Pluto-Charon binary or in solid material captured from the protoplanetary debris disk. If the satellites have masses close to their minimum masses, our analysis suggests that capture of material into a circumplanetary or circumbinary debris disk is a viable mechanism for satellite formation. If the satellites are more massive, they probably form in debris from the giant impact. After the impact, Pluto and Charon accrete some of the debris and eject the rest from the binary orbit. During the ejection, high velocity collisions among debris particles produce a collisional cascade, leading to the ejection of some debris from the system and enabling the remaining debris particles to find stable orbits around the binary. Our numerical simulations of viscous diffusion, coagulation, and migration show that collisional evolution within a ring or disk of debris leads to a few small satellites orbiting Pluto-Charon. These simulations are the first to demonstrate migration-induced mergers within a particle disk. The final satellite masses correlate with the initial disk mass. More massive disks tend to produce fewer satellites. For the current properties of the satellites, our results strongly favor initial debris masses of 3-10 x 10^{19} g and current satellite albedos A = 0.4-1. We also predict an ensemble of smaller satellites with radii of 1-3 km or less and very small particles with radii of 1-100 cm and optical depth $\tau < 10^{-10}$. These objects should have semimajor axes outside the current orbit of Hydra.

Methods: To explore satellite formation in the Pluto-Charon system, we derive simple analytic estimates for the evolution of debris and then examine results from several types of numerical simulations. For the formation and migration of satellites in a circumbinary disk of particles, we use our hybrid coagulation + n-body code Orchestra [1,2]. To investigate the radial evolution of particles in a disk around an expanding binary, we develop a new diffusion code within Orchestra [3]. Currently, we consider diffusion, satellite growth, and satellite migration in distinct calculations. In the future, we plan to treat these processes in a single calculation.

Results: Our analytic results favor satellite formation in debris from a giant impact. Capturing debris from collisions of primordial KBOs in the Hill sphere of Pluto-Charon appears to be too inefficient. Once Pluto-Charon is surrounded by a disk of debris, satellite formation occurs on time scales of 10^3 to 10^5 yr. Satellites form more rapidly closer to the binary.

Figure: Predicted system configuration for the Pluto–Charon system. The Pluto–Charon binary (represented by the two largest white disks), the four small satellites – P5, Nix, P4, and Hydra (represented by the four small white disks), and three smaller satellites (represented by the green disks) lie within an extended ensemble of solid particles shown as small blue dots. This configuration is the result after twenty years of a computer simulation with two million massless tracer particles surrounding the known and predicted moons. On this short time scale, the small satellites clear out most of the tracers along their orbits. On much longer time scales, satellites will clear tracers from a larger fraction of their orbits.

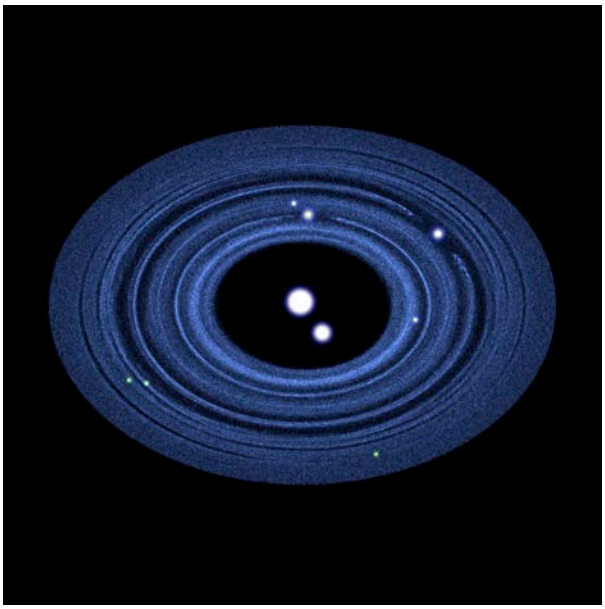

References:

[1] Kenyon, S. J. & Bromley, B. C. (2008) *ApJS, 179,* 451-483. [2] Bromley, B. C. & Kenyon, S. J. (2013) *ApJ, 764,* id 192 (19pp), [3] Kenyon, S. J. & Bromley, B. C. (2013*) arXiv, 1303.0280*.

Additional Information: The full text of the paper is on the arXiv at http://arxiv.org/abs/1303.0280

SIMULATION OF EFFECT OF CHARON ON ESCAPING MOLECULES IN THE PLUTO-CHARON SYSTEM.

N. S. Knerr,[1] D. B. Goldstein[2], L. M. Trafton[3] and P. L. Varghese[5]. [1]University of Texas at Austin (nknerr@utexas.edu), [2]University of Texas at Austin (david@cfdlab.ae.utexas.edu), [4]University of Texas at Austin (lmt@astro.as.utexas.edu), [5]University of Texas at Austin (varghese@mail.utexas.edu)

Introduction: Recent work by authors such as Strobel [1] and Erwin et al. [2] have established atmospheric escape of N_2 molecules with a flux of ~$2x10^{27}$ molecules/sec.

The present work attempts to characterize the behavior of the fastest molecules escaping from the atmosphere under the combined influence of Pluto and Charon. It differs from previous work in that it uses a rotating frame and hence structure among the escaping particles is visible [3].

Model Formation: As the focus of this work is the contribution of the fastest particles in the outermost region of the atmosphere, a free-molecular model is used with a rotating continuum solid-body model for the inner atmosphere.

Because the eccentricity of the Pluto-Charon orbit is small [4], we approximate the Charon orbit around Pluto as a circle. When fixing the frame of reference to rotate with Pluto's surface, the fact that Pluto and Charon are tidally locked implies that Pluto and Charon appear fixed in space.

Velocity Variation Results: The particles are initialized at the exobase at a uniformly random position with a radial velocity and uniform speed (as viewed in the Pluto-fixed frame). At low initial velocities, some particles are thrown outwards and some might escape, but the majority remains bound and increase the density field between the planets.

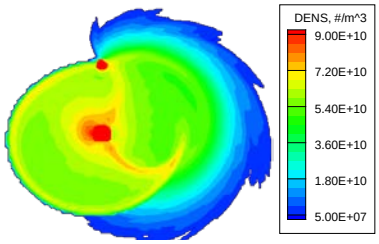

Unsteady density field at one instant in the orbital plane for 85% of the system escape velocity.
Notice: All images are in a Pluto-fixed reference system

However, if we increase the velocity and assume a steady supply of particles from the exosphere then we find the single-velocity particles form a forked tail at steady state in the orbital plane.

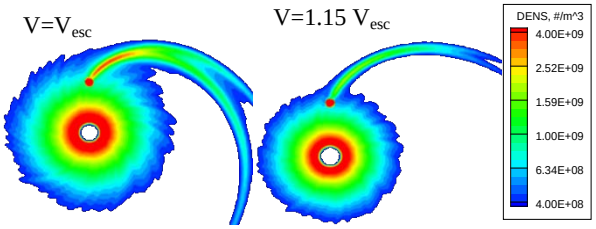

Steady density field in the orbital plane

As the velocity increases, the tail becomes narrower, weaker and peaks farther from Charon.

Single-Velocity Tail Formation: The formation of this tail is due to the disturbance of Charon on the molecular trajectories. When viewed as a wave of positions at some time after being released from the exobase, the trajectories appear to be a spherical shell.

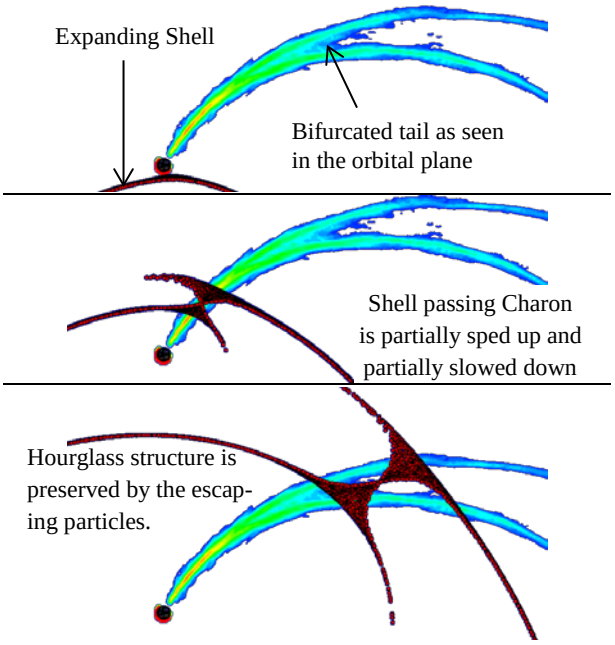

Illustration of tail formation from trajectories

Tail Shape: Particle paths cross as they pass Charon and this causes out-of-plane spreading. The crossing creates a region of high density immediately following Charon and the spreading and differences in the trajectories passing close to Charon implies creates a diamond shape.

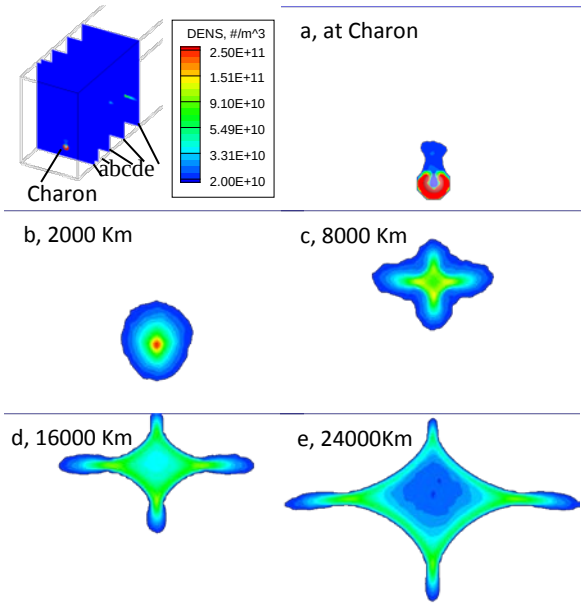

Single velocity ($V=V_{esc}$) tail viewed perpendicular to the plane of orbit and formation of diamond pattern

Notice that the forked shape tail seen in the orbital plane corresponds to the top and bottom in the diamond and causes a concentration of density in the plane of orbit—not only will other velocity classes share the same space but there are two tails per velocity class in the orbital plane.

Steady System Results: To visualize a composition of velocity classes, particles are generated uniformly over the surface of the exobase of Pluto with a velocity distribution obeying a Maxwellian distribution in speed and direction. The result is a continuous tail of elevated density following Charon. When examining the density above or below the orbital plane, the tail is preserved but becomes weaker with distance:

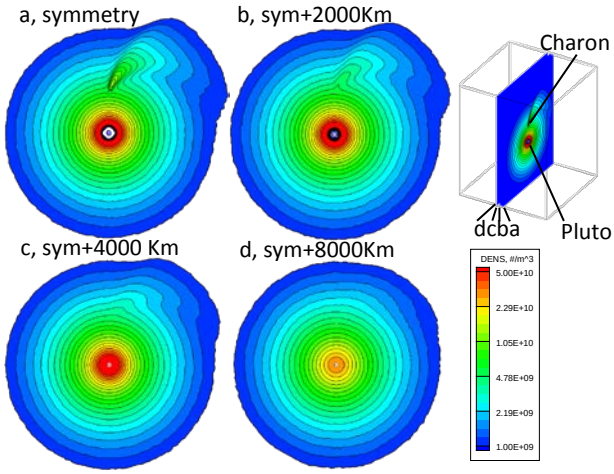

Steady density field in four places parallel to the orbital plane with Maxwellian speeds from V_{esc} to $5V_{esc}$

Examining the plane perpendicular to the orbital plane, it is clear that the tail is a disturbed region surrounding the orbital plane but the disturbance is peaked and much taller than wide.

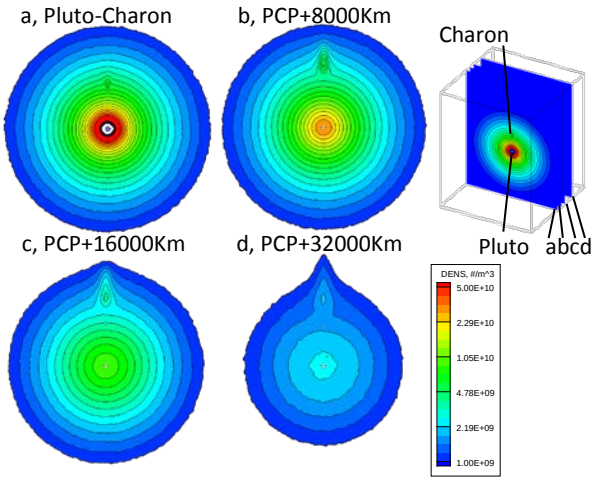

Steady density field perpendicular to the orbital plane. With displacements from the Plane Containing Pluto (PCP)

As is clear, Charon has an effect on the structure formed by escaping particles. It is worth reiterating, however, that this structure will rotate with the system so if the system is imaged in an inertial frame for multiple rotations then the structure will vanish and be replaced with a rotationally-symmetric outer atmosphere.

References: [1] D. F. Strobel (2008), *Icarus*, *193*, 612-619. [2] J. Erwin, O. J. Tucker, and R. E. Johnson (2012) , *arXiv*, *1211.3994*. [3] O. J. Tucker, J. T. Erwin, J. I. Deighan, A. N. Volkov, R. E. Johnson (2012), *Icarus*, *217*, 408-415. [4] Williams, D. R. *nssdc.gsfc.nasa.gov*.

PLUTO'S PHOTOCHEMISTRY: COMPARISON WITH TRITON AND TITAN.

Vladimir A. Krasnopolsky, Department of Physics, Catholic University of America, 620 Michigan Avenue, N. E., Washington, DC 20064, vlad.krasn@verizon.net.

Introduction: There are three bodies with N_2/CH_4 atmospheres in the Solar System: Titan, Triton, and Pluto. However, Titan's atmosphere exceeds that of the Earth while those of Triton and Pluto are of a few tens μbars. This huge difference is caused by the position of Titan at 10 AU with the surface temperature T_S = 94 K and almost all N_2 and CH_4 in the gas phase. Triton and Pluto are at 30 AU with $T_S \approx 40$ K, and their tiny atmospheres are in equilibrium with ices of these species. If Titan could be moved to 30 AU, its atmosphere would have been similar to those of Triton and Pluto. Titan and Triton have been studied by spacecraft; some lessons from their studies may be helpful for Pluto.

Parent Species (N_2, CH_4, and CO): Recently observed abundances of CH_4 and CO are compared with those adopted in photochemical models in Table 1. Overall, the agreement is good and the model assumptions are reasonable.

Table 1.
Observed mole fractions of CH4 and CO on Triton and Pluto and those in photochemical models.

	f_{CH4}[a]	f_{CO}	CO/CH4
Triton, L10	$\sim 2 \times 10^{-4}$	$\sim 7 \times 10^{-4}$	3.7
Triton, KC95	10^{-4}	3×10^{-4}	3
Pluto, L11	$0.6^{+0.6}_{-0.3}$ %	$5^{+10}_{-2.5} \times 10^{-4}$	~0.08
Pluto, KC99	0.9%[b]	5×10^{-4}	0.06
Titan	1.5%[c]	4.5×10^{-5}	0.003

L10 and L11 are Lellouch et al. (2010, 2011); KC95 and KC99 are Krasnopolsky and Cruikshank (1995, 1999).

Major Differences in Observational Data for Titan and Triton: Table 2.

Table 2. Some observed data for Titan and Triton.

	CH_4	e_{max}	$[N]_{max}$
Titan	1.5%	3000	10^5
Triton	10^{-4}	3×10^4	5×10^8

In spite of the large heliocentric distance, the ionosphere of Triton is more prominent than on Titan, and atomic nitrogen is more abundant by four orders of magnitude. This is caused by the low CH_4 on Triton.

Major Differences in Photochemistry: Column photolysis rate of methane is equal to the solar photon flux at Lyman-alpha and does not depend on CH_4 mixing ratio. Therefore the photolysis weakly affects the CH_4 mole fractions on Titan and Pluto ($CH_4 \approx 1\%$) and strongly depletes it on Triton ($CH_4 \approx 0.01\%$).

Because of the low CH_4 on Triton, production of hydrocarbons and nitriles occurs below 100 km. For the same reason the methane thermostat does not work on Triton, and its lower atmosphere is very cold. Therefore the basic photochemical products are removed by condensation.

Production of N by photon and photoelectron dissociation and dissociative ionization of N_2 and recombination of N_2^+ occurs in the upper atmosphere of Triton with no loss in reactions with hydrocarbons and nitriles. The abundant N atoms either escape or diffuse down to 100-150 km. Atomic composition of Triton's thermosphere results in atomic ions C^+ and N^+ with very slow radiative recombination and the dense F-type ionosphere.

The low methane on Tritone stimulates indirect photolysis of N_2 and production of HCN in the lower atmosphere via

$CH + N_2 + N_2 \rightarrow HCN_2 + N_2$
$HCN_2 + h\nu \rightarrow CH + N_2$
$HCN_2 + H \rightarrow HCN + NH$
$NH + H \rightarrow N + H_2$
Net $CH + N_2 + 2H \rightarrow HCN + N + H_2$.

This cycle is confirmed by detection of HCN in ice on Triton and its lack on Pluto.

Basic Features of Pluto's Photochemical Model (KC99): (1) This is a self-consistent model of coupled neutral and ion chemistry and includes the ionosphere up to r = 3500 km; (2) only N_2, CH_4, and CO are fixed at thelower boundary r = 1200 km; (3) the model simulates a slow hydrodynamic escape in the atmosphere; (4) the model involves 191 reactions of 44 neutral and 23 ion species and (5) effects of cosmic rays and escape of ions. Two versions of the model were calculated. Vertical profiles of basic hydrocarbons and H_2 from the model are shown in the figure.

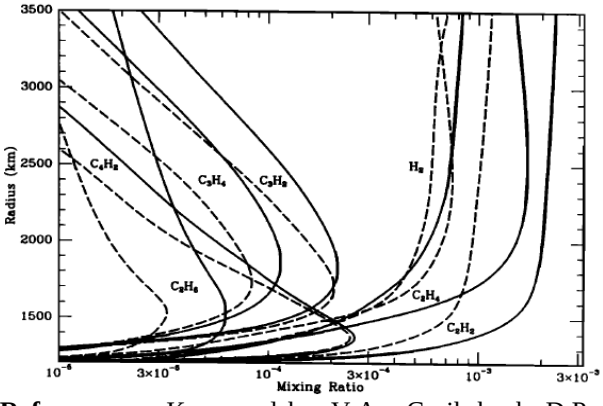

References: Krasnopolsky V.A., Cruikshank D.P., 1995, JGR 100, 21271;1999, JGR 104, 21979; Lellouch E. et al. 2009, AA 495, L17; 2011, AA 512, L8.

Realizing an Elusive Goal: The exploration of Pluto with New Horizons

By

Stamatios M. Krimigis
Johns Hopkins University Applied Physics Laboratory, Laurel MD, 20723, USA

The quest for completing the reconnaissance of all nine planets of the solar system had been a recurring recommendation of advisory committees since the mid-seventies of both, the Space Science Board (SSB) of the Academy and of NASA panels such as SSAAC/Solar System Exploration Subcommittee. The first attempt to define a program for flying by Pluto was made in the late seventies through a NASA AO soliciting proposals for a Voyager-type mission named MJP (Mariner-Jupiter-Pluto) that were never evaluated due to cancellation of the program for budgetary reasons (a familiar process, as it was repeated often in later years). The era of miniaturization begun by Mr. Goldin as NASA Administrator resulted in assertions that small spacecraft (~ 25 kg) with tiny payloads (5 kg) could actually enable the acquisition of significant data from a Pluto flyby. By the late 90s, however, it had become clear that such efforts were unlikely to succeed soon, so more conventional approaches were being pursued. The horrific cost overruns of the so-called X-2000 spacecraft bus that was expected to accommodate three missions-Pluto-Kuiper Express, Europa Orbiter, and Solar Probe-caused the cancellation of Pluto-Kuiper Express in the Fall of 2000. The resulting outcry caused NASA headquarters to look for alternatives and led to an AO in December of that year for a competed mission with a $500 million cost cap. New Horizons won the competition, but the new Bush administration canceled the project. Congressional pressure, however, forced implementation of the Phase-A study, and eventually led to the acceptance of the project by NASA as the first of a new series of «Discovery Plus» missions, named New Frontiers. Thus, the decades-long effort to initiate a probe to the last unexplored planet (now a nanoplanet), involved a contest of wills by individuals in the science community, the administration represented by OMB personnel, and the Congress, that in the end has benefited planetary science with a new line item in the budget that can address more effectively new science questions as they arise, without the agony of the perennial «new start».

PLUTO'S ATMOSPHERE: CURRENT KNOWLEDGE AND OPEN QUESTIONS

E. Lellouch[1] [1]Observatoire de Paris-LESIA F-92195 Meudon, France; emmanuel.lellouch@obspm.fr

Introduction: In this talk, I will review current knowledge on Pluto's atmosphere and summarize some open questions.

Current knowledge: Direct observations of Pluto's atmosphere are available from stellar occultations and high-resolution infrared spectrsocopy. Established facts are (i) a 10-microbar class atmosphere showing evolution on year/decade timescales (ii) a N_2 – dominated atmosphere including significant amounts of CH_4 and probably of CO, and whose composition is controlled to first order by equilibrium with surface ices (iii) a non-isothermal thermal structure with a near-surface ~50 K temperature and an ~100 K temperature at the µbar level, mostly resulting from the heating properties of CH_4 gas.

Open issues:

Beyond this gross picture, many questions are still unsolved or controversial, such as:

- What are the precise mixing ratios of the minor species and how do they vary spatially?
- What are the detailed physical processes controlling the surface/atmosphere interactions?
- What is the stratospheric composition ?
- What is the thermal structure in the lower atmosphere? How steep is the stratospheric temperature gradient? Does Pluto have a troposphere?
- How does the thermal structure vary with latitude or local time? What drives turbulence?
- Are there hazes or clouds in Pluto's atmosphere?
- Is there any relation between the observed changes on the surface and the atmospheric evolution?
- What are the magnitude and mechanisms for atmospheric escape? How extended is the escaping atmosphere?

PLUTO'S THERMAL LIGHTCURVES AS SEEN BY HERSCHEL

E. Lellouch[1], P. Santos-Sanz[1,2], S. Fornasier[1], T. Lim[3], J. Stansberry[4], E. Vilenius[5], Cs. Kiss[6], T. Müller[5], A. Pàl[6], S. Protopapa[7], W. Grundy[8], P. Panuzzo[1], R. Moreno[1], F. Forget[9].
[1] Observatoire de Paris-LESIA F-92195 Meudon, France; emmanuel.lellouch@obspm.fr; [2] Instituto de Astrofisica de Andalucìa, Spain; [3] Rutherford Appleton Laboratory, United Kingdom; [4]Space Telescope Science Institute, USA; [5] Max Planck Institute for Extraterrestrial Physics, Germany; [6] Konkoly Observatory, Hungary; [7] University of Maryland, USA; [8] Lowell Observatory, USA; [9] Laboratoire de Météorologie Dynamique, France

Introduction: Thermal lightcurves of the Pluto-Charon system have been observed in 1997 by ISO at 60 and 100 µm (Lellouch et al. 2000) and more recently (2004, 2007, 2008) by Spitzer at 20-37 µm (IRS) and 24, 70 and 160 µm (Lellouch et al. 2011). Thermal lightcurves appear generally anti-correlated with the optical lightcurve of the system and provide a means to determine thermal inertia and surface emissivities. Highlights of the Spitzer observations include (i) the observation of a clear decrease the of mean brightness temperatures with increasing wavelength (ii) separate measurements of the Pluto and Charon thermal inertias (iii) a hard-to-interpret evidence of a fading of the system (by 2-3 K at 70 µm) from 2004 to 2007.

Herschel observations and early results:

Additional thermal observations of Pluto-Charon have been obtained in in February-March 2012 with Herschel, using both PACS (70, 100, and 160 µm) an SPIRE (250, 350 and 500 µm). In both cases, 9 visits to Pluto were observed. The thermal lightcurve is detected at all wavelengths, though only marginally at 500 µm. A preliminary assessment of the data indicates that (i) the trend of decreasing brightness temperatures with increasing wavelengths continues over 70-500 µm (ii) the cooling of the system observed by Spitzer in 2007 is not confirmed.

References: Lellouch et al. Icarus 147, 220 (2000); Lellouch et al. Icarus 214, 701 (2011)

The New Horizons (NH) Radio Science Experiment, REX

I.R. Linscott[1], D.P. Hinson[2], G.L. Tyler[1], M.K. Bird[3,5], D.F. Strobel[4], M. Patzold[5], M.E. Summers[6]

[1] Dept. of Electrical Engineering, 350 Serra Mall, Stanford, CA 94305-4020, U.S.A. (linscott@stanford.edu)
[2] Carl Sagan Center, SETI Institute, 189 Bernardo Ave., Mountain View, CA 94043, USA
[3] AIfA Radioastronomie, Universitat Bonn, Auf dem Hugel 71, 53121, Bonn, Germany
[4] I121 Olin Hall, 34th and North Charles Streets, Johns Hopkins University, Baltimore,Maryland 21218, U.S.A.
[5] Rheinisches Institut fur Umweltforschung, Dep. Planetary Research, Universitat zu Koln, Aachenerstrasse 209, 50931 Koln, Germany
[6] Dept. of Physics and Astronomy, George Mason University, 4400 University Drive, MS-3F3, Fairfax, Virginia 22030-4444, U.S.A

Abstract

The New Horizons (NH) Radio Science Experiment, REX, is designed to determine conditions on Pluto as manifest in the atmospheric state at the surface and a few scale heights higher. Expected absolute accuracies in n, p, and T at the surface are $4 \cdot 10^{19}$ m^{-3}, 0.1 Pa, and 3 K, respectively, obtained by radio occultation of a 4.2 cm-wavelength signal transmitted from Earth at 10 to 30 kW and received at the NH spacecraft. The threshold for electron density for detection of the ionosphere is roughly $2 \cdot 10^{9}$ m^{-3}. Radio occultation experiments are planned for both Pluto and Charon, but the level of accuracy is expected to be useful for the neutral gas only at Pluto. REX will also measure the nightside 4.2 cm-wavelength thermal emission from Pluto and Charon during the time NH is occulted. At Pluto, the thermal scan provides about five half-beams across the disk; at Charon, only disk integrated values can be obtained. Two additional thermal scans of Pluto will be performed during closest approach, one with an equatorial crossing and another crossing the pole. The equatorial scan will intercept the specular point as seen from Earth, and thus the bistatic scattering echo of the uplink transmission. A combination of two-way tracking and occultation signals will determine the Pluto system mass to about 0.01 percent, and improve the Pluto-Charon mass ratio. REX flight equipment augments the NH radio transceiver used for spacecraft communications and tracking. Implementation of REX required realization of a new CIC-SCIC signal processing algorithm; the REX hardware implementation consumes 0.33 W, and has mass of 3.5 g in 1.25 cm^3. Commissioning tests conducted after NH launch demonstrate that the REX system is operating as expected. Two Lunar Occultations with the NH spacecraft in 2011 and 2012 served as a stringent test of the performance and precision of the radio occultation method.

July 2013 Meeting: The Pluto System on the Eve of Exploration by New Horizons: Perspectives and Predictions

Abstract

Chandra Observations of Pluto's Escaping Atmosphere in Support of the New Horizons Mission

C.M. Lisse (APL), R.L. McNutt (APL), T.E. Cravens (University of Kansas)

Pluto is known to have an atmosphere which changes size and density with its seasons (Elliot *et al.* 2003; Elliot *et al.* 1989; Elliot *et al.* 2007) and current models of its atmosphere (McNutt 1989; Strobel 2008; Tian & Toon 2005) formulate a majority N_2 atmosphere with scale height ~3000 km and free escape of ~10^{28} mol/sec (Erwin *et al.* 2012, Tucker *et al.* 2012). This is very similar to the physical situation of a JFC comet observed by Chandra at 1 AU (Lisse *et al.* 2001, 2005, 2007, 2013; Bodewits *et al.* 2007; Wolk *et al.* 2009; Christian *et al.* 2010). In many ways Pluto and its atmosphere may be behaving like a very large comet (Bagenal *et al.* 1997; Bagenal & McNutt 1989; Delamere & Bagenal 2004), quite consistent with the physical picture of KBOs as the parents of the inner system Centaurs and Jupiter Family Comets.

Current models of Pluto's extended atmosphere (thought to be dominated by N_2 and CH_4) are still very uncertain (McComas *et al.* 2008) leading to difficulties in optimizing the *in situ* New Horizons (NH) observation plan. Applying the knowledge gained by studying cometary X-ray emission, Chandra ACIS-S photometric imaging of X-rays produced by charge exchange between the solar wind and Pluto's atmosphere (McNutt *et al.* 2008) can address both the run of atmospheric density with distance from Pluto and the interaction of the solar wind with the extended Plutonian atmosphere. Pinning down the atmosphere's extent and exact amount of free molecular escape can corroborate the exospheric emission measurements of the NH ALICE instrument (Stern *et al.* 2008), while determining the x-ray luminosity will help the NH PEPSSI instrument (McNutt, *et al.* 2008) determine the solar wind particle environment at Pluto, and the ultimate fate of escaping gas, i.e. by charge exchange with the solar wind or photoionization from solar UV radiation.

The major concern with a Chandra Pluto observation is the distance of Pluto from Chandra and the strength of the solar wind at Pluto. While the solar wind strength decreases by ~1/332, Chandra's 0.5" pixels are 332 larger, about 12,000 km on a side. The neutral gas escaping from Pluto should extend ~33 times farther out from the planet as compared to the gas emitted by a comet nucleus at 1 AU from the Sun, and the total amount of X-ray emission should be the same as detected for a medium bright JFC comet by Chandra (e.g. 2P/Encke, Lisse *et al.* 2005, or 9P/Tempel 1, Lisse *et al.* 2007). The expected total ACIS-S count rate for Pluto is on the order of 0.001 cps. Thus the major concern with observing Pluto is that any local heliospheric or instrumental backgrounds could possibly dominate the observed X-ray signal.

However, the potential benefit of such an observation to the NH mission and Pluto science is large. As there is one Chandra Guest Observer (GO) cycle available during NH cruise, and the next available during the NH flyby, a prudent use of Chandra is a small, test-pilot observation of the Pluto system in Cycle 15 to verify the potential of Chandra observations, followed up in Cycle 16 by detailed monitoring of the system during the week around NH closest flyby in July 2015 if there is a positive detection in the Cycle 15 observation.

References

- Bagenal, F., & McNutt, R. L., Jr. 1989, *Geophys Res Lett* **16**, 1229
- Bagenal, F., Cravens, T. E., Luhmann, J. G., McNutt, R. L., Jr., & Cheng, A. F. 1997, in *Pluto and Charon*, eds. S. A. Stern, & D. J. Tholen (Tucson: University of Arizona Press), 523
- Bodewits, D. *et al.* 2007, *Astro. Astrophys.* **469**, 1183
- D. Christian *et al.* 2010, *Astrophys. J. Suppl* **187**, 447
- Delamere, P. A., & Bagenal, F. 2004, *Geophys Res Lett* **31**, doi:10.1029/2003GL018122
- Elliot, J. L. *et al.* 1989, *Icarus* **77**, 148
- Elliot, J. L., *et al.* 2003, *Nature* **424**, 165
- Elliot, J. L., *et al.* 2007, *Astron. J.* **134**, 1
- Lisse. C.M. *et al.* 2001, *Science* **292**, 1343
- Lisse, C.M. *et al.* 2005, *Astrophys. J.* **635**, 1329
- Lisse, C.M. *et al.* 2007, *Icarus* **190**, 391
- Lisse, C.M. *et al.* 2013, *Icarus* **222**, 752
- McComas, D., *et al.* 2008, *Space Science Reviews* **140**, 261
- McNutt, R. L., Jr. 1989, *Geophys Res Lett* **16**, 1225
- McNutt, R. L., *et al.* 2008, *Space Science Reviews* **140**, 315
- Stern, S. A., et al. 2008, *Space Science Reviews* **140**, 155
- Strobel, D. F. 2008, *Icarus* **193**, 612
- Tian, F., & Toon, O. B. 2005, *Geophys Res Lett* **32,** L18201, doi:10.1029/2005GL023510
- Tucker, O. J., Erwin, J. T., Deighan, J. I., Volkov, A. N., & Johnson, R. E. 2012, *Icarus* **217**, 408
- Wolk, S. *et al.* 2009, *Astrophys. J* **694**, 1293

EVALUATING THE GLOBAL TECTONIC HISTORIES OF ICY BODIES: ENCELADUS AS A CASE EXAMPLE

E. S. Martin[1] and S. A. Kattenhorn[1], [1] Department of Geological Sciences, University of Idaho (875 Perimeter Drive MS 3022, Moscow, ID 83844-3022, mart5652@vandals.uidaho.edu, simkat@uidaho.edu).

Introduction: Large-scale tectonic deformation in icy shells can manifest itself as fractures that form in response to stresses sourced from a range of mechanisms including polar wander, despinning, changes in volume caused by freezing or thawing of a subsurface ocean, orbital recession/decay, diurnal tides, and non-synchronous rotation (NSR) [1,2]. Icy shells often preserve this record of tectonic deformation as patterns of fractures which can be used to identify the source of stress. Enceladus's surface shows an extensive geologic record [3,4], and the fracture patterns observed in the south polar terrains (SPT) provide direct geologic evidence for NSR [3].

While the surface of Pluto has yet to be revealed, numerous studies have attempted to predict the likelihood of tectonic activity, and the possible stress mechanisms including despinning [5] and polar wander [6] that may have produced them. Additionally, [5, 7] discuss that the possibility of a subsurface ocean during periods of Pluto's evolution under certain conditions. For these reasons, establishing Enceladus's global tectonic history provides a useful analog for Pluto, until the surface of Pluto and Charon are unveiled by the New Horizons mission July of 2015.

Establishing Fracture Histories: Fractures often form within a *fracture set* where cracks are evenly spaced and parallel to one another in response to a stress field. If the stress field changes, a new fracture set may form in a different orientation dictated by the orientation and magnitude of the new stress field. Therefore, multiple fracture sets, each with distinct orientations, can form within the same region. Detailed fracture mapping can resolve the different sets, and their relative age relationships (Fig. 1 & 2).

Global stress models are required to identify the stress mechanism responsible for creating observed fracture patterns. With the help of programs like SatStress [8] and SatStressGUI [9], we can make assumptions about the rheological properties of an ice shell and the source of stress, and produce a theoretical pattern of failure. If predicted fracture patterns produced with SatStress match mapped fracture patterns we can infer which sources of stresses produced the observed fractures.

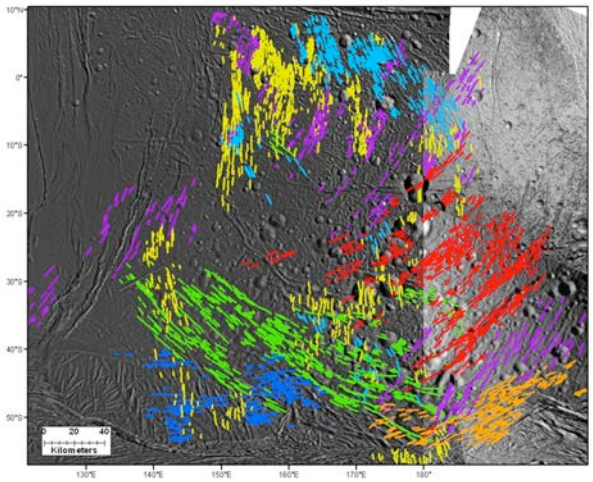

Figure 1: Systematic fracture sets revealed on Enceladus's leading hemisphere.

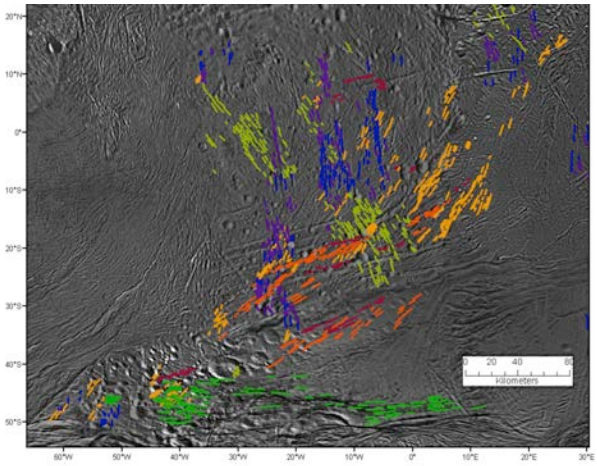

Figure 2: Systematic fracture sets revealed on Enceladus's trailing hemisphere.

A Record of Normal Fault Formation: Enceladus's cratered terrains are overlooked as being heavily tectonized, and are undergoing tectonic dissection by early-stage normal faults called pit chains. Enceladus's cratered terrains show fracture orientations rotating through time, from which we infer a change in the stress field in which the fractures formed (Fig. 1 & 2). Similar observations in the SPT by [3], attributed the observed systematic change in fracture orientations to NSR of Enceladus's ice shell.

Strike-slip Faulting: In the outer solar system normal faulting is the dominant tectonic process; however, strike-slip faults have been identified on a number of icy bodies, including Europa [10], Ganymede [11],

Enceladus [12], and Triton [13]. Right-lateral strike-slip faults predominantly formed in the southern hemisphere and left-lateral strike-slip faults in the northern hemisphere [10], suggesting they were formed in the past by stresses induced by diurnal tidal forces, and then rotated ~60° by NSR [10]. Deviations from this general pattern in equatorial regions of Europa are dependent on fault orientation but may also be explained by polar wander [14]. The global distribution of strike-slip faults on Enceladus (Fig. 3) reveals a seemingly random pattern of left- and right-lateral strike-slip faults across its surface. While this pattern may suggest that diurnal tides may not apply to the formation strike-slip faults on Enceladus, multiple stress mechanisms may be at work creating the observed strike-slip fault distribution. Further work modeling global stresses will be necessary to understand this pattern on Enceladus.

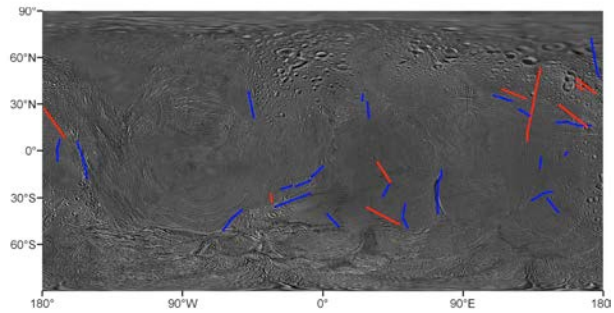

Figure 3: Global distribution of strike-slip faults on Enceladus. Blue indicates left-lateral faults, and Red indicates right-lateral faults.

Conclusion: As seen by global scale mapping of normal and strike-slip faults on Enceladus, details of the tectonic history of an icy body can be probed. If tectonic features are resolved on the surface of Pluto or Charon, previous modeling, and global-scale mapping of tectonic features may provide a window into the evolution of Pluto, and the Pluto system.

References: [1] Kattenhorn & Hurford (2009), in *Europa*, UA Press, 199-236. [2] Collins et al., (2009) in *Solar System Tectonics*, Cambridge U. Press. [3] Patthoff & Kattenhorn (2011) *GRL*, 38, L18201. [4] Martin & Kattenhorn (2013), *44th LPSC, Abs.* 2047. [5] Collins & Barr (2008) *AGU* Abs. #P51C-1425. [6] Rubincam (2003) *Icarus*, 163, 469-478. [7] Robuchon & Nimmo (2011) *Icarus* 216, 426-439. [8] Wahr et al., (2009) *Icarus* 200, 188-206. [9] Kay & Kattenhorn (2010) *LPSC Abs.* 2046. [10] Hoppa et al., (1999) *Icarus* 141, 287-298. [11] Pappalardo et al., (1998) *Icarus* 135, 276-302. [12] Smith-Konter & Pappalardo (2008) *Icarus* 198, 435-451. [13] Croft (1993) 24th *LPSC Abs.* 1176. [14] Rhoden et al., (2011) *Icarus*, 211, 636-647.

Acknowledgements: This work is funded by NESSF Grant #NNX11AP30H.

RADIATION CHEMISTRY ON PLUTO: A LABORATORY APPROACH.

C. K. Materese[1], D. P. Cruikshank[2], S.A. Sandford[3], H. Imanaka[4], and D.W. White[5], [1]Oak Ridge Associated Universities, Moffett Field, CA 94035 Christopher.K.Materese@nasa.gov, [2]NASA Ames Research Center, Moffett Field, CA 94035 Dale.P.Cruikshank@nasa.gov, [3]NASA Ames Research Center, Moffett Field, CA 94035 scott.sandford@nasa.gov, [4]Lunar and Planetary Lab., U. Ariz., [5]*(formerly)* Oak Ridge Associated Universities, Moffett Field, CA 94035

With the New Horizons spacecraft fast approaching its rendezvous with Pluto and its satellites, we will soon have a unique opportunity to obtain data on the chemical compositions of their surfaces with a level of detail yet unmatched. In preparation for this event, we are conducting a series of laboratory experiments designed to mimic the surface conditions of Pluto in order to both make predictions about what the spacecraft may observe, and to help understand the data that are eventually returned.

Previous laboratory experiments related to Pluto surface chemistry have been reviewed by Hudson *et al.* [1]. The present work has focused on ultraviolet (UV) photolysis of ices relevant to Pluto and analysis of the resulting photoproducts with a special focus on refractory non-ice components. We irradiated (during deposition) a mixture of N_2, CH_4, CO, and C_2H_6 (100:1:1:0.1) and studied the resulting photoproducts using parallel and complimentary chemical analysis techniques: 1. *In situ* Infrared (IR) analysis of the resulting ice and refractory residue. 2. *Ex situ* analysis of refractory residue with gas chromatography coupled with mass spectrometry (GC-MS). The IR data are useful for identifying specfic compounds and radicals in the ice phase while providing some general information the chemical moities in the refractory material. The GC-MS data provide a means for identifying specific compounds in the refractory material after it has been extracted from the vacuum chamber.

To date, our experiments have yielded several main results: 1. The ice phase radiation products identified via IR spectroscopy closely match previous experiments conducted by other groups on simpler two- and three-component ice mixtures. 2. The Mid-IR (2.5-20 μm) spectra of the refractory residue is consistent with the presence of $-CH_2-$, $-CH_3$, -OH, C=O, and -C≡N groups. 3. The GC-MS data (Figure 1) have identified at least 13 individual compounds in the refractory residue most of which are carboxylic acids or hydroxy-carboxylic acids. While these acids may not be the predominant component of the radiation residues, their presence indicates the importance of an oxygen-bearing molecule in the reactions occurring in a mixture of ices otherwise dominated by reduced compounds.

We plan to use the data collected in these experiments in conjunction with future experiments to derive optical constants for some of these refractory materials in the 1-2.5 μm range so that through radiative transfer models for reflectance they can be compared directly with data returned from the New Horizons spacecraft.

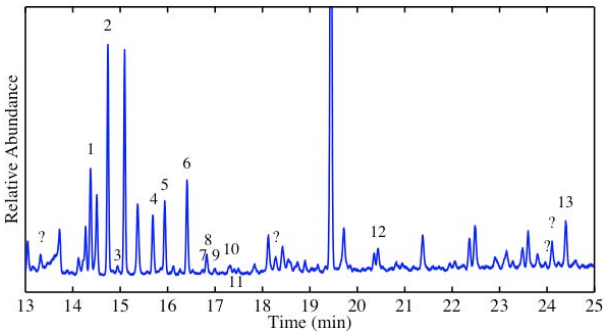

Figure 1. The following compounds have been positively identified using the GC-MS with purchased chemical standards: (1) 2-hydroxypropanoic acid, (2) glycolic acid, (4) oxalic acid, (5) 2-Hydroxybutyric acid, (6) 3-Hydroxypropanoic acid, and (13) 2,3-dihydroxypropanoic acid. The following compounds have been tentatively identified using the GC-MS Xcalibur™ software (Thermo Finnigan): (3) 2-Hydroxy-2-methylpropionic acid (7) 3-Hydroxybutanoic acid (8) 3-Hydroxy-2-methylpropanoic acid (9) 2-Hydroxy-3-methylbutanoic acid or 2-Hydroxypentanoic acid (10) 2-Hydroxy-3-methylbutanoic acidor 2-Hydroxypentanoic acid (11) 2-Hydroxy-2-butenoic acid (12) 2-hydroxyhexanoic acid or 2-hydroxy-4-methylpentanoic acid.

References:

[1] Hudson, R.L., Palumbo, M.E., Strazzulla, G., Moore, M.H., Cooper, J.F., Sturner, S.J., (2008) Laboratory studies of the chemistry of transneptunian object surface materials. In: Barucci, A., Boehnhardt, H., Cruikshank, D., Morbidelli, A. (Eds.), *The Solar System Beyond Neptune.* Univ. of Arizona Press, Tucson, pp. 507–523

THE SOLAR WIND AROUND PLUTO (SWAP) INSTRUMENT ON NEW HORIZONS

D.J. McComas[1,2,3], [1]Southwest Research Institute, P.O. Drawer 28510, San Antonio, TX 78228, USA (dmccomas@swri.edu), [2]University of Texas at San Antonio, San Antonio, TX 78249, USA, [3]On behalf of the entire SWAP Science Team

---

Introduction: The Solar Wind Around Pluto (SWAP) instrument on New Horizons measures ions with energy/charge (E/q) from 35 eV/q to 7.5 keV/q. Constrained to fit within minimal resources, SWAP is optimized to make measurements as the New Horizons spacecraft scans to image Pluto and Charon over all scan angles planned at the time of launch. To meet these unique requirements, we produced a wide field-of-view top-hat analyzer with electrostatic deflectors, and a redundant/coincidence detection scheme. SWAP has already provided unprecedented observations of the plasma environment down the deep Jovian magnetotail and of interstellar pickup protons out to >20 AU. This brief talk summarizes 1) the SWAP instrument, 2) some of the important discoveries and results already published using SWAP data, and 3) the plans for making critical observations of the solar wind interaction through the Pluto/Charon flyby. These latter measurements are designed to characterize Pluto's total atmospheric loss rate and allow us to examine the complex plasma interactions at Pluto for the first time.

PROVENANCE OF PLUTO: IMPLICATIONS FOR COMPOSITION AND STRUCTURE

William B. McKinnon

Department of Earth and Planetary Sciences and McDonnell Center for the Space Sciences, Washington University in St. Louis, Saint Louis, MO 63130, USA (mckinnon@wustl.edu)

New Horizons will revolutionize our understanding of the Pluto system in 2015, but understanding of Pluto's provenance has been strongly evolving for years. From escaped satellite to surviving protoplanet [1–3], and from caught in resonant migration [4,5] to scattered during a solar-system-wide dynamical instability [6,7], Pluto has emerged as a surviving oligarch/dwarf planet of the primordial planetesimal disk beyond the initial compact planetary configuration. In early studies of possible planetary migration, Pluto's eccentricity implied 3:2 resonant migration from ~33 AU to its present position [4,5]. This view has been supplanted by the arguably dominant paradigm of the Nice instability model, in which a close-in Neptune (at ~12 AU) jumps the outer planetesimal disk more-or-less "in a single bound" to ~27–28 AU, where its orbit circularizes through dynamical friction and then completes its outward migration to 30 AU [6]. Neptune scatters planetesimals from the disk into the present range of the Kuiper belt and beyond, and as its orbit stabilizes, the surviving planetesimals (both resonant and non-resonant) are trapped "for eternity" [6]. Both the resonant migration and Nice models predict that Pluto originally accreted well inside its present position, and the Nice model in particular implies formation somewhere in the 20-to-34 AU range [6,8]. In terms of statistical likelihood, formation in the outer part of the planetesimal disk (≥29 AU) is favored, but Pluto's high inclination is more consistent with accretion inside of 29 AU [6]. It also makes sense, that as one of the largest known survivors of the original disk (along with Eris and Triton), Pluto formed closer to the Sun. Growth times are a strong function of heliocentric distance [e.g., 9], and formation of 1000-km-sized oligarchic planetesimals is estimated have taken 5–10 m.y. between 20–25 AU and 15–30 m.y. between 30–34 AU [9]. These growth times are interesting when compared to likely nebular gas disk lifetimes of 3–10 m.y. [10], and imply that Pluto accreted in full within a gas-free environment or at best during the waning stages of nebular gas loss.

In terms of composition, extensive studies of comets, asteroids, meteorites (especially the more recent falls Tagish Lake and Sutter's Mill), interstellar dust particles (IDPs), interstellar molecular clouds and star-forming regions support the concept that the planetesimal disk that birthed Pluto and other Kuiper belt objects (KBOs) was composed of subequal amounts of volatile ices (including volatile organics), less volatile carbonaceous matter, and refractory "rock" [see references in 11]. Volatile ice compositions are best represented by cometary comae [e.g., 12,13], but differences may exist among cometary dynamical classes [14-16]. Macromolecular carbonaceous compounds (CHON) were seen at Halley [17,18], are seen in Stardust particles [19], and inferred from infrared emission spectra [e.g., 20]. The rock component can be usefully compared with the most primitive carbonaceous chondrites, as exemplified by Tagish Lake: a fine-grained, opaque matrix of phyllosilicates, sulfides, and magnetite, surrounding aggregates of olivine, pyroxene and other minerals and inclusions, showing evidence for pervasive but incomplete low-temperature, aqueous alteration [21,22]. This is not to suggest that Tagish Lake is a precise mineralogical model for cometary rock or rock within Pluto, but 1) such rock should be solar in composition or close to it (with respect to non-volatile elements) and 2) as planetesimals accreted and evolved between ~20-and-34 AU, various degrees of aqueous alteration likely occurred prior to final incorporation into Pluto.

The following compositional features should be noted: 1) The *carbon abundance* of carbonaceous chondrites is ~5 wt%, much less than solar [23,24], but comets as a whole are not depleted in carbon [17,18,25], so there must have been a large carbonaceous component to the planetesimals that built Pluto

[26]; 2) the *N/C ratios* in IDPs and Stardust particles are non-trivial [19], so the carbonaceous component could have been a more important source of N_2 and nitrogen compounds for Pluto than volatile ices, which are N-depleted [12]; 3) the rock and carbonaceous fractions are likely have been a mélange of *unequilibrated* nebular condensates, chondrules, and interstellar grains, reflecting extensive radial mixing in the early nebula [27,28]; 4) the most recent *solar abundances* [24] have higher C/O and substantially higher Si/O ratios when compared with the standard reference of Anders and Grevesse [29], consistent with Pluto's relatively high density [cf. 30]; 5) *sulfur*, an important rock-forming element, is moderately volatile, and its abundance in the Pluto-forming region may have been affected by draw-down of nebular H_2S by FeS formation in the terrestrial planet region [31,32]; and 6) a number of novel explanations have been advanced to explain the unforeseen abundance pattern measured by the *Galileo* probe at Jupiter [33-35], some of which could change our understanding of cometary compositions if valid (in this regard, forthcoming results from *Juno* should prove enlightening).

Pluto's rock/ice ratio is ~0.7 by mass, calculated on an anhydrous basis and neglecting its less volatile carbonaceous component. Pluto's differentiation state was debated in [26], but the case for Pluto being differentiated has strengthened considerably since then: 1) convection is now seen as a less efficient mechanism of interior heat transport, implying greater adiabatic (internal) temperatures, all other things being equal [e.g., 36]; 2) Charon's lower density than Pluto implies at least partial differentiation of one of the precursor bodies, prior to the Charon-forming collision [37]; 3) at least one other major KBO, Haumea, is clearly differentiated [38]; and 4) new rock mineralogical models created by the author for major icy satellites/bodies [39], reflecting varying states of hydroxylation and carbonation, are somewhat less dense (for likely degrees of oxidation, given internal pressures). The latter push rock volume fractions higher (higher still if refractory carbonaceous material is considered), increasing ice+rock viscosities and the likelihood of internal water-ice melting. *New Horizons* will not pass close enough to Pluto (or Charon) to measure degree-2 gravity, but shape determination from imaging offers the possibility of determining differentiation state as long as hydrostatic equilibrium is attained post tidal evolution.

References: [1] McKinnon W.B. (1984) *Nature 311*, 355-358; [2] Stern S.A. (1991) Icarus 90, 271-281; [3] Stern S.A. et al. (1997) in *Pluto and Charon*, Univ. Ariz. Press, 605-663; [4] Malhotra R. (1993) *Nature 365*, 819-821; [5] Malhotra R. (1995) *Astron. J. 110*, 420-429; [6] Levison H.F. et al. (2008) *Icarus 196*, 258-273; [7] Levison H.F. et al. (2011) *Astron. J. 142*, 152; [8] Gomes R.S. (2004) *Icarus 170*, 492-507; [9] Kenyon S.J. et al. (2007) in *The Solar System Beyond Neptune*, Univ. Ariz. Press, 293-313; [10] Haisch K.E. et al. (2001) *Astrophys. J. Lett. 553*, L153-L156; [11] McKinnon W.B. et al. (2007) in *The Solar System Beyond Neptune*, Univ. Ariz. Press, 213-241; [12] Bockelée-Morvan D. et al. (2004) in *Comets II*, Univ. Ariz. Press, 391-423; [13] Crovisier J. et al. (2009) *Planet. Space Sci. 57*, 1162-1174; [14] Fink U. (2009) *Icarus 201*, 311-334; [15] Hartogh P. et al. (2011) *Nature 478*, 218-220; [16] A'Hearn M.F. et al. (2012) *Astrophys. J. 758*, 29; [17] Jessberger E.K. et al. (1988) *Nature 332*, 691-695; [18] Fomenkova M.N. (1999) *Space Sci. Rev. 90*, 109-114; [19] Sandford S. et al. (2006) *Science 341*, 1720-1724; [20] Lisse C.M. et al. (2007) *Icarus 187*, 69-86; [21] Brown P.G. et al. (2000) *Science 290*, 320-325; [22] Zolensky M.E. et al. (2002) *Meteor. Planet. Sci. 37*, 737-761; [23] Lodders K. (2003) *Astrophys. J. 591*, 1220-1247; [24] Asplund M. et al. (2009) *Annu. Rev. Astron. Astrophys. 47*, 481-522; [25] Greenberg J.M. (1998) *Astron. Astrophys. 330*, 375-380; [26] McKinnon W.B. et al. (1997) in *Pluto and Charon*, Univ. Ariz. Press, 295-343; [27] Brownlee D.E. (2006) *Science 314*, 1711-1719; [28] Brownlee D.E. and Team Stardust (2011) *AGU Fall Meeting*, abstract #P42A-01; [29] Anders E. and Grevesse N. (1989) *Geochim. Cosmochim Acta 53*, 197-214; [30] Wong M.E. et al. (2008) in *Oxygen in the Solar Sysetm, Rev. Mineral. Geochem. 68*, 219-246; [31] Pasek M. A. et al. (2005) *Icarus 175*, 1-14; [32] Ciesla F.J. (2013) *44th LPSC*, abs. #1315; [33] Lodders K. (2004) *Astrophys. J. 611*, 587-597; [34] Guillot T. and Hueso R. (2006) *Mon. Not. R. Astron. Soc. 367*, L47-L51; [35] Mousis O. et al. (2012) in *Astrophys. J. Lett. 751*, L7; [36] McKinnon W.B. (2006) *Icarus 183*, 435-450; [37] Canup R. (2005) *Science 307*, 546-550; [38] Brown M.E. (2007) in *The Solar System Beyond Neptune*, Univ. Ariz. Press, 335-344; [39] McKinnon W.B. and Bland M.T. (2010) *42nd LPSC*, abs. #2768.

THE SHAPES OF THINGS TO COME: ROTATIONAL AND TIDAL FIGURES OF EQUILIBRIUM FOR PLUTO AND CHARON. William B. McKinnon, Department of Earth and Planetary Sciences and McDonnell Center for the Space Sciences, Washington University in St. Louis, Saint Louis, MO 63130, USA (mckinnon@wustl.edu).

New Horizons will not pass close enough to Pluto (or Charon) to measure degree-2 gravity, but shape determination from imaging offers the possibility of determining differentiation state as long as hydrostatic equilibrium is attained post tidal evolution.

With the decision to maintain the nominal trajectory as the best option from a hazard point-of-view, the closest approach distances to Pluto and Charon are set to be ~13,000 km and 30,000 km (COM), respectively. At approach distances >10 Pluto radii, flyby speeds of nearly 14 km/s, and radio tracking constraints, degree-2 or higher gravity will not be obtained. The situation is not entirely hopeless, however. Both radio tracking and optical navigation should determine the individual masses of Pluto and Charon ("J_0") to a high degree of accuracy. This will put to rest a long-standing limitation on modeling and understanding Pluto and Charon's internal structure and evolution [1]. The internal structures and geophysical histories of these bodies will also be reflected in their shapes. In the ideal situation of perfect hydrostatic equilibrium, their triaxial shapes will reflect their moments-of-inertia (MOI) and thus degree of differentiation.

The figure below illustrates the potential magnitudes of shape distortions due to rotation and mutual tidal interaction (a = tidal axis, c = spin axis). Present-day system parameters are based on [2] for definiteness. Differentiated structures assume hydrated rock for Charon and dry rock for Pluto (which minimizes the latter's normalized MOI ≈ 0.3); undifferentiated assumes uniformity (not precisely true due to high-pressure ice phases, but NMOI = 0.4 maximizes hydrostatic deformation). As can be seen, Charon is strongly triaxial, while Pluto is nearly biaxial. Detecting flattenings is only the beginning of the *New Horizons* experiment, however. We want to *discriminate between differentiated and undifferentiated figures*. This will be a challenging task for limb fitting [e.g., 3], especially as *all* of the values below are <1 km. Charon's $a - c$ is larger, as is the delta between the differentiated and differentiated case, than for Pluto, and measurements of the required precision may be within reach for Charon. Charon will have to cooperate, though, as it may be considerably topographically rougher than Pluto, if Triton is a useful guide/analogue for Pluto [4].

We should also not be too surprised if we measure *larger* second-degree figures than estimated here. In this case we may be looking at a *fossil* bulge or bulges, from before complete spin-orbit synchronism was achieved early in solar system history [5] (e.g., a fossil bulge is thought to contribute to the Moon's dynamic figure, and is painfully obvious for Iapetus). In such a case for Pluto or Charon, we would not learn anything about differentiation state, but a fossil bulge would nevertheless be very interesting and would constrain thermal history [6,7]. Additional possibilities for (apparently non-hydrostatic) long-wavelength topographic interpretation abound [e.g., 8,9].

References: [1] McKinnon W.B. et al. (1997) in *Pluto and Charon*, Univ. Ariz. Press, 295-343; [2] Buie M.W. et al. (2006) *Astron. J. 132*, 290-298; [3] Thomas P.C. (2010) *Icarus 208*, 395-401; [4] Thomas P.C. (2000) *Icarus 148*, 587-588; [5] Dobrovolskis A.R. et al. (1997) in *Pluto and Charon*, Univ. Ariz. Press, 159-190; [6] Castillo-Rogez J.C. et al. (2007) *Icarus 190*, 179-202; [7] Singer K.N. and McKinnon W.B. (2011) *Icarus 216*, 198-211; [8] Nimmo F. and Bills B.G. (2010) *Icarus 208*, 896-904; [9] McKinnon W.B. (2013) *JGR Planets*, submitted.

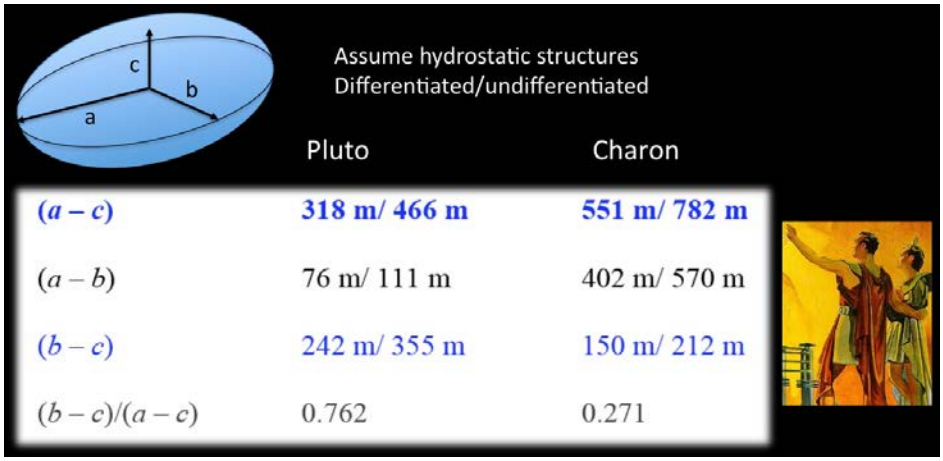

PICK-UP IONS AT PLUTO: THE PLUTO ENERGETIC PARTICLE SPECTROMETER SCIENCE INVESTIGATION (PEPSSI).

R. L. McNutt, Jr.[1] and M. E. Hill[2], L. E. Brown[2], R. S. Gurnee[2], D. K. Haggerty[2], G. C. Ho[2], S. M. Krimigis[2,3], C. M. Lisse[2], S. Livi[4], D. G. Mitchell[2], N. Paschalidis[5], E. C. Roelof[2], J. H. Westlake[2], [1]Johns Hopkins University Applied Physics Laboratory (11100 Johns Hopkins Road, Room 200-E258, Laurel, MD 20723, USA, ralph.mcnutt@jhuapl.edu), [2]Johns Hopkins University Applied Physics Laboratory (11100 Johns Hopkins Road, Laurel, MD 20723, USA), [3]Academy of Athens (28 Panapistimiou, 10679 Athens, Greece), [4]Southwest Research Institute (San Antonio, TX 78228, USA), [5]Heliophysics Science Division, NASA Goddard Space Flight Center (Greenbelt, MD 20771, USA).

Introduction: There has been speculation about the interaction of the solar wind with Pluto from the time of the "Grand Tour" studies in the early 1970's [1]. At the same time Trafton and others considered the potential atmosphere, which might be escaping from this planet [2-8]. Subsequently, initial occultation measurements of Pluto revealed evidence for an atmosphere [9-11] and led to further speculation about the extent of atmospheric escape [12] and what consequences this might have for the integration of the planet with the solar wind [13].

As models for the atmosphere became more detailed [14-18], it also became clear that pickup ions could dominate a large space around the planet [19] and provide significant information on the composition and extent of atmospheric escape via *in situ* measurements by an appropriately instrumented flyby spacecraft [20, 21]. Continued investigation provided more evidence of the potential scientific importance of tenuous atmosphere at Pluto, its implications for the evolution of the surface, and the potential for a significant interaction with the solar wind in the distance heliosphere [22-27].

Pick-up Ions: Although the basic properties of the solar wind at the distance of Pluto are well known from Voyager measurements [27], the nature of the interaction with Pluto's atmosphere is highly dependent upon the outflow strength, which is unknown over several orders of magnitude. At its the strongest, the interaction may be similar to that of the solar wind with a comet for which there can be significant mass loading of the solar wind, stagnating the flow [28-34]. In this case, the detection and measurement of picked up cometary ions provide insight into the net production rate by the comet. Especially with the continuing presence of the atmosphere of Pluto even as it recedes from perihelion [35-37], ongoing modeling efforts suggest that something of this sort may be present at the time of the New Horizons encounter in 2015 [38-42]. If this is the case, then the measurement of heavy ions from Pluto's atmosphere remote for the planet can provide a discriminating outer boundary condition for the atmospheric escape [29].

Instrumentation: To detect the pickup ions, which can be accelerated to relatively high energies in the integration, an energy range up to the ten's of keV was required along with mass discrimination. The Pluto Energetic Particle Spectrometer Science Investigation (PEPSSI) is a class of "hockey puck" energetic particle spectrometer designed to make such measurements while minimizing the use of spacecraft resources, notable mass and power [43]. By combining time-of-flight and total energy measurements into a compact package with six sectors to provide angular resolution over the instantaneous look direction, PEPSSI accomplishes its task in a 1.475 kg package using ~2.5 W of electrical power. PEPSSI measurements during and after the Jupiter flyby have demonstrated the instrument performance [44-46], and ongoing operation of the instrument in the far heliosphere during hibernation periods of the spacecraft show that the instrument is "good to go" for providing the required measurements during the Pluto encounter.

References: [1] Dryer M., et al., *Astrophys. Space Sci., 22* (1973) 329-351. [2] Trafton L.M., *Icarus, 44* (1980) 53-61. [3] Trafton L.M., Stern S.A., *Astrophys. J., 267* (1983) 872-881. [4] Golitsyn G.S., *Sov. Astron. Lett., 1* (1975) 19-20. [5] Hart M.H., *Icarus, 21* (1974) 242-247. [6] Fink U., et al., *Icarus, 44* (1980) 62-71. [7] Hunten D.M., Watson A.J., *Icarus, 51* (1982). [8] Trafton L.M., et al., *Bull. Amer. Astron. Soc., 19* (1987) 1071-1072. [9] Hubbard W.B., et al., *Nature, 336* (1988) 452-454. [10] Eshleman V.R., *Icarus, 80* (1989) 439-443. [11] Elliot J.L., et al., *Icarus, 77* (1989) 148-170. [12] McNutt R.L., Jr., *Geophys. Res. Lett., 16* (1989) 1225-1228. [13] Bagenal F., McNutt R.L., Jr., *Geophys. Res. Lett., 16* (1989) 1229-1232. [14] Clarke J.T., et al., *Icarus, 95* (1992) 173-179. [15] Trafton L.M., *Astrophys. J., 359* (1990) 512-523. [16] Hubbard W.B., et al., *Icarus, 84* (1990) 1-11. [17] Yelle R.V., Lunine J.L., *Nature, 339* (1989) 288-290. [18] Yelle R.V., Lunine J.I., *Nature, 339* (1989) 228-290. [19] Kecskemety K., Cravens T.E., *Geophys. Res. Lett., 20* (1993) 543. [20] Neugebauer M., et al., Space physics objectives for the Pluto Fast Flyby mission, Report to NASA Space Physics Division, in, 1993. [21] Lunine

J.L., et al., Pluto Express: Report of the Science Definition Team, in, 1995, pp. 65. [22] Krasnopolsky V.A., Cruikshank D., *J. Geophys. Res., 104* (1999) 21,979-921,996. [23] Krasnopolsky V.A., *J. Geophys. Res., 104* (1999) 5955-5962. [24] Young L.A., et al., *Icarus, 127* (1997) 258-262. [25] Trafton L.M., et al., Escape processes at Pluto and Charon, in: S.A. Stern, D.J. Tholen (Eds.) Pluto and Charon, University of Arizona Press, Tucson, 1997, pp. 475-521. [26] Summers M.E., et al., Chemical models of Pluto's atmosphere, in: S.A. Stern, D.J. Tholen (Eds.) Pluto and Charon, University of Arizona Press, Tucson, 1997, pp. 391-434. [27] Bagenal F., et al., Pluto's interaction with the solar wind, in: S.A. Stern, D.J. Tholen (Eds.) Pluto and Charon, University of Arizona Press, Tucson, 1997, pp. 523-555. [28] Galeev A.A., et al., *Astrophys. J., 289* (1985) 807-819. [29] Gloeckler G., et al., *Geophys. Res. Lett., 13* (1986) 251-254. [30] McKenna- Lawlor S., et al., *Nature, 321* (1986) 347-349. [31] Mendis D.A., et al., *Geophys. Res. Lett., 13* (1986) 239. [32] Richardson I.G., et al., *Geophys. Res. Lett., 13* (1986) 415-418. [33] Sagdeev R.Z., et al., *Geophys. Res. Lett., 13* (1986) 85-88. [34] Sanderson T.R., et al., *Geophys. Res. Lett., 13* (1986) 411-414. [35] Elliot J.L., et al., *Nature, 424* (2003) 165-168. [36] Hubbard W.B., *Nature, 424* (2003) 137-138. [37] Sicardy R., et al., *Nature, 424* (2003) 168-170. [38] Delamere P.A., Bagenal F., *Geophys. Res. Lett., 31* (2004) doi:10.1029/2003GL018122. [39] Harnett E.M., et al., *Geophys. Res. Lett., 32* (2005) doi:10.1029/2005GL023178. [40] Tian F., Toon O.B., *Geophys. Res. Lett., 32* (2005). [41] Strobel D.F., *Icarus, 193* (2008) 612-619. [42] Tucker O.J., et al., *Icarus, 217* (2012) 408-415. [43] McNutt R.L., Jr., et al., *Space Sci. Rev., 140* (2008) 315-385. [44] McNutt R.L., Jr., et al., *Science, 318* (2007) 220-222. [45] Haggerty D.K., et al., *Journal of Geophysical Research (Space Physics), 114* (2009) 02208. [46] Hill M.E., et al., *Journal of Geophysical Research (Space Physics), 114* (2009) 11201.

GLOBAL SURFACE-ATMOSPHERE INTERACTIONS ON PLUTO.

T. I. Michaels[1], [1]SETI Institute (189 Bernardo Ave Suite 100, Mountain View, CA 94043; tmichaels@seti.org).

Introduction: Pluto is known to have complex albedo patterns which exhibit changes on relatively short timescales (a small number of Earth-years) [1-3]. This world also currently possesses an atmosphere significant enough (e.g., [4-6]) to exhibit organized dynamic behavior (e.g., [7]) that may strongly modulate the (re)distribution of surface ices. A wealth and variety of observations and other work have provided constraints and tantalizing clues into the nature of Pluto's climate system, but the fact remains that little is known or understood in a spatially- or temporally-comprehensive manner. Fortunately, numerical modeling may be used to begin to bridge these knowledge gaps, and to better anticipate what the *New Horizons* spacecraft may observe on Pluto in July 2015.

Current Investigative Approach: A three-dimensional global climate model (GCM) for Pluto has been exercised to better elucidate some key aspects of Pluto's contemporary global surface-atmosphere interaction(s). This GCM (based on the terrestrial model OLAM [8]) uses an unstructured horizontal grid, assumes no topography, and simulates the surface/subsurface and the lowest ~100 km of the atmosphere. It incorporates a surface/subsurface submodel capable of tracking the seasonal and diurnal transfer of volatile surface ices, and full surface layer and boundary layer turbulence parameterizations. The "contemporary" climate epoch to be investigated (1988-2018) was chosen partly because it spans the seasonally interesting times of Pluto's perihelion and equinox. Since the atmosphere of Pluto is thought to be in (or near) vapor pressure equilibrium with the surface ices, the changes in insolation during this period should have a large impact on the surface pressures. This epoch was also chosen because it encompasses the existing observational constraints and an expected future dataset from the NASA *New Horizons* spacecraft. Existing observations and other constraints have been used as model inputs where possible, and/or as items that the model aims to reproduce and further interpret.

Some Preliminary Examples: Some preliminary examples of the output of the GCM are presented below (Figs. 1-5), with an emphasis on atmosphere-surface interactions. Note that the runs shown are for equinox insolation conditions, include only beta-phase N_2 ice, and are all plotted from the global state at the same instant in time.

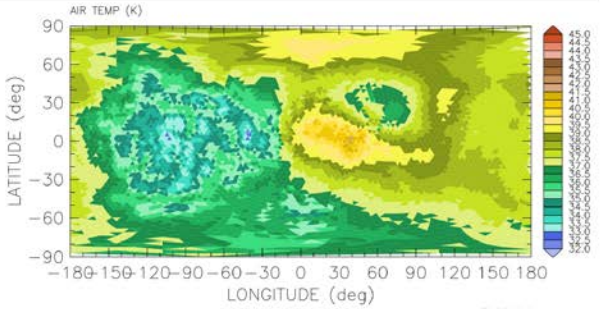

Figure 1. Horizontal (lat/lon) plot of instantaneous near-surface air temperature [K]; the left half (roughly) of the plot is the dayside; surface sublimation/deposition and atmospheric dynamics result in this time-varying asymmetric pattern.

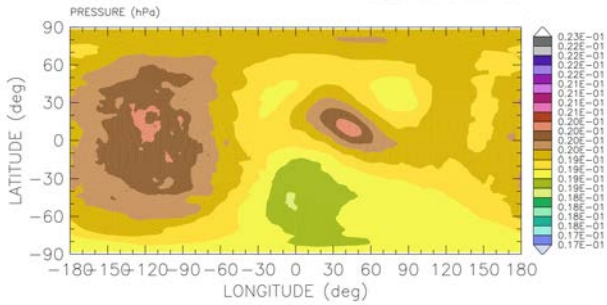

Figure 2. As in Fig. 1, but shows surface air pressure [hPa]; greatest pressure in the afternoon, but also areas of predawn high pressure due to atmospheric dynamics.

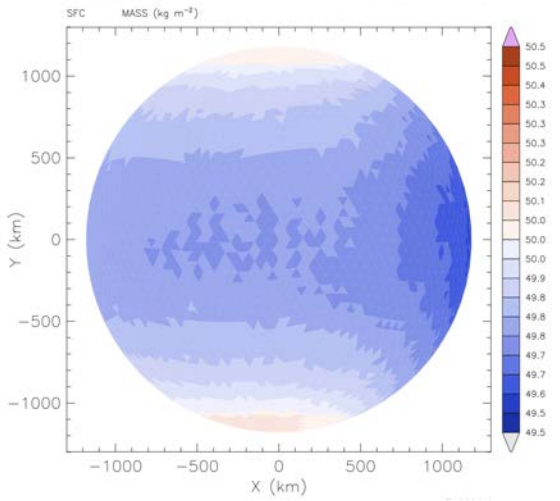

Figure 3. Equatorial orthographic projection (mostly the nightside, dayside at right), showing the surface nitrogen ice mass [kg m^{-2}]; in this equinox season, only the polar regions exhibit a net gain of surface ice (white and reddish colors).

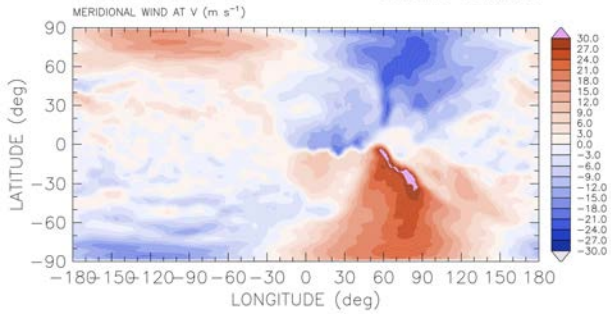

Figure 4. As in Fig. 1, but shows near-surface meridional (N-S) wind velocity [m s^{-1}]; greatest meridional wind magnitudes occur before dawn and in the high latitudes during the afternoon/evening.

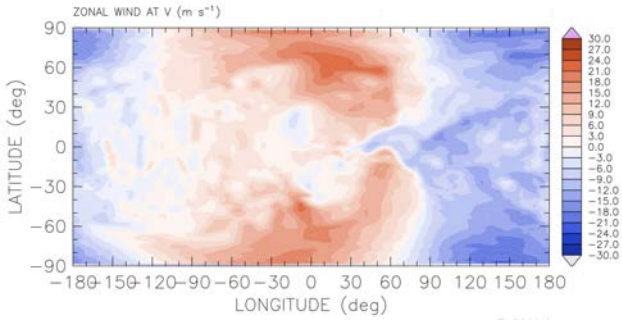

Figure 5. As in Fig. 1, but shows near-surface zonal (E-W) wind velocity [m s^{-1}]; greatest zonal wind magnitudes occur before dawn and in the higher latitudes during the day.

Outlook: The examples of GCM output shown in Figs. 1-5 illustrate some ways in which contemporary Pluto is a dynamic world, particularly with respect to atmosphere-surface interactions. Although it is quite thin, the atmosphere should not be ignored, especially with regard to the global (re)distribution of minor constituents such as methane (carried efficiently by near-surface winds).

It is hoped that the modeled phenomena in these and future GCM simulations will help unravel unexplained details of past and future observations. Further simulations targeting the conditions expected on Pluto in 2015 will be presented at the meeting.

References:

[1] Buie M. et al. (1992) *JGR, 90,* 1151–1154. [2] Stern S. A. et al. (1997) *JGR, 90,* 1151–1154. [3] Buie M. et al. (2010) *AJ, 139,* 1128–1143. [4] Elliot J. et al. (1989) *Icarus, 77,* 148–170. [5] Millis R. et al. (1993) *Icarus, 105,* 282–297. [6] Young E. F. et al. (2008) *AJ, 136,* 1757–1769. [7] Zalucha A. M. and Michaels T. I. (2013) *Icarus, 223,* 819–831. [8] Walko R. L. and Avissar R. (2008) *MWR, 136,* 4045–4062.

On the Possible Noble Gas Deficiency of Pluto's Atmosphere

O. Mousis[1,2], J. I. Lunine[3], K. E. Mandt[4], E. Schindhelm[5], H. A. Weaver[6], S. A. Stern[5], J. H. Waite[4], R. Gladstone[4] and A. Moudens[7], [1]Université de Franche-Comté, Institut UTINAM, CNRS/INSU, UMR 6213, Besançon Cedex, France, olivier.mousis@obs-besancon.fr, [2]Université de Toulouse; UPS-OMP; CNRS-INSU; IRAP; 14 Avenue Edouard Belin, 31400 Toulouse, France, [3]Center for Radiophysics and Space Research, Space Sciences Building Cornell University, Ithaca, NY 14853, USA, [4]Space Science and Engineering Division, Southwest Research Institute, San Antonio, TX 78228, USA, [5]Southwest Research Institute, 1050 Walnut Street, Boulder, CO 8030223, USA, [6]Space Department, Johns Hopkins University Applied Physics Laboratory, 11100 Johns Hopkins Road, Laurel, MD 20723-6099, USA, [7]LERMA, Université de Cergy-Pontoise, Observatoire de Paris, ENS, UPMC, UMR 8112 du CNRS, 5 mail Gay Lussac, 95000 Cergy Pontoise Cedex, France.

Abstract: We use a statistical-thermodynamic model to investigate the formation and composition of noble-gas-rich clathrates on Pluto's surface.

By considering an atmospheric composition close to that of today's Pluto, and a broad range of surface pressures, we find that Ar, Kr, and Xe can be efficiently trapped in clathrates if they formed at the surface, in a way similar to what has been proposed for Titan. The formation on Pluto of clathrates rich in noble gases could then induce a strong decrease in their atmospheric abundances relative to their initial values. A clathrate thickness of order of a few centimeters globally averaged on the planet is enough to trap all Ar, Kr and Xe, if these noble gases were in protosolar proportions in Pluto's early atmosphere.

Because atmospheric escape over an extended period of time (millions of years) should lead to a noble gas abundance that either remains constant or increases with time, we find that a potential depletion of Ar, Kr and Xe in the atmosphere would best be explained by their trapping in clathrates. A key observational test is the measurement of Ar, since the Alice UV spectrometer aboard the New Horizons spacecraft will be sensitive enough to detect its abundance 10 times smaller than in the case considered here.

EXOTIC SODAS: CAN GAS EXSOLUTION DRIVE EXPLOSIVE CRYOVOLCANISM ON PLUTO AND CHARON?

M. Neveu[1], D. C. Napolitano[2], A. D. Edwards[2], S. J. Desch[1], C. R. Glein[3], and E. L. Shock[1,2]. [1]School of Earth and Space Exploration, Arizona State University, Tempe, AZ 85287, USA. [2]Department of Chemistry and Biochemistry, Arizona State University, Tempe, AZ 85287, USA. [3]Geophysical Laboratory, Carnegie Institution of Washington, 5251 Broad Branch Rd. NW, Washington, DC 20015, USA. (mneveu@asu.edu).

Explosive Cryovolcanism in the Outer Solar System: Active outgassing of volatiles has been observed on Triton (N_2) [1] and Enceladus (H_2O) [2]. The radii (1350 and 250 km) and densities (2 and 1.6 g·cm^{-3}) of these moons bracket those of the Kuiper Belt Objects (KBOs) Pluto and Charon (1150 and 600 km; 2 and 1.6 g·cm^3), suggesting similar bulk compositions, internal structures, and thermal histories. Internal evolution models have hinted at liquid water layers inside Pluto [3] and Charon [4]. Detections of short-lived species on the surface of Charon [5,6] are also compatible with recent cryovolcanism.

A Mechanism for Explosive Cryovolcanism: We assume that Pluto and Charon partially or fully differentiated into rocky cores and icy mantles, and retained liquid layers in between. Crawford and Stevenson [7] investigated a gas-driven mechanism for the ascent of denser aqueous cryolava through a water ice mantle. Liquid-filled cracks spontaneously propagate through the ice layer up to the hydrostatic level, at depth $(1 - \rho_{\rm ice}/\rho_{\rm water}) \cdot d$ from the surface of the ice layer, where d is the ice layer depth. Overshooting the hydrostatic level to reach the surface requires an additional drive. As liquid rises, the overburden pressure decreases, leading to the exsolution of dissolved volatiles. Gas rises to the top of the water column and drives crack propagation by positive buoyancy, pumping some liquid to the surface [7]. This would happen too fast (10^5 s) for liquid to refreeze on the cold walls of a 1-m diameter cylindrical conduit, because the latent heat of freezing takes about 10^6 s to be conducted away [7]. The pressure-driven exsolution is slightly mitigated by the temperature drop in the rising fluid, which favors dissolution. Were KBOs to retain an undifferentiated crust [4], fluid-filled cracks would rise by positive buoyancy through that ice-rock mixture.

The Volatile Culprits: Accreted volatiles were presumably initially trapped in amorphous ice or as clathrate hydrates. Subsequent softening or melting of ice due to heating by short- and long-lived radionuclides, tidal interactions, differentiation, or exothermic water-rock reactions would have released volatile impurities into the aqueous melt. Thus, the icy mantle may be purer water than the liquid layer, whose dissolved volatiles would act as antifreezes to preserve it on geological time scales [3,4]. Which volatiles do we expect in the liquid? Comet spectroscopy has shown that key species are carbon monoxide CO (coma abundance of 0.4 to 30% with respect to water), carbon dioxide CO_2 (2 to 30%), methane CH_4 (0.4 to 1.6%), methanol CH_3OH (0.2 to 7%), ammonia NH_3 (0.2 to 1.4%), and hydrogen sulfide H_2S (0.12 to 1.4%) [8]. Diatomic and atomic species such as N_2 and Ar, not accessible with this technique, should also be considered. These abundances are consistent with observations of extrasolar protoplanetary disks [9] and measurements of the Enceladus plume [2]. We assume that these species were also accreted by KBOs. H_2 resulting from water-rock reactions may also be present.

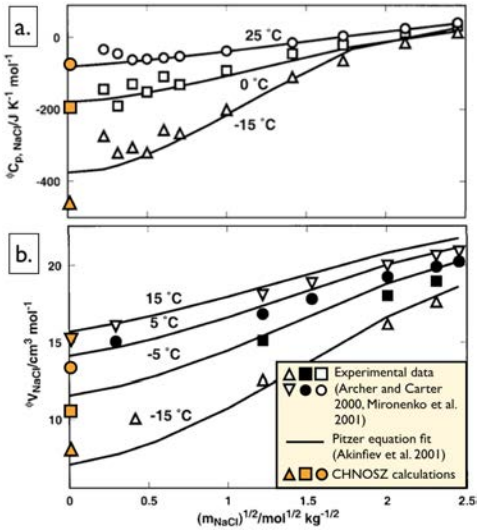

Figure 1: Apparent molar heat capacity (*a.*) and volume (*b.*) of NaCl at subzero temperatures as a function of the square root of the NaCl molality. CHNOSZ predictions are as accurate as the Pitzer fits [14] to experimental data [15,16] at low T. Modified from [14].

Testing the Validity of Subzero Geochemical Calculations: At chemical equilibrium, the number of moles of a given dissolved volatile per kilogram of water, or molality m, is given by:

$$logK(T,P) = log\frac{\gamma_{\rm volatile\ (aq)} m_{\rm volatile\ (aq)}}{\phi_{\rm volatile\ (g)} P_{\rm volatile\ (g)}} \qquad (1)$$

where K is the equilibrium constant for the reaction Volatile (g) → Volatile (aq) at given temperature T and pressure P, γ is the activity coefficient of the solute, and ϕ and $P_{\rm volatile}$ are the fugacity coefficient and partial pressure in bars of the volatile gas. To evaluate the propensity of volatiles to exsolve as fluid rises, we consider the ideal case of a single volatile dissolved in pure water ($\gamma = 1$). The exsolved gas is assumed to

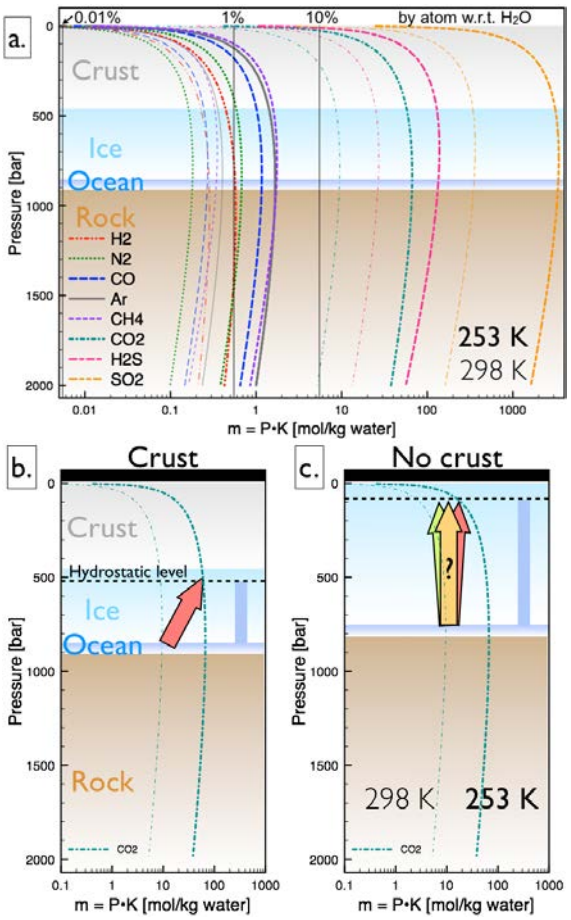

Figure 2: *a.* Ideal solubilities of key volatiles as a function of P (i.e., depth), for T=253 K (thick lines) and 298 K (thin lines). A possible internal structure for Charon [4] is superimposed. *b. and c.* An ice-rock crust inhibits gas exsolution in the mantle, because m seldom varies with P, but increases with decreasing T.

be ideal and composed of the pure volatile ($\phi = 1$ and $P = P_{\rm volatile}$).

T and P range between about 50 K, 0 bar at the surface and 273 K, >1 kbar at the base of the ice [3,4]. Geochemical codes provide $K(T, P)$ from thermodynamic datasets referenced at 298.15 K and 1 bar, using an equation of state for solutes. The Pitzer [10] and HKF [11] equations are commonly used. The former equation has been used down to 173 K in the FREZCHEM code [12], but is derived from polynomial fits to experimental data. Thus, it has little predictive power and is restricted to species for which data are available at given T and P. The semi-empirical HKF equation models interactions between solute molecules in water, and does have predictive capabilities. However, it was developed using data above 273 K. We used the software package CHNOSZ [13] to test the accuracy of the HKF equation down to 253 K (the minimum T achievable with CHNOSZ) to predict solute properties in supercooled water, and found close agreement with experimental data (Fig. 1).

Does Exsolution Occur? Fig. 2a shows the molality m of relevant volatiles as a function of pressure (or depth) at 253 K and 298 K. NH_3 and CH_3OH are not shown because they are very soluble in water, which inhibits degassing. All volatiles follow a similar m vs. P trend, but compounds with greater solubility (higher m) are more sensitive to T. With our assumptions, exsolution occurs at P for which $m(T, P)$ decreases below the bulk concentration, represented by vertical lines in Fig. 2: 10% (primordial CO), 1% (primordial CH_4) and 0.01% (endogenic H_2). Unless it was accreted at less than a few percent, CO never fully dissolves, because the $K(T, P)$ curve is always to the left of the 10% line. The expected trend of m decreasing as pressure drops occurs only at $P < 200$ bar, close to the surface. At higher P, exsolution is offset by the decrease of log K with increasing P, keeping m roughly constant at a given T. As a consequence, undifferentiated crusts *inhibit* exsolution at the liquid/ice hydrostatic level by shifting this level to $P > 200$ bar (Fig. 2b), where m is governed by T which should decrease by 40 to 100 K through the mantle [4], roughly the ΔT between the thick and thin curves. Without a crust, exsolution at the hydrostatic level depends on ΔT through the mantle, which need be just small enough to slightly decrease m (Fig. 2c).

Moving to Lower T and Gas Mixtures: Scarce experimental data on supercooled solutes make calculations below 253 K speculative. The HKF equation goes singular at 228 K where water has a liquid-liquid critical point [17], but in principle calculations can be done at arbitrarily low T. In real cases, $P_{\rm volatile} < P$ and m, which scales with $P_{\rm volatile}$, is decreased.

Acknowledgements: We thank J. M. Dick for modifying the CHNOSZ R geochemistry package to work at subzero temperatures.

References: [1] Smith B. A. et al. (1989) *Science 246*, 1422-1449. [2] Waite J. H. et al. (2009) *Nature 460*, 487-490. [3] Robuchon R. and Nimmo F. (2011) *Icarus 216*, 426-439. [4] Desch S. J. et al. (2009) *Icarus 202*, 694-714. [5] Cook J. C. et al. (2007) *Ap. J. 663*, 1406-1419. [6] Merlin F. et al. (2010) *Icarus 210*, 930-943. [7] Crawford G. D. and Stevenson D. J. (1988) *Icarus 73*, 66-79. [8] Mumma M. J. and Charnley S. B. (2012) *ARAA 49*, 471-524. [9] Carr J. S. and Narita J. R. (2008) *Science 319*, 1504-1506. [10] Pitzer K. S. (1973) *J. Phys. Chem. 77*, 268-277. [11] Helgeson H. C. et al. (1982) *AJS 281*, 1249-1516. [12] Marion G. M. et al. (2012) *Icarus 220*, 932-946. [13] Dick J. M. (2008) *Geochem. Trans. 9*, 10. [14] Akinfiev N. N. et al. (2001) *J. Sol. Chem. 30*, 1065-1080. [15] Archer D. G. and Carter R. W. *J. Phys. Chem. B 104*, 8563-8584. [16] Mironenko M. V. et al. (2001) *J. Phys. Chem. 105*, 9909-9912. [17] Speedy R. J. and Angell C. A. (1976) *J. Chem. Phys. 65*, 851-858.

INTERIORS OF PLUTO AND CHARON

F. Nimmo[1] and I. Matsuyama[2], [1]Dept. Earth & Planetary Sciences, University of California Santa Cruz, fnimmo@es.ucsc.edu, [2]Lunar & Planetary Laboratory, University of Arizona, isa@lpl.arizona.edu

Introduction: Pluto and Charon have somewhat different surface appearances, densities (2.03 vs. 1.65 g/cc) and radii (1153 vs. 604 km). Nonetheless, both probably underwent rather similar evolutionary trajectories, with a few important caveats (see below). The key question addressed here is how to use necessarily limited *New Horizons* observations to infer the internal structures and histories of these bodies.

Similarities and Differences: Charon's smaller radius and density make it less likely to have undergone thermally-controlled processes such as differentiation or convection. On the other hand, if Charon formed during a giant impact [1], its initial mean temperature could have been higher than Pluto's. Circularization of Charon's orbit would have provided a source of energy and stress not available to Pluto, though Charon's current eccentricity is probably zero [2]. Charon's present-day tidal bulge is larger (in relative terms) than Pluto's.

Differentiation and Hydrostatic Equilibrium: Titan is significantly larger than Pluto, yet it does not appear to have fully differentiated [3], so differentiation even of Pluto is not guaranteed [cf. 4]. One way of determining moment of inertia (and thus differentiation state) is by shape measurements [5] – as long as the body is in hydrostatic equilibrium. Smaller bodies are in general less likely to be hydrostatic; Iapetus is comparable in size to Charon and is strongly non-hydrostatic [6], while Titan is hydrostatic [3]. The presence of a subsurface ocean makes a hydrostatic shape more likely (see below). The small orbital inclination of Charon makes using obliquities to provide an independent estimate of moments of inertia very difficult.

Subsurface oceans?: In the presence of an anti-freeze such as NH_3, even Charon could plausibly possess a present-day ocean [4]. Charon's putative formation via impact could have produced an initial ocean, while for Pluto, the main source of energy driving melting is radioactive decay; despinning represents a minor addition [7]. Whether an ocean develops after formation depends on the competing rates of heat production and heat removal, with convection favouring no ocean [7,8].

Signatures of an ocean. If an ocean is present, there will likely be no "fossil bulge" – unlike Iapetus – and the body will be close to hydrostatic [7]. An ocean which formed and then froze will generate early compressional and more recent extensional stresses, while an ocean-free body will exhibit early extension and more recent compression, from thermal expansion effects [7]. An ancient ocean would have permitted larger diurnal tidal stresses on Charon [9]. A near-surface ocean would also change the appearance of large impact features [10]. A freezing ocean could in principle generate large enough pressures to cause cryovolcanism, potentially detectable at the surface [11].

Thermal evolution: A baseline thermal evolution model for a differentiated Pluto [7] results in ice-shell convection, no ocean developing, predominantly extensional surface tectonics and a pronounced fossil bulge. However, the presence of NH_3 could permit an ocean to develop. For Charon, convection is less vigorous but radioactive heating is smaller, so it is currently unclear whether a subsurface ocean is plausible. As at Iapetus, the extent to which large impact basins have relaxed will provide constraints on the thermal evolution of the ice shell [12]. Other tectonic features, such as Ithaca Chasma on Tethys [13], would provide additional constraints on thermal history.

Surface tectonics: Several mechanisms capable of generating global surface tectonic patterns exist. Despinning and orbital recession [9,14] are both likely, but were probably overwhelmed by the much larger effects of thermal contraction/expansion [15]. Diurnal tidal stresses may have been important for Charon [9] and could perhaps have given rise to double ridges similar to those seen at Triton [16]. Both Pluto and Charon are rotationally unstable, so reorientation due to impacts is another potential source of stress [17].

References:

[1] Canup R.M. (2005) *Science 307*, 546.[2] Buie M.W. et al. (2012) *AJ 144*, 15. [3] Iess L. et al. (2010), *Science 327*, 1367-69. [4] Hussmann H. et al. (2006) *Icarus 185*, 258-273. [5] Dermott S.F. and Thomas P.C. (1988) *Icarus 73*, 25-65. [6] Castillo-Rogez J.C. et al. (2007), *Icarus 190*, 179-202. [7] Robuchon G. and Nimmo F. (2011) *Icarus 216*, 426-439. [8] McKinnon W.B. (2006) *Icarus 183*, 435-450. [9] Collins G.C. and Barr A.C. (2008) *Fall Mtg AGU P51C-1425* [10] Schenk P.M. (2002) *Nature 417*, 419-421. [11] Manga M. and Wang C.-Y. (2007) *GRL 34*, L07202. [12] Robuchon G. et al. (2011) *Icarus 214*, 351-355. [13] Giese B. et al. (2007) *GRL 34*, L21203. [14] Collins G.C. and Pappalardo R.T. (2000) *LPSC 31*, 1035. [15] Matsuyama I. and Nimmo F (2013), *LPSC 44*, 1399. [16] Prockter L.M. et al. (2005) *GRL 32*, L14202. [17] Nimmo F. and Matsuyama I. (2007), *GRL 34*, L19203.

The May 4, 2013 Stellar Occultation by Pluto and Implications for Pluto's Atmosphere in 2015

C. B. Olkin[1], A. Pickles[2], L. A. Young[1], D. Borncamp[1], B. Sicardy[3], F. Bianco[2], Martin Norbury[2], L. H. Wasserman[4], R. French[5], M. Buie[1]

[1]Southwest Research Institute, 1050 Walnut Street, Boulder, CO, USA, colkin@boulder.swri.edu. [2] Las Cumbres Observatory Global Telescope Network, Goleta, CA, USA. [3] Observatoire de Paris, Meudon, France. [4]Lowell Observatory, Flagstaff, AZ, USA. [3]Wellesley College, Wellesley, MA, USA.

On May 4 2013, Pluto passed in front of a V~14 star and the shadow was well observed from multiple occultation groups. This paper presents initial results from the three light curves observed at Las Cumbres Observatory Global Telescope Network (LCOGT) from their Cerro Tololo site. The three LCOGT telescopes have 1.0 m apertures and used identical off-axis FLI ML4720 cameras unfiltered. The cameras currently have a 2 second readout time therefore autonomous observations were scheduled with different exposure times to give good time resolution of the event.

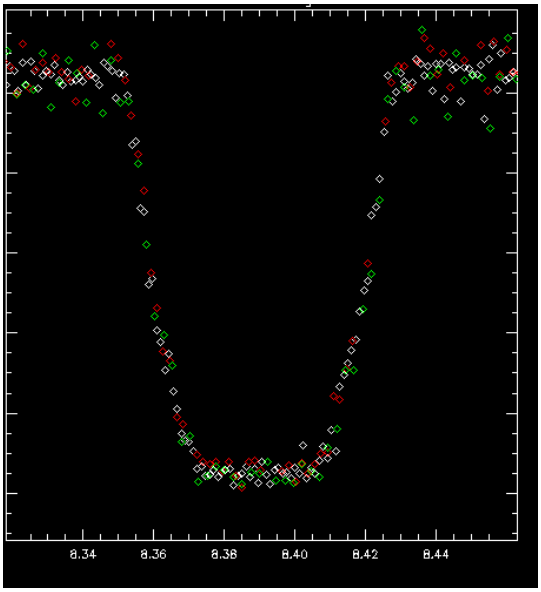

Figure 1. Initial reduction of the LCOGT stellar occultation light curves. The three colors correspond to the three different telescopes.

We will combines these observations with an astrometric solution provided by B. Sicardy and colleagues and carry out a model fit to determine the atmospheric pressure in Pluto's atmosphere in May 2013. This result will be compared with volatile transport models from Young (2012).

References:

[1] Young, L.A., et al. (2013) *ApJL, submitted*

A Detailed Look at Selected Ralph Observations Near Closest Approach

C. B. Olkin[1], A. S. Stern[1], L. A. Young[1], J. Spencer[1], D. Reuter[2], W. Grundy[3], [1]Southwest Research Institute, 1050 Walnut Street, Boulder, CO, USA, colkin@boulder.swri.edu. [2] NASA Goddard Spaceflight Center, Greenbelt, MD, USA. [3] Lowell Observatory, Flagstaff, AZ, USA.

The Ralph instrument is a visible/near infrared multi-spectral imager and a short wavelength infrared spectral imager. Ralph has one input aperture and two sets of focal planes: MVIC (Multi-spectral Visible Imaging Camera) and LEISA (Linear Etalon Imaging Spectral Array). Another paper at this conference describes the Ralph instrument and science objectives (Stern et al.). This paper focuses on presenting details of selected Ralph observations that are either key to addressing Group 1 science objectives [1] or are the best Ralph observations of the small moons of Pluto.

An example of a set of observations that will be described in detail are the 4 LEISA scans that will be used to produce our Group 1 composition map of Pluto. These observations take place 2-3 hours before closest approach to Pluto. The combination of the four scans builds up the coverage of Pluto's illuminated disk and the SNR level.

For each of the key observations, details such resolution, solar phase angle, exposure time and time from closest approach will be given, as in Table 1 for the 4 Group 1 composition map scans.

Table 1. Details of the 4 LEISA scans that address the global composition map objective.

Observation Name	Time from c/a, hr	Resn (km)	Phase Angle, deg.	Exp Time, sec
P_LEISA_Alice_1a	-3.1	0.7	20.1	0.61
P_LEISA_Alice_1b	-2.9	0.7	20.5	0.61
P_LEISA_Alice_2a	-2.6	0.7	21.7	0.58
P_LEISA_Alice_2b	-2.1	0.7	22.5	0.58

The details of spatial coverage for these key observations will be provided by Systems Tool Kit (STK, formally Satellite Tool Kit) simulations or our New Horizons geometric visulizer tool (NHGV). The STK graphics for the four observations targeted to producing the global composition map are presented in Figures 1-4.

Other observations also contribute to the global composition map such as our high resolution approximately one hour before closest approach. This is a regional scan with a resolution of ~1.2 km per pixel.

The depth and redundancy of the Ralph observations near closest approach will be explored.

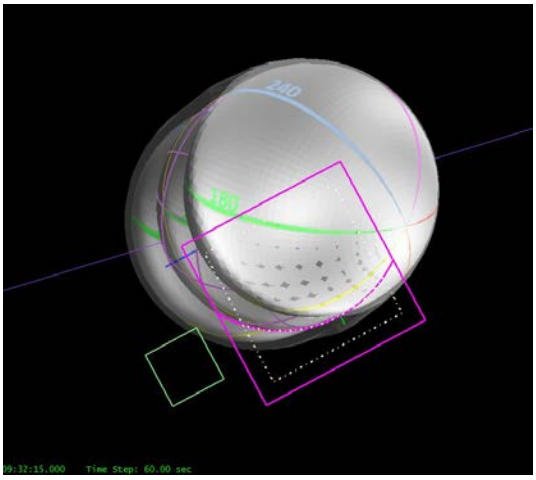

Figure 1. The location of the LEISA field of view (pink box) relative to the Pluto disk (center globe) near the midtime of the P_LEISA_Alice_2a scan across Pluto. The three globes are the 3-sigma positions of Pluto relative to the spacecraft at time of the scan. Lines of longitude are shown on the globe. The nominal limb of Pluto is shown in pink and the deadband uncertainty is depicted by the white dotted line inside the LEISA field of view. The green box is the LORRI field of view used to orient the viewer to the orientation of the spacecraft.

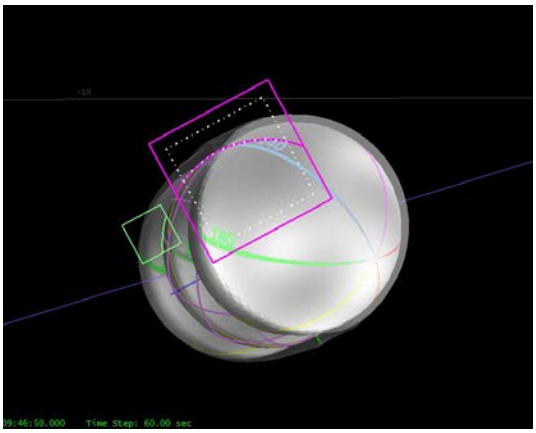

Figure 2. Same STK image as above except for the complementary scan P_LEISA_Alice_2b

References:

[1] Young, L.A., et al. (2008) *Space Sci. Rev, 140*, 93

Mass Determination of Pluto and Charon from New Horizon REX Radio Science Observations

M. Pätzold[1], T.P. Andert[2], G.L. Tyler[3], M.K. Bird[1], D.H. Hinson[3] and I.R. Linscott[3]
[1] Rheinisches Institut für Umweltforschung, Dep. Planetary Research, Cologne University, Köln, Germany (mpaetzol@uni-koeln.de)
[2] Institut für Raumfahrttechnik und Weltraumnutzung, Universität der Bundeswehr München, Neubiberg, Germany
[3] Department for Electrical Engineering, Stanford University, Stanford, CA, USA

Abstract: The anticipated 14 July 2015 New Horizons fly-through of the Pluto system provides the first opportunity to determine both the total system mass and the individual masses of Pluto and Charon by direct observation. This will be accomplished by use of: i) two-way Doppler radio frequency tracking data during intervals along the fly-in and -out trajectory, and ii) one-way uplink Doppler frequency recorded by the on-board radio science instrument, REX, during the day of closest approaches to Pluto and Charon. Continuous tracking is not feasible as a result of pointing sharing with the instruments during the encounter phase. Needed radio tracking will be obtained during time slots shared with i) two-way Doppler tracking for navigation, ii) 'plasma rolls' with the spacecraft antenna pointing to Earth, and iii) during the ingress and egress phases of the occultations. Simulations of the NH encounter indicate the potential accuracies of the combined and individual mass determinations of Pluto and Charon in the order of 0.1%.

Long-Range Kuiper Belt Object Observations: Prospects and Scientific Value

Alex H. Parker[1†], Darin A. Ragozzine[11,1], Marc W. Buie[2], David J. Osip[3], Stephen D.J. Gwyn[4], Matthew J. Holman[1], David M. Borncamp[2], John R. Spencer[2], Susan D. Benecchi[5], Richard P. Binzel[6], Francesca E. DeMeo[6], Sébastian Fabbro[4], Cesar I. Fuentes[7], Pamela L. Gay[8], JJ Kavelaars[4], Brian A. McLeod[1], Jean-Marc Petit[9], Scott S. Sheppard[5], S. Alan Stern[2], David J. Tholen[10], David E. Trilling[7], Lawrence H. Wasserman[12]. [1]Harvard-Smithsonian Center for Astrophysics, [2]Southwest Research Institute, [3]Carnegie Observatories, Las Campanas Observatory, [4]Canadian Astronomy Data Centre, National Research Council of Canada, [5]Carnegie Institute of Washington, Department of Terrestrial Magnetism, [6]Massachusetts Institute of Technology, [7]Northern Arizona University, [8]Southern Illinois University, [9]Universite de Franche Comte, CNRS, UTINAM, [10]University of Hawaii, Institute for Astronomy, [11]University of Florida, [12]Lowell Observatory. †: `aparker@cfa.harvard.edu`

Introduction: After its 2015 Pluto encounter, the New Horizons spacecraft will sweep outward through the Kuiper Belt. We are conducting a survey to identify a Kuiper Belt object for the New Horizons spacecraft to redirect toward and study at close range. In the course of this survey, we have identified a number of Kuiper Belt objects that, while too distant to be reached by the spacecraft, are nevertheless close enough ($0.1-0.2$ AU at closest approach) to be easily detectable by the spacecraft's *LOng-Range Reconnaissance Imager* (LORRI) instrument. Observations by LORRI will allow unique measurement of Kuiper Belt Object phase curves at high phase angles, possibly constrain shape models for a handful of these objects, and permit a search for close binary companions.

Potential targets: To date, the most promising candidates for long-range reconnaissance that we have identified in our survey are 2011 JW_{31}, 2011 JY_{31}, and 2011 HZ_{102}. These three objects are all consistent with being Cold Classical Kuiper Belt objects, on low-inclination, low-eccentricity orbits, with diameters of 50-100 km. All three make their closest approach to the spacecraft in 2018. Figure 1 illustrates their flyby trajectories and visibility from New Horizons, and demonstrates that each will remain detectable to *LORRI* for many months.

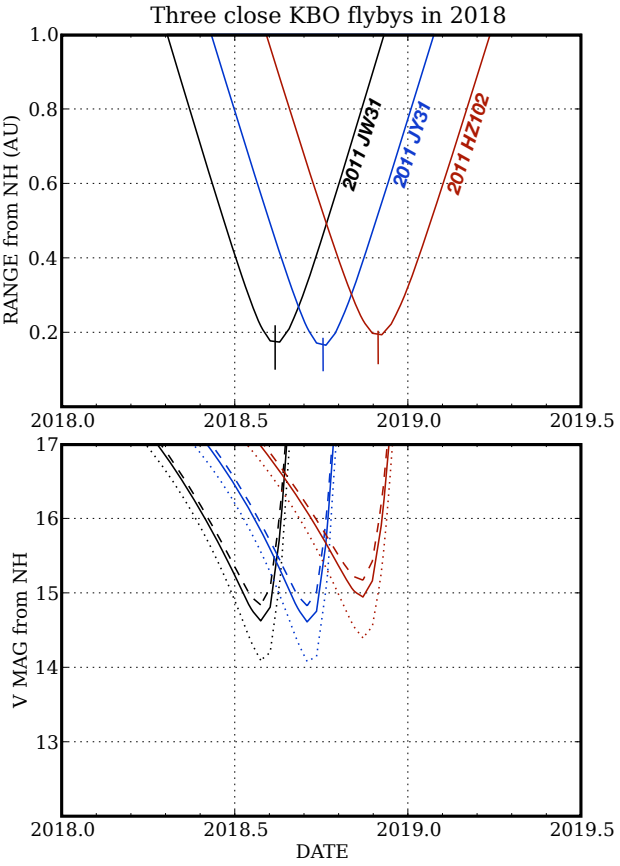

Figure 1: Illustration of the New Horizons long-range flyby circumstances for 2011 JW_{31}, 2011 JY_{31}, and 2011 HZ_{102}, three objects we discovered in the course of our search for a post-Pluto flyby candidate. Top panel illustrates physical range vs. time, and bottom panel illustrates apparent V-band magnitude vs. time. Bottom panel bands indicate range of plausible phase functions. *LORRI* is capable of detecting objects to $\sim 17^{th} - 18^{th}$ magnitude[1], though the faintest end requires long (resource-intensive) exposure times.

Scientific Value: Even though these objects' closest approaches are too distant to allow New Horizons to clearly resolve them, and the remaining fuel onboard the spacecraft is insufficient to reach them, New Horizons will still provide a unique vantage point to study these objects. As it flies by, it will view each object over a very large range of phase angles that are impossible to view from Earth, providing otherwise unobtainable information about the surface properties of "ordinary" Kuiper Belt objects. Monitoring rotational variability as the spacecraft flies by may provide unique measurements of these objects' shapes. Finally, while binary systems are extremely common in the Cold Classical Kuiper Belt, the binary fraction at extremely small separation is poorly constrained[2]. At a range of $\sim$ 0.1 AU, New Horizons *LORRI* has an angular resolution many times better than HST and will be able to search for very close binary companions. Such observations will provide novel constraints on the origin of these binary systems, their component bodies' physical structures, planet formation processes in the distant solar system, and the Kuiper Belt's collisional environment[3,4].

Ongoing Survey: Our search for a post-Pluto Kuiper Belt target for New Horizons to visit continues. We expect that other long-range candidates will be identified by our survey in the near future, expanding the sample of these distant objects that we can uniquely investigate from New Horizons.

References: [1] Cheng, A., and 15 co-authors. (2008) Space Science Reviews 140, 189. [2] Kern, S. & Elliot, J. (2006) ApJL 643, L57. [3] Parker, A. & Kavelaars, JJ. (2012) ApJ 744, 139. [4] Nesvorný, D., Vokrouhlický, D., Bottke, W., Noll, K., Levison, H. (2011) AJ 141, 159.

ON (ANY) PLUTO'S COMETARY FAMILY

N. I. Perov[1], D. V. Kolesnikov[2] and E. N. Tikhomirova[3], [1] State Pedagogical University, Respublikanskaya, 108, 150000, Yaroslavl, Russian Federation, e-mail: n.perov@yspu.yar.ru, [2,3] Tereshkova's Cultural and Educational Centers, Tchaikovskogo, 3, 150000, Yaroslavl, Russian Federation, e-mail: en_tihomirova@mail.ru

Introduction: There are 10^{12}-10^{13} comets, moved along elliptical orbits, in the Oort's cloud [1]. Stars and gigantic molecular clouds, passing by near the Sun, set some comets of Oort's cloud move into the internal part of the Solar system and these comets turn into short-periodic comets, long-periodic comets, parabolic comets or hyperbolic comets. The major planets may play an important role in this process [2]. There are only about 4557 comets in modern cometary's catalogues [3], [4], [5]. Development of *theoretical* methods of localization in space-time of undiscovered comets, radiants of meteor streams and forecasting appearances near Pluto uncatalogued minor bodies are of a special interest [6]. (It is considered up to day the discoveries of comets are random and unpredictable [7], [8], [9]).

A model of localizing of undiscovered yet any Pluto's cometary family, based on the hypothesis of interaction of these bodies is presented below.

A Model of Pluto's Cometary Family Origin: Let us consider a model of interaction of a comet with a preliminary parabolic heliocentric orbit, and a planet of mass M_{pl} [10], [11], [12]. The comet at the perihelion of the heliocentric orbit closes with the planet, which moves along circle orbit radius of which equals r_{pl} with velocity V_{pl}. An initial angle between the orbital planes of the comet and the planet is equal to i_0 . The process of interaction of the comet and the planet will be considered like momentary turn of velocity vector V_c of the comet, experienced the closest approach of the planet. An angle of turn θ of the comet velocity vector (in the sphere of action of the planet) is maximum, if the comet approaches with the planet at the minimal distance without destroying. For this distance we take the radius of the planet R_{pl}. (Roche limit is not taken into account). A target parameter of the comet is ρ should be in excess of ρ_{crit} (for the ρ_{crit} $r_{min}=R_{pl}$), otherwise the comet will collide with the planet and recover from further existence in the given model of motion. The comet with velocity of V enters into the sphere of influence of the Sun - mass is M_{Sun}. Setting for the heliocentric motion $r_{pl} \approx r$ (for the moment of time of "collision' of comet and planet) we determine by analytically tractable an angle of turn θ of a velocity vector of the comet in the sphere of influence of the planet, a semimajor axis a, an eccentricity e, true anomaly v of the comet for the new heliocentric orbit (after scattering) the comet by gravitational field of the planet and egress of this object from the sphere of the planet influence) and an angle α between the heliocentric radius–vector of comet $\boldsymbol{r}$ and the vector of the heliocentric velocity $\boldsymbol{V}$. The new perihelion distance of the comet denote by $q=r_P$. The new aphelion distance of the comet denote by $Q=r_A$. The parameters of the final orbit of the comet are concerned with some parameters of the original (parabolic in accordance with the model) orbit of the comet as well as the parameters of the planet by the following formulae, corrected with reference to [10], [11], and [12]:

$$\nu' = \frac{1}{\left[\frac{M_{Sun}}{M_{pl}} \cdot \frac{R_{pl}}{r_{pl}}(3-2\sqrt{2}\cos i_0) \ +1\right]^2}. \qquad (1)$$

$$a = \frac{r_{pl}}{4 \cdot \nu'(\sqrt{2}\cos i_0 - 1)}, \qquad (2)$$

$$e^2 = 1 - 8\nu'(\sqrt{2}\cos i_0 - 1)\{[1 - \sqrt{2}\,\nu'(\sqrt{2} - \cos i_0)]^2 + 2\nu'^2 \sin^2 i_0\} \qquad (3)$$

$$\tan i = \pm \frac{\sin i_0 (1 - 2\nu')}{\cos i_0 - \sqrt{2}\nu'(\sqrt{2}\cos i_0 - 1)} \qquad (4)$$

Further, in the expressions (1) – (4), will be put - the planet moves in the plane of ecliptic. (Here an analytical model of migration of comets is used, but the most of researchers prefers to use numerical integration of equations of motion of celestial bodies in order to clear out the details of this migration process and especially details of the process migration of minor bodies from the Kuiper's belt).

Parameters of Pluto's Cometary Orbits Family: In this section parameters of the cometary orbits after the *unobserved before now* comets, moved from the periphery of the Solar system into the Pluto's orbit, closest approach with Pluto are presented. Using numerical values of the known parameters of Pluto and equations (1) – (4), for various numerical values of i_0 , it is easy to find parameters of the final cometary's orbit: i, ν', a, e, v and then it is possibly to determine the instant of time and the true anomaly of the comet, when it crosses (or only approaches) the orbit of Pluto. These facts are proposed to use for searching for unknown comets, "meteor streams" and meteoroids near Pluto.

For an example let consider two parabolic comets.

Both of them at the perihelion of the heliocentric orbit pass near Pluto. We assume [6] $a_E = 149.597 \cdot 10^9$ m, $M_{Sun} = 1.989 \cdot 10^{30}$ kg, $M_{pl} = 13.09 \cdot 10^{21}$ kg, $r_p = 5.906440628000 \cdot 10^{12}$ m. $R_{pl} = 1150000$ m.

In accordance with the given above model and using formulae (1)–(5) put the result of calculation into the Table 1.

Table 1. Parameters of hypothetical final heliocentric orbits of comets (meteoroids) after close approach up one radius of Pluto. The original heliocentric orbits of the comets are parabolic. Initial inclinations of the orbital planes of these comets equal i_0=0º and $i_0 = \pi/5$. (See also text).

i_0 , deg	0	35.99999
v'	0.02708	0.002055
a, AU	879.71988	33319.97411
e	0.95554	0.99881
i, deg	0	35.9019
cos(v)	0.98062	0.99415
q, AU	39.1086	39.3669
Q, AU	1720.3311	66600.5813

In figures 1, 2, 3 some parameters – *i*, *e*, *a* - of Pluto's cometary family final orbits depended on i_0 are presented.

Conclusion: The observational and theoretical works of such kind will be favor the development of methods for searching of unknown minor bodies based on the known positions of major bodies of the Solar and exosolar systems [10]. It is interesting to check up these results with help of "New Horizons".

References: [1] Wiegert P., Tremaine S. (1999) *Icarus.* V. 137. P. 84-121. [2] Levison H.F., Morbidelli A., Dones L., et.al. (2002) *Science.* V. 296. № 5576. P. 2212 – 2215. [3] http://cfa-www.harvard.edu/iau/mpc.html. [4] Marsden B.G. and Williams G.V. (2000) *Catalogue of Cometary Orbits, 17th edition. SAO. Solar, Stellar Planetary Science Division*. Cambridge. 196 p. [5] http://www.johnstonsarchive.net/astro/sslist.html. [6] Tholen D. J. and Buie M. W. (1997) In *Pluto and Charon*. P. 193–219. (Eds. S. A. Stern and D. J. Tholen. University of Arizona Press, Tucson). [7] Fernandez J.A., Gallardo T. (2002) *Icarus.* V. 159. P. 358 – 368. [8] Jedicke, Morbidelli A., Spahar T. et al. (2003) *Icarus*. V. 161. P. 17 – 33. [9] Kresak L. (1994) Proc. *of the IAU symposium. N 160.* "Asteroids, comets, meteors 1993" (June 14-18, 1993, Belgirate, Italy). P. 77-94. [10] Perov N.I. (2005) *SSR, 39,* 247-253. [11] Perov N.I. (2004) *LPS XXXV,* Abstract #1040. [12] Perov N.I. (2005) *LPS XXXVI,* Abstract #1049.

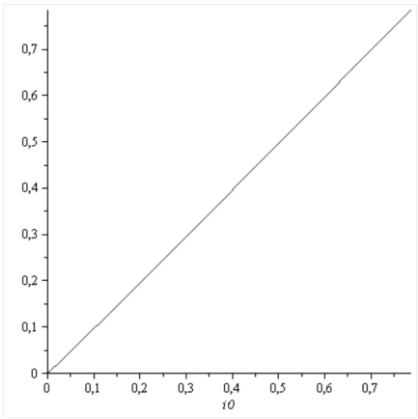

Fig. 1. Initial (i_0, *rad*) and final inclinations (*rad*) of (any) Pluto's cometary family in the considered celestial mechanical model.

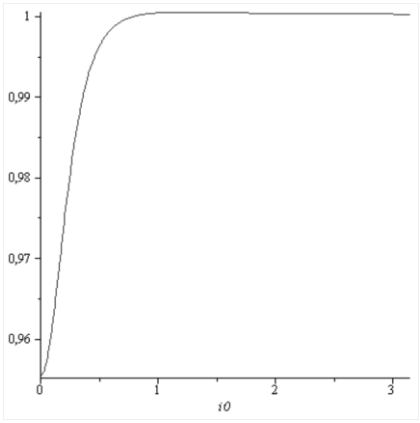

Fig. 2. Initial inclinations (i_0, rad) and final eccecentricities of (any) Pluto's cometary family in the considered celestial mechanical model.

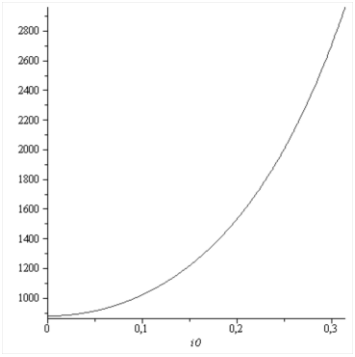

Fig. 3. Initial inclinations (i_0, rad) and final semimajor axis of (any) Pluto's cometary family in the considered celestial mechanical model.

DOES PLUTO'S RING EXIST?

N. I. Perov, State Pedagogical University, Respublikanskaya ul, 108, 150000, Yaroslavl, Russian Federation, E-mail: n.perov@yspu.yar.ru

Introduction: Evolution of the Pluto's system is one of the modern astronomy unsolved problem [1], [2]. Now it is known 5 natural satellites of Pluto and is not revealed any ring near this dwarf planet [3].

At Pulkovo, using 62-years series observations, new effects in the system of Pluto–Charon have been discovered [4]. Particularly, periodic variations of the magnitude of Pluto with period of P=7.76 years are found.

In the frame of celestial mechanics we put forward and investigate a hypothesis of the orbital evolution of a ring or an unclosed ring (system of any rings) spaced near Pluto introduces the period P to account for the time dependence of magnitude of Pluto (or Pluto's system).

A Method of Localizing of (Any) Ring of Pluto: From the epoch of Lagrange to the present time there are several striking examples of successful theoretical predicting of the existence of unknown celestial bodies. These bodies are observed in reality years after they have been advanced theoretically [5], [6].

The integrable in closed form celestial mechanics problems play the most important role in such theoretical methods of localizing previously unobserved astronomical bodies [7].

We shall try to consider (any) ring of Pluto using the integrable (in quadrature) problem of evolution of a satellite orbit under the combined effect of flattening of the central planet and attraction of a sufficiently distant external body. As a first approximation the secular evolution of the satellite orbit is described by equations in elements with mean of the perturbed function with respect to short-period variables e.g., mean anomalies of the satellite and perturbed point (only Charon is considered), barring commensurabilities of the lowest orders between periods. Such averaging is performed independently and gives (in Hills' approximations) the following expression for the secular part of perturbed function [8]

$$W=(3/16)\mu_1 a^2 a_1^{-3}[2(e^2-\sin^2(i))+e^2\sin^2(i)(5\cos(2g)-3)]+(3/8)\mu a_0^2 c_{20} a^{-3}(1-e^2)^{-3/2}[-1/3-\cos(2i)+2s(1-s^2)^{1/2}\sin(2i)\cos(\Omega)+2s^2(\sin^2(i)\sin^2(\Omega)+\cos(2i))]. \quad (1)$$

If the equatorial plane of Pluto and the orbital plane of Charon coincide (inclination i_1=0º) then $\sin(i_1)=s=0$. Here, i is the inclination, Ω is the longitude of the ascending node, *and g* is the argument of periapses. These elements of the osculating particle's orbit refer to the plane of Charon's orbit an the first Point of Aries; a is the semimajor axis and e is the eccentricity of the particles orbit; μ and μ_1 are the products of the gravitational constant by the mass of Pluto and Charon respectively, c_{20} is the the coefficient of the second zonal harmonic of the gravitational field of Pluto (at the first time approximately estimated in the work [6]); a_0 is the mean equatorial radius of Pluto, t is Newton's uniform time; a is the semimajor axis of the circular orbit of Charon (e_1=0.0030 [1]) Using the equation (1) we may derive the equation for determination of an admissible regions of parameters of orbits of hypothetical particles with known evolutionary period P. Computing the value of the corresponding integral [2]:
we consider only the case of circulation of the parameter g (we ignore the libration of g that is no less practically important case). The numerical values of the hypothetical particles orbits parameters with known evolutionary period P are received using the parameters of the Pluto–Charon system [1], [2], [6].

Let the initial value of the particle periapses argument equal g_0=0º, and the final one (quarter period passes) equal $g_k=\pi/2$. The results of calculating in accordance with considered model is presented in fig.1. The figure shows the arrangement of the isochrones P=7.76 years. The isochrone is in agreement with the period of the hypothetical particles orbital motion. The motion of the particle's orbits line nodes (Ω) and evolution of inclination (i) do not consider at once. The extracted celestial mechanical model results for small values of e and i show *there is a spatial region in the system of Pluto-Charon where the keplerian periods are equal and the periods of the particles orbits argument motion are also equal* (the error is about 1%) and the values of e and i of these orbits distinctly differ. In the figure the curve steeply slopes down in this region. The corresponding periapses of hypothetical particles orbits lie between the limits 2510 km and 2520 km from the center of Pluto's mass. The orbital periods are distinguished from each other by about $\Delta T/T=(3/2)\cdot(\Delta a/a)\sim 0.01$. The characteristic size of the spherical layer in the considered region is equal to h=440 km (a=2515 km, i=10º). So, if the region with periodic varying of concentration of the non-interacting particles in the Pluto's system has such size then the scope for the new interpretation of periodic time-varying brightness of Pluto is revealed.

Modeling of the Lifetime of Ring Particles in the Presence of Pluto's Atmosphere: In order to estimate the lifetime of the hypothetical ring particles located

near Pluto and moving in a resisting medium the equation (2) will be under consideration [9].

$$d^2\mathbf{r}/dt^2 = -GM_{Pl}\mathbf{r}/r^3 - (1/2)\rho_A \mathbf{V}\mathbf{V}SC_D/m \qquad (2)$$

Here, **r** is a radius vector of the ring's particle with respect of Pluto's mass center? G and M_{Pl} are the gravitational constant and mass of Pluto, respectively, m is mass of the particle, ρ_A – is density of Pluto's atmosphere, S is a drag area, C_D is a dimensionless drag coefficient, **V** is a vector of velocity of the particle in respect of the surrounding medium. In accordance with data of [1] we may estimate the lifetime of different ring's particles/ The lifetime of the large–size (R=1 m) and dense (ρ=1000 kg/m^3) particles (T=35 K, P_S=0.1 Pa) are in factor of 10^7 excess over the life time of small dimensioned (R=0.1 m) and the friable (ρ=100 kg/m^3) particles (T=45 K, P_s=1 Pa), where T and P_s are temperature and pressure (CH_4, NH_3, H_20) near the surface of Pluto. It means an old ring of Pluto (the life-time equals 10^9 years) must contain large-sized objects and a new one (the life-time equals 10^5 years) may contain small –sized objects and, possibly, the large sized objects. The hypothesis considered here in respect of the origin of the period 7.76 years in the Pluto's system, we see: the applicable bodies are not discovered yet, but their lifetime may be of cosmogony order (10^9 years) in rare Pluto's atmosphere. It should be noted that the model of restricted three body problem (The SUN–Pluto–Charon) the life4time of Charon before its collision with Pluto is estimated about $5.5\cdot10^8$–$3.4\cdot10^{11}$ years [2].

It will be interesting to compare the results given here with the results of forthcoming investigation of Pluto's system (and others triple systems).

References: [1] Tholen D. J. and Buie M. W. (1997) In *Pluto and Charon*. P. 193–219. (Eds. S. A. Stern and D. J. Tholen. University of Arizona Press, Tucson). [2] Perov N.I. and Sadovnikova A.A. (1994) *SSR, 28,* N 4–5, 470–476. [3]http://nssdc.gsfc.nasa.gov/planetary/factsheet/plutofact .html. [4] Rylkov V. P., Viyazev V. V, and Dementieva A. A. (1995) *Astronomical and Astrophysical Transactions, 6,* 265–281. [5] Szebehely V. (1967) *Theory of Orbits. The Restricted Problem of Three Bodies.* Yale University. New Haven Connecticut. Academic Press New York and London. [6] Perov N. I. (1989) *Astron. Tsirk., N 1538,* 33. [7] Seidelmann P. K. (1986) *Celestial Mechanics, 31*, N2, 141–146. [8] Washkovyak M. A. (1996) *Astromomy Letters, 22,* N 3, 231–240. [9] King-Hele D. (1964) *Theory of Satellites Orbits in an Atmosphere*. Butterworths. London.

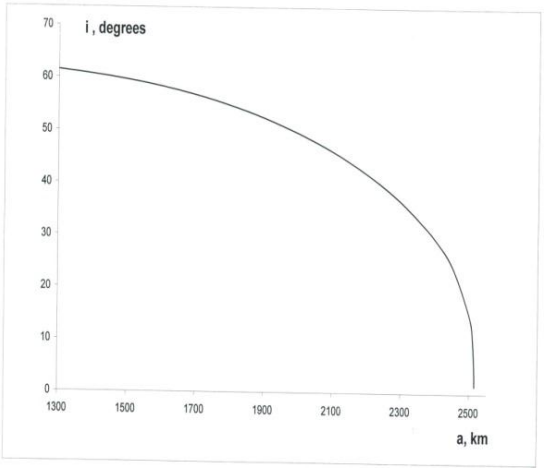

Fig.1. Isochrone (7.76 years) in the plane "**s**emimajor axis (*a*) and inclinations (*i*)" for perturbed motion of periapses of any hypothetical particles moved near Pluto. Moreover, for small inclinations (i<10º) particles moves around Pluto almost with one and the same Kepler's period, forming a thor. Only gravitating of Charon is taken into account.

Trends in Pluto's Atmosphere from Stellar Occultations

M. J. Person, Massachusetts Insitute of Technology (MIT Bldg. 54-418, 77 Massachusetts Ave., Cambridge, MA 02139 – mjperson@mit.edu).

Introduction: Since the first clear measurements of Pluto's atmosphere via stellar occultation in 1988 (*1*), observing these events has remained the most practical means of monitoring Pluto's atmosphere from Earth. In this time, we've seen remarkable changes in Pluto's global atmosphere, such as the doubling of surface pressure between 1988 and 2002 (*2*), as well as tantalizing hints of continuing change in detailed dynamics, such a planetary waves (*3*), and evolution of the atmosphere's low level thermal gradients and haze layers, when present.

Global Changes: Aside from the notable increase in pressure between 1988 and 2002 seen by several groups (*2, 4*), Pluto's overall global pressure has remained fairly stable through the last decade, though with a statistically significant decrease in half-light pressure level of about -1.2 ± 0.2 km/year (*5*). (See Figure 1.) It is expected that this slow decline pressages a total collapse of the atmosphere (*6*), but models differ on the exact timing of this seasonal event (*7*).

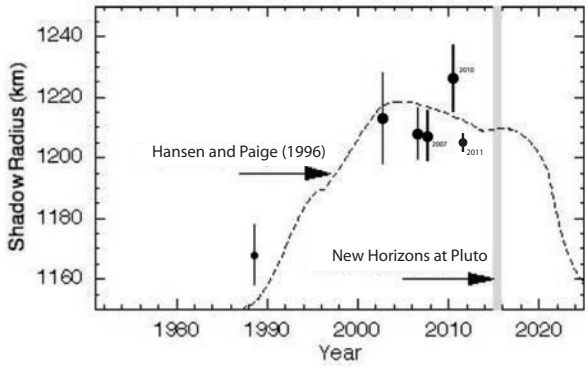

Figure 1: The half-light radius of Pluto's atmosphere as measured by stellar occutlations. Stellar occultation measurement are plotted versus year of obseravation with the dark points and error bars, while a representative pressure model (*6*) is over plotted with the dashed line. Note the decreasing slope in recent years, with the exception of the anomalous 2010 measurement.

Detailed Changes: Beyond these basic changes however, are trends in detailed wave activity (*3, 5, 8, 9*), and lower atmospheric behavior. Evidence of particulate haze in the lower atmosphere has appeared (*1, 10, 11*) and vanished (*3, 12*) over the last decade. Also, the transition level from the upper-atmospheric behavior (a shallow thermal gradient to a severe gradient or haze layer) has dropped over the last several occultations (*5, 13, 14*) and the lower atmospheric onset has changed from a sharp transition (*1*) to a more gradual onset (*5, 15*) over this same period.

References:

1. R. L. Millis *et al.*, *Icarus* **105**, 282 (1993).
2. J. L. Elliot *et al.*, *Nature* **424**, 165 (2003).
3. M. J. Person *et al.*, *Astron. J.* **136**, 1510 (2008).
4. B. Sicardy *et al.*, *Nature* **424**, 168 (2003).
5. M. J. Person *et al.*, *Astron. J.* **submitted**, (2013).
6. C. J. Hansen, D. A. Paige, *Icarus* **120**, 247 (1996).
7. L. A. Young, *Astrophys. J. Lett.* **766**, L22 (2013).
8. W. B. Hubbard *et al.*, *Icarus* **204**, 284 (2009).
9. D. McCarthy *et al.*, *Astron. J.* **136**, 1519 (2008).
10. J. E. Thomas-Osip, J. L. Elliot, K. B. Clancy, *American Astronomical Society Meeting* **34**, 1212 (2002).
11. M. J. Person *et al.*, *Bull. Amer. Astron. Soc.* **34**, 1211 (2002).
12. M. J. Person *et al.*, *(in preparation)*, (2013).
13. M. J. Person, Ph. D., Massachusetts Institute of Technology (2006).
14. J. M. Pasachoff *et al.*, *Astron. J.* **129**, 1718 (2005).
15. A. A. S. Gulbis *et al.*, *Bull. Amer. Astron. Soc.* **38**, 541 (2006).

Acknowledgements: This work was supported, in part, by a NASA Planetary Astronomy grant to MIT (NNX10AB27G).

Preserving Pluto's atmospheric evolution record by archiving stellar occultation data sets in the Planetary Data System (PDS)

M. J. Person[1], L. A. Young[2], and R. G. French[3] [1]MIT (MIT Bldg. 54-418, 77 Massachusetts Ave., Cambridge, MA 02139 – mjperson@mit.edu), [2]SWRI (Southwest Research Institute, Boulder, CO 80302 – layoung@boulder.swri.edu)., [2]Wellesley College (Department of Astronomy Wellesley College, 106 Central St., Wellesley, MA 02481 – rfrench@wellesley.edu).

Introduction: In all the time Pluto has been observed since its discovery in 1930 (*1*), we have seen it pass through only one third of its orbital period. Even worse, from the first occultation observations providing clear evidence of an atmosphere (*2*), we've witnessed only 10% of a Plutonian seasonal cycle. A full understanding of Pluto's seasonal evolution will require decades (if not centuries) of more data, and constant reinterpretation of past data throughout this period.

Thus it is imperative to preserve past data, not only from simple destruction or loss, but also against failures in understanding of previous work, or lack of the necessary context needed to compare the data to future efforts.

Here we present a framework for structuring data acquired from stellar occultation probes of Pluto's atmosphere, and a consistent format for storing this data in a fully accessible archive such as the Planetary Data System.

Occultation Data Framework: For the foreseeable future, we expect stellar occultations to remain the only plausible means of regularly monitoring changes in the pressure and temperature structure of Pluto's atmosphere. Even assuming the hoped-for revelations of the New Horizons flyby, maintaining a reliable occultation record to establish long-term trends in atmospheric conditions will be crucial to providing a baseline for the instantaneous observations made during the flyby.

We present a framework for archiving Pluto stellar occultation data, in order to preserve this vital information for future investigators.

The framework has been developed based upon the following guiding principles:

1) Independent occultation observers should be able to add their data to the archive without requiring contact with or information from previous observers of the same event or reference to their analyses/pipelines.
2) The framework should be flexible enough to include occultation data from varying sources, methods, and analysis techniques, without losing the richness provided by each individual measurement system, but also without requiring numerous inappropriate entries for datasets that do not need them (e.g. simultaneous multi-wavelength light curves versus simple optical timing measurements).
3) Researchers wishing to use data from the archive should be able to do so without needing to contact any outside source (such as the original observers) to explain or otherwise provide context for the archived data.

Archive Progress: Data are being currently archived in the PDS Small Bodies Node. We present a list of occultations that are currently archived as of this posting, including those that had to be rearchived in our new format, and an approximate schedule for the archiving of other datasets available to the authors. We also encourage others groups to similarly archive their data with the PDS using this framework, and provide recommendations for expanding this effort to other bodies beyond Pluto.

References:

1. F. C. Leonard, *Astronomical Society of the Pacific Leaflet* **1**, 121 (1930).
2. R. L. Millis *et al.*, *Icarus* **105**, 282 (1993).

Acknowledgements: The authors gratefully acknowledge the generous assistance provided by the PDS staff, especially Mike A'Hearn and Carol Neese, for their continuing patience with our evolving formats.

This work was supported, in part, by a NASA Planetary Atmospheres grant to Wellesley College (NNX11AD83G) and NASA Planetary Astronomy grants to MIT (NNX10AB27G) and SWRI (NNX12AG25G).

IRAC/SPITZER photometry of the Pluto-Charon System.

N. Pinilla-Alonso[1];J. P. Emery[1]; D. P. Cruikshank [2] [1]Department of Earth and Planetary Sciences, University of Tennessee, Knoxville, TN, USA (npinilla@utk.edu), [2] NASA Ames Research Center, Moffett Field, CA, USA.

Abstract: We present photometry of the Pluto-Charon system obtained with IRAC/Spitzer at eight different longitudes on Pluto's surface. Our aim is to study the surface composition of this icy object and how it changes with rotation.

Introduction: Pluto's surface is known to be covered by volatile ices (e.g N_2, CH_4, C_2H_6 and CO, [1],[2],[3],[4]). It is also known to show patches of different albedo, attributed to differences in composition, with the brightest regions being richer in these volatiles [5]. The composition of the darkest regions is not well known, but it is thought to include complex organic materials. These materials are expected to be photochemical byproducts of the photolysis of Pluto's atmosphere and the radiolysis of its surface.

Recently, [6] obtained the first ultraviolet reflectance spectrum of Pluto that shows a clear absorption in the ultraviolet. Although the authors cannot identify a unique absorber as the origin of this feature, it is also present on the reflectance of complex organic materials. Therefore the possibility of detecting complex organics on the surface of Pluto is promising.

IRAC/Spitzer data have proven to be very useful for investigation of the surface composition of icy objects in the Kuiper Belt. Using IRAC photometry, [7] detects methane and water ice on the surface of the Dwarf Planet Sedna, and [8] suggests the presence of nitrogen on the KBO, Quaoar. Red complex organics are needed as well to model the shape of the reflectance spectra of both KBOs in the visible and NIR.

Results and Analysis: We present fluxes at 3.6, 4.5, 5.8 and 8 microns. These data were acquired at 8 equally spaced observer sub-longitudes. As expected from the heterogeneity on the surface composition of Pluto, the IRAC data show rotational variability.

Comparing these fluxes with the reflectances of ices and complex organics, we aim to shed light on the nature of the different materials present on the surface of Pluto. For example: the band at 3.6 microns is particularly sensitive to the presence of methane, water ice and/or complex organics (e.g., tholins). The band at 4.5 microns is sensitive to the presence of nitrogen, carbon dioxide, and carbon monoxide ices. The spectral region covered by the 5.8 and 8.0 μm channels is less well-studied than shorter wavelengths and therefore offers the possibility of unexpected signatures.

We will also study how these materials are distributed over the surface by comparing the photometry at different longitudes on the surface of Pluto. The IRAC lightcurves do not all follow published visible or compositional lightcurves [e.g., 9]. We will discuss these results in the context of secular evolution, different scattering properties of known ices at IRAC wavelengths, and the possibility of ices not detected at shorter wavelengths (e.g., CO_2).

References:

[1] Cruikshank et al. 1984, Icarus, 58, 306; [2] Cruikshank et al. 1976, Science, 194, 835; [3] De Meo et al. 2010, Icarus, 208, 412; [4] Owen et al. 1993, Science, 261, 745; [5] M. W. Buie, et al. AJ 139, 1128-1143 (2010); [6] Stern et al. (2012) AJ,143,id.22. [7] Emery et al. (2007) A&A, 466, 395; [8] Dalle Ore et al. (2009) A&A, 501, 349; [9] Grundy et al. (2013) Icarus, 223, 710.

Analysis on the dynamics of the Pluto system during Neptune scattering as predicted by the Nice model

P. M. Pires dos Santos[1], S. M. Giuliatti Winter[1], R. S. Gomes[2], [1]Unesp (Ariberto Pereira da Cunha Avenue, 333, 12.516-410 - Guaratinguetá, SP; pos09032@feg.unesp.br), [2]Observatório Nacional (General José Cristino Street, 77, Rio de Janeiro, RJ; rodney@on.br).

Introduction: The planetary migration of the giant planets as suggested by the Nice model [1] creates a dynamical mechanism to reproduce the distribution of objects currently observed in the Kuiper Belt. Through this mechanism planetesimals interior to about 14 AU were delivered to the belt after a temporary eccentric phase of Uranus and Neptune's orbits. At this time, the region interior to 1:2 mean motion resonance (MMR) with Neptune is no longer chaotic, then the bodies transported from orbits closer to the Sun outward can remain trapped [2]. Since there were multiple planetesimal-planet encounters in this scenario, we performed N-body simulations of the Nice model [1], and recorded the trajectories of the planetesimals during close approaches with the giant planets. The effects of the formation scenario as proposed by [1] were tested on passing binaries like Pluto-Charon.

Pluto-Charon binary was proposed to be formed through a collision between two massive protoplanets orbiting the Sun [3],[4]. The current low total mass estimated in the Kuiper belt is unable to form ≥ 100 km sized TNOs [5] around them. Thus, it is more likely that the system is primordial. The idea that Pluto's small satellites grew up from material ejected from Charon's forming impact [4] is not totally accepted. Since the Pluto system is associated with the gravitational scattering by Neptune, then it is necessary to investigate what are the effects of such event on Pluto's members.

At this time, we know that the Pluto-Charon system has 4 small satellites: P5, Nix, P4 and Hydra (in increasing distance from Pluto, respectively) moving in circular orbits and coplanar with Charon. The results of our analysis naturally put some constraints on the formation of Pluto-Charon binary and its small satellites.

Metodology: Initially we analyzed close encounter histories of objects like Pluto-Charon through numerical simulations of the original Nice model, starting at about 875 My. This time is very close to the moment when Neptune changes its position with Uranus and becomes the farthest planet to the Sun. The numerical simulations using the original model are chaotic, so a small change in the program produces very different outcomes.

These numerical simulations were performed to obtain the current configuration of the giant planets and close encounter trajectories of the planetesimals. In those simulations Neptune has a period in highly eccentric orbit, after 2.5 My its eccentricity was damped. When the eccentricities of both ice giants are large, close approaches between planetesimals and the planets are very common. We recorded the encounters passing smaller than 1 Hill's radius of each planet during 4 My.

We selected particles, only those in hyperbolic trajectories with respect to Neptune, with $30 < a < 47.5$ AU, $e < 0.5$ and $4^\circ < i < 40^\circ$. We placed one Pluto-sized object on the trajectory of each close approach with Neptune and the secondary (Charon-sized body) with a equals to the current Pluto-Charon distance, $e<0.90$, the inclination, the initial longitude of the ascending node, and the mean longitude were randomly selected.

Results: Since the encounters with Neptune is the most common, we only use trajectories of encounters with this planet. About 19% of the binaries was destroyed: about 93% due to collisions between binary components, while destruction due to the mutual distance is enlarged to 1 Pluto's Hill radius contributed at 7%.

A large fraction (80%) of Pluto-Charon-like binaries do not become unbound at the end of all close encounter histories. However, we have some issues for which we are working on, for example: the number of planetesimals in the MMRs with Neptune, like 3:2 or 5:3, is too small, even if we consider the classical Kuiper belt (a larger region of non-resonant objects). Therefore, we have changed our approach and now we use the model proposed by [2]-Run A to have a large number of captured objects as Plutinos, and to eliminate the chaotic behavior of the integrator.

Firstly, we performed numerical simulations to obtain the successful configuration of bodies captured in the 3:2 MMR with Neptune, as Run-A by [2]. We used the same initial conditions to planets and the disk of particles, and the same timespan of integration. Then, we have particles caught into 3:2 MMR with Neptune in enough number to integrate binary orbits, or multiple systems like Pluto system. The results of these simulations will be presented.

References:

[1] Tsiganis, K. et al. (2005) Nature, 435, 459-461.

[2] Levison, H. et al. (2008), Icarus, 196, 258-273.

[3] Canup, R. M. (2005) Science, 307, 546-550.

[4] Canup, R. M. (2011) AJ, 141, 35-43.

[5] Stern, S. A. and Colwell, J. E. (1997) AJ, 114, 841-881.

INTERPLANETARY DUST INFLUX TO THE PLUTO SYSTEM: IMPLICATIONS FOR DUSTY EXOSPHERE AND RING PRODUCTION

A. R. Poppe, Space Sciences Laboratory, University of California at Berkeley, Berkeley, CA, 94720 (poppe@ssl.berkeley.edu)

Introduction: The influx of interplanetary dust grains (IDPs) to the Pluto-Charon system is expected to drive the formation of tenuous dusty rings and/or exospheres via bombardment. The characteristics of any potential dusty exosphere or ring systems are directly dependent on the total incoming mass, variability, and composition of interplanetary grains; however, our knowledge of the IPD environment in the Edgeworth-Kuiper Belt (EKB) has, until recently, remained rather limited. Newly-reported measurements by the New Horizons Student Dust Counter combined with previous Pioneer 10/11 meteoroid measurements and a dynamical IDP tracing model have improved the characterization of the IDP environment in the outer solar system, including at Pluto-Charon. Here we report this modeling & data comparison effort, including a discussion of the IDP influx to Pluto and its moons, and the implications thereof.

Interplanetary Dust Model: We use an interplanetary dust grain tracing code to model the dynamical behavior of dust grains originating from the EKB in the range of 0.5 – 25 μm. Each grain is subject to variety of forces, including solar and outer planetary gravitation, solar radiation pressure, Poynting-Robertson drag, and the electromagnetic interaction with the interplanetary magnetic field. The code also follows the size evolution of individual grains due to solar wind sputtering and sublimation, as applicable. The assumed composition of the dust grains is critical to modeling the IDP density and structure as differing composition can yield sputtering and sublimation rates that vary more than two orders of magnitude [1]. To date we have separately considered two distinct dust grain compositions: silicate and ice.

To provide an absolute measure of the EKB density throughout the solar system, the model has been compared to both Pioneer 10 and New Horizons Student Dust Counter (SDC) measurements [2,3]. Since SDC measures grains larger than approximately 0.5 μm while Pioneer 10 measured grains larger than approximately 3.5 μm, both the overall dust production rate from the EKB and the slope of the corresponding mass distribution have been constrained [4]. From these constraints, the density and mass distribution of micron-sized EKB grains can be calculated throughout the solar system. Figure 1 shows the density of 10 μm EKB-generated grains in (a) the ecliptic plane and (b) in the vertical plane. Mean-motion resonances dominate the behavior of dust grains outside the orbit of Neptune,

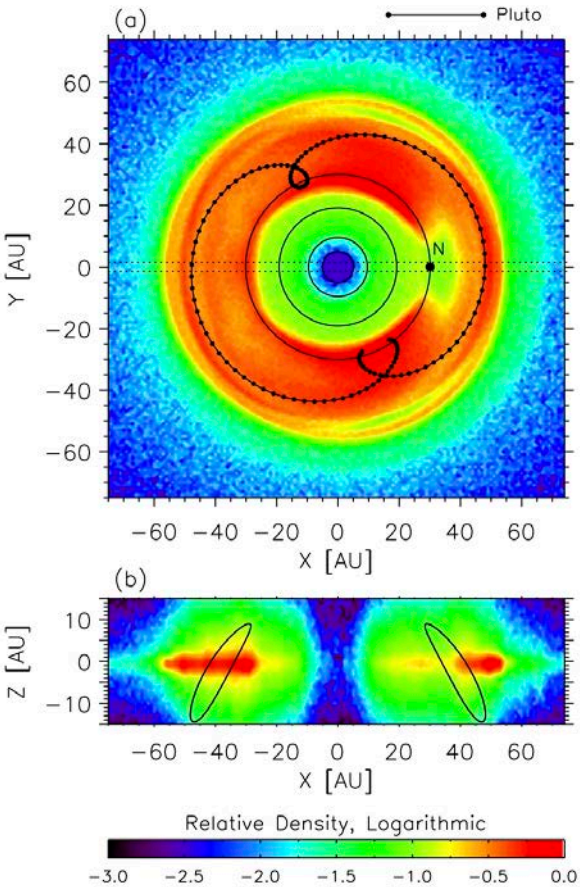

Figure 1: The relative density of 10 μm EKB dust grains in the Neptune-rotated frame both (a) in the ecliptic plane and (b) vertically. In (a), the orbits of the outer planets and Pluto are plotted. Additionally in (b) the Pluto trajectory in the r-z plane is overplotted.

yielding the complex density structure both radially and azimuthally. The character of these structures depends on the parent bodies (EKB classical, scattered or resonant objects) as well as the dust grain size and composition.

Influx to the Pluto System: Using the interplanetary dust model of EKB-generated grains, we trace through the model along Pluto's orbit (rotated into the Neptune-centric frame) and interpolate local dust grain densities and velocity distributions for each grain size. As seen from Figure 1, the interplanetary dust environment at Pluto varies significantly along Pluto's orbit as it repeatedly crosses the ecliptic plane (in addition to dust density variations circumferentially). At Pluto's

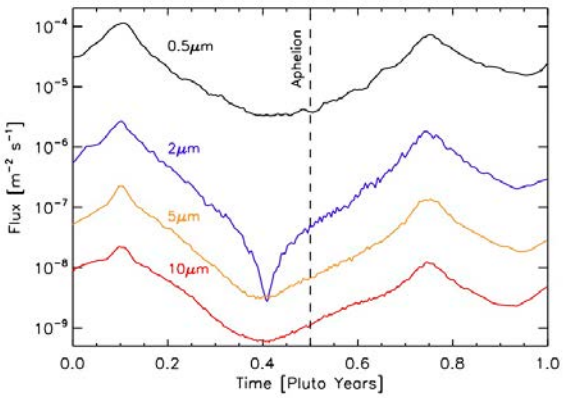

Figure 2: The influx of 0.5, 2, 5, and 10 μm EKB grains into the Pluto system as a function of time. Pluto's aphelion is marked as the dashed line, while perihelion is at t=0 or 1 Pluto years.

greatest extent above or below the ecliptic plane, the dust density drops by more than an order of magnitude. Using the density interpolated along Pluto's orbit, combined with the dust velocity distribution and Pluto's orbital velocity, we calculate the interplanetary dust influx to the Pluto system as a function of time (throughout one Pluto year), shown in Figure 2. Across all grains sizes, the flux peaks twice per Pluto year (t = 0.1 and 0.75 Pluto yrs) corresponding with crossings of the ecliptic plane. Relative minimums occur at approximately t = 0.4 and 0.9 Pluto yrs corresponding with the maximum vertical extent above or below the ecliptic plane. Notably, the IDP influx to Pluto changes by two orders of magnitude as it crosses the ecliptic and the main EKB dust disk.

Implications: The influx of IDP grains is thought to drive the formation of tenuous dusty rings roughly centered on the orbits of Nix and Hydra, with relatively small contributions from Pluto and Charon [5-7]. To date, optical searches have not detected any signature of rings or tori in the Pluto system [8], yet theoretical and computational models have predicted their existence at levels just below current limits. Figure 3 shows the geometric optical depth of a simulated 5 μm ring originating mainly from Nix and Hydra [6]. These previous models, however, have relied on IDP influx estimations using well-known fluxes at 1 AU that are not valid in the outer solar system. Using the newly calculated IDP influx rate and mass distribution, we will re-visit our earlier simulation work on the Pluto-Charon ring/tori system [6]. In addition, we will address the role that external variation in the IDP influx to Pluto has in generating variability in the Pluto ring/torus system.

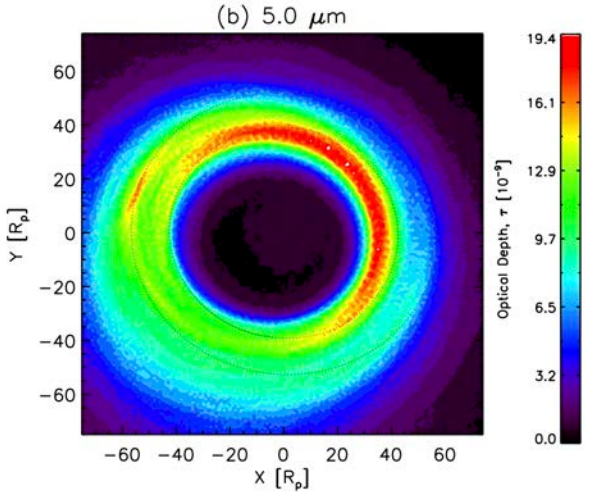

Figure 3: The geometric optical depth of a simulated 5 μm ring in the Pluto-Charon system [6]. The dust torus is centered on the orbits of Nix and Hydra.

References:

[1] Mukai T. and G. Schwehm (1981) *Astron. Astrophys.*, *95* [2] Humes D. H. (1980) *JGR*, *85*(A11), 5841–5852. [3] Poppe A. et al. (2010) *GRL*, *37*(L11101). [4] Han D. et al. (2011) *GRL*, *38*(L24102). [5] Thiessenhusen K.-U. et al. (2002) *Plan. Space Sci.*, *50* [6] Poppe A. and M. Horányi (2011), *Plan. Space Sci.*, *59* [7] Pires dos Santos P.M. et al. (2013), *MNRAS* [8] Steffl A. J. and S. A. Stern (2007) *Astro. J.*, *133*.

Ejecta Transfer within the Pluto System

Simon B. Porter[1,2] and William M. Grundy[1], [1]Lowell Observatory, [2]Arizona State University (**porter@lowell.edu**)

Motivation: Pluto and its satellites form a uniquely complex dynamical system. The small outer satellites (P/5, Nix, P/4, and Hydra) are significantly smaller than Pluto and Charon, small enough that even low velocity impacts can produce ejecta that is moving faster than their surface escape velocity. This produces inter-satellite dust that orbits the Pluto-Charon barycenter until it is either ejected from the system or impacts one of the objects. Very low velocity ejecta can produce relatively long-lived dust orbits, which are a potential hazard for spacecraft navigation. However, the slightly higher velocity ejecta (>25 m/s) can be swept up by a different object from the one it was launched off of. This ejecta generally transfers inward, producing secondary impacts on the more massive objects. The small satellites could have transfered a considerable amount of material to the surfaces of Pluto and Charon.

Simulations: We performed a number of computational simulations of dust trajectories after being ejected from a small satellite. These simulations used a variable-timestep implicit 8th-order integrator to evolve the N-Body system. For each combination of source satellite (Nix or Hydra) and ejecta velocity, we ran a large number of simulations randomizing the start time and the initial direction of the dust particle relative to the source satellite. Due to the short lifetimes of the dust (<1000 days for nearly all impactors), we did not consider solar radiation pressure, Poynting-Robertson or other non-gravitational effects.

Dust Trajectories: The majority of dust trajectories fast enough to not be immediately swept up by their source satellite will quickly leave the Pluto system. However, a fraction of the dust ejected from the small satellites will impact a different satellite. Most of these impacts are on to Pluto and Charon, though there is some transfer between the small satellites. In general, dust which leaves the smaller satellites at low velocities is more likely to impact Charon, while higher velocity dust favors Pluto impacts. The velocities required for the dust transfer are quite low (>25 m/s), and can thus be produced by a wide range of primary impacts on to the small satellites. Transfer from Charon to Pluto is possible, but requires much higher velocity ejecta, and that ejecta mush come from Charon's Pluto-facing hemisphere.

Most low velocity trajectories do not impact on the first orbit, but rather make several passages within the orbit of Charon, or even Pluto's barycentric orbit, before encountering Pluto or Charon and either impacting or being ejected from the system at high velocity. On the other hand, impacts from high-velocity trajectories generally happen on the first orbit, if at all.

Impact Locations: The trajectory that the dust particle takes before it impacts will influence the location it impacts. In general, low-velocity ejecta impacts onto Charon are more likely on the leading, anti-Pluto quadrant. At higher ejecta velocities, though, the impacts on Charon are uniform in longitude. On Pluto, the low velocity ejecta is mostly on the trailing hemisphere, while the higher velocity ejecta favors the leading hemisphere.

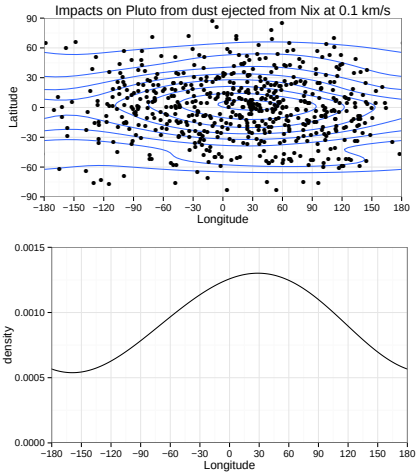

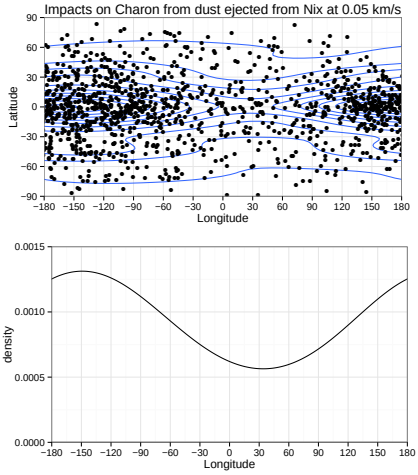

Simultaneous N-Body Fits of the Pluto System

Simon B. Porter[1,2] and William M. Grundy[1], [1]Lowell Observatory, [2]Arizona State University (**porter@lowell.edu**)

Motivation: The small satellites of the Pluto system provide a unique opportunity to make close observations of <100 km trans-Neptunian objects. However, the New Horizons spacecraft has very tight pointing requirements, and so their positions need to determined with high accuracy to allow observations during the encounter. This is difficult, as they are in a tight-packed system orbiting the Pluto-Charon barycenter, with many mutual perturbations. Pluto and Charon can be modeled very well by a circular Keplerian orbit. However, there is additional precession in the orbits of the small satellites from Pluto and Charon, and P/4 and P/5 are likely perturbed by the larger Nix and Hydra. Thus, we sought develop a method to simultaneously fit the entire Pluto system as an N-Body system, allowing all perturbations to fall out naturally. In addition, determination of the masses of the small satellites will allow an estimate of their density, thus hinting at their composition.

Fitting Methodology: To fit the system, we sought a methodology that not only minimized the observed minus predicted error (χ^2), but also minimized the uncertainty of the fitted parameters. This was especially important, as we chose the parameters to be the masses, positions, and velocities of the objects on the day of the New Horizons encounter (JD 2457218.5). Thus, the fit will naturally produce an estimate of the uncertainty of the position of the objects at the encounter, as well the uncertainty in the mass of the small satellites.

The basic configuration of the system is well known: Pluto and Charon in a near-circular mutual orbit, and the small satellites in near-coplanar, near-circular orbits centered at the Pluto-Charon barycenter. Thus, the fitting algorithm can assume any initial solution it is given is close to the real answer, but needs to be further optimized. In addition, since the observational error is primarily due to PSF-fitting, it can be approximated as Gaussian. This allows the entire problem to treated as multivariate normal distribution. Following after Muinonen et al. [1], we assumed the probability of a particular solution is proportional to $w = \sqrt{\mid \Sigma^{-1} \mid}\ exp[-\frac{1}{2}\chi^2]$, where $\Sigma^{-1} = \Phi^T \Lambda^{-1} \Phi$ is the Fisher information matrix of the input parameters, Λ^{-1} is the weight matrix of the observations, and Φ is the matrix of the partial derivatives of the error with respect to the input parameters. $\chi^2 = \Psi^T \Lambda^{-1} \Psi$, where Ψ is a matrix of the observations minus the predicted positions. $\sqrt{\mid \Sigma^{-1} \mid}$ is the Jeffreys prior of the parameters, while $exp[-\frac{1}{2}\chi^2]$ is the Gaussian prior of the observations. To fit, we performed a Markov Chain Monte Carlo optimization to maximize w.

The inverse of the information matrix is the covariance matrix of the parameters, and the square root the diagonal elements of covariance matrix correspond to the 1-σ uncertainty for each parameter. We used this uncertainty to scale the perturbations for the Markov Chain Monte Carlo fitting.

Implementation: Many N-Body integrations were needed to perform the fits. This was difficult, as the Pluto system cannot really be modeled as a central-body problem. So, for most integrations we used an adaptive 12th-order explicit Runge-Kutta-Nystrom integrator with tight tolerance control. For the few times when this failed to reach the required accuracy, the program would fall back to more robust (but slower) implicit 8th-order Runge-Kutta-Nystrom method.

The fitting program is designed to take in a given state vector and then run a given number of optimization iterations. The basic algorithm for this is:

1. Read in a given state vector.
2. Calculate its weight and uncertainty.
3. Perturb the state vector by random Gaussians using the width of the vector's uncertainty.
4. Calculate the χ^2 of the new vector; if too large, return to step 3.
5. Calculate the full weight of the new vector.
6. If the new weight is higher than the old, save the new and calculate its uncertainty.
7. Return to step 3 for as many times as requested.

Step 4 is especially important, as the calculation of the partial derivatives is the slowest part of the program, and should be avoided for poor solutions.

Results: We will present our fits for the masses and positions of the small satellites using the best available data, including at least Nix, Hydra, and P/4.

References

[1] K. Muinonen, J. Virtanen, and E. Bowell. Collision Probability for Earth-Crossing Asteroids Using Orbital Ranging. *Celestial Mechanics and Dynamical Astronomy*, 81: 93–101, 2001.

Absorption Coefficients of Methane Ice Diluted in Nitrogen at different mixing ratios: Implications for Pluto

S. Protopapa[1] and W. Grundy[2] and S. Tegler[2] and H. Boehnhardt[3] and L. Barrera[4] and J. Bergonio[5], [1]University of Maryland, Department of Astronomy, College Park, MD 20742, USA, [2]Lowell Observatory, 1400 W. Mars Hill Rd., Flagstaff, AZ 86001, USA, [3]Max-Planck Institute for Solar System Research, Max-Planck-Str. 2, 37191 Katlenburg-Lindau, Germany, [4]Universidad Metropolitana de Ciencias de la Educacion, Santiago, Chile, [5]Department of Physics and Astronomy, University of Hawai'i at Manoa Honolulu, HI 96822

Seen at high spectral resolution, the near infrared methane (CH_4) ice absorption bands in Pluto's spectrum are shifted toward shorter wavelengths compared to the central wavelengths of pure CH_4 obtained in the laboratory. This shift, described by Schmitt and Quirico (1992), occurs when CH_4 is dissolved at low concentrations in a matrix of solid N_2, and the magnitude of the shift varies from one CH_4 band to another. In particular, the complex structure of the CH_4 bands in Pluto's spectrum indicates that there are two phases contributing to the absorptions. One component is formed by CH_4 dissolved in N_2, with shifted wavelengths as described above, and another arising from CH_4-dominated ice with little or no wavelength shifts. The mixing ratio of pure and diluted CH_4 ice can be studied via the wavelength shift and depth of the CH_4 absorptions in the near infrared.

We performed laboratory transmission spectroscopy experiments of CH_4 ice diluted in N_2 and N_2 ice diluted in CH_4. In particular, a systematic study of changes in CH_4:N_2 mixtures spectral behavior with mixing ratio has been conducted, in order to understand whether blueshifts of CH_4-ice bands correlate with the amount of N_2-ice. We report absorption coefficients of CH_4 ice diluted in N_2-ice for different mixing ratio. These data are applied to interpret high dispersion H and K bands spectra of Pluto acquired with the NACO instrument at the ESO VLT on 27 June 2008.

PREDICTIONS FOR CRYOVOLCANIC FLOWS ON THE SURFACE OF PLUTO.

Lynnae C. Quick[1,2] and Louise M. Prockter[2], [1]Johns Hopkins University Earth and Planetary Sciences Department, 3400 North Charles Street, Olin Hall, Baltimore, MD 21218, lquick5@live.johnshopkins.edu, Johns Hopkins University Applied Physics Laboratory, 11101 Johns Hopkins Road, Laurel, MD 20723, Louise.Prockter@jhuapl.edu.

Abstract

We are investigating the likely formation conditions of effusive cryovolcanic features on the surface of Triton, as an analog for the types of features that might be expected on the surface of Pluto. We examine candidate lava conditions and rheologies, and how they are expressed on the surfaces of these two icy bodies.

Introduction

Candidate cryovolcanic features have been identified on Europa, Enceladus, Titan and Triton, among other outer solar system satellites. Given that Triton is thought to be a captured Kuiper Belt object, its composition may be analogous to that of Pluto, and its surface features may be similar.

Voyager 2 flybys of Triton showed signs of recent geological activity, as evidenced by the paucity of impact craters on its surface [1]. Geyser-like plumes were observed, measuring up to 8 km high, apparently comprised of nitrogen gas and entrained dust [2]. These result in dark streaks on the surface (Fig. 1). It is thought that the plumes form through the overpressurization of shallow (a few meters) subsurface nitrogen, resulting in eruption through the overlying surface ice [2,3].

Other candidate features on Triton's surface appear to have formed from, or to be associated with, widespread effusive volcanism (Fig. 1). These include vast "*walled plains*", subcircular depressions 100-400 km in diameter, which appear to be almost filled with smooth, relatively young plains material; *ring paterae*, subcircular features 50-100 km in diameter which are defined by a scarp or a ring of coalescing pits, and may contain smooth plains material; *pitted cones*, small conical hills typically 4-7 km in diameter with summit pits; and *pit paterae*, circular to elongate depressions which may have raised rims, are typically 10-20 km in diameter, may occur singly or in chains, and which are associated with larger patches of smooth material. In addition Triton's surface exhibits terrain containing numerous quasi-circular, closely-spaced shallow depressions called cavi, ~25-35 km in diameter with slightly raised rims, which are interpreted to have formed from diapiric upwelling of subsurface material [4]. Triton's most enigmatic surface features are the guttae, huge lobate features 100-200 km across and inferred to be at least tens of meters thick, which are surrounded by a bright aureole ~20-30 km wide (Fig. 1). The smooth surfaces and lobate edges of the guttae suggest extrusive materials that have flowed in a viscous manner. The dual albedo of these features is highly unusual.

Triton's surface composition is primarily comprised of frozen nitrogen (55%), water ice (25-35%) and carbon dioxide ice (10-20%), along with traces of methane, ethane and carbon monoxide [5]. Ammonia dihydrate is predicted in the lithosphere [6] but no ammonia has been detected on the surface.

Pluto's surface appears very similar to Triton's, and is predominantly comprised of nitrogen, with traces of methane, carbon monoxide and ethane. Water ice and carbon dioxide have not yet been detected. Methane is found to be widespread in high albedo surface regions, and in some locations appears to be pure ice [7].

The temperatures of Triton and Pluto are similar; Triton's average surface temperature is ~40K, and Pluto's surface temperature varies across the surface, from ~40K regions where N_2 ice is actively sublimating, to ~60K where N_2 ice is not abundant, probably as a result of strong winds and corresponding lateral transport of material across the surface [7].

Method

We use analytical modeling to investigate the cooling times of a suite of candidate lavas on the surface of Triton. Using the dimensions of several effusive volcanic features as constraints, we infer the conditions necessary to form them. We then extrapolate our results to anticipate the types of features that might be found on Pluto.

Previous workers have suggested that H_2O would be the most abundant component of magmas on Triton, of which CH_4, N_2, CO, and CO_2 may also be constituents [8]. Based on cosmochemical arguments and the proposed rigidity of putative volcanic constructs, it has also been suggested that ammonia–water lavas, in the form of NH_3-$2H_2O$, may be prevalent on Triton's surface [5, 9-11]. We consider lavas that would be produced from melting in the NH_3-H_2O and CH_4-CO systems, as well as pure compounds that are components of these systems (e.g. pure H_2O, NH_3, CH_4, etc.), and CO_2 and pure N_2 as candidate lavas on Triton's surface. Based on cosmochemical grounds and its projected bulk composition [e.g. 7] we expect that lava flows of similar composition may exist on Pluto. All candidate lavas are assumed to erupt at temperatures greater than or equal to their eutectic temperatures and lava flows

are presumed to be rendered immobile when they have completely cooled to the background temperature of their surroundings. Cooling times for lava flows are represented by:

$$t = \frac{y^2}{4\kappa b^2} \quad (1)$$

where y is the thickness of the flow, in meters, κ is the thermal diffusivity of the lava, in m^2/sec, at the background surface temperature, and b is an empirical constant describing the ratio between the energy required to change the temperature of the flow and its latent heat of crystallization [12].

Preliminary results suggest that a 50-m thick NH_3-$2H_2O$ lava flow erupting at 176 K into Triton-like conditions, where the surface temperature is approximately 40 K, κ = 1 x 10^{-5} m^2/sec, and b = 0.47, may take as long as ~ 8 years to completely crystallize. In order for such a flow to fill a circular depression that is 100 km across, such as might be found in the *walled plains* units, before complete solidification occurs, it must have a discharge rate of ~ 1500 m^3/sec, or a mass eruption rate of 1.4 x 10^6 kg/sec. For a surface temperature of 60 K, as would be the case in some regions on Pluto, κ would equal 4.5 x 10^{-6} m^2/sec, b = 0.5, and the flow would take almost twice as long as the time quoted above to cool. A smaller discharge rate on the order of 700 m^3/sec (mass eruption rate of 6.6 x 10^5 kg/sec) would be required to form a similar feature under these conditions. These calculations assume an NH_3-$2H_2O$ lava density of 945 kg/m^3 [4] and viscosities O(10) Pa-sec, similar to terrestrial basalt [9].

These results indicate that lavas erupting at 176 K would take more time to cool to a 60 K background surface temperature than they would to cool to a 40 K background surface temperature. Warmer average surface temperatures (i.e. T ~ 60 K) in some areas on Pluto may mean that volcanic features similar to those observed on Triton can be formed on Pluto by lavas with lower discharge rates than their counterparts on Triton. This concept will be further explored in our final analysis.

Imagery suggests that several candidate volcanic features on Triton are rigid enough to preserve impact craters. Hence, lava more viscous than NH_3-H_2O, such as ammonia-water lavas containing methanol, or pure CO_2 lavas, may have formed these features. In our final analysis we will explore other candidate lava compositions and their rheologies and further investigate the implications for the formation of volcanic features on Pluto.

References [1] Stern A. S., and McKinnon, W. B. (2000) *AJ,119*, 945. [2] Soderblom, L. A. et al. (1990) *Science, 250*, 410. [3] Kirk, R. L. et al. (1990) *Science, 250*, 424. [4] Schenk, P. and Jackson, M. P. A. (1993) *Geology, 21*, 299. [5] McKinnon, W. B. and Kirk, R. L. (2007) *Encyclopedia of the Solar System 2nd Ed*, 483. [6] Ruiz, J. (2003) *Icarus, 166*, 436. [7] Stern, S. A. (2007) *Encyclopedia of the Solar System 2nd Ed.*, 541. [8] Croft, S. K. et al. (1995) *Neptune and Triton*, 879. [9] Kargel, J. S. et al. (1991) *Icarus, 89*, 93. [10] Kargel, J. S. (1992) *Icarus, 100*, 556. [11] Hogenboom, D. L. et al. (1997) *Icarus 128*, 171. [12] Marsh, B. D. (2013) Magma Physics, *In Preparation*.

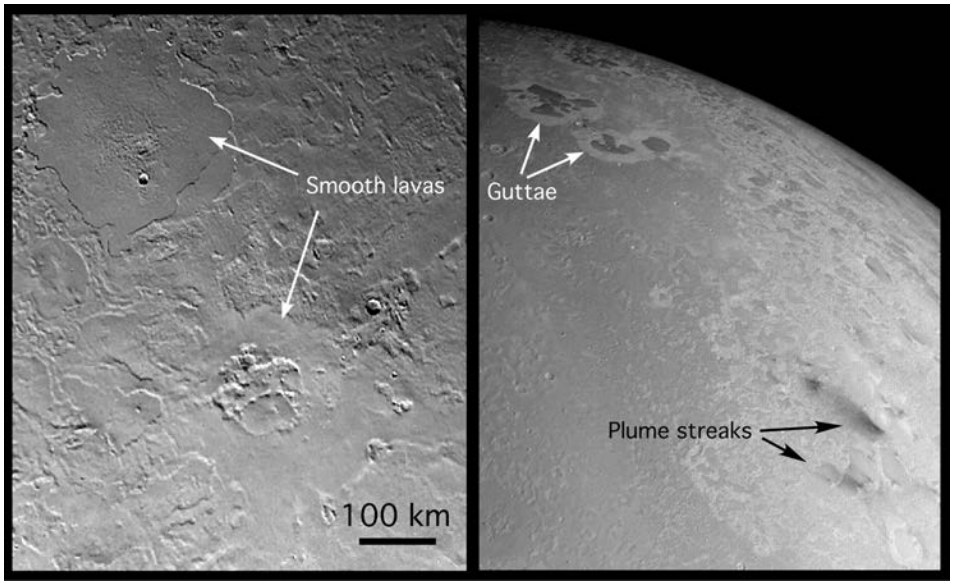

Figure 1: Triton's candidate volcanic features include smooth lavas (left), and guttae and plume streaks (right).

Distant Cousins: What the asteroids can teach us about the Pluto system, and vice versa

A. S. Rivkin[1] [1]JHU/APL (andy.rivkin@jhuapl.edu)

Introduction: Pluto, Charon, and the other bodies in that system are typically compared to transneptunian objects (TNOs) due to similar histories and compositions. However, as we learn more about the largest asteroids and the overlap betwteen the asteroidal and cometary populations, it seems clear that the asteroids can provide interesting context for the exploration of the Pluto system, and what we learn about that system will inform asteroidal studies.

The largest asteroids: Ceres is the only object inside the orbit of Neptune classified as a "dwarf planet" by the IAU criteria. Its density (2077 +/- 36 kg/m3) and the HST-derived shape model has been interpreted as requiring an icy shell above a rocky core, consistent with models of Ceres' interior and thermal history. Ceres' density is comparable to that of bodies typically thought of as icy, including the Galilean satellites, Quaoar, Triton, and Pluto itself.

However, the surface temperature of Ceres (and, indeed, all main-belt asteroids) is too warm to maintain volatiles at its surface. Its surface reflectance spectrum is low albedo and relatively featureless in the visible-near IR (0.5-2.5 μm), reminiscent of the carbonaceous chondrite meteorites. However, at longer wavelengths several absorption features are seen that are not found in carbonaceous chondrites: bands at 3.07 and 3.35 μm interpreted as brucite and carbonates (though interpreted as due to ammoniated phyllosilicates by earlier workers), and additional carbonate bands in the 3.8-3.9 μm region.

These brucite and carbonate features indicate heavy aqueous alteration of olivine in the presence of carbon dioxide. Interior modeling of Ceres suggests that these alteration products could have been brought to the surface either via cryovolcanism and left behind after the sublimation of the ice lava, or a direct lag deposit if the ice shell had access to the vacuum of space.

It was long thought that Ceres was unique among the asteroids in its 3-μm spectra, but several other of the largest asteroids, including 10 Hygiea and 704 Interamnia, also appear to have similar absorption features. This suggests similar surface mineralogies and the possibility of similar histories. It is also the case that the largest asteroids tend to be low-albedo and carbonaceous in composition, with notable exceptions. Could the similar-sized objects in the TNO region have also shared similar histories?

Dynamical arguments: The possibility of similar histories for asteroids and TNOs is also raised via dynamical models that have been developed over the last decade. Taken as a whole, the Nice Model and Grand Tack suggest post-formation mixing between volatile-poor/silicate and volatile-rich/carbonaceous populations of small bodies may have occurred on a large scale. However, competing models are also under development that do not require such mixing. At this point, it is not obvious which model will be most consistent with additional data, but it does seem obvious that additional constratints will be generated through the New Horizons visit to the Pluto system and additional TNOs.

Some hand-wavy specifics: We might imagine the interior evolution of ~few 100km scale objects to be functions of composition, size, radiogenic elements etc.. The surface temperature, while very different between 3 and 30 AU, seems unlikely to have much of an effect besides the thickness of any original, unmelted layer. If both Ceres and a similar-sized TNO (like Quaoar) formed at similar distances and accreted similar materials, we might expect similar interior evolution. In the case of the TNO, any erupted volatiles would remain on the surface rather than subliming away, but a comparison of the non-ice material on the surfaces of TNOs to the surfaces of large asteroids could provide insight into how similar or different their original composition and subsequent evolution was.

CONSTRAINTS ON THE INTERIOR STRUCTURES OF PLUTO AND CHARON BASED ON TIDAL PARAMETERS

J. H. Roberts[1], [1] Johns Hopkins University Applied Physics Laboratory, 11100 Johns Hopkins Road, Laurel, MD 20724 (James.Roberts@jhuapl.edu

Introduction: The thermal evolution of Pluto and Charon is a key question in planetary geophysics [1,2]. In particular, the possibility of subsurface oceans beneath the ice shells of these dwarf planets is of particular interest to astrobiological investigations [3] as their existence may significantly extend the habitable zone of our Solar System [2]. Models of thermal evolution [2,4] are strongly dependent upon the interior structure [4,5]. At present, only the orbital parameters [6] and masses of these bodies are at all well known [7,8]; there is significant uncertainty even as to the radius of Pluto [9]. Information regarding the silicate fraction, differentiation state, and depth to and extent of any putative subsurface oceans are model-dependent [2,4,5]. However these parameters strongly control the thermal evolution of icy satellites and Kuiper Belt objects [1,2,10-12]. For example, recent studies [2] suggest that the existence of an ocean strongly depends on the radioactive heat production and ice viscosity.

The New Horizons mission [9,13] will enable measurements that will improve constraints on these key geophysical parameters. Here I describe a method in which imaging and topographic data returned by the spacecraft can be used to develop a shape model, determine tidal parameters, and thereby constrain the interior structures of Pluto and Charon.

Shape modeling: The primary science objectives of New Horizons include characterizing the global geology and morphology of Pluto and Charon, and involves hemispheric imaging data at 0.5 km/px [9,13], and regional data as high as 75 m/px at closest approach [13]. These imaging data can be used to construct topographic maps of the surfaces using stereophotoclinometry (SPC), a technique by which images at different illuminations are used to solve for topography and albedo in small "maplets." A key strength of SPC is the ability to use a variety of images at different illumination angles, viewing geometries, and resolutions, as will be obtained during the Pluto flyby. The topography can then be solved to the resolution of the best images used [14]. Another objective of New Horizons is the acquisition of a number of stereo pairs which can be used to independently infer heights. The stereo and SPC topography reconstructions will be used to create a new shape models for Pluto and Charon.

Tidal parameters: Pluto and Charon are mutually synchronous, and indicate the end state of tidal evolution [6], where each body has deformed the other into a prolate ellipsoid. Although determining time-variability of the tidal bulge and potential is impossible during a single flyby (and is likely to be small), the static equilibrium tidal amplitude H should be discernable. Analysis of the shape models can reveal the long-wavelength displacement of the surface with respect to the ellipsoid; that is, the degree-2 displacement Love number h_2. For a homogeneous body, this cam be written simply as

$$h_2 = \frac{H}{R} = \frac{M_T}{M}\left(\frac{R}{a}\right)^3$$

where R and M are the radius and mass respectively of the body, M_T is the mass of the tide-raising body, and a is the semi-major axis of the orbit. h_2 for layered bodies is somewhat more complicated and diagnostic of the interior structure, as discussed in the next section.

Interior Structure: h_2 is essentially a measure of the globally-averaged rigidity of a planetary body, and can be used to infer the interior structure. In particular, h_2 will be helpful in assessing the differentiation state of the interior, as a differentiated body will deform less than a homogenous one [15]. I use the propagator-matrix tidal code TiRADE [16] to compute the Love numbers for a sequence of Pluto and Charon internal structures consistent with the observed bulk mass and radius, but with different degrees of mass concentration in the center. Figure 1 shows these curves for Pluto as a function of core density.

I note that the solutions are inherently non-unique. There is a strong tradeoff between the rigidity and thickness of the outer layer (e.g. ice shell above a subsurface ocean). However, identification of tidal deformation from the shape models will improve constraints. Moreover, it is to be hoped that estimates of long-wavelength gravitational parameters J_2 and C_{22} can be inferred from radio tracking. These can be used to estimate the potential Love number k_2. Knowledge of this parameter serves as a further constraint on the interior. In particular the ice shell thickness is more uniquely dependent on the tidal tilt parameter $\Delta = 1 - h_2 + k_2$ which largely filters out density variations and core properties.

Conclusions: Shape models of Pluto and Charon derived from imaging data obtained during the New Horizons flyby should be of sufficient measure the stat-

ic equilibrium tidal bulge, and to obtain estimates of the degree-2 displacement tidal Love number. This estimate can be used to constrain models of the interiors of Pluto and Charon; in particular, their degrees of differentiation, and likelihood of subsurface oceans, and estimates of their depths. The fidelity of these estimates can be improved if simultaneous measurements of degree-2 gravitational parameters can be made (e.g. with radio science).

References: [1] Schubert G. et al. (2010). *Space Sci. Rev., 153*, 447–484. [2] Robuchon G. and Nimmo F. (2011) *Icarus, 216*, 426-439. [3] Mottl M. J. et al. (2007) *Chem. Erde, 67*, 253-282. [4] McKinnon W. et al. (1997) In *Pluto and Charon*, pp. 295-343. [5] Collins G. C. and Barr A. C. (2008) *AGU Fall Meet.* Abs. 1425. [6] Dobrovolskis A. R. et al. (1997) In *Pluto and Charon*. Arizona Press, pp. 159–190. [7] McKinnon W. B. et al. (2008) In *The Solar System Beyond Neptune*, pp. 213-241. [8] Olkin C. B. et al. (2003) *Icarus, 164*, 254-259. [9] Young L. A. (2008) *Space Sci. Rev., 140*, 93-127. [10] Hussmann H. et al. (2006) *Icarus, 185*, 258–273. [11] McKinnon W. B. (2006) *Icarus, 183*, 435-450. [12] Desch S. J. et al. (2009). *Icarus, 202*, 694–714. [13] Stern S. A. (2008) *Space Sci. Rev., 140*, 3-21. [14] Gaskell, R. W. et al. (2008) *Meteorit. Planet. Sci., 43*, 1049-1061. [15] Moore W. B. and Schubert G. (2000) *Icarus, 147*, 317-319. [16] Roberts J. H. and Nimmo F. (2008) *Icarus, 194*, 675-689.

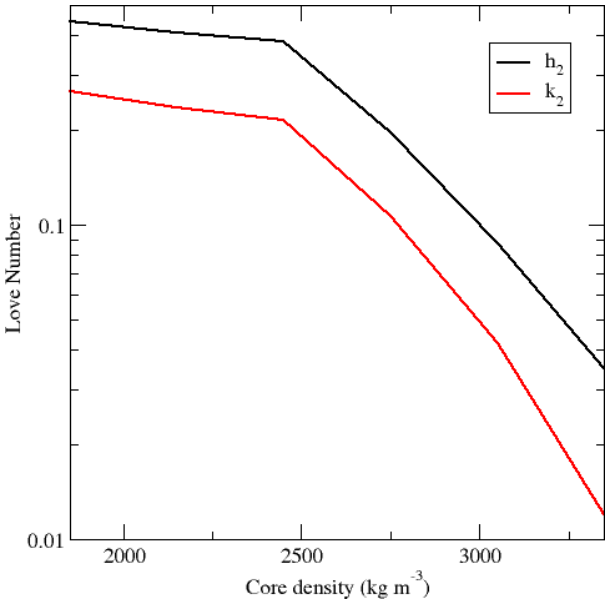

Figure 1: Degree-2 tidal Love numbers for Pluto interior structures consisting of a pure water-ice shell above a rock-ice core, assuming no ocean. Left-most point is for a homogeneous interior; right-most is fully differentiated.

MASKING SURFACE WATER ICE FEATURES ON SMALL DISTANT BODIES.

G. Sarid[1,2] , R. Brunetto[3,4] , F. E. DeMeo[5], [1]Earth and Planetary Sciences, Harvard University, 20 Oxford Street, Cambridge, MA 02138, USA. [2]NASA Astrobiology Institue, University of Hawai'i, 2680 Woodlawn Drive, Honolulu, HI 96822, USA, galsarid@fas.harvard.edu. [3]Institut d'Astrophysique Spatiale, CNRS, UMR-8617, Universite Paris-Sud, batiment 121, F-91405 Orsay Cedex, France. [4]European Space Astronomy Centre (ESAC), European Space Agency, Apartado de Correos 78, 28691 Villanueva de la Canada, Madrid, Spain. [5]Earth, Atmospheric, and Planetary Sciences, Massachusetts Institute of Technology, Cambridge, MA 02139, USA.

Introduction: Surface compositions of small bodies in the outer Solar System are derived mostly through analysis of measurements in the visible and near-infrared (NIR), with estimates of albedo, photometric colors and diagnostic spectral features [1]. Centaurs and trans-Neptunian objects exhibit low surface albedos. Some of the widest color variation of any other Solar System population, ranging from neutral gray to the reddest colors and lack distinguishing absorption features apart from some hints of water ice, for all but the largest objects [2, 3].

Small bodies in the outer Solar System are believed to be rich in ices, hydrocarbons, complex organics, and more refractory carbon-rich materials, such as amorphous carbon [4]. A mixture of these materials, together with other rock compounds, should be responsible for the spectral colors of small icy bodies. Complex organic materials on such surfaces likely include a primary native component that accreted during planetesimal formation epoch, and a secondary component that is a by-product of ion and photon irradiation of simpler C-bearing volatile compounds.

Additional insight into the surface composition of small icy bodies comes from the laboratory study of cometary grains, such as some interplanetary dust particles (IDP) collected in the Earth's stratosphere [5, 6], or grains collected from comet 81P/Wild 2 by the *Stardust* spacecraft [7]. These studies indicate the presence of refractory carbonaceous units that are usually sub-micron in size. This indicates that the size of every sub-unit is much smaller than the wavelengths commonly covered in surface spectroscopy. Based on this evidence, it has been suggested that reddening of small icy bodies may be caused by sub-micron particles from organic material of pre-solar or protoplanetary origin trapped in ice [8].

To extend these results, We have developed a spectral model for small icy bodies that is compatible with volatile loss and surface processing by solar and cosmic ions. This model is based on results derived from laboratory measurements of collected cometary grains and IDPs [9].

Model: Following the approach presented in [8], we use Maxwell-Garnett effective medium theory to approximate the effect of sub-wavelength refractory inclusions. This procedure takes the optical constants of several components and mixes them according to their respective mass fractions and densities. If all inclusions are considered spherical and the dielectric properties of the medium and inclusions are similar, we can compute the average wavelength-depnedent dielectric function. Next, we employ the Hapke model to calculate multiple scattering by the aggregate particles and produce disk-integrated albedo spectra.

We focus on the nature of the refractory dust and examine a broad range of compositions, in particular including silicate and iron sulfide components and a more realistic representation for the carbon component. While it is true that a-priori we do not know the composition of refractory components in the outer Solar System, we can certainly assume the cometary dust composition as the best currently known analog for small outer Solar System bodies and a good starting point to explore the visible-NIR spectral effects of the different mixtures (silicates vs. carbons, etc.). The materials we consider in our model are: Crystalline and amorphous silicates (olivine and pyroxene), iron sulfides, and a large variety of carbonaceous materials. We assume the composition of a well-characterized cometary IDP as a sort of ``reference dust" [9], from which we let vary the different relative abundances.

We choose three key parameters that we calculate from the synthetic spectra, which are used to characterize outer Solar System bodies [10, 11]: Depth of the 2 micron water ice band, R-band albedo (as well as V-band) and a color index (B-V and V-R).

Results: We refer here to our derived results as a scheme for the effects of sub-micron inclusions on the reflectance spectra.

Fig. 1 shows a mapping of the 2 micron fractional band depth onto the ice-carbon mass fraction space. These fractions cover the range from pure-refractory to pure-ice grains (x-axis, 0 to 1) and from carbon-depleted to completely carbonaceous refractory inclusions (y-axis, 0 to 1). These results are for the small-scale grains and low-sensitivity observations. We have also calculated the same for larger grains (20 and 50 microns) and for high-sensitivity observations. Even small inclusions of carbon, in terms of mass fraction, are extremely efficient at masking the icy

composition of a grain, at both the small and large size limits.

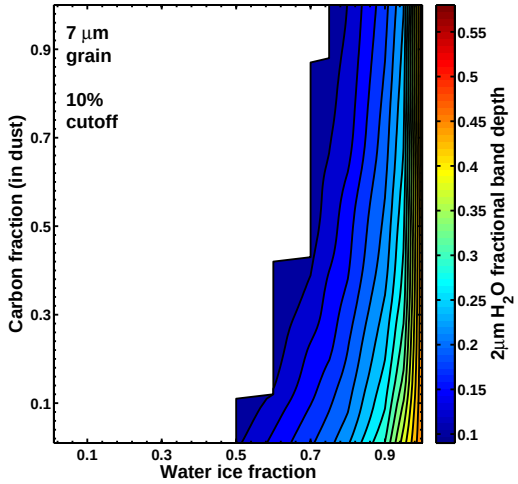

Figure 1: Fractional band depth of the 2 micron band for different proportions of water ice and carbon fractions in the dust.

Fig. 2 presents our calculated R-band albedo for the large and small grain sizes, as a function of water ice mass fraction in the grain. We can see that the sub-resolution mixing of water-ice and refractory components renders the albedo independent of composition and grain size, up to ~0.35 water ice mass fraction. At the mass fraction range where the curves differ, only small grains with dust components moderately-enriched in carbon have albedo values similar to the estimates relevant for icy objects in the outer Solar System [10].

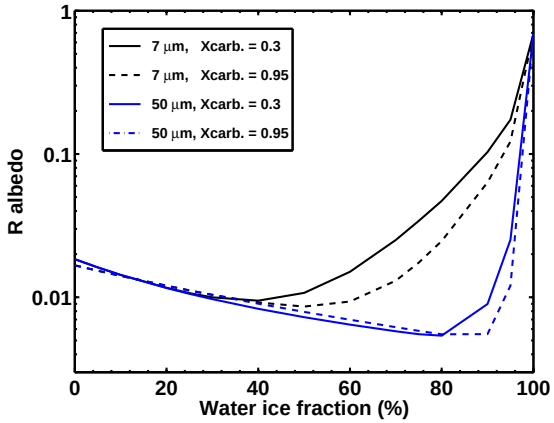

Figure 2: R albedo variation, as a function of water ice fraction in the grains, for "average" and enriched carbon fraction inclusions in the dust.

Our models show that a lack in detectable water ice band depth does not necessarily mean a lack of considerable fraction of water ice, if it is mixed in the grain-aggregate level. We find that over 50% (by mass) of water ice can be spectroscopically masked at 10% detection sensitivity due to the strong absorption of the carbonaceous sub-inclusion component. This effect is roughly similar to the one found for carbon-enriched crusts [12]. Comparing with ion irradiation experiments [13], we find that sublimation induced volatile loss and destruction of volatiles due to space weathering display a very similar spectral trend (flat-bright/red/flat-dark).

Acknowledgements: This material is based upon work supported by the National Aeronautics and Space Administration through the NASA Astrobiology Institute under Cooperative Agreement No. NNA09DA77A issued through the Office of Space Science. This material is based upon work supported, in part, by the National Science Foundation under Grant 0907766. Any opinions, findings, and conclusions or recommendations expressed in this material are those of the authors and do not necessarily reflect the views of the National Science Foundation. We are grateful to T.L. Roush for providing Hapke scattering codes and for precious suggestions. We thank G. Strazzulla and E. Dartois for useful discussions.

References: [1] Barucci M. A. et al. (2008) *The Solar System Beyond Neptune*, 143-160. [2] Barkume K. M., Brown M. E. and Schaller E. L. (2008) *AJ, 135*, 55-67. [3] Guilbert A. et al. (2009) *Icarus 201*, 272-283. [4] de Bergh C. et al. (2013) *The Science of Solar System Ices*, 107. [5] Bradley J. P. (2003) *Treatise on Geochemistry*, *1*, 689-711. [6] Flynn G. J. et al. (2003) *Geochim. Cosmocim. Ac., 67*, 4791-4806. [7] Sandford S. A. et al. (2006) *Science, 314*, 1720-1724. [8] Grundy W. M. (2009) *Icarus, 199*, 560-563. [9] Brunetto R. et al. (2011) *Icarus, 212*, 896-910. [10] Stansberry J. et al. (2008) *The Solar System Beyond Neptune*, 161-179. [11] Fornasier S. et al. (2009) *A&A, 508*, 457-465. [12] Brunetto R. and Roush T. L. (2008) *A&A, 481*, 879-882. [13] Kanuchova, Z. et al. (2012) *Icarus, 221*, 12-19.

THE IMPROBABLE ART OF PREDICTING PLUTO-CHARON GEOLOGY.

P. Schenk,[1] J. Moore,[2] and W.B. McKinnon[3], and A. Howard,[4] [1]Lunar and Planetary Institute, Houston, TX (schenk@lpi.usra.edu), [2]NASA Ames Research Center, Moffett Field, CA, [3]Washington University at Saint Louis, MO, [4]University of Virginia, Charlottesville, VA.

Introduction: On the eve of the first reconnaissance of the Pluto-Charon system (and indeed KBO objects generally), we might ask ourselves the basic question: "What will we find when we get there? How geologically evolved are these bodies?" The history of space exploration (e.g., *Voyager* and it's litany of surprises) should suggest the futility of posing such a question, but we have in the Outer Solar System a family of 17+ major icy moons that provide a rich set of examples of how diverse icy bodies can be (Fig. 1). In this report we review what we have learned so far about the geologic evolution of these icy worlds and attempt to place them in a Pluto context.

We can take two approaches to the problem. 1. We can survey the variety of geologic features found on icy satellites (and how they differ from those on silicate planets). 2. We can attempt to understand how icy bodies work geologically as worlds. Because New Horizons is approaching essentially a binary planetary system with two different sized icy bodies (one large: Pluto; one midsize: Charon; the small "rocks" are unlikely to be geologically inspiring), we examine each type seperately. For Pluto the relevant comparisons are the three icy Galilean satellites and Triton. Titan can be included but the pervasive rainfall there (plausible if Pluto had an ancient dense atmosphere, though what the precipitate would be is unlcear) has 'clouded' our understanding of its geologic history. For Charon these are the midsize satellites of Saturn and Uranus. To do this we rely on a vast body of referreed work exists detailing the geology of these bodies.

Geology on Large Icy Satellites: Geologic features on planetary bodies are commonly divided into endogenic and exogenic features. Endogenic features are tectonics (faulting and other forms of crustal deformation), volcanic (intrusive and extrusive redistribution of lavas), and erosional (mass wasting, and atmospheric modification in the case of Pluto). Exogenic features include impact cratering and erosional effects due to the space environment.

Let us consider Charon first, we commonly observe extensional fracturing commonly on midsize satellites, from Tethys, Dione and Rhea to Titania and Ariel. These tend to be km to tens of km is scale and hemispheric in scope. They are provisionally attributed to late stage lithopheric cooling and/or global expansion, even on ancient-looking Rhea. Putative volcanism takes the form of broad low plains, caldera-like dwalled depressions, and narrow ridges up to 1-2 km high. Although we have no credible identification of lava compositions (except for Enceladus' plumes), there may be a trend toward more complex lava chemistries and thicker volcanic deposits with distance from the Sun due to increased low-T non-water ice abundances. Pluto may support such an idea. The dynamical environments of these satellite systems have provided prolonged (tidal) heat sources that were more limited at Pluto, however.

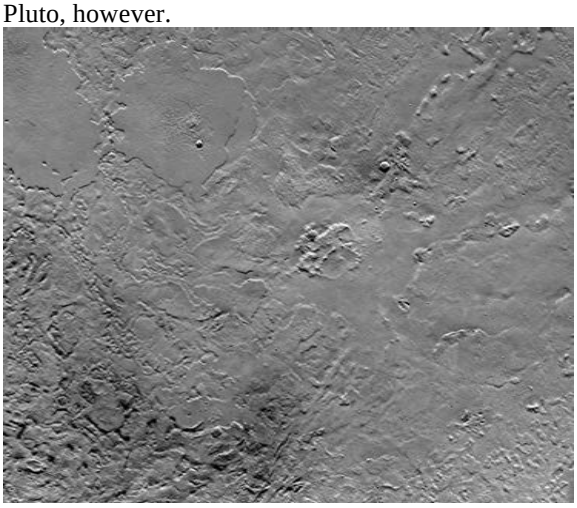

Figure 1. Geologic features on icy satellites. Example: Triton. In this 700-km-wide region we see a wide variety of fatures, including diapirism and frost deposition on peaks (lower left), scarp erosion (upper left and lower right), volcanism (center and upper right), tectonism (lower center), and the odd impact crater. Voyager mosaic at 0.6 km/pixel.

Mass wasting is not well documented on these bodies, but landslides are abundant on most of the saturnian midsize satellites, suggesting some degree of slope instability will be prevalent on both Pluto and Charon. Erosion on Charon is likely to otherwise be dominated by slow micrometeorite bombardment. Whether a massive ring system ever existed at Pluto or Charon might be recorded by a heavy flux of small impacts or by accumulation of an equatorial ridge as on Iapetus, or equatorial "Blue Pearls" as on Rhea.

Charon is most similar in size to the satellites Ariel, Umbrial, Dione and Tethys. These range from ancient to heavily resurfaced. Charon is unlikely to be Enceladus-like, and is likely to be cratered. Some degree of

fracturing is also likely, though tidal stresses have probably been negligible.

Pluto may be more evolved geologically than Charon, as suggested by its composition and albedo variations, but there is little to go by in predicting its appearance. We have only one example of a large icy body with similar volatile composition: Triton. Volcanism is extensive there, including a large caldera and volcanic pit chains. Tectonism is less extensive, perhaps surprisingly, with only a few stray extensional fractures. The rest of the surface is dominated by diapiric cells (cantaloupe terrain) and by the mysterious south polar terrains. The geysers at Triton may be geothermal or solar driven exhalation of nitrogen or other volatiles. They are poorly understood. Seasonal solar-driven volatile transport is likely to have eroded some features. Scarp retreat, pitting, dark ice precipitation on local highs, and other manifestations are likely and will require high resolution and stereo imaging, volatile mapping and global mapping to unravel.

Impact craters are one of the few features we are essentialy guaranteed to see on both bodies. They will by nature be 60-70% shallower than lunar craters and exhibit distinct morphologies (from central dome craters to palimpsests), but may also have been subject to post-impact viscous relaxation. One might expect interesting differences: 1) relatively low impact speeds compared with other sats; 2) novel effects from (weak) ice compositions. Here, a straightforward determination of the pristine crater shape statistics will allow a determination of the degree of relaxation and constrain heat flow. We might also predict a differential impact flux on the two sides of Charon but not on Pluto. Of course our track record in observing asymmetries is weak. Besides Charon's orbital velocity is only 0.2 km/s, so won't generate much of an antapex-apex difference immersed in a 1 km/s background kbo flux. Impacts also excavate buried materials and may be key to unraveling the stratigraphy (if any) of Pluto. Any large impact events, similar to those observed on Tethys or Dione, will affect large areas and redistribute ejecta and possibly fracture the crust.

An outstanding question is the impact flux in the Kuiper-Edgeworth Belt, which will determine the degree to which ancient features will be preserved. A comparison of crater densities on bodies throughout the Pluto system will provide some constraints on relative ages of the bodies and the flux of impactors involved.

Geology of Ice Worlds: Looking at icy worlds as whole bodies, we are drawn to those most active, such as Europa, Enceladus, Ganymede, and Triton. Prolonged geologic activity is usually ascribed to tidal heating, but cannot be due completely to it as recent fracturing is seen on Rhea and Dione. Forces at work include tidal distortion and fracturing, tidal heating, secular cooling, and impact flux. Thermal history is manifest in subtle ways as well. Aside from Iapetus, the global-scale topographies of Saturn's midsize icy satellites are highly relaxed, likely due to some ancient episode of global heating not experienced by Iapetus. The degree of global relaxation, and hence early thermal effects, should be discernable on Charon. Iapetus is also relaxed, just to an earlier spin state. It is an interesting question of who will win the race in the cases of P & C: thermal cooling or tidal evolution? The results may well be recorded in the topography of these bodies and features thereon

Europa, with a "thin" shell of mostly water-ice, may have limited applicability to Pluto. It is dominated by pervasive tidally-driven fracturing, a scenario that may be unlikely on Pluto. The mixed record of ancient eroded terrains, localized volcanism, and intense but confined tectonism on Ganymede might be more applicable to Pluto with its less dynamic thermal history. That Pluto is "Callisto with frost" seems unlikely but not implausible.

Though Pluto did not experience Triton's massive tidally-induced thermal history, Triton/Europa analogs may be applicable in the sense of surface geology being driven by shallow oceans as an underlying heat reservour. Each moon is different but heat-driven diapirism occurs across Europa, and the widespread diaprism on Triton may be heat- or density-driven, or both. If Pluto ever had an ocean near the surface, similar geological manifestations may be their signature.

New Horizons at Pluto-Charon: New Horizons will address key issues. How did Pluto, with its unique dynamical history, evolve and what was its thermal history? This will be expressed in the geologic record, which will be documented in imaging, spectrocopy and topography. Comparisons to midsize icy satellites, especially the revelations from *Cassini* at Saturn, will be key. Does Charon betray any geologic activity and does it exhibit any significant low-T ice fraction in its icy crust? How does the abundance of low-T ice phases control or modify geologic evolution on icy worlds? The (likely) large impact event that brought about the complex Pluto system profoundly affected the thermal state of the resulting bodies. Will we see any effects of this in the geoligc record? Will we see ancient volcanoes eroding slowly under the cold but persistent Sun for eaons? Will we see extensional fractures indicating slow secular cooling? How have impact events large and small altered the outer layers and do they reveal the inner compositionsal and thermal histories of these strange new worlds? Regardless of the answers, the Pluto system will open a vast region of Solar System for the first time and no doubt surprise us.

VOYAGER AT TRITON (AND CASSINI AT SATURN): A REHEARSAL FOR NEW HORIZONS AT PLUTO.

P. Schenk, Lunar and Planetary Institute, Houston, TX (schenk@lpi.usra.edu).

Introduction: Despite a very different dynamical and thermal history, Neptune's large satellite Triton remains the only Solar system object visited by mankind comparable in size and composition to Pluto. Here we examine a reprocessed and improved Voyager data for Triton, with an eye toward how it will help us in understanding bodies similar to Pluto. The Voyager encounter was also broadly similar to that planned for New Horizons, and the Voyager experience at Triton also gives us an insight into how New Horizons will be mapping Pluto.

The Voyager Encounter at Triton: The August 1989 Voyager high-velocity encounter with Triton provided an excellent but limited view of this satellite. A new global mosaic has been assembled from the best of the Voyager images (Fig. 1) ranging eastward from ~45 to 0.35 km/pixel in resolution (resolution is a function of longitude here due to the 6 day rotation period and fast encounter velocity, as it will be for Pluto). The mosaic is combined with identical mosaics in 4 colors (UV, V, B and Orange), and are assembled in O-B-V (approx. natural color) and O-V-UV (exaggerated color) combinations. High-phase angle crescent imaging supplements lower-resolution approach imaging.

With similar rotation periods and physical diameters and similar approach velocities, the New Horizons encounter with Pluto in 2015 is broadly similar to Voyager at Triton, and will produce a global map of similar character. Key differences are a high-resolution (<100 m) capability (LORRI) and spectral coverage into the red and near- and mid-infrared (RALPH) on New Horizons, both of which were lacking on Voyager. Although coverage will extend to higher northern latitudes on Pluto, departure imaging will have a higher phase angle than for Triton and will be somewhat less though still useful.

The Geology of Triton: The last examination of Triton's global geology took place several years after the encounter. Since that time we have matured considerably in our understanding of icy body geologic evolution (thanks to Galileo and Cassini) and a reexamination of Triton geology is in order. The basic geologic sequence remains valid (i.e., icy volcanic terrains overlying potentially diapiric cantaloupe terrain, subsequently or continuously degraded by scarp retreat and mass wasting) but additional insights can be had. Tectonism is limited compared to Europa or Ganymede, though the origins of those linear features observed remains unclear. Several of the equatorialequatorial units can now be traced at least to the east into the low-resolution mapping areas.

The southern hemisphere is the great enigma of Triton, having been observed under high solar illumination and at limited resolution ($\geq$1 km/pixel). This hemisphere is relatively brighter than the northern hemisphere, with a well-defined if uneven boundary, but has been erroneously referred to as a "South Polar Cap." The inference has been that it is a monolithic deposit formed from the seasonal deposition of nitrogen or other frosts. The new mapping and color mosaics, coupled with (weak, low-resolution) stereo images, confirms that this hemisphere is in fact geologically complex, with several different terrain types, some of which are as cratered as areas to the north and therefore long-lived [4]. Much of the southern hemisphere terrains (SHTs) consist of smooth plains with bright and dark units. The dark units form nearly featureless amoeboid-shaped patches densely scattered across a variable bright unit. To the south lies a more rugged unit consisting of short discontinuous ridges, smooth patches, and rolling hills. Aside from the known 7-9 km high dark plumes observed after encounter [3], stereo imaging also reveal a second class of possible plumes, these being only a few kilometers high and more umbrella shaped.

A Preview of the Pluto System: In addition to the global mosaic, a variety of views of Triton will be shown, as will selected Voyager observations of relevance to the New Horizons encounter. Also, a series of views of icy bodies similar in size to Pluto and Charon will be shown. These will be selected from the Galileo and Cassini imaging libraries to highlight views most similar to the planned New Horizons observations. These views will provide a glimpse of the types of features we might expect to resolve at various times as we enter the Pluto system in 2015.

References: [1] Smith et al. (1989) *Science, 246*, 1442–1449. [2] Croft et al., (1995) in *Neptune and Triton*, Univ Ariz. Press. [3] Soderblom et al., (1990). *Science*, 250, 410-415. [4] J. Moore and J. Spencer, (1990). *Geophys. Res. Lett.*, 10, 1757-1760.

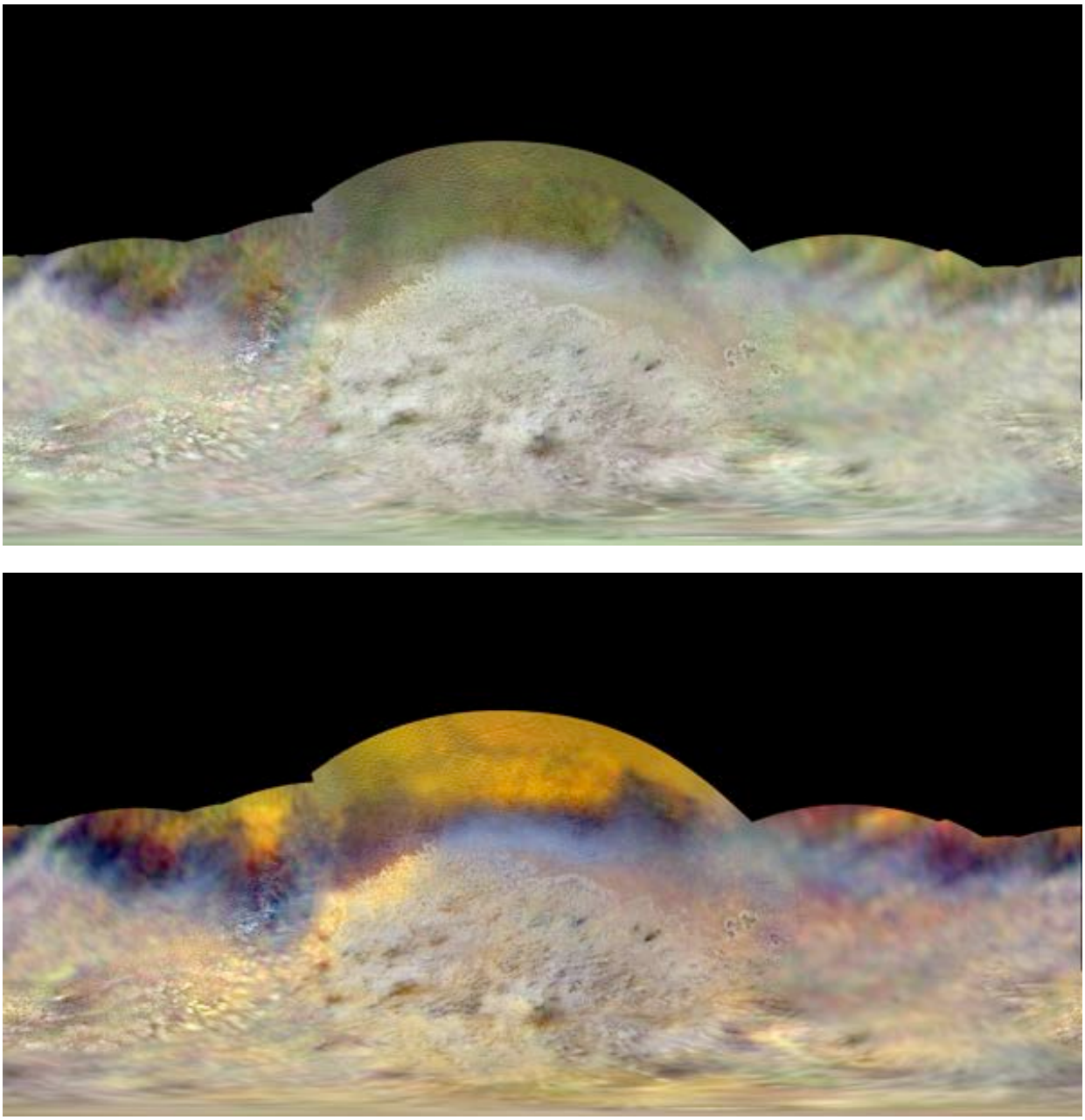

Figure 1. New global mosaic of Triton, based on Voyager imaging. (top) Approx. natural color (O-B-V); (bottom) enchanced color (O-V-UV).

FUV Studies of Pluto and Its Satellites: From IUE to New Horizons

Eric Schindhelm[1] , Alan Stern[1], and Randy Gladstone[2], [1]Southwest Research Institute, Boulder CO 80302, [2]Southwest Research Institute, San Antonio, Texas

---

The Alice far-ultraviolet (FUV) imaging spectrograph onboard the New Horizons spacecraft was designed to measure electronic transitions of species in Pluto's atmosphere, to study Pluto's atmosphere and search for an atmosphere around Charon with solar and stellar occultations, and to quantify the FUV surface reflectivity of other bodies in the system [1].

We predict FUV airglow emission originating from Pluto's atmosphere using the Atmospheric Ultraviolet Radiance Integrated Code program (AURIC, [2]) for various atmospheric model assumptions. Observation distances and phase angles are selected from several actual planned Alice activities in the nominal New Horizons encounter.

We also examine the expected surface reflectivity in the FUV by modeling the emergent spectrum through surface hazes and gases in the atmosphere. We correct the mid-ultraviolet albedo curves from previous *IUE* and *HST*-Faint Object Spectrograph observations [2,3] using recent modifications to the Pluto latitude-longitude coordinate system, and estimate the surface vs. atmospheric contributions to these spectra. These archival albedo data are also adjusted according to a more recent and accurate radius, and extrapolated to the FUV. We consider a range of surface ice compositions including N_2, CH_4, CO, and H_2O in our surface models using laboratory FUV reflectance data.

References: [1] Stern, S.A., Slater, D.C., Scherrer, J., et al. (2008) *Space Sci. Rev., 140*, 155-187. [2] Use the brief numbered style common in many abstracts, e.g., [1], [2] Stern S.A., Brosch N., Barker E., Gladstone G.R. (1991) *Icarus, 92*, 332-341. [3] Trafton L.M. & Stern S.A. (1996) *AJ, 112*, 1212-1224.

NEAR-INFRARED SPECTRA OF SIMPLE ORGANIC MOLECULES CANDIDATE FOR THE COMPOSITION OF PLUTO'S SURFACE.

B. Schmitt[1] and E. Quirico[1], [1] Institut de Planétologie et Astrophysique de Grenoble (IPAG), UJF-Grenoble 1 / CNRS-INSU, Grenoble, France (Bernard.Schmitt@obs.ujf-grenoble.fr).

Introduction: One important information to understand the evolution of Pluto is the composition of its surface ices that should trace its endogeneous and exogeneous chemical evolutions.

Several observations were aimed at investigating the possible presence of non-methane hydrocarbons [1, 2, 3, 4, 5, 6] on Pluto's and Triton's surfaces with hints for trace of ethane while higher hydrocarbons and nitriles escaped identification up to now.

Numerical models of Pluto's atmosphere [7] predict a production of hydrocarbon and nitrile species more similar to Titan than to Triton due to its high methane abundance.

The Ralph / LEISA imaging spectrometer onboard the New Horizons spacecraft will record numerous spectral images of Pluto and its satellites, as well as possibly of Kuiper Belt Objects, from 1.25 to 2.5 µm at a resolving power of 250 (and at higher resolution in the 2.10-2.25 µm range). This spectral range has many diagnostic features of solid hydrocarbons and nitriles.

Laboratory experiments:

The composition and photochemistry of Pluto atmosphere being similar to that of Titan, although at much lower pressure and temperature, we can expect also some similarities in the composition of its surface. We have recorded, or reanalyzed a first series of laboratory spectra of solid hydrocarbons and nitriles in the 15-100 K range in the near and mid-infrared, both overlapping the Ralph / LEISA spectral range, with the aim to provide reference data for the possible identification of these molecules at the surface of Pluto.

We present absorption coefficient spectra of C_2H_2, C_2H_4, C_2H_6, C_3H_4, C_3H_8, C_6H_6, HC_3N, CH_3CN, C_2H_3CN and C_2H_5CN and compare them with that of other solid species existing (CH_4, CO, N_2) or possibly existing (H_2O, CO_2, NH_3, CH_3OH, …) at the surface of Pluto.

In particular we are searching for diagnostic features of some of these molecules that could be identifiable on Pluto, i.e. that did not interfere with the very strong bands of methane. These laboratory data and their products, once fully analyzed, will be available digitally through the Grenoble Astrophysics and Planetology Solid spectroscopy and Thermodynamics (GhoSST) database, as well as all other spectra, absorption coefficient or optical constant data published on ices relevant for Pluto, its satellites and KBOs: N_2 [8], CH4 [9], CO_2, CH_4, C_2H_4, C_2H_6 and their mixtures in N_2 [10, 11], CO [12], H_2O [13], CH_3OH [14], …

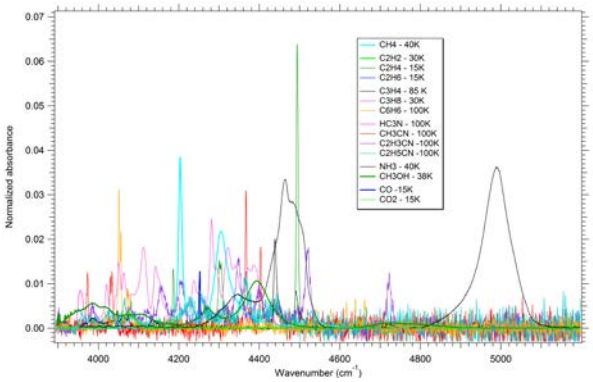

Figure 1: absorbance spectra in the 1.9-2.6 µm range of hydrocarbons and nitriles, compared with CO, CO_2, NH_3 and CH_3OH.

Pluto's spectra simulations:

We are currently running radiative transfer simulations in order to determine at which concentration each of these molecules could be detectable in the whole near-infrared and specifically in the Ralph / LEISA spectral range. The main difficulty is the interference of the strong CH_4 bands that preclude weak band observation, so transparencies regions, such as around 1.25-1.3, 1.5-1.6, 1.85-2.1 and 2.45 µm are the most promising.

References:

[1] Quirico et al. (1999) *Icarus, 139*, 159-178. [2] Douté et al. (1999) *Icarus, 142*, 421-444. [3] Sasaki T. et al. (2005) *Astrophys. J.*, 618, L57-L60. [4] Cruikshank D.P. et al. (2006) *Bull. Am. Astr. Soc. 38*, 518. [5] Olkin et al. (2007) *Astron. J. 133*, 420–431. [6] DeMeo F.E. et al. (2010) *Icarus, 208*, 412-424. [7] Krasnopolsky V.A. and Cruikshank D.P. (1999) *JGRE, 104*, 21979-21996. [8] Grundy W., Schmitt B. and Quirico E. (1993) *Icarus, 105*, 254-258 [9] Grundy W., Schmitt B. and Quirico E. (2002) *Icarus, 155*, 486-496. [10] Quirico and Schmitt (1997a) *Icarus, 127*, 354-378. [11] Quirico E. et al. (1996) *Planet. Space Sci. 44*, 973-986. [12] Quirico and Schmitt (1997b) *Icarus, 128*, 181-188. [13] Grundy, W., and B. Schmitt (1998) *J. Geophys. Res. E, 103*, 25809-25822. [14] Merlin et al. (2012) A&A 544, A20.

Additional Information: The GhoSST database can be foud at http://ghosst.osug.fr/

ORBITS AND PHYSICAL PROPERTIES OF PLUTO'S SMALL MOONS "P4" AND "P5"

M. R. Showalter[1], H. A. Weaver[2], M. W. Buie[3], D. P. Hamilton[4], W. Merline[3], M. Mutchler[5], A. J. Steffl[3], S. A. Stern[3], H. Throop[6], and L. A. Young[3], [1]SETI Institute (189 Bernardo Ave., Mountain View, CA 94043, mshowalter@seti.org), [2]APL/JHU (11100 Johns Hopkins Rd, Laurel, MD 20723), [3]SwRI (1050 Walnut St #300, Boulder, CO 80302), [4]University of Maryland (College Park, MD 20742), [5]STScI (3700 San Martin Drive Baltimore, MD 21218), [6]PSI (1700 E Fort Lowell Rd #106, Tucson, AZ 85719).

Introduction: We report on the analysis of "P4" (S/2011 (134340) 1) and "P5" (S/2012 (134340) 1), based on the complete set of available data from the Hubble Space Telescope (HST). Although discovered in 2011 and 2012, the moons have been recovered from earlier HST programs, providing an extensive body of data from which to infer orbital elements and photometric properties. Within this data set, we use Hydra and Nix for reference and as "reality checks" on our results.

Data Set: Pluto was imaged repeatedly by the HST Wide Field Camera 3 (WFC3) during 2010–2012 (GO-11556, 12436, 12725, 12801). From these images, we have assembled 179 detections of P4 and 64 of P5. In addition, P4 was detected in one ACS (Advanced Camera for Surveys) image in 2005 and six in 2006 (GO-10427, 10774). Particularly in the shorter exposures, it is necessary to co-add multiple images to obtain these detections. Nevertheless, once suitably processed, they are astrometrically and photometrically reliable.

Orbits: The orbits of Pluto's outer moons are complicated by the non-spherical and time-variable gravity field of the central binary planet, Pluto and Charon. As a result, orbits show marked deviations from simple Keplerian orbits. In particular, the pericenter longitudes precess and the ascending nodes regress, much as they would for orbits about an oblate planet. Charon's motion around Pluto also induces higher-frequency "wiggles" into the motions of these moons; these cannot be measured directly in the astrometry, but may increase the fit residuals. Orbits show measurable variations from one year to the next, which probably reveal the mutual interactions among the four outer moons; this information should eventually lead to constraints on the masses of Nix and Hydra.

We describe the orbits using nine orbital elements: semimajor axis a, mean motion n, mean orbital longitude θ, eccentricity e, pericenter longitude ω, pericenter precession rate $d\omega/dt$, inclination i, longitude of ascending node Ω, and nodal regression rate $d\Omega/dt$. The model is accurate to first order in e and i. Values are defined relative to the Pluto-Charon barycenter, using an inertial frame with the Z-axis along the system's angular momentum vector. Longitudes are measured from the J2000 ascending node of the Pluto-Charon orbit plane at epoch July 1, 2011 UTC.

Our best-fit values for the orbital elements are as follows. For P4: a = 57,731 ± 28 km; n = 11.19124 ± 0.00008 °/day; θ = 94.216 ± 0.035°; e = 0.0031 ± 0.0003; ω = 194 ± 6°; $d\omega/dt$ = 0.128 ± 0.013 °/day; i = 0.35 ± 0.05°; Ω = 214 ± 9°; $d\Omega/dt$ = -0.105 ± 0.010°/day. For P5: a = 42,487 ± 81 km; n = 17.85564 ± 0.00041 °/day; θ = 276.90 ± 0.12; e = 0.0034 ± 0.0013; ω = 307 ± 22°; $d\omega/dt$ = 0.452 ± 0.058 °/day; i = 0.56 ± 0.27°; Ω = 122 ± 28°; $d\Omega/dt$ = -0.223 ± 0.112 °/day. Quoted uncertainties are one sigma. By extrapolation, the orbital longitudes can now be predicted to ~ 1° precision at the time of the New Horizons flyby.

Photometry: P4 and P5 have integrated reflectivities of 29 ± 12 km^2 and 19 ± 5 km^2, respectively. Here reflectivity is defined by the dimensionless ratio I/F, where I is the reflected intensity and πF is solar flux density; by this definition, a perfectly diffusing "Lambert" surface has unit reflectivity when illuminated at normal incidence. At the small phase angles observed ($\leq$ 1.8°), these values represent the product of the moon's cross-sectional area and its geometric albedo.

If P4 and P5 have albedos of ~ 0.35, comparable to the value for Charon, then the moons have radii of 5.1 ± 1.1 km and 4.1 ± 0.5 km, respectively. If the albedos are very small, say ~ 0.04, then the radii are 15 ± 3 km and 12 ± 2 km instead. These values are ~ 20% smaller than those quoted in the original IAU circulars [1,2] announcing the discoveries. Quoted error bars represent the standard deviation among all available measurements; a rotational light curve and/or opposition effect could be contributing to the relatively large uncertainties. This possibility is still under investigation.

References:

[1] Showalter M. R. et al. (2011) *IAU Circ.* 9221, 1.

[2] Showalter M. R. et al. (2012) *IAU Circ.* 9253, 1.

Acknowledgments: We thank Matt Mountain for very generous allocations of HST Director's Discretionary Time to support this research. This work was supported in part by the New Horizons Project, via subcontract E99013LM from SwRI. This work was also funded by STScI through program GO-12436 and by NASA's Outer Planets Research Program through grant NNX12AQ11G.

CHAOTIC ROTATION OF NIX AND HYDRA

M. R. Showalter[1], [1]SETI Institute (189 Bernardo Ave., Mountain View, CA 94043, mshowalter@seti.org).

Introduction: HST photometry of Nix and Hydra from 2010–2012 reveal distinct variations in integrated brightness, suggesting that the moons are irregular in shape. However, the variations show no correlation with orbital longitude, as one would expect for bodies in synchronous rotation. I show that Nix and Hydra are probably rotating chaotically, and that this can be a natural outcome of orbiting a binary planet.

Measurements: The Pluto system was imaged repeatedly by the HST Wide Field Camera 3 (WFC3) during 2010–2012 (GO-11556, 12436, 12725, 12801). I have measured the disk-integrated brightness *D* of Nix and Hydra during each set of observations, which consist of 1–3 consecutive orbits of HST around the Earth. We have 12 observing epochs from 2010, 6 from 2011, and 14 from 2012. All measurements were obtained through either the long-pass filter F350LP or the broad V filter F606W. Measurements show no dependence on which of these filters was used.

Phase Curve: A plot of *D* vs. phase angle α shows distinct evidence for an opposition surge, which is common for near-backscatter from rough surfaces. This component of the phase function *P*(α) must be accounted for before the other brightness variations are investigated. I model the opposition surge as identical for Hydra and Nix, using a simple parametric model (Fig. 1). Upon dividing out this function, it became apparent that the moons vary in brightness year by year. Nix has brightened by ~ 30% from 2010 to 2012 (Fig. 1), whereas Hydra has been more stable.

Rotation Periods: To identify the rotation period *p* of each moon, I fit the available measurements to a model consisting of a constant plus two sinusoids, one with period *p* and the other with period *p*/2. Models consisting of a single sinusoid were much less successful, and it is not uncommon for the light curves of irregularly-shaped bodies to have a strong second harmonic. Fits were applied to the complete data set and also to data from 2010 and 2012 separately; measurements from 2011 are too few in number for fitting.

Figure 2 shows the root-mean-square (RMS) residuals for values of *p* between 4 and 100 days. In no case does a period fit the full data set with acceptable residuals. During 2010, Nix shows peaks at 32.64 and 27.22 days, but the former is strongly favored when the phase function and period are modeled simultaneously rather than sequentially. Neither of these periods is compatible with the 2012 data, where 18.84 days provides the best

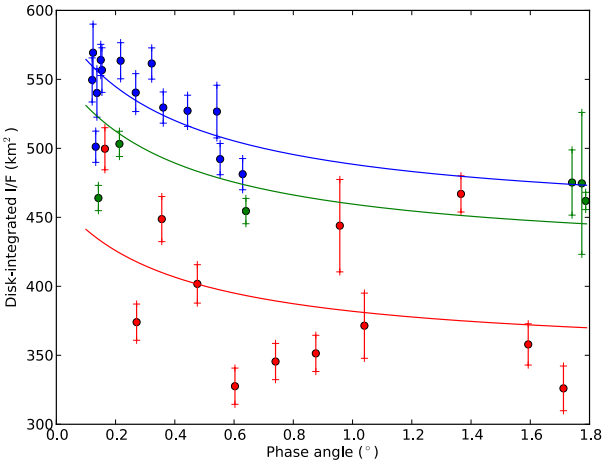

Figure 1. Best-fit phase function for Nix and Hydra, scaled to the Nix photometry from 2010 (red), 2011 (green) and 2012 (blue). Nix shows a ~ 30% increase in brightness between 2010 and 2012.

fit. For Hydra, *p* = 21.62 days in 2010, but the 2012 data show no evidence for any similar period; instead, a much shorter period of 7.82 days is favored.

These measurements indicate radical changes in the rotation rates of Nix and Hydra over 1-year time scales. The year-by-year changes in Nix's mean brightness could also be explained by a wobble in Nix's rotation axis. What could account for these peculiar results?

Dynamics: Most regular satellites in the solar system are in synchronous lock with their central planet. However, the Pluto system is unique in that the outer moons orbit a "binary planet" consisting of two bodies. Youdin et al. [1] demonstrated the influence that this has on the orbital motions of the outer moons. I have integrated both the orbital motion and the rotation state of bodies in orbit around Pluto and Charon, and find that the variations of the central gravity field can prevent synchronous lock. Fig. 3 shows one excerpt from an integration of Nix's motion and rotation. While Nix's long-term average rotation period is similar to that of its orbit (dashed line in Fig. 3a), it is common for *p* to change up or down by factors of ~ 2 for months at a time. Nix will often librate around a synchronous orientation (corresponding to 0° or 180° in Fig. 3b) but it can jump between these orientations and can temporarily go into an entirely different rotation state. Not every integration leads to chaos, at least within the ~ 100 year time scales I have investigated; for example, if

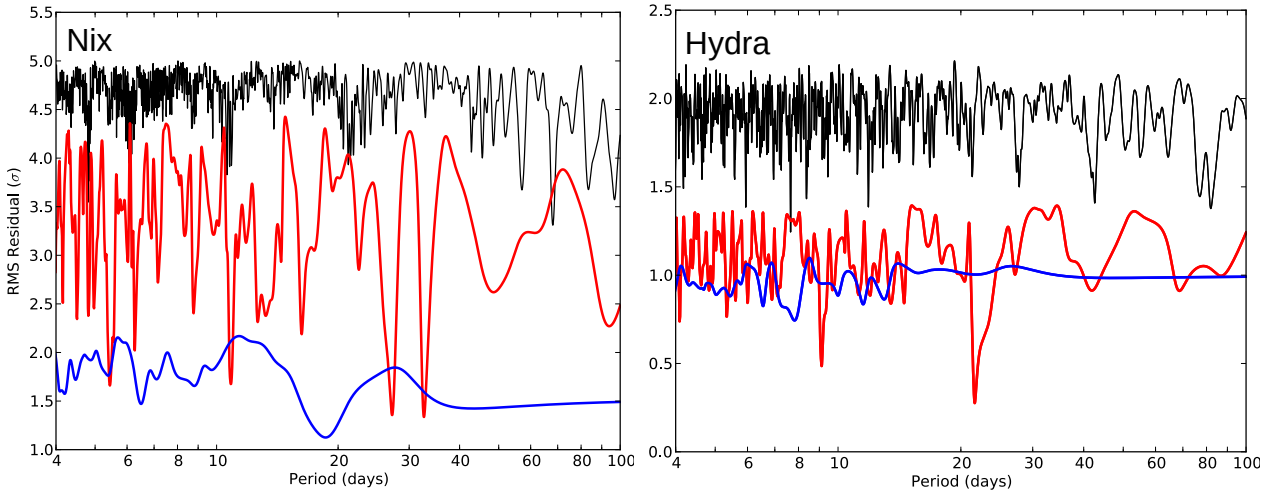

Figure 2. RMS residuals to assumed rotation periods ranging from 4 to 100 days for Nix and Hydra. A fit to 3 years of data (black) shows unacceptable residuals. Fits to data from 2010 (red) and 2012 (blue) show statistically plausible residuals for individual years, but those periods are incompatible.

an integration begins with Nix in synchronous lock, Nix stays there except for a small wobble. However, if Nix began its life with a different period, these simulations suggest that synchronous lock might never be achieved.

Simulations of Hydra show generally similar phenomena, although jumps out of libration states are rarer. Nevertheless, the slow speeds and potentially large amplitudes of Hydra's libration are sufficient to alter its rotation period by ~ 50% for periods of a few months, comparable to the durations of our three data sets.

Nix and Hydra have very little influence of their own on these integrations. Available photometry of P4 and P5 is too sparse to study their rotations, but they may well also be rotating chaotically. Further integrations will be required to determine whether Charon's perturbations can induce a significant wobble in Nix's rotation pole, which is needed to explain its changes year by year.

References: [1] Youdin A. N., Kratter K. M, and Kenyon S. J. (2012) *Astrophys. J. 755*, 17–27.

Acknowledgments: This work was supported by NASA's Outer Planets Research Program through grant NNX12AQ11G.

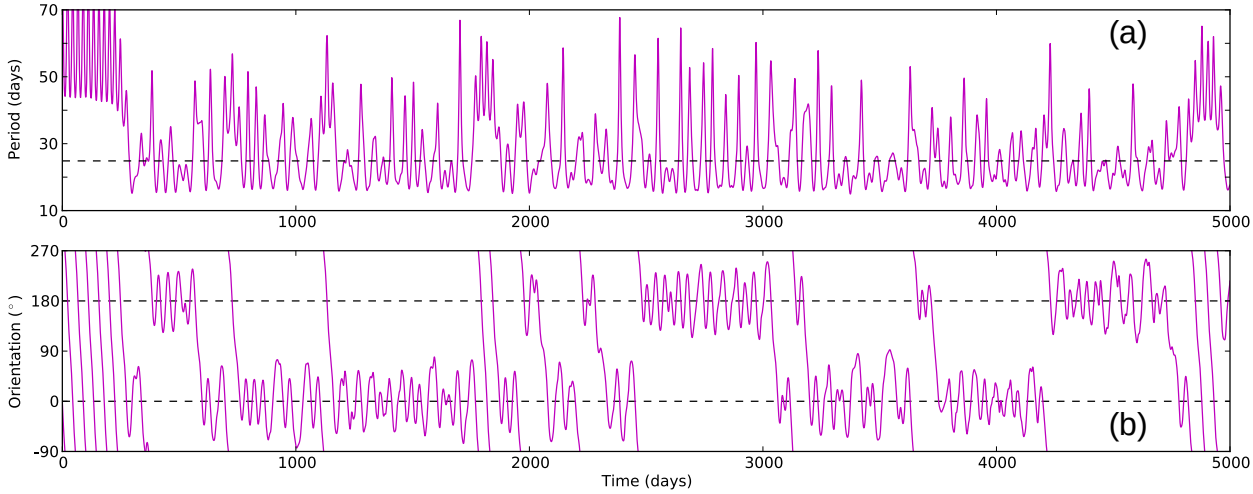

Figure 3. (a) Instantaneous rotation period of Nix during a 5000-day integration. The dashed line indicates Nix's orbital period of 24.85 days. (b) Longitude of Nix's long axis relative to the radial direction; note its tendency to oscillate around 0° or 180°, but only temporarily.

PLUTO'S ATMOSPHERIC PRESSURE FROM STELLAR OCCULTATIONS: 2002-2012*

B. Sicardy[1], E. Lellouch[1], A. Doressoundiram[1], F. Roques[1], T. Widemann[1], F. Colas[2], A. Dias de Oliveira[1,3], A. H. Andrei[3], M. Assafin[4], F. Braga-Ribas[1,3], J. I. B. Camargo[3], R. Vieira-Martins[3], D. N. da Silva Neto[5], J. L. Ortiz[6], C. Dumas[7],V. D. Ivanov[7] and E. Jehin[8]
[1]Observatoire de Paris/LESIA, 5 place J. Janssen, 92195 Meudon cedex, France, aoliveira@obspm.fr
[2]Observatoire de Paris-Meudon/IMCCE – 77 Av. Denfert-Rochereau, 75014 Paris, France
[3]Observatório Nacional/MCTI – Rua Gal. José Cristino 77, 20921-400 Rio de Janeiro RJ Brazil,
[4]Observatório do Valongo/UFRJ – Ladeira do Pedro Antônio 43, 20080-090 Rio de Janeiro RJ Brazil
[5]Centro Universitário Estadual da Zona Oeste – Av. Manuel Caldeira de Alvarenga 1203, 23070-200, Rio de Janeiro RJ Brazil
[6]Instituto de Astrofísica de Andalucía, CSIC, Apartado 3004, 18080 Granada, Spain
[7]European Southern Observatory, Alonso de Córdova 3107, Vitacura, Casilla 19001, Santiago 19, Chile
[8]Institut d'Astrophysique de l'Université de Liège, Allée du 6 Août 17, B-4000 Liège, Belgium

Introduction: Ground-based stellar occultations are presently the unique way to provide temperature, pressure and density profiles of Pluto's atmosphere. They probe radii between about 1190 and 1550 km from the dwarf planet center, which corresponds to a pressure range of ~8 µbar-10 nbar.

Here we report results derived from twelve stellar occultations observed between 2002 and 2012. These events are used to assess Pluto's atmospheric pressure, thus providing estimates of putative time evolution of Pluto's atmosphere, before the New Horizons flyby of July 2015.

Observation: Multi-chord occultations observed at the following dates were included in our study: 21 August 2002, 12 June 2006, 18 March 2007, 14 June 2007, 22 June 2008, 24 June 2008, 25 August 2008, 14 February 2010, 4 June 2010 and 4 June 2011. The results derived from two further events, yet to be analyzed (14 June 2012 and 18 July 2012) will be included in the presentation, providing a total pool of twelve occultations.

Results: For each event, we performed a simultaneous fit to the light curves obtained at various sites. A ray tracing code generates a synthetic light curve corresponding to the geometry of each chord, using a common prescribed temperature profile, with a lower inversion layer with a gradient of 7 K km^{-1} and an upper isothermal branch at 107 K. The results shown here are little dependent on the values of those parameters, inside their respective allowed ranges. For a given occultation, the free parameters of the fit are the location of Pluto's center in the plane of the sky and the value p_{1215} of the pressure at the chosen radius 1215 km.

This approach provides a homogeneous analysis of all events and furnishes the value of p_{1215} as a function of time (Fig. 1). After the drastic surge of pressure by a factor of more than two between 1988 and 2002, the pressure appears to have stabilized. A slight increase in the last decade is suggested in our data, but remains marginally significant, considering our error bars. Comparison with models ([1]) and other observations ([2],[3]) will be presented.

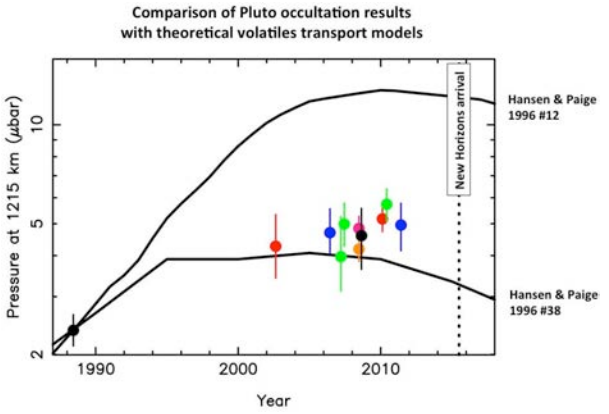

Figure: 1 – Colored dots: our results showing the time evolution of Pluto's atmospheric pressure at radius 1215 km. Black dot: pressure obtained from the 9 June 1988 occultation [4]. Dotted line: date of New Horizons flyby. Black lines: the particular models #12 and #38 of [1].

References: [1] Hansen, C.J. and Paige, D.A. (1996), *Icarus,* 120, 247-265. [2] Elliot, J.L. et al. (2007), "Changes in Pluto's atmosphere: 1988–2006", *Astron. J.,* 134, 1-13. [3] Young, E.F. *et al*. (2008), *Astron. J.*, 136, 1757-1769. [4] Yelle, R. V. and Elliot, J. L. in *Pluto and Charon* (eds Stern, S. A. & Tholen, D. J.) 347–390 (Univ. Arizona Press, Tucson, 1997).

*Results are partly based on runs 077.C-0283, 276.C-5052, 079.C-0345 and 089.C-0314 of the European Southern Observatory.

PHYSICO-MECHANICAL PROPERTIES AND GRAVITATIONAL DEFORMATION OF KUIPER BELT OBJECTS.

E. N. Slyuta[1] and S. A. Voropaev[1], [1]Vernadsky Institute of Geochemistry and Analytical Chemistry, Russian Academy of Sciences, 119991, Kosygin St. 19, Moscow, Russia. slyuta@mail.ru.

Introduction: Kuiper Belt objects to which some comets and Saturn's satellite Phoebe belongs [1-3], on composition considerably differ from icy Solar system bodies (Saturn's satellite Hyperion and so on). The fact of tidal destruction of a cometary nucleus suggests that the nucleus consists from fragile and weak enough material and on the physical and mechanical properties considerably differs from a usual solid body. Progressive cometary meteor fragmentation caused by aerodynamic pressure in the Earth's upper atmosphere is also diagnostic of general fragility and porosity of cometary meteoroids. The difference in composition assumes distinction of physico-mechanical properties of a material, so as tensile strength, compressive strength and yield strength. In processes where physico-mechanical properties are determining, for example, gravitational deformation, this distinction also should be appeared.

Physico-mechanical properties: According to the model [4], Si, Mg, and Fe compounds (silicates) make up about 26% of a cometary nucleus mass; complex organic compounds and the inclusions of minor particles or large molecules make up about 23% and 9%, respectively. Nearly 42% falls at ice of a different composition; water ice dominating (about 30%); and 2–3% falls at each of the following: CO, CO_2, CH_3OH, CH_4, H_2CO, and other exotic ices. The data obtained on the dust/ice mass ratio for the Tempel 1 comet also show that an "icy dirtballs" model is more preferable than a "dirty snowball" one [5].

Analytical, observed and experimental data on strength properties of cometary material and its analogues are shown that tensile strength of cometary material is distinct enough from strengthless material and is about 2 kPa [6]. This value corresponds approximately to average and conservative value of tensile strength, satisfying to almost all considered data which have been received by different methods and with a different degree of uncertainty.

Gravitational deformation: Gravitational loading in small bodies in the form of stress deviator caused by mass and a nonequilibrium figure of bodies, is constant and actually exists from the moment of their formation [7]. There's no creep in small Solar system bodies [8]. All small Solar system bodies irrespective of their structure from icy to metal including Kuiper Belt objects are elastic bodies which possess ultimate and yield strength. An analysis of mechanical properties of Kuiper Belt objects has been carried out with a model, which uses the elastic theory with ultimate strength for a three-dimensional self-gravity body, and allows the exact solution of differential stresses in a solid elastic body to be received and to carry out their analysis. The value and distribution of stress deviator in small body depends on mass, size, density, figure eccentricity and Poisson coefficient and defined by equation $\tau_{max}=\sigma_0 F(\varepsilon,\nu)$ (1), where dimension factor $\sigma_0 = \frac{9}{8\pi}\frac{GM^2}{a^2bc}$, where G - gravitational constant, M – mass ($M = \frac{4}{3}\pi\rho_0 R_m^3$, where Rm – mean radius), a, b and c – main semiaxes, and $F(\varepsilon,\nu)$ – dimensionless function, which depends on figure eccentricity (ε) and Poisson coefficient (ν).

For 19P/Borrelly comet [9], 67P/Churyumov-Gerasimenko comet [10], 81P/Wild 2 comet [11], 9P/Tempel 1 comet [12] and Halley comet [13] stress deviators obtained are small and are of two orders of magnitude lower than the cometary material tensile strength (Table 2).

Table 2. Cometary nucleus stress deviator*

Comet	Semiaxes (a×c), km	Density, g cm^{-3}	Stress deviator, ×10^{-2} kPa
Borrelly	4×1.6	0.3	2.2
Churyumov–Gerasimenko	2.43×1.85	0.5	2.5
Halley	8×4	0.28	3.4
Tempel 1	3.8×2.45	0.6	6.0
Wild 2	2.75×1.65	0.6	3.3

*- References are in the text.

Taking a cometary nucleus density equal to a conserva-tive value of 300 kg m^{-3} [6] and a Poisson coefficient of 0.31 [14], we obtain a cometary nucleus radius of 41×24.6 km (Rm=29 km), at which the stress deviator is equal to the cometary material tensile strength (2 kPa). That is the size of the largest comet Hale-Bopp within its size estimation uncertainty [15]. This means, that cometary nuclei less than ~60 km in diameter (which is the case practically all of the known comets) have a constant tensile strength of about 2 kPa, which is determined by structure only. At achievement of tensile strength as a result of tidal destruction, collision, or ram pressure at sublimation, bodies of less than ~60 km in diameter irrespective of their mass would be split easily enough, increasing a population of ones. Effective tensile strength of the bodies more than ~60 km in size is determined by a body mass and shape parameters and increases under the square-law depending on a body size and mass (Fig. 1). Such increase of the tensile

strength can explain an observed deficiency of cometary nuclei more than ~60 km in diameter.

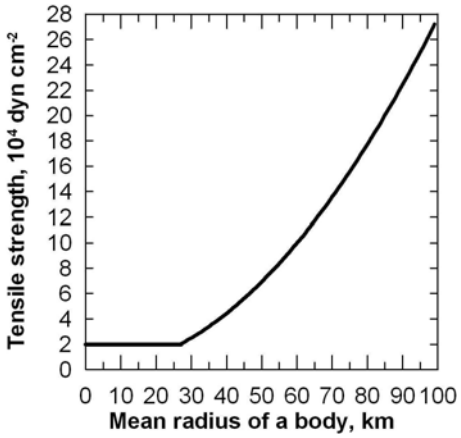

Fig. 1. Dependence of effective tensile strength on size of a cometary nucleus.

If comets are small bodies with an irregular shape, Phoebe is large enough a body to have developed a sphere-like shape. The mean radius of the satellite is 106.6 km [16]. As the satellite has a very low albedo (0.06) it was considered, that Phoebe is a rocky body [17]. But among small rocky bodies Phoebe differed by anomalous shape parameters [7]. With regards to the shape parameters, Phoebe belongs to the planetary bodies [16, 18]. Phoebe is less than Mimas (icy planetary body), and is less than Hyperion (icy small body) [7]. Its volume makes 55% from volume of Hyperion and 17% from volume of Mimas. According to the most recent data, Phoebe's composition is similar to that of Kuiper Belt objects [19, 20]. The orbital properties of Phoebe suggest that it was captured by Saturn's gravitational field.

Cometary nuclei are characterized by high porosity and low density [21, 22]. The maximum density of a fully packed cometary nucleus due to gravitational deformation would be ≈ 1650 kg m^{-3} [23]. Phoebe's density is 1638 kg m^{-3} [16] and corresponds to the above-stated value for a fully packed cometary nucleus. It means that the minimal stress deviator for Phoebe exceeds yield strength of material and gravitational deformation has already taken place. Gravitational deformation is accompanied by gravitational densification and gravitational strengthening of a material at the entire body due to three-dimensional gravitational compression accompanied by two basic mechanisms of plastic deformation [7]. Taking shape parameters of the satellite of a=109.3, b=108.5 km, c=101.8 km [24], and density of 1638 kg m^{-3} [16], and a Poisson coefficient of 0.31 [14], and using the stress deviator equation (1) we obtain a stress deviator of 0.49 MPa. Hence, the yield strength of a material of Kuiper Belt objects is within the range $0.002<\sigma_p<0.49$ MPa, where the minimum value corresponds to a cometary nucleus tensile strength [6].

It is necessary to note, that if to take a yield strength of 0.49 MPa, the mean radius of a small body not exposed to gravitational deformation (i.e. with a density of about 300 kg m^{-3} [21]), would reach 643×386 km. Hence, among Kuiper Belt objects small bodies with irregular shape which sizes exceed Phoebe's size may be observed. Perhaps, large Kuiper object 1994 VK_8 (280×190×190 km in diameter) and 1998 SM165 (600×360×360 km in diameter) may be considered such examples [25]. But it is necessary to take into account that under equal temperature conditions and similar composition the mass of such bodies should be less than critical one, and accordingly, less than mass of Phoebe, due to their high porosity. If the upper limit value take the yield strength of 0.49 MPa, ν=0.31, ε=0.8, we can estimate the upper limit for the density of the object 1998 SM165, when this cannot be done by any other methods. Hence the upper limit of the density values of Kuiper Belt object 1998 SM_{165} is estimated as $\rho_0<647$ kg m^{-3}. This value agrees well with the average optimal value of density of cometary nuclei (~300 kg m^{-3}) [21], as well as with known density of some transneptunian objects, which varies in the range from 110 up to 670 kg m^{-3} [26].

Thus, Kuiper Belt objects are characterized by the lowest value of yield strength among Solar system bodies, due to their composition. Obtained data on the rheology of Kuiper Belt objects shows that even subordinated amount of exotic ices can result in the change of rheologic properties of a material. Such dependence of transition parameters on composition can serve as a good indicator of the distinction between the bulk composition of numerous Kuiper and transneptunian objects studied by remote sensing. Phoebe can be considered such an example.

References: [1] Mumma M. J. et al. (2005) *Science*, 310, 270. [2] Clark R. N. et al., (2005) *Nature*, 435, 66. [3] Johnson T. V. and Lunine J. I. (2005) *Nature*, 435, 69. [4] Greenberg J.M., et al. (1995) *A&A.*, 295, 35–38. [5] Küppers M., et al. (2005) *Nature*, 437, 987–990. [6] Slyuta E.N. (2009) *Solar Sys. Res.*, 43, #5, 459-469. [7] Slyuta E.N. and Voropaev S.A. (1997). *Icarus*, 129, 401-414. [8] Slyuta E.N. (2013) *LPSC XXXXIV*, Abstr. #1117. [9] Britt D.T. et al. (2004) *Icarus*, 197, 45-53. [10] Davidsson B.J.R. and Gutierrez P.J. (2005) *Icarus*, 176, 453-477. [11] Davids-son B.J.R. and Gutierrez P.J. (2006) *Icarus*, 180, 224-242. [12] A'Hearn M.F. et al. (2005) *Science*, 310, 258-264. [13] Rickman H. (1989) *Adv. Space Res.*, 9, 59-71. [14] Hobbs P.V. (1974) Ice Physics. Clarendon Press. Oxford, England. [15] Fernández Y.R. (2002) *Earth, Moon, and Planets*, 89, 3-25. [16] Porco, C. C. et al. (2005) Science, 307, 1237-1242. [17] Burns, J. A. (1986) In Satellites (Tucson: Arizona Univ. Press), 1-38. [18] Slyuta E.N. (2006) *LPSC XXXVII*, #1088. [19] Clark, R. N. et al. (2005) *Nature*, 435, 66-69. [20] Johnson, T. V., and Lunine, J. I. (2005) *Nature*, 435, 69-71. [21] Sin-iti Sirono, and Greenberg, J. M. (2000) *Icarus*, 145, 230-238. [22] Davidsson, B. J. R., and Gutierrez, P. J. (2004) *Icarus*, 168, 392-408. [23] Greenberg, J. M. (1998) *A&A*, 330, 375-380. [24] Thomas P.C. (2010) *Icarus*, 208, 395-401. [25] Romanishin, W. et al. (2001), *PNAS*, 98, #21, 11863-11866. [26] Dotto E., et al. (2008) *A&A.*, 490, 829-833.

PROCESSES INVOLVED IN THE EVOLUTION OF PLUTO'S INTERIOR STRUCTURE

C. Sotin[1], [1]Jet Propulsion Laboratory-California Institute of Technology, Pasadena, CA 91109, USA (Christophe.Sotin@jpl.nasa.gov).

Introduction: The dwarf planet Pluto will be observed by the New Horizons spacecraft in 2015. This planet is part of the large family of icy bodies that have a large fraction of silicates. Most of these bodies are moons of gas giants and icy giants. The icy moons of Jupiter and Saturn have been studied by the Galileo spacecraft and the Cassini/Huygens mission, respectively. The data collected by these two missions have strongly modified our understanding of their interior structure and dynamics. Small moons such as Enceladus have revealed to be very active with jets of vapor and particles being ejected from a large fault system [1]. Gravity data suggest a large variety in the differentiation state of the large icy satellites [2]. Pluto also bears interesting similarities with Ceres, another dwarf planet that will be visited by the Dawn spacecraft in the Spring of 2015. This paper focuses on the differentiation state of icy bodies and describes some processes that may be important in driving Pluto's evolution.

	Ceres	Callisto	Enceladus	Pluto
Mass (10^{22} kg)	0.0943	10.76	0.0108	1.31
Radius (km)	475	2403	252.3	1153
density	2.10	1.851	1.608	2.03
T (K)	165-235	134 (80-165)	75 (30-270)	44
Eccentricity (%)	7.9	0.7	0.47	24.5
Spin rate (days)	0.378	16.7	1.37	6.4

Table 1: Some characteristics of Ceres, Callisto, Enceladus, and Pluto.

The degree of differentiation of icy bodies: The Galileo mission to Jupiter and the Cassini/Huygens mission to Saturn have revealed that the three large Jovian icy moons and Titan, Saturn's largest satellite, are at least partly differentiated. Their normalized moments of inertia (C/Ma2) are smaller than 2/5, which is the value for undifferentiated moons. However, the value is quite different for Ganymede than for Callisto. The low value for Ganymede is consistent with a fully differentiated body consisting of an inner iron rich core, a silicate shell, a high-pressure ice shell, a liquid shell and an outer low pressure (ice I) layer [3]. One explanation for the larger values of the moment of inertia of Titan and Callisto is that they have not undergone complete differentiation and that their interior would be, at least partly, composed of hydrated silicates [4,5] which are much less dense than the silicates that compose the mantle of terrestrial planets. The case of Europa is different since its lower mass and its large density imply a much thinner outer H_2O layer. For Enceladus, its large activity means that it is most likely differentiated with an ocean in between the ice crust and the inner silicate core.

The presence of an hydrated silicate core within Pluto was proposed 25 years ago by McKinnon [6] based on the value of its density. Such a structure was also proposed for Ceres by McCord and Sotin [7]. The stability of an hydrated silicate core is now addressed.

Thermal evolution model: A 1D spherical model is used to calculate the thermal profile in the silicate core as a function of time for a variety of initial conditions and parameters. The core is overlaid by a H_2O layer. In the nominal case, the initial amount of radioactive heat is $2x10^{-11}$ W/kg. At each time step, the likelihood of convection is assessed. The simulations start after the accretion phase during which temperatures were large enough to allow for partial melting and the formation of a hydrated core made of antigorite. The core heats up due to the decay of radioactive elements. The amount of ^{40}K is a free parameter because potassium is easily leached during processes involving circulation of water. The simulations use thermal parameters recently reviewed [8]. These values are based on several laboratories studies on antigorite whose properties play a key role in the geodynamics of subduction zones on Earth [9]. As the interior temperature increases, the inner part of the core can dehydrate. One interesting question is whether the water trapped at depth can migrate to the rock/H_2O interface, bringing with it salts and key elements.

At each time step, the density profile is computed using an equation of state based on recent laboratory experiments [9,10]. Using the parameters of their Birch-Murnagham equation, we determine a linear fit between pressure and density (correlation coefficient of 0.999) that provides a simple equation of state linking the density to temperature and pressure. The stability against convection is then assessed.

Onset of convection: Convection processes can start if the density profile is unstable (density decreases with pressure because of the temperature increase) and if the viscosity of the material is low enough for buoyancy forces to overcome viscous forces. It starts when the Rayleigh number becomes larger than a critical value that depends on the viscous behavior of the material [11]. The viscosity of antigorite is very strongly stress-dependent. The value of the critical Rayleigh number for non-Newtonian viscosity with no temperature dependence has been estimated using both laboratory and numerical data [11]. It must be noted that in such fluids, the meaning of the boundary between conductive and convective regimes is that if the Rayleigh number is below some critical value, no convective motion is possible with any initial conditions; if it is above this critical value, convection is possible but initiation of convection requires sufficiently large initial perturbations. In Pluto, the perturbations may be the tidal forces acting on the core. If the amount of ^{40}K is large (CI chondrites) the critical value can be reached in less than 1 Gyr. With an Earth-like amount of ^{40}K, the critical value is reached much later. In both cases, convection would only affect the outer layer of the core while the inner core would be subject to dehydration. The implications for the evolution of the interior structure are being investigated

Structure of the ice layer: Owing to its low surface temperature, the ices that constitute Pluto's outer ice layer my include methane clathrates and CO2 ices. The thermal conductivity of those ices is much lower than that of ice I, leading to much larger temperature gradients at similar values of the heat flux. Models of heat transfer in the ice I layer are being conducted. Implications for the formation of an ocean [12] and the presence of a high-pressure ice layer are being investigated.

Conclusions: The numerical simulations presented in this study suggest that the inner part of the hydrated core of Pluto would dehydrate for a large range of parameters, the most important of which is the amount of ^{40}K. The outer core would remain hydrated. The onset of convection has been investigated for antigortite whose viscosity is mostly stress-dependent. It is shown that convection could start in the outer core for large values of internal heating. Forthcoming observations of Pluto's surface composition, density, and shape will help constrain some of these models.

Acknowledgements: This work was performed at the Jet Propulsion Laboratory, California Institute of Technology, under contract to NASA. Support by NASA Outer Planets Research Program and the NASA Astrobiology Institute is acknowledged.

References: [1] Spencer J.R. et al. (2006) Science, 311, 1401. [2] Sotin C. and G. Tobie (2004) CRAS, 5, 769. Grinrod P.M. et al. (2008) Icarus 197 137–151. [3] Schubert et al. (2004) In: Bagenal, F., T.E. Dowling, and W.B. McKinnon (Eds.), Jupiter. The planet, satellites, and magnetosphere. Cambridge University Press, Cambridge, UK, pp. 281 – 306. [4] Grinrod P.M. et al. (2008) Icarus 197 137–151. [5] Castillo-Rogez J.C.and J.I. Lunine (2010) Geophys. Res. Lett., 37, L20205. [6] McKinnon W.B. (1988) Nature, 335, 240. [7] McCord T.B. ans Sotin C. (2005) JGR, 110, E05009. [8] Osako M. et al. (2010) Phys. Earth Planet. Int., 183, 229-233. [9] Hilairet N. et al. (2007) Science, 318, 1910-1913. [10] Nestola F. et al. (2010) Contrib. Mineral. Petrol., 160, 33–43. [11] Solomatov V.S. (1995) Phys. Fluids 7, 266. [12] Hussmann H. et al. (2006) Icarus, 185, 258.

.

THE SEARCH FOR KBO FLYBY TARGETS FOR NEW HORIZONS

J. R. Spencer[1], A. H. Parker[2], M. W. Buie[1], D. J. Osip[3], M. J. Holman[2], D. M. Borncamp[1], JJ Kavelaars[4], S. D. Benecchi[5], S. A. Stern[2], R. P. Binzel[6], F. E. DeMeo[6], S. Fabbro[4], C. I. Fuentes[7], S. D. J. Gwyn[4], P. L. Gay[8], B. A. McLeod[2], J.-M. Petit[9], S. S. Sheppard[5], D. J. Tholen[10], D. E. Trilling[7], D. A. Ragozzine[11], L. H. Wasserman[12], [1]Southwest Research Institute (spencer@boulder.swri.edu), [2]Harvard-Smithsonian Center for Astrophysics, [3]Carnegie Observatories, Las Campanas Observatory, [4]Canadian Astronomy Data Centre, National Research Council of Canada, [5]Carnegie Institute of Washington, Department of Terrestrial Magnetism, [6]Massachusetts Institute of Technology, [7]Northern Arizona University, [8]Southern Illinois University, [9]Universite de Franche Comte, CNRS, UTINAM, [10]University of Hawaii, Institute for Astronomy, [11]University of Florida, [12]Lowell Observatory

Introduction: After its Pluto flyby in July 2015, New Horizons will continue deeper into the Kuiper Belt, providing the opportunity for one or more flybys of smaller Kuiper Belt Objects (KBOs). Because no known KBOs are reachable by New Horizons, we are engaged in a deep ground-based search for accessible flyby targets.

Expected Number of Accessible KBOs: After the Pluto encounter, New Horizons is expected to have sufficient delta-V to change the direction of its trajectory by about 0.5°, allowing access to a narrow cone of space beyond Pluto. Current understanding of the Kuiper Belt population, based on the CFEPS survey [1], indicates that this cone should contain about 2 KBOs with ground-based R magnitude < 26.0, and about 4 KBOs with R < 26.5, a brightness range that is within the reach of 8-meter class telescopes.

Search Strategy: Though preliminary surveys were carried out with the Subaru telescope in 2004 and 2005, we began our primary KBO search in 2011. The start date was chosen to be early enough to allow several years for the discovery and characterization of potential targets before a post-Pluto targeting burn in late 2015, but late enough that the search area had shrunk to a manageable size for a deep search. By 2013, most accessible KBOs will be situated in a region of sky about 1 square degree in extent, which can be covered by a few pointings with available wide-field CCD imagers. The search area is currently centered near RA 18h 40m, Dec -21°, in the constellation Sagittarius.

Our primary search tools so far are the SuprimeCam camera on the Subaru telescope in Hawaii, and the IMACS and Megacam cameras on the Magellan telescopes in Chile. We obtained deep imaging of the search area on multiple nights spread over several months in 2011 and 2012, and have telescope time for a similar search in 2013.

Crowded Fields: The major challenge in the search is the very high density of background stars, owing to the low Galactic latitude of the search area. Detection of KBOs requires careful subtraction of background stars using a template generated from the best images of each field, with the PSF matched as accurately as possible between the template and the images to be searched. Astrometry of discovered objects is referenced to an astrometric grid obtained for the purpose at the Canada-France-Hawaii telescope.

Because of the crowded fields, our discovery rate is extremely dependent on image quality. We have reached our targeted limiting magnitude for new discoveries when seeing is better than ~0.6", though we can recover known objects in somewhat poorer seeing conditions. We had excellent seeing in early 2011, but poorer seeing later that year, and below-average seeing for most of 2012.

Results: Table 1 shows all objects near or beyond Neptune's orbit discovered by our search in the 2011 and 2012 data sets. We have found 27 of these objects, and 7 have already received official designations from the MPC. One of our discoveries is the second known trailing Neptune Trojan, the highest-inclination Neptune Trojan yet discovered [2]. Objects are being found at the rate expected from known constraints on the KBO magnitude/frequency distribution [3] given our limiting magnitudes. Because we have not yet been able to cover the entire search area with sufficiently good seeing, our discoveries do not yet include a targetable KBO. However, several discovered objects could be reached if New Horizons had twice the available delta-V, and we expect to find targetable KBOs once seeing conditions permit a search of the entire search area to our target magnitude of R=26.0 – 26.5. Several of the objects already discovered are close enough to the New Horizons trajectory to permit distant observations from the spacecraft.

References: [1] Kavelaars, J.J. et al. (2009) *Astron. J. 137,* 4917. [2] Parker, A. H. et al. (2013) *Astron. J., 145*, 96. [3] Fuentes, C. I. et al. (2010). *Astrophys. J. 722*, 1290.

Table 1: Kuiper Belt Objects Discovered So Far

	Orbital Elements				Closest Approach to New Horizons			
Name	a (AU)	e	i (deg)	R Magni-tude	Date	Range (AU)	Δv required for close encounter (m/s)	Observation Arc (days)
2011HM102	30.1	0.081	29.4	22.2	2013/11/02	1.22 — 1.22	pre-Pluto	355
VNH0002	51	0.223	6.4	—	2018/03/31	0.21 — 0.44	360 — 560	66
VNH0003	50.4	0.345	5.4	—	2017/01/15	0.18 — 0.40	520 — 850	66
VNH0004	39	0.355	3.8	23.5	2014/10/08	0.34 — 1.14	>5000	34
VNH0005	51.5	0.455	3.1	24.5	2017/04/25	0.48 — 0.94	880 — 2200	65
VNH0006	50.8	0.016	2.5	26	2021/02/13	0.17 — 1.13	140 — 810	4
2011JW31	46	0.142	1.9	25.2	2018/05/30	0.14 — 0.21	230 — 290	358
2011JY31	44	0.041	2.6	25	2018/07/19	0.14 — 0.16	220 — 240	358
2011JX31	44.9	0.107	3.3	24.5	2020/06/18	0.41 — 0.42	390 — 400	448
2011HZ102	43.2	0.004	2.4	25.4	2018/09/07	0.15 — 0.20	210 — 280	358
VNH0011	42.3	0.161	14.5	23.2	2016/03/11	1.33 — 1.44	>5000	66
2011HE103	43.7	0.083	6.8	—	2019/08/13	0.90 — 0.96	850 — 1000	358
VNH0013	56.9	0.467	13	24	2015/05/16	0.93 — 1.14	>5000	64
2011JA32	62.6	0.536	3.2	25.8	2017/06/24	0.35 — 0.42	690 — 870	356
VNH0015	34.8	0.034	18.8	25.4	2012/06/30	0.55 — 2.59	>5000	6
2011HD103	53.1	0.49	5.8	25.3	2020/08/07	1.35 — 1.37	720 — 1270	359
VNH0019	46.4	0.021	2.7	24.7	2016/12/06	0.38 — 1.96	420 — 1420	3
VNH0020	54	0.02	18.1	—	2017/12/31	1.20 — 4.32	>1000	2
VNH0021	44.2	0.085	3.3	—	2014/07/30	0.07 — 0.45	>1000	3
VNH0022	44.5	0.044	6.2	—	2016/03/21	0.38 — 0.98	860 — 1180	3
VNH0023	38.8	0.011	19.3	—	2015/08/04	1.28 — 2.58	>1000	3
VNH0024	41.8	0.155	4.5	—	2015/05/06	0.18 — 0.48	>1000	3
VNH0025	46.5	0.021	2.9	—	2019/08/03	0.96 — 1.18	>1000	2
VNH0026	45.4	0.022	9.1	—	2018/06/19	1.02 — 2.17	>1000	1
VNH0027	44.3	0.023	3	—	2018/01/10	0.73 — 1.82	900 — 2440	1
VNH0029	67.1	0.022	2.8	—	2025/03/04	0.19 — 5.36	80 — 1840	6
VNH0031	23.8	0.199	6.6	—	2012/08/09	0.39 — 2.33	>5000	6

WHAT WILL PLUTO LOOK LIKE?

J. R. Spencer, Southwest Research Institute (spencer@boulder.swri.edu).

Pluto is unlike any object yet visited by spacecraft, and surprise is the only certainty in the upcoming New Horizons data. However, we know enough to indulge in informed speculation about what the New Horizons images and spectra may reveal about Pluto's appearance.

The nearest analog to Pluto for which we have close-up data is of course Triton, a world of similar size, surface composition, and probable origin. The two objects suffered very different traumas in their early history- the probable Charon-forming impact in Pluto's case, and the Neptune capture event in Triton's case (though it is possible that Triton suffered both traumas, if it was captured as a member of a disrupted binary system [1]). However, while Triton probably suffered massive tidal heating during the impact event [2], its surface is probably less than 100 my old [3], much younger than plausible dates for that event or any lingering direct thermal effects. Its surface features thus formed at a time when tidal heating is negligible. Unless even very minimal current tidal heating can significantly affect Triton's thermal evolution, as has been argued recently [4], the geological activity that dominates Triton's surface likely to be driven by radiogenic heating, a heat source that should be almost as effective on Pluto. We can thus plausibly expect that Pluto has a surface that is as sparsely cratered as Triton's, and is dominated, like Triton's, by endogenic processes. The great variety of Triton's endogenic landforms, and the fact that many are completely enigmatic, makes any speculation about the precise nature of Pluto's endogenic geological features dangerous. However, New Horizon's vastly superior imaging coverage compared to that of Voyager at Triton (Fig. 1), coupled with its compositional mapping capabilities that were completely absent on Voyager, makes it much more likely that we will understand what we see at Pluto. If similarities do exist, the higher quality of the New Horizons data may well lead to improved understanding of the geological features on Triton.

One way in which we know Pluto will look very different from Triton is in the contrast of its albedo features. Triton's visible lightcurve amplitude was less than 5% at the time of the Voyager encounters, (though it may have increased recently [5]), compared to ~30% for Pluto, and HST images show regions of very low albedo on Pluto's surface [6] that have no analogs on Triton. The difference is plausibly related to the much higher CH_4 content of Pluto's atmosphere and surface, resulting in a much higher abundance of low-albedo carbon-rich photochemical products (tholins) on its surface. These may have become spatially segregated on the surface by a process analogous to the thermal segregation that is probably responsible for the extreme albedo contrasts on Iapetus [7]. While the segregation process will differ in detail because of Pluto's dense, collisional, atmosphere, it is at least plausible that the high albedo contrasts inferred from the HST images will persist to small spatial scales. Loss of volatiles from somewhat warmer and darker regions, leading to further darkening [8], may result in a piebald surface lacking regions of intermediate albedo, as on Iapetus. In fact non-volatile surfaces may be largely covered with dark photochemical products, accounting for the low abundance of exposed non-volatiles like H_2O and CO_2 [8,9], in contrast to CH_4-poor Triton where even non-volatile surfaces can remain clean.

References: [1] Agnor, C. B., and Hamilton, D. P. (2006) *Nature, 441*, 192. [2] McKinnon, W. B.. (1984) *Nature, 311*, 355. [3] Schenk, P. M. and Zahnle, K. (2007) *Icarus 192*, 135. [4] Gaeman, J. et al. (2012) *Icarus 220*, 339. [5] Buratti et al. (2011) *Icarus 212*, 835. [6] Buie M. W. et al. (2010) *Astron. J. 139*, 1128. [7] Spencer, J. R. and T. Denk (2010) *Science 327*, 432. [8] Grundy, W. M. and M. W. Buie (2002) *Icarus 157*, 128. [9] Grundy, W. M. et al. (2013) *Icarus 223*, 710.

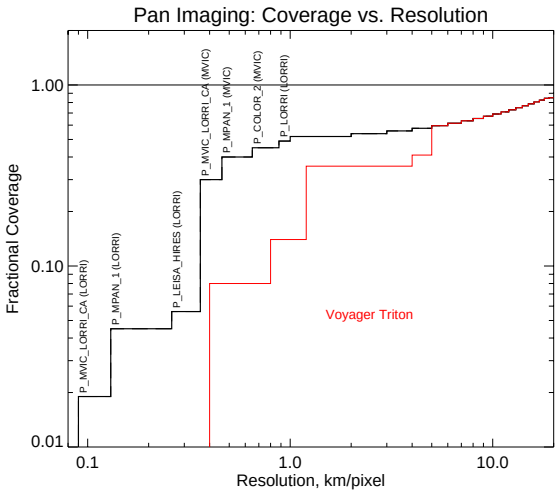

Figure 1. Comparison of New Horizons coverage and resolution at Pluto with Voyager 2's coverage of Triton (red). Steps in the Pluto curve correspond to the resolution and coverage of specific planned observations, which are named in the figure. Pluto coverage and resolution will be greatly superior to Voyager at Triton.

Interactions Between Pluto's Surface and Atmosphere.

J. A. Stansberry[1,2], [1]Steward Observatory, University of Arizona, Tucson AZ 85721 (until June, 2013), [2]Space Telescope Science Institute, 3700 San Martin Dr., Baltimore MD 21218 (beginning June, 2013).

Introduction: Pluto's atmosphere, composed primarily of N_2, is strongly coupled to deposits of that ice on the surface. This situation is quite different from most of the atmospheres of the other planets and satellites, but is analogous to the situation on Mars (where CO_2 is the relevant molecule), Triton (which also has an N_2 dominated atmosphere), and perhaps to atmospheres that may at times arise around other large trans-Neptunian objects.

Many aspects of Pluto's atmosphere and surface indicate that the atmosphere is currently supported in vapor-pressure equilibrium with N_2 ice on the surface. The latent heat of sublimation of N_2 is so large that tiny pressure differences (<0.1 μbar) drive latent heat fluxes comparable to the flux of absorbed insolation (or radiated thermal emission). As a result, the atmospheric pressure is determined by the global energy balance of the N_2 ice, and that ice is expected to have the same temperature regardless of where it occurs on the surface. Since the discovery of Pluto's atmosphere, it appears that the N_2 ice temperature is around 38K, and the surface pressure is 10-30 μbar.

Sublimation-driven transport from areas of high insolation to darker regions is expected to control winds in the lowest ~scale height or so. Because Pluto's orbit is significantly eccentric, and it's rotation is highly oblique, Pluto's vapor-pressure atmosphere is expected to experience significant seasonal variations. An open, and very interesting, question is whether Pluto's atmosphere will freeze-out on the surface at some point in the orbit, and when freeze-out will occur.

Models: Models of seasonal N_2 ice transport are the framework in which Pluto's (and Triton's) surface-atmosphere interactions have been studied (*e.g.* [1], [2]). These models have been informed by stellar-occultation, spectroscopic, resolved-imaging, and thermal-emission measurements of Pluto's surface and atmosphere. Recent advances have been made in implementing highly efficient volatile transport models [3], which will allow for more thorough exploration of the relevant parameter space, and for timely interpretation of New Horizons results. Global circulation models for Pluto have also been recently implemented ([4], [5]), and offer the chance to incorporate additional processes into attempts to understand the surface-atmosphere interaction in a global sense. Ultimately, all such models attempt to predict the distribution of Pluto's N_2 ice (and, presumably, accompanying albedo patterns), atmospheric pressure, circulation and temperature, and their evolution over seasonal timescales.

Second Order Interactions: There are numerous ways in which the surface-atmosphere interaction is more complex than the simple vapor-pressure paradigm might suggest. These interactions can have observable effects on atmospheric pressure and temperature structure, the appearance of the surface (assuming that N_2 ice has a distinct albedo relative to other surface units), atmospheric circulation, and the seasonal evolution of atmospheric bulk.

Composition and Atmospheric Temperature Structure. Pluto's ices include other somewhat less volatile species such as CO and CH_4, and their distribution on the surface and state of microphysical cohabitation with the N_2 ice is expected to be complex. Furthermore, these factors will influence, and be influenced by, their relative abundance in the atmosphere. This interaction is also important because the radiative properties of CO and CH_4 are thought to form a thermostat that gives an upper-atmospheric temperature of about 100K.

Atmospheric Heating. Heating of the atmosphere by the surface will affect the temperature structure of the lower atmosphere. Regions not covered by N_2 ice (*i.e. bedrock*, for lack of a better term) will (necessarily) be warmer than that ice. Buoyancy created by such heating will drive convection, although the strength of the convection is unknown. Models of this process [6] suggest Pluto's atmosphere could include a troposphere. Convective flows would also interact with the global-scale sublimation-driven winds, and could lead to the formation of clouds.

Thermal Inertia. The temperature of bedrock on Pluto will depend on the thermal inertia, Γ, of that material. The applicable value of Γ probably depends on whether one considers diurnal temperature variations (which will only affect the upper few cm of the subsurface) or seasonal temperature variations (which will affect the upper meters of the subsurface). Thermal inertia is an important parameter when trying to understand atmospheric heating, but will also have strong influence on the movement of N_2 ice in response to diurnal and seasonal variations in insolation (because the N_2 can only condense in areas cooler than the N_2 ice temperature).

Diurnal Sublimation and Condensation. To date models have not accounted for transport of N_2 ice on diurnal timescales. While the amount that could be transported is small, there could be important effects on

longer-term transport if the diurnal layer increases the albedo of the surface locally. This would result in a (strongly) non-linear positive feedback that would modify the overall distribution (and therefore energy balance) of the N_2 ice.

Topographic Effects. Topography may also have a strong effect on the distribution of N_2 ice. The decrease of pressure with altitude means that a patch of ice at higher altitude, but receiving the same insolation as a patch at lower altitude (and therefore with the same equilibrium temperature), will tend to sublimate while the lower patch would tend to experience condensation. This process operates very efficiently (much faster than seasonal transport rates, for example), and so locally will tend to drive the N2 ice into low-lying areas, leaving higher areas bare. This process may also have important effects in the presence of regional or global topographic disparities.

Sublimation at Depth. Spectroscopic observations require very large path-lengths of near-IR photons through N_2 ice in order to produce even the very weak 2.15μm band. It is likely that visible-light photons also travel significant distances through the ice, and that they may preferentially be absorbed deep within the ice, or at the interface between the N_2 ice and bedrock. On Triton, such absorption at depth is a possible driver for the geyser-like plumes detected in Voyages images, but requires a competent 'lid' of N_2 ice to collect and direct the sublimation flow to a vent. If the N_2 ice is instead fractured or granular, flow would locally be towards the surface. Some of the flow would likely condense in the upper layers of the ice deposit, causing vertical evolution and stratification of the ice texture, and potentially causing sublimating N_2 ice to evolve to higher albedo. This process has been dubbed 'solar gardening' [7].

Atmospheric Pressure Gradients & Freeze-out. Pluto's atmosphere is currently dense enough that sublimation-driven winds will have low velocities, requiring only small pressure gradients to overcome Corriolis forces and result in transport between the hemispheres [8]. Because the required pressure gradient is small, the simplifying assumption that the N_2 ice can be characterized by a single temperature is valid. If convection is strong, complex flow patterns might develop in the global circulation, and the isothermal-ice assumption might be less accurate, and there could be localized effects on the patterns of sublimation and deposition on N_2 ice. Pluto's eccentric orbit will result in significant reductions in insolation over the coming decades, and the atmospheric pressure will decrease as the N_2 ice cools in response. If the surface pressure gets as low as about 0.1 μbar (corresponding to an N_2 ice temperature of 31K), sublimation driven transport will require winds with velocities approaching the sound speed. Such strong winds can only flow in the presence of strong pressure gradients, and the atmosphere can no longer be considered to be in hydrostatic equilibrium at that point, and the isothermal ice assumption will also be violated. This state has been referred to as atmospheric collapse or freeze-out. Current models for seasonal transport and atmospheric flow will not be applicable in such a regime, but should hold at somewhat higher pressures and temperatures, and so can be used to try and predict the onset of atmospheric collapse. There is one further complication in attempting to bridge the gap between current conditions and the few μbar/35K – 31K regime.

Solid State Phase Changes. At 35.6K N_2 ice undergoes a phase transition from a more disordered phase (β) to the highly ordered (α) phase. As Pluto's recedes from the Sun, the N_2 ice on the surface will reach the α – β phase-transition temperature. The phase transition latent heat is about 0.1 times that of the sublimation latent heat, and so will retard further cooling as the ice converts to the α phase. The phase change also has implications for the absorption and emission spectrum of the ice. Existing near-IR data show no evidence for the presence of the α phase (placing a lower bound on the atmospheric pressure of 4 μbar), which has a much narrower absorption band. The far-IR spectrum is also quite different for the two phases, with α having two very narrow absorption bands near 140 μm and 200 μm while β has an extremely broad absorption band from about 100 – 500 μm. Hapke models predict a much lower emissivity for α- N_2 than for β [9]. If a major mechanism for the radiative cooling of the N_2 ice is emission in these bands (as opposed to from contaminants within the ice or from the substrate), the reduction in ice emissivity that accompanies the phase transition results in significantly higher equilibrium temperatures for the α phase. Because the atmosphere is hydrostatic at the phase transition temperature (and the ice isothermal), the α and β phases are energetically coupled via the atmosphere, and the N_2 ice remains at the phase transition temperature until all of the β phase is converted to α. For fairly conservative assumptions, this mechanism can prevent atmospheric collapse for decades, or prevent it entirely.

References: [1] Hansen, C.J. and Paige (1996) *Icarus, 120,* 247. [2] Spencer, J.R. (1990) *GRL 17,* 1769. [3] Young, L.A. (2013) *AJ Lett. 766,* L22. [4] Vangvichith, M., Forget, F. and Wordsworth (2011) *EPSC 6,* 1165. [5] Zalucha, A.M. *et al.* (2011) *Icarus 214,* 685. [6] Yelle, R.V. and Elliot (1997) in *Pluto and Charon (S.A. Stern, D.J. Tholen, Eds.),* 347. [7] Grundy, W.M and Stansberry (2000) *Icarus 148,* 340. [8] Spencer, J.R. *et al.* (1997) in *Pluto and Charon (S.A. Stern, D.J. Tholen, Eds.),* 435. [9] Stansberry, J.A. and Yelle (1999) *Icarus 141,* 299.

ALICE: THE ULTRAVIOLET IMAGING SPECTROGRAPH ABOARD THE NEW HORIZONS SPACECRAFT

S. A. Stern[1], J. Wm. Parker[1], G. R. Gladstone[2], L. A. Young[1], M. W. Davis[2], A. J. Steffl[1], and E. Schindhelm[1].

[1]*Southwest Research Institute, Boulder, CO 80302-5143, USA*
[2]*Southwest Research Institute, San Antonio, TX 78238-5166, USA*

Introduction: The *Alice* instrument is a lightweight (4.4 kg), low-power (4.4 W), ultraviolet imaging spectrograph aboard the *New Horizons* mission to the Pluto system and the Kuiper Belt. Its primary job is to detect a variety of important atomic and molecular species in Pluto's atmosphere, and to determine their relative abundances so that a complete picture of Pluto's atmospheric composition and vertical structure can be determined for the first time. *Alice* will also be used during the flyby for numerous purposes, including to 1) search for an atmosphere around Pluto's largest moon, Charon, 2) observe the FUV reflectance of Pluto's various satellites and Pluto itself, 3) study hazes, and 4) search for a hydrogen corona and tail around Pluto. Its design incorporates an off-axis telescope feeding a Rowland-circle spectrograph with a 52-187 nm spectral passband, a spectral point spread function of 0.3-0.6 nm FWHM, and an instantaneous spatial field-of-view of 6 degrees. Two separate input apertures feed the telescope and allow for both airglow and solar occultation observations during the mission. The focal plane detector is an imaging microchannel plate (MCP) double delay-line detector with dual solar-blind opaque photocathodes (KBr and CsI) and a focal surface that matches the 15-cm diameter Rowland-circle. Data taking modes include both histogram and pixel list exposures. We will describe the scientific objectives, design, and capabilities of *Alice* in this review talk.

CONSTRAINTS ON SATELLITES OF PLUTO INTERIOR TO CHARON'S ORBIT AND PROSPECTS FOR DETECTION BY NEW HORIZONS

S.A. Stern[1], H.A. Weaver[2], D. Kaufmann[1], J. Spencer[1], R. Gladstone[3]
[1]Southwest Research Institute, Boulder, CO, USA, [2]Johns Hopkins Applied Physics Laboratory, Laurel, MD, USA
[3]Southwest Research Institute, San Antonio, TX, USA

Introduction: The discovery of Pluto's system of small satellites has prompted both searches and modeling work to determine how extensive the population of Pluto satellites is. Conventional wisdom argues that all of Pluto's satellites should lie exterior to Charon, as Charon's tidal evolution outward would have swept up or ejected extant satellites as it migrated outward. However, more recently Winter et al. (2010) have discovered a class of exotic stable orbits that include orbits inside of Charon's orbit.

Synopsis: In this report we collect together all dynamical, observational, and other constraints on satellites of Pluto orbiting inside Charon's orbit. We also report on new dynamical simulations that constrain the masses of any such satellites. And we report on aerodynamic drag calculations which show that Pluto's extended atmosphere constrains the population of small satellites out to ~4000 km from Pluto, significantly beyond the Roche limit. Finally, we report on HST imaging and groundbased occultation work that also constrains the population of such satellites. We then review the ability of New Horizons to detect satellites inside Charon's orbit during its approach to and close flyby of Pluto in 2015.

References:

Winter, S.M.G., et al., (2010), MNRAS, 404, 442-450

THE NEW HORIZONS MISSION TO THE PLUTO SYSTEM

S.A. Stern[1]

[1]Southwest Research Institute, Boulder, CO, USA

Introduction: NASA's New Horizons (NH) Pluto-Kuiper Belt (PKB) mission was selected for development in 2001 following a competitive selection process. New Horizons is the first mission to the Pluto system and the Kuiper belt, and will complete the reconnaissance of the classical planets. The mission was launched on 19 January 2006 on a Jupiter Gravity Assist (JGA) trajectory toward the Pluto system, for a 14 July 2015 closest approach to Pluto; Jupiter closest approach occurred on 28 February 2007. The ~400 kg spacecraft carries seven scientific instruments, including imagers, spectrometers, radio science, a plasma and particles suite, and a dust counter built by university students. NH will study the Pluto system over a 7-month period beginning in early 2015. Following that, NH will go on to reconnoiter one or two 30-50 kilometer diameter Kuiper Belt Objects (KBOs) if the spacecraft is in good health and NASA approves an extended mission. New Horizons has already conducted a successful encounter with Jupiter, collected valuable cruise science data, and demonstrated the ability of Principal Investigator (PI) led missions to use nuclear power sources and to be launched to the outer solar system. As well, the mission has demonstrated the ability of non-traditional entities, like the Johns Hopkins Applied Physics Laboratory (JHU/APL) and the Southwest Research Institute (SwRI) to explore the outer solar system, giving NASA new programmatic flexibility and enhancing the competitive options when selecting outer planet missions. The NH flyby of the Pluto system will represent a watershed in the scientific exploration of a the solar system, which will include exploring new class of planets in the solar system—dwarf planets, and its satellite system. In this review talk I will provide a more in depth overview of the spacecraft, payload, and mission objectives.

RALPH: THE PANCHROMATIC AND COLOR IMAGER AND INRARED IMAGING SPECTROGRAPH ABOARD THE NEW HORIZONS SPACECRAFT

S.A. Stern[1], C. Olkin[1], D. Reuter[2], D. Jennings[2], L. Young[1], W. Grundy[3], J. Moore[4], H.J. Reitsema[5], and J. Spencer[1]

[1]Southwest Research Institute, Boulder, CO, USA; [2]NASA Goddard Space Flight Center, Greenbelt, MD, USA; [3]Lowell Observatory, Flagstaff, AZ, USA; [4]NASA Ames Research Center, Moffett Field, CA, USA; [5]Ball Aerospace & Technologies Corp, Boulder, Colorado, USA.

Introduction: Ralph is a low mass (10.5 kg), low power (7.1 W), visible and IR remote sensing instrument aboard the New Horizons spacecraft en route to the Pluto/Charon system and the Kuiper Belt. Ralph's primary purpose is to map the geology, albedo, surface composition, and temperature fields on the surfaces of Pluto and its satellites. Ralph's telescope feeds two sets of focal planes, the Multispectral Visible Imaging Camera (MVIC) a visible, near-IR imager and the Linear Etalon Imaging Spectral Array (LEISA), a short-wave IR spectral imager. MVIC will use a large format (5000x32 pixel) CCD array to provide panchromatic (400 to 1000 nm) hemispheric maps of Pluto at a double sampled spatial resolution of 1 km or better. Four additional 5000x32 CCDs will provide hemispheric maps in blue (400 nm to 550 nm), red (550 to 700 nm), Near IR (780 nm to 1000 nm) and a narrow band methane channel (860 to 910 nm). These arrays operate primarily in time delay integration (TDI) mode to increase the integration time and therefore the signal to noise ratio of Ralph datasets. MVIC also contains a 5000x128 element, framing array, providing data for both optical navigation and science. LEISA is an IR spectral imager that operates in a push-broom mode. It images through a wedged filter (linear variable filter, LVF) placed close to a two-dimensional HgCdTe 256x256 pixel detector array. The filter has two segments. One covers 1.25 to 2.5 microns at a spectral resolving power (l/Dl)≥240 to obtain surface composition maps with a spatial resolution of 10 km or less. The other covers 2.1 to 2.25 microns with a spectral resolving power ≥560 obtain surface temperature maps using the spectral shape of solid N_2 near its 35° K phase transition, and other thermally-diagnostic features in the LEISA bandpass. Ralph's optical system uses an all-aluminum, three-mirror f/8.6 anastigmatic design to provide a 5.7°x1.0° instantaneous field of view. We will describe the scientific objectives, design, and capabilities of Ralph in more detail during this review talk.

COMETARY IMPACTS PRODUCE TRANSIENT ATMOSPHERES ON CHARON

S.A. Stern[1]
[1]Southwest Research Institute, Boulder, CO, USA.

Introduction: Although Charon's H_2O-ice surface has long suggested a lack of a permanent atmosphere (e.g., Stern et al. 1988), impacts from KBO and Oort Cloud comets must import N_2, CH_4, and other cometary super-volatiles that can create temporary atmospheres around Charon from time to time. Impacts may also excavate volatiles below Charon's surface, though this possibility is uncertain and model dependent.

Synopsis: In this report I estimate the frequency of cometary impacts on Charon and the imported mass of super-volatiles from each such impact. I then examine certain aspects of such atmospheric transients, including number and column densities, mean molecular weights, scale heights, loss timescales, and dynamical regimes. I then estimate the probability that Charon currently has such a transient atmosphee in place and suggest telltale signatures of such atmospheres that may reveal themselves in New Horizons imagery or spectra.

References:
Stern, S.A., Trafton, L.M., and Gladstone, G.R., 1988. Icarus, 75, 485-498.

PLUTO'S ULTRAVIOLET AIRGLOW

M. H. Stevens[1], J. Scott Evans[2] and G. R. Gladstone[3],
[1]Space Science Division, Naval Research Laboratory, Washington, DC 20375 (michael.stevens@nrl.navy.mil).
[2]Computational Physics Inc., Springfield, VA 22151.
[3]Southwest Research Institute, 6220 Culebra Rd., San Antonio, TX 78238.

Abstract: The Ultraviolet (UV) airglow observation of a planetary atmosphere provides an excellent way of remotely inferring composition and its spatial and temporal variability. The impending arrival of the New Horizons spacecraft at Pluto in 2015 offers an opportunity to test our understanding of airglow production in a nitrogen (N_2) atmosphere. This understanding has developed from decades of analysis using observations from the nitrogen bearing atmospheres of Earth, Titan and Triton. We use an airglow model with heritage derived from spectral analysis of these atmospheres to identify the UV features expected from New Horizons observations of Pluto using the Alice ultraviolet spectrometer. We find significant differences with earlier modeling studies of the Pluto airglow, including the absence of the N_2 CY′(0,0) band near 958 Å which was previously reported to be the brightest feature in the extreme UV.

Introduction: Based on observations from other N_2 bearing atmospheres of the solar system[1,2], we assume that the Pluto airglow is dominated by photoelectron excitation of N_2 and photofragmentation of N_2. We employ the Atmospheric Ultraviolet Radiance Integrated Code (AURIC) in order to simulate the expected emission features from the upper atmosphere of Pluto. Using a model atmosphere for Pluto derived from earlier work[3] and a solar irradiance appropriately scaled to the distance of Pluto during the New Horizons flyby, we calculate photoelectron fluxes and production rates using laboratory measured emission cross sections. The Alice instrument on New Horizons is sensitive to wavelengths between 465-1881 Å, with a spectral resolution between 3-9 Å[4]. We take inventory of all emergent extreme ultraviolet (EUV) and far ultraviolet (FUV) emission features expected at Pluto. For the special case of the extremely optically thick N_2 CY(0,0) band near 958 Å we use a separate multiple scattering algorithm developed for the Earth's atmosphere, which has also been applied to the atmosphere of Titan to explain EUV airglow observations there[5,6].

Results: Nadir-viewing radiances for some important features at Pluto are shown in Table 1. We use a measured solar irradiance from 21 June 2011 scaled to the distance of Pluto during the 2015 encounter to simulate the expected solar irradiance. We find that the brightest feature within the Alice passband arising from processes on N_2 is N I 1200 Å, with a radiance of 0.7 R. Other important N I and N II multiplets produced primarily by photofragmentation are also listed. N_2 FUV features such as those within the Lyman-Birge-Hopfield or Vegard-Kaplan systems are present but weaker. The resonant N_2 CY(0,0) band is strongly photoelectron excited but optically thick to self-absorption and below the detection threshold of Alice (~0.1 R), in contrast to results from previous studies[4,7]. The emission within this system undergoes multiple scatterings, after which much of the emission ends up in the more optically thin CY(0,1) band near 980 Å. In contrast to previous studies[4,7], we also find that emission features from carbon as well as those in the CO (4P) system should be weak and below the detection threshold of Alice.

Table 1.

Expected Radiances of Important Features at Pluto

Feature	Wavelength (Å)	Radiance (R)
N I	**1200**	**0.7**
N I	**1493**	**0.2**
N II	**1085**	**0.2**
N_2 CY(0,1)	**980**	**0.2**
N_2 CY(0,0)	**958**	**0.0**
CO (4P)	**1200-1900**	**0.0**
C	**1657**	**0.0**

Summary: We take inventory of all emission features from the upper atmosphere of Pluto expected within the passband of the Alice spectrometer on New Horizons. The most prominent feature arising from processes involving N_2 is the N I 1200 Å multiplet produced primarily from photofragmentation of N_2. Although the CY(0,0) band is strongly photoelectron excited, it is optically thick and below the detection threshold of Alice. We find that emission features of the CO (4P) band are also undetectable.

References: [1] Stevens, M.H. *et al.* (2011), *JGR, 116*, A05304, doi:10.1029/2010JA016284. [2] Stevens, M.H. (2002), AGU-Geophysical Monograph 130, 319-328. [3] Krasnopolsky, V.A. and D.P. Cruikshank (1999), *JGR, 104*, 21979-21996. [4] Young, L.A. *et al.* (2008), *Space Sci. Rev., 140*, 93-127. [5] Stevens, M.H. *et al.* (1994), *JGR, 99*, 417-433. [6] Stevens, M.H. (2001), *JGR, 106*, 3685-3689. [7] Stern, S.A. *et al.* (2008), *Space Sci. Rev., 140*, 155-187.

Pluto's Atmosphere: Escape and the relationship to its Density and Thermal Structure

D. F. Strobel[1], [1]Dept. Earth & Planetary Science, Johns Hopkins University, 3400 N. Charles St., Baltimore, MD 21218, strobel@jhu.edu.

Abstract: This talk will review the historical background on various approaches and predictions for atmospheric escape rates from Pluto. The basic theory underlying the various escape regimes will be discussed. The importance of accurately knowing the solar EUV and FUV heating fluxes and associated heating efficiencies as well as the stratospheric heating rates that control the underlying atmospheric structure will be reviewed. The escape problem will be illustrated with simple analytic models and thought experiments. It will be argued that constructing model atmospheres for Pluto and other KBOs must include dynamical, adiabatic cooling, because it is not negligible in the lower stratosphere where dT/dr is large. Although the range of atmospheric models for Pluto are hydrostatic with vertical velocities associated with atmospheric escape that are low, the low Mach number radial expansion does impact the thermal structure of the stratosphere and provides an important feedback process between escape rate and thermal structure.

Temporary capture of planetesimals in the Kuiper belt

Ryo Suetsugu, Keiji Ohtsuki. Department of Earth and Planetary Sciences, Kobe University

Introduction: When planetesimals encounter with a planet, the typical duration of close encounter during which they pass within or near the planet's Hill sphere is smaller than or comparable to the planet's orbital period. However, in some cases, planetesimals are captured by the planet's gravity and orbit about the planet for an extended period of time, before they escape from the vicinity of the planet. This phenomenon is called temporary capture. Temporary capture may play an important role in the origin of Kupier-belt binaries and irregular satellites [1, 2]. Recently, we investigated temporary capture of planetesimals initially on eccentric orbits, and found that temporary capture orbits can be classified into four types [3, 4; Figure 1]. Their orbital size and direction of revolution around the planet change depending on planetesimals' initial eccentricity and energy. When initial eccentricity is so small that Kepler shear dominates relative velocity between planetesimals and the planet, temporary capture typically occurs in the retrograde direction in the vicinity of the planet's Hill sphere, while large retrograde capture orbits outside the Hill sphere are predominant for large eccentricities. Long prograde capture occurs in a very narrow range of eccentricity and energy of planetesimals. We obtained rates of temporary capture of planetesimals and found that the rate of long capture increases with increasing eccentricity at low and high eccentricity but in intermediate values of eccentricity decreases with increasing eccentricity.

In the above studies, we mainly focused on the case of temporary capture by Jupiter. These results are not necessarily directly applicable to the Kuiper Belt, because the size of the Hill radius of planetesimas increases with increasing distance from the Sun and temporary capture occurs more easily in the outer part of the Solar system. In the present work, we investigate temporary capture of planetesimals in the Kuiper belt.

Numerical Methods: We examine temporary capture using three-body orbital integration (i.e. the Sun, two planetesimals). When the masses of two planetesimals are much smaller than the solar mass and their orbital eccentricities and inclinations are sufficiently small, the motion of one planetesimal in the rotating coordinate system centered on the other is represented by Hill's equation. We integrate Hill's equation for planetesimals with various initial orbital elements, using the eighth-order Runge-Kutta integrator.

We will discuss the characteristics and rates of temporary capture in the Kuiper belt.

Acknowledgment: This work was supported by JSPS KAKENHI.

References: [1] Goldreich P,. Lithwich Y., Sari T., 2002, Nature, 420, 643 [2] Cuk M., Burns J. A., 2004, Icarus, 167, 369. [3] Suetsugu R., Ohtsuki K., Tanigawa T., 2011, Astron, J., 142, 200 [4] Suetsugu R., Ohtsuki K., 2013, Mon. Not. R. Astron. Soc., 431, 1709

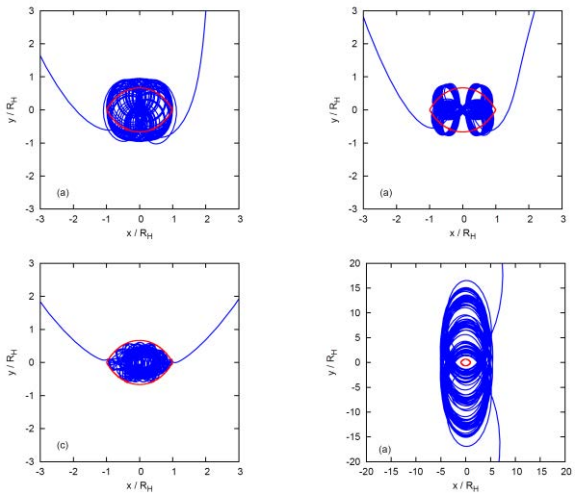

Figure 1: Examples of temporary capture from heliocentric eccentric orbits. These figures show planetesimals' orbits on the rotating coordinate system with a planet at the origin [3].

The Student Dust Counter: Status Report at 26 AU

J. R. Szalay,[1,2] and M. Horanyi[1,2], [1]University of Colorado Boulder (jamey.szalay@colorado.edu), [2]Laboratory for Atmospheric and Space Physics.

Introduction: The Student Dust Counter (SDC) is an impact dust detector on board the New Norizons Mission to Pluto. SDC was designed to resolve the mass of dust grains in the range of $10^{-12} < m < 10^{-9}$ g, covering an approximate size range of 0.5-10 μm in particle radius, in order to map the spatial and size distribution of interplanetary dust particles. These measurements are used to validate the existence of predicted structures in our interplanetary dust disk. SDC provides the first dust measurements beyond 18 AU, where the Pioneer sensors stopped working. After the Pluto-Charon fly-by, SDC will continue to measure dust as it transits through the Edgeworth-Kuiper Belt (EKB). These observations will provide insight about the dust production at the outskirts of our solar system and enable comparisons with dust disks around other start.

Comparison to Model Results: SDC data provide a unique opportunity to validate model results of the IDP distribution past 18 AU with direct measurements. The model we use to compare SDC data to is described in [1]. Briefly, we traced dust grains over a range of grain radii from the EKB throughout the solar system under the influence of gravity, solar radiation pressure and solar wind drag in order to establish a statistical equilibrium density distribution for each grain size. All grains in the model were started with initial conditions randomly selected from known KBO's. By keeping track of each grain's position, a relative statistical equilibrium density map can be calculated for each grain size. As an example, Fig. 1 shows the column density for grains with radius 10 μm. The white line shows the trajectory of New Horizons integrated out to the Pluto encounter at 33 AU.

In order to compare the model-predicted densities with the experimental measurements, the model densities at each grain radius are added together after appropriately weighting by an assumed power law distribution [2,3]. SDC's results are compared to the model to derive estimates for the mass production rate and the ejecta mass distribution power law exponent.

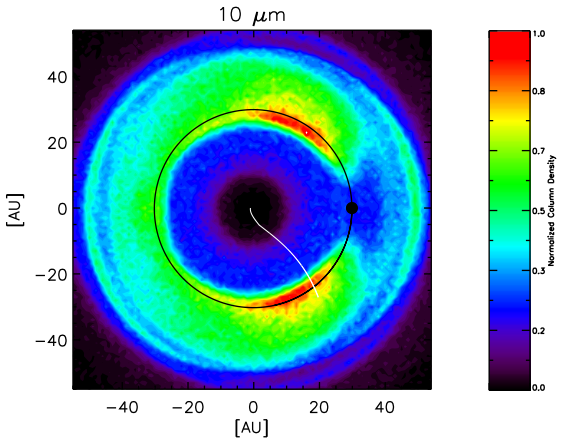

Figure 1. Modeled column density of 10 μm dust within ± 0.5 AU of the ecliptic plane, rotated into the Neptune co-rotating frame.

References: [1] Han, D., et al. (2011) *Geophys. Res Lett.*, doi: 10.1029/2011GL050136 [2] Stern, S. A., (1996), *A&A*, 310:999-1010 [3] Yamamoto, S. and Mukai, T., (1998) *A&A*, 329:785-791

Pluto's small satellites: what to expect, what they might tell us.

P. C. Thomas[1] and K. S.Noll[2], [1]Center for Radiophysics and Space Research, Cornell University, Ithaca NY 14853, pct2@cornell.edu [2]NASA GSFC (Goddard Space Flight Center, B34 S154A, 8800 Greenbelt Rd., Greenbelt, MD 20771

Introduction: Small satellites (less than 150 km radius) orbit all planets from Mars outward. Binaries and satellites in this size range are also present in small body populations, including the Kuiper Belt. Because bodies of this size generally are not thought to have internally driven processes, they are regarded as possible markers of the evolution of material in each planet's system, or as gravitationally captured samples from the early history of the solar system.

Information on small satellites varies greatly, with repeated surveys of Phobos, and the multiple-object surveys by Cassini providing much of the spacecraft-based knowledge. Cassini's survey of the small Saturnian satellites shows surface morphology and shapes depend upon their dynamical niche. Groundbased techniques add a wealth of information, albeit spatially unresolved, on a large number of objects in virtually every Solar System small body population.

Pluto's four small satellites potentially share many qualities with other similar-sized objects found throughout the solar system. Nix, Hydra, P4 and P5 may be reaccreted collisional debris. In this regard they may have analogs in the irregular satellites of the giant planets and with the small satellites of Haumea. In terms of initial composition the four small Pluto satellites may have much in common with other Kuiper Belt objects, although, because they share a common gravitational well their surfaces may be homogenized by regolith exchange.

Data from New Horizons will be of modest spatial resolution, such that comparisons to other systems will be on the basis of overall shapes, colors, and photometry. Shapes (axial ratios) of most small objects are non-diagnostic, but the exceptions may be revealing of history or formation conditions. Color nonuniformity may give clues about formation and resurfacing processes. Despite observational limitations, however, Nix, Hydra, P4 and P5 will emerge from the New Horizons encounter as four of the best characterized 100-km class objects in the Kuiper Belt.

LIMITS ON PLUTO'S RING SYSTEM FROM THE JUNE 12 2006 STELLAR OCCULTATION.

H. B. Throop[1], R. G. French[2], K. Shoemaker[3], C. R. Ruhland[4], L. A. Young[4], and C. B. Olkin[4]
[1]Planetary Science Institute, Pretoria, South Africa, throop@psi.edu, [2]Wellesley College, Wellesley, MA, [3]Shoemaker Labs, Lafayette, CO, [4]Southwest Research Institute, Boulder, CO

Abstract: We present new detection limits on Pluto's ring system from the stellar occultation of P384.2 by Pluto, as observed from the Anglo-American Telescope. Our analysis to date has not found any evidence for a ring system or other unknown detectable material within the bounds of Hydra's orbit.

Introduction: Pluto's occultation of the R=14.8 magnitude star P384.2 on 2006 Jun 12 was visible from the southern hemisphere. Results from the occultation of Pluto in our dataset have been published elsewhere [4]. In this work, we took advantage of the 2.5 hour length of our dataset to search it for additional occultations of P384.2 caused by material in the Pluto system, such as rings or additional satellites. Dusty rings at Pluto might naturally exist at the orbits of the satellites, which would provide a source of material as ejecta from micrometeoroid impacts is placed into the local environment.

Observations: We (RF and KS) observed P384.2 using the 3.9 meter Anglo-Australian Telescope at Sliding Springs, Australia. Images were taken for using a Roper Instruments CCD at 10 Hz (3.5 km/sample), binned on-chip to 64x64 pixels [5]. Observations started roughly two hours before the occultation and ended 30 minutes afterwards, yielding approximately 86,000 individual frames spanning 2.5 hours. Data were taken continually, with short gaps every 20 minutes. The time for the orbits of Charon, Nix, and Hydra to all pass directly over P384.2 on both ingress and egress is approximately one hour, and our dataset spans this period completely.

Data analysis: We used aperture photometry to measure the brightness of Pluto, P384.2, and four field stars on every frame. Photometry apertures were typically 6.5 pixels in diameter, increasing somewhat when Pluto and P3484.2 approached each other in the field. After processing, the P384.2 light curve is extremely stable, with SNR ~ 100. Using SPICE, we determined the times at which the projected orbits of Charon, Nix, Hydra, and the Pluto barycenter would cross the line-of-sight to P384.2.

We searched the data set for any signals arising from additional occultations. We searched in particular for events which correlated with orbital crossing times, with the expectation that meteoroid impacts into the satellites could be the source of ring material, as they are in the dusty rings of the giant planets. We found no such detectable features at the several-percent level.

Conclusions: We have found no evidence for previously unknown material in the Pluto system, either correlated with known satellite locations or elsewhere. We will present our formal upper limits for material in this region, and compare it to limits from occultations [1, 2] and direct imaging [3].

Acknowledgements: This work was supported by NASA PAST program NNG-05GF05G and the New Horizons mission.

References:

[1] Boissel, Yannick, Sicardy, B., Roques, F., Widemann, T., Gaulme, P., Ageorges, N., Ivanov, V., Marco, O., Mason, E., Mousis, O., Rousselot, P., Assafin, M., Braga Ribas, F., Camargo, J., da Silva Neto, D., Andrei, A., Vieira Martins, R., Albert, L., Veillet, C., Behrend, R., Search for small satellites and rings orbiting Pluto through stellar occultations, BAAS, 40, #48.01, 2008.

[2] Pasachoff, Jay M.; Babcock, B. A., Souza, S. P., Gangestad, J. W., Jaskot, A. E., Elliot, J. L., Gulbis, A. A., Person, M. J., Kramer, E. A., Adams, E. R., Zuluaga, C. A., Pike, R. E., Francis, P. J., Lucas, R., Bosh, A. S., Ramm, D. J., Greenhill, J. G., Giles, A. B., Dieters, S. W.A: Search for rings, moons, or debris in the Pluto system during the 2006 July 12 occultation, BAAS, 38, #25.02, 2006.

[3] Steffl, A. and Stern, S. A.: First constraints on rings in the Pluto system, Astron. J. Lett, pp. L1485-L1489, 2007.

[4] Young, E. F., French, R. G., Young, L. A., Ruhland, C. R., Buie, M. W., Olkin, C. B., Regester, J., Shoemaker, K., Blow, G., Broughton, J., Christie, G., Gault, D., Lade, B., and Natusch, T.: Vertical Structure in Pluto's Atmosphere from the 2006 June 12 Stellar Occultation. Astron. J., 136, pp. 1757-1769, 2008.

[5] Young, E. F., Young, L. A., Olkin, C. B., Buie, M. W., Shoemaker, K., French, R. G., Regester, J., Development and performance of the PHOT (Portable High-Speed Occultation Telescope) systems. PASP 123, 735-745.

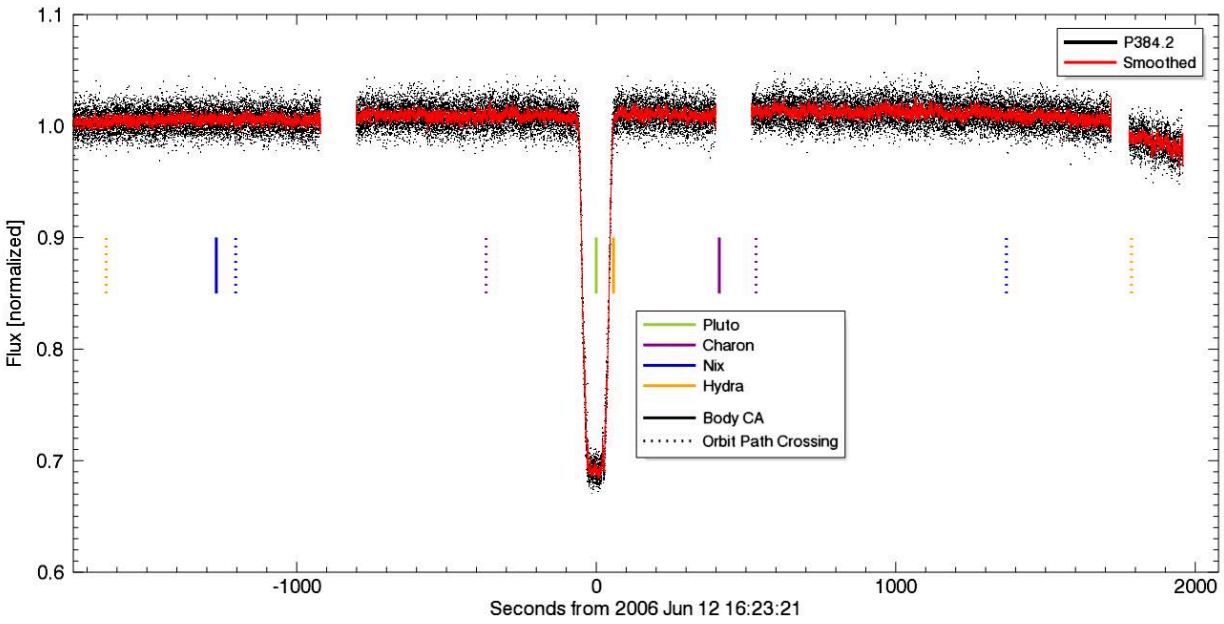

Figure 1: Light curve from the 3.9-meter AAT observations of Pluto's occultation of P384.2. Shown here is the central hour of our 2.5-hour data set; this plot spans the ingress and egress of the orbits of Charon, Nix, and Hydra across P384.2 (dashed colored lines). The two-minute gaps are for data readout and timer synchronization. We find no obvious signature of rings at these orbit crossings or elsewhere in the dataset.

MARS SEASONAL CAPS AS AN ANALOG FOR PLUTO: JETS, FANS, AND COLD TRAPPING

T. N. Titus[1] and T. I. Michaels[2], [1]United States Geological Survey, 2255 North Gemini Drive, Flagstaff, AZ 86001 (ttitus@usgs.gov), [2]SETI Institute (189 Bernardo Ave Suite 100, Mountain View, CA 94043; tmichaels@seti.org) .

Introduction: With the impending Pluto flyby of New Horizons in 2015, it seems reasonable to look elsewhere in the solar system for potential analogs that may provide insights into what we might observe on the surface of Pluto. There are at least 4 solar system bodies where the primary atmospheric constituent is in vapor-pressure equilibrium with surface volatiles: Mars, Io, Triton, and Pluto. Of these, Mars is the best studied. This study uses Mars as an analog to identify potential processes that may be observed on Pluto.

Table 1: Mars-Pluto Atmospheric Comparisons.

Atmosphere	Mars	Pluto
Major Constituent	CO_2 [1]	N_2 [2]
Fraction of Atmos.	95%	99%
Pressure	200-1000 Pa [1]	.3-7.1 Pa [3]
Minor Volatiles	H_2O	CH_4, CO

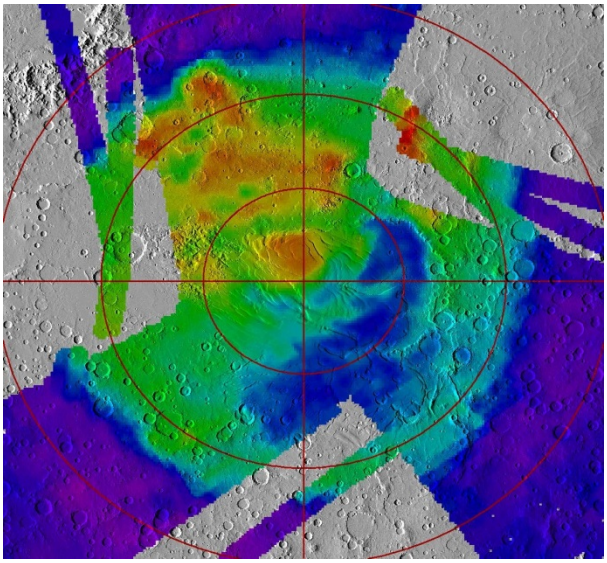

Figure 1: Mars south polar TES albedo mosaic overlaid on MOLA shaded-relief. Warm colors indicate bright regions, such as the perennial cap and the Mountains of Mitchel. Cool colors indicate dark regions, such as volatile-free soil and the "cryptic region."

Comparison of Mars and Pluto: Both Mars and Pluto have highly elliptical orbits. Mars' atmosphere is 95% CO_2 and 25-30% of that atmosphere is seasonally frozen onto the winter hemisphere [4-6]. Pluto's atmosphere is 99% nitrogen, at least part of which is also seasonally deposited on the surface as ice [2]. Mars has three polar climate zones with differing processes: (1) north polar seasonal cap (NPSC) with access to H_2O reservoirs [7], (2) south polar seasonal cap between 30^0E and 210^0E (SPSC-E) which remains dark during the spring sublimation season [8-11], and (3) the south polar seasonal cap extending from 210^0E through the prime meridian to 30^0E (SPSC-W), which brightens with increasing insolation [9-11]. Each of these three polar climate zones provides examples of processes that may be observed on Pluto.

.

Figure 2: Mars South Polar Fans as observed by HiRISE. The dark fans are composed of dust. The bluish fans are composed of fine-grained CO_2 [14].

The Cryptic Region of Mars' Southern Springtime Seasonal Cap (SPSC-E): The seasonal caps of Mars generally appear bright, with the notable exception of the cryptic region [8-9,11]. Plumes from the jets have yet to be directly observed, but the presence of dark and bright fans that appear to originate from dark spots provide strong circumstantial evidence [9,12-13]. NIR spectroscopic evidence suggests that the dark fans are composed of dust that was exuviated from under the ice and propelled into the air as part of the CO_2 gas jets. The bright fans, which are more transitory, are composed of fine-grained CO_2 ice, and are likely the result of the gas recondensing due to adiabatic expansion [14]. At least for the southern hemisphere, H_2O ice does not seem to play a role in the jet-forming process or as a major component of either the bright or dark fans [14]. However, on Pluto – the volatile minor ices may be apparent. If fans caused by jets are observed, the fans could be composed of N_2 ice from adiabatic cooling of the jet, CH_4 ice if mixed with the N_2 ice in sufficient quantities, or perhaps "Plutonian dust" composed of tholins.

Bright Albedo Part of the Southern Cap (SPSC-W): This part of the southern cap brightens with increasing

insolation [15]. Fans have been observed but only in the early spring while the CO_2 ice remains dark (or cryptic) [16]. As an analog for Pluto, some of the N_2 ice may brighten as solar insolation increases. On Pluto, this brightening effect could be the result of changes in light scattering properties due to the transition between the cubic α and hexagonal β ice phases at 35.61 K [17].

The H_2O Ice Annulus of Mars Northern Springtime Seasonal Cap (NPSC): MGS TES observed a bright annulus of intermediate temperatures (~ 180 K) surrounding the retreating seasonal CO_2 ice cap.[18]. Kieffer and Titus speculated that this bright annulus consisted of water ice. Later NIR spectroscopic observations by OMEGA and CRISM confirmed that the annulus was composed of H_2O ice. The process that creates this H_2O ice annulus was first suggested by Houbin et al. [20]. They describe a process by which the H_2O ice is initially left as a sublimation lag after the CO_2 ice sublimes. Ultimately, the H_2O ice also sublimes, but due to eddies at the edge of the seasonal cap, much of the H_2O vapor is cold-trapped back onto the CO_2 cap, thus increasing the H_2O ice content. This process continues until all of the seasonal CO_2 has sublimed.

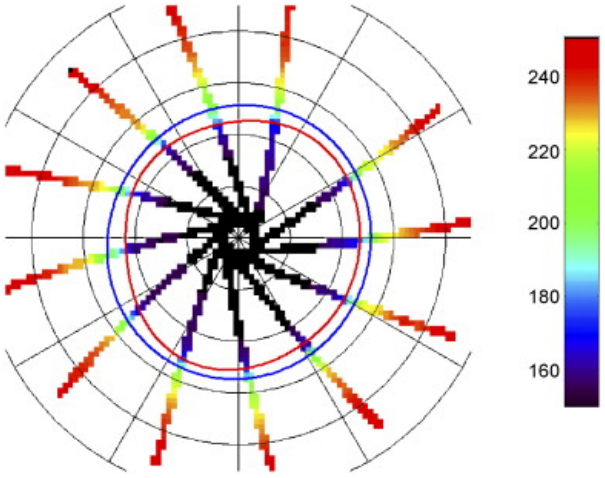

Figure 3: Mars Southern Cap Edges with TES temperatures [K]: H_2O (blue outline) and CO_2 (red outline). (This is Fig. 2 from [19]).

In addition to the presence of an H_2O ice annulus that tracks the seasonal cap retreat, occasional brightening of the entire seasonal cap will occur [20]. This temporary brightening of the cap albedo (referred to as "flashing") typically lasts for a day, and then returns to normal. This type of flashing is most likely due to a sudden exposure of an H_2O ice reservoir, followed by cold trapping of water vapor across the entire cap, resulting in a thin and temporary layer of bright water frost.

The equivalent processes on Pluto may be a methane ice annulus that tracks the treating seasonal N_2 ice cap or a sudden brightening of the seasonal N_2 ice due to cold-trapping of methane after a large methane reservoir is released into the atmosphere.

Simple Model Results*:* Results from a simple thermal model will be presented. Fig. 4 shows the results from a single model run with a constant albedo and emissivity of 0.8. Future runs of this model will include albedo changes due to the α-β N_2 phase transitions.

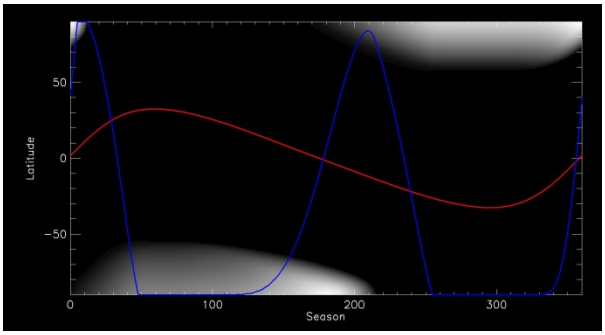

Figure 4: Simple thermal model run showing column density of seasonal ice (whiter = more ice), latitude of the subsolar point (red) and the atmospheric pressure (blue). Axis units are in degrees.

Conclusions: New Horizons should look for:

- N_2/CH_4 gas jets.
- Evidence of past jet activity could be bright N_2 or methane "frost" fans, or dark "tholan" fans.
- A methane annulus that may surround the retreating seasonal N_2 ice cap.
- Sudden changes in albedo of the entire seasonal cap due to sudden release and recondensation of methane.

References: [1] Owen et al. 1977, *JGR*, *82*, 4635. [2] Owen et al. 1993, *Sci*, *261*, 745. [3] Young, 2013, *ApJ*, *766*, 22. [4] Tillman et al., 1993, *JGR*, *98*, 10963. [5] Forget & Pollack, 1996, *JGR*, *101*, 16865. [6] Kelly et al., 2006, *JGR*, *111*, E03S07. [7] Jakosky & Barker, 1984, *Icarus*, *57*, 322. [8] Titus et al.,1998, *30th DPS*, #20.05. [9] Kieffer et al., 2000, *JGR*, *105*, 9653. [10] Colaprete et al., 2005, *Nature*, *435*, 184. [11] Titus et al., 2008, *in Ch25*, *Mars Surface Composition.* [12] Kieffer 2000 [13] Kieffer et al 2006, *Nature*, *442*, 793. [14] Titus et al 2007, *AGU*, #P24A-05. [15] Paige, 1985, *Ph.D. Calif. Inst. Of Tech.* [16] Piqueux et al. 2003, *JGR*, *108*, 5084. [17] Duxbury & Brown, 1993, *Sci.*, *261*, 748. [18] Kieffer & Titus, 2001, *Icarus*, *154*, 162. [19] Wagstaff et al. 2008, PSS [20] Houbin et al. 1995, J. Geophys. Res., 100, 5501-5523.

The Atmosphere and Nitrogen Cycle on Pluto as Simulated by the PlutoWRF General Circulation Model

A. D. Toigo[1], R. G. French[2], P. J. Gierasch[3], and M. I. Richardson[4], [1]Johns Hopkins University Applied Physics Laboratory, 11100 Johns Hopkins Road, Laurel, MD 20723, USA (Anthony.Toigo@jhuapl.edu), [2]Wellesley College, Wellesley, MA 02481, USA, [3]Cornell University, Ithaca, NY 14853, [4]Ashima Research, Pasadena, CA 91106.

Introduction: Extending our linear classical tidal model [1] to a full 3D general circulation model (GCM), we describe early application of the planetary Weather Research and Forecasting (WRF) General Circulation Model [2,3] to Pluto. The PlutoWRF GCM includes treatment of the energy balance at the surface due to subsurface thermal diffusion, sensible heat exchange with the atmosphere, solar and thermal infrared heating, and latent heating due to N_2 phase changes. Heating within the atmosphere has thus far been treated using relaxation to the observed profile described in Toigo et al. (2010) [1], though the explicit radiative heating scheme detailed in Strobel et al., 1996 [4] is currently being implemented in the model.

Simulations With No N_2 Cycle: We will initially show results from simulations with inactive nitrogen cycling and with an observed thermal profile used for radiative relaxation at all latitudes. In this case, the imposed strong thermal inversion and uniform meridional heating limits the development of overturning circulation and the result is a rather quiescent and primarily zonal flow with little meridional heat transport or circulation. These results are similar to those published in Zalucha and Michaels (2013) [5] using the MITgcm. Qualitative differences between our results, following the observed occultation-derived profile of Toigo et al. (2010) [1] and those with the MITgcm are the location of the "tropopause" (the top of the thermal inversion), which we place at approximately 25 km vs. the MITgcm results; and, the temperature of the isothermal layer above this, which we place at about 100 K, vs. about 75 K for the MITgcm. Since the thermal structure in the PlutoWRF GCM directly reflects the thermal forcing (the very weak circulation is unable to significantly modify the thermal structure via adiabatic heating, as also found by Zalucha and Michaels (2013) [5]) differences between the models result almost entirely from differences in thermal forcing. While the MITgcm uses an explicit radiative forcing, the selection of thermal structure "fits" is by forward modeling of observed light curves. The differences in thermal structure between PlutoWRF and the MITgcm thus amount to differences in the quality of the light curve fitting rather than anything intrinsic to the respective dynamical models.

Simulations With An Active N_2 Cycle: The addition of an active nitrogen cycle makes the GCM simulations far more sensitive to initial conditions, especially to the initial choice of ice distribution, pressure, and (sub)surface temperatures. This results rather directly from the fact that heated ice deposits will sublime and add significant atmospheric mass to the model, while cooled regions will act as "cold finger" sinks [6].

We conducted simulations to explore the effect of different assumptions regarding initial state (and vigor of the N_2 cycle) on the circulation and thermal structure. Integrations were performed at the season (and orbital parameters) with solar and thermal forcing appropriate to the observed temperature profile of Toigo et al. (2010) [1]. With uniform initial ice and approximately equinoctial solar forcing, ice rapidly sublimes from the subsolar latitudes. If the atmospheric and surface radiative timescales are made short, this results in a rapid dayside-to-nightside flow. With longer radiative timescales, the flow switches from subsolar-to-polar. The effect of the initial thermal inversion imposed in the lower atmosphere is to concentrate this flow in the lowest layers, generating very rapid winds. However, this transient solution rapidly results in atmospheric heating and the strong modification of the thermal structure extending from the surface up above 100 km. As such, while interesting as an ideal state, active ice at all latitudes can be excluded on the basis of breaking model agreement with the observed thermal structure (in addition to not being viable in multi-annual thermal modeling [6]).

We have conducted additional simulations with evolution of surface ice away from the subsolar latitudes. This is equivalent to seeking a "steady state" ice distribution (although the history-dependence of the ice distribution is itself dependent on the total ice inventory, which is not well constrained [6]). We find that as we allow the surface ice deposits to more closely approximate a balance state, the condensation flow weakens and the thermal structure becomes more strongly radiatively controlled and reverts to better agreement with occultation-derived thermal profile observations. This is equivalent to noting that as we remove the source of the condensation flow (which is driven by ice instability), the circulation and thermal state revert to those that characterize the simulation with no N_2 cycle (as we would expect).

Conclusions: Initial results of simulations with the PlutoWRF GCM reconfirm the idea that in the absence of a strong condensation cycle, the atmosphere will be quiescent and dominated by a strong thermal inversion

in the lowest few scale heights. Our results further suggest that the vigor of the N_2 cycle on Pluto can be constrained to a significant degree by the influence of the associated condensation flow on the thermal structure. In order to retain agreement with the occultation-derived observed atmospheric thermal structure, and assuming a simple "ice / no ice" system, our simulations suggest an ice distribution that is very close to its ideal, instantaneous thermal-balance distribution, *i.e.*, showing little "memory" of prior states for earlier seasons.

References:

[1] Toigo, A. D., et al. (2010), *Icarus*, **208**, 402–411. [2] Skamarock, W. C., et al. (2005), *NCAR Tech. Note 468+STR*. [3] Richardson, M. I., et al. (2007), *J. Geophys. Res.*, **112**, doi:10.1029/2006JE002825. [4] Strobel, D. F., et al. (1996), Icarus, **120**, 266–289. [5] Zalucha, A. M. and Michaels, T. I. (2013), *Icarus*, **223**, 819–831. [6] Hansen, C. J. and Paige, D. A. (1996), *Icarus*, **120**, 247–265.

DRIVING SEASONAL SUBLIMATION AND DEPOSITION ON PLUTO – UNCERTAINTIES IN EVALUATING THE VAPOR PRESSURE

L. M. Trafton[1], [1]University of Texas at Austin (lmt@astro.as.utexas.edu)

Introduction: Pluto's high obliquity and orbital eccentricity, as well as its cryogenically supported atmosphere, are expected to result in extreme seasonal changes in the atmospheric bulk and surface distribution of volatile ices. The primary driver is the diurnally-averaged insolation absorbed by these ices, consisting of N_2, CO, and CH_4, which determines their temperature. The resulting vapor pressure, which supports the atmosphere and drives "sublimation winds" across the seasonal hemispheres that redistribute the upper few mm of ice while greatly affecting the atmospheric bulk, depends on the ice composition and structure, as well as on the temperature. The success of general circulation models in predicting the seasonal changes and in characterizing the sublimation winds will depend critically on how the vapor pressures of these ices are evaluated self-consistently. For pure ices, the vapor pressure is given simply by the temperature, which also determines the phase of the ice at Pluto's low atmospheric pressure. However, for solid solutions, the vapor pressure is additionally a function of the ice mole fractions, which for the deposition phase is a function of the atmospheric composition. Pluto's spectrum reveals CH_4 bands that are both shifted in wavelength, consistent with solid CH_4 dissolved in solid N_2, and unshifted, consistent with the pure ice. There has not yet been any resolution between the two models proposed for explaining Pluto's spectrum and high (~1%) atmospheric mixing ratio: The "detailed balancing" model (DBM) [1], which assumes thermodynamic equilibrium in the kinetic interaction between the ice surface and atmosphere to explain the phenomena in terms of solid solutions. The "hot methane patch" model [2] assumes that rapid, non-equilibrium sublimation produces a relatively involatile, essentially pure, surface lag deposit that heat up enough to explain the observations. According to this model, a hot spot area of 1-3% of Pluto's surface explains the observed CH_4 mixing ratio. With net sublimation and deposition, Pluto's atmosphere cannot be in strict thermal equilibrium with the surface yet there is no explanation of what can be so special about 1-3% of Pluto's surface to generate the relatively warm methane deposits. We discuss below the interpretation of further observations from the viewpoint of the DBM that further highlight the vapor pressure ambiguity.

Interpretation of Spectra: It is noteworthy that Triton's spectrum does not show the unshifted CH_4 band while showing lower CH_4 mole fraction in the ice and mixing ratio in the atmosphere. This and Pluto's double-lined CH_4 spectrum suggest that CH_4 is more abundant in Pluto's ice than on Triton, fully saturating solid N_2 with the excess forming a CH_4-rich solid solution of N_2 saturated in CH_4. This would explain Pluto's double-lined spectrum. On Triton, the absence of detected unshifted lines would indicate an abundance of CH_4 too small to produce a detectable amount of the CH_4-rich component. In equilibrium, the relative proportion of these two solid solutions does not affect the vapor pressure (or thermodynamics), which therefore should be equal for the separated saturated components. Raoul's law breaks down here because of chemical activity. Further laboratory data are needed to resolve the uncertain vapor pressure of these phases. With the CH_4-rich saturated grains likely being lighter than the N_2-rich ones, the dispersal by winds may explain the compositionally varying longitudes of Pluto observed spectrally, thus explaining the apparent segregation of species.

Constraint of the Elevated CH_4 Mixing Ratio: Since hot CH_4 patches are constrained to 1-3% of Pluto's surface area by the observed mixing ratio (through the ratio of the upward and downward CH_4 mass fluxes of the model), it cannot explain the continent-sized apparent segregation of species and of pure methane in particular. This supports our interpretation of these large areas as mixtures of two solid solutions of longitudinally varying proportions. But even in the hot spots, the vapor pressure is not given by that of pure CH_4; it is much less in this model due to suppression by impacts from the mostly N_2 atmosphere. This further complicates the task of assessing a vapor pressure for constraining predictions of seasonal change.

References:

[1] Trafton L. M. (1990) *ApJ 359*, 512-523

[2] Stansberry, J. A., Spencer, J. R., Schmitt, B., Benchkoura, A., Yelle, R. V., and Lunine, J. I. (1996) *Planet. Space Sci. 44*, 1051-1063

UNRAVELING THE EARLY DYNAMICAL EVOLUTION OF THE OUTER SOLAR SYSTEM

K. Tsiganis[1] and R. Gomes[2], [1]Aristotle University of Thessaloniki, Dept. of Physics, GR 54124 Thessaloniki, Greece (tsiganis@auth.gr), [2]Observatorio Nacional/MCT, Rio de Janeiro, RJ 20921-400, Brazil (rodney@on.br).

Introduction: In recent years a lot of effort has been devoted to understanding how the outer solar system has evolved into its current dynamical state, following the formation of the giant planets. Planet migration, caused by the gravitational interaction of the planets with a massive disk of planetesimals [1], is nowadays considered to have played a decisive role in this evolution and different migration models have been proposed, attempting to explain the orbital evolution of the planets and the distribution of trans-Neptunian objects. In this talk we will review the basic premises of these models and, especially, their predicitons concerning the formation of Pluto and the Kuiper Belt.

Smooth planet migration: Already since the mid-90's, a "smooth", outward migration of the major planets was invoked to explain Pluto's capture into resonance with Neptune and its unusually high eccentricity [2][3]. According to this model, the major planets formed closer to the Sun than nowadays observed (e.g. Neptune formed near ~23 AU) and smoothly migrated towards their current orbits. In order for its eccentricity to reach its current value, Pluto must have formed near ~34 AU; its eccentricity increased due to adiabatic invariance as Pluto migrated outwards, along with the 3:2 resonance.

In the same context (smooth planet migration), [4] and [5] examined the possibility that parts of the Kuiper belt did not form in situ but, rather, KBOs were transported to their current orbits during planet migration. In particular, [4] suggested that the "hot" population originated in the interplanetary region and KBOs were implanetd in the Kuiper Belt region, after being scattered outwards by the planets, while [5] suggested that also the "cold" population is non-local, cold KBOs having been transported into the Kuiper Belt after getting trapped and dragged along by the 2:1 resonance with Neptune.

The Nice model: One of the main reasons that lead to an alternative migration model was that smooth migration was leading to almost perfectly circular and coplanar planetary orbits, due to dynamical friction with the disk particles. This argued for a dynamical mechanism that could excite the planetary orbits to the observed level. [6] realized that such a mechanism could be the crossing of a mean motion resonance between two migrating planets, the most promising one being the 1:2 resonance between Jupiter and Saturn. Indeed, [6] showed that, provided that Jupiter and Satrun were formed on orbits with a period ratio smaller than 2, the outer solar system could become temporarily unstable upon resonance crossing, the planetary orbits becoming eccentric. As the planetesimal disk is depleted, the system could become stable again, the planets settling on orbits very similar to their current ones, As shown in [7]-[8], such an instability would have system-wide consequences and, provided it can occur late enough, it could produce an intense bombardment of the inner solar system, with similar characteristics to the LHB.

Following the publication of the "Nice model", as it became known, a number of papers were published, demonstarting how such a "violent" migration of the planets could explain a number of observations, such as e.g. the Neptune Trojans [9] and the irregular satellites of the giant planets [10].

In 2008, [11] showed that the Kuiper Belt could be formed during the instability phase of the Nice model, suggesting that *all* KBO sub-populations (hot, cold and resonant) are essentially non-local in origin, having formed closer to the Sun. Their different physical properties were mostly attributed to their different formation location (inner/outer disk). It is worth noting that this formation scenario also suggests that Pluto could have formed much closer to the Sun than previously thought. It is likely that the collisional history of Pluto could be quite different in this case, as opposed to the smooth migration scenario.

Model refinement: The main drawbacks of the original Nice model can be summarized to (a) the "made-up" initial conditions for the planets (this is also true for the smooth migration models though) and (b) the seemingly critical dependence of the instability time on the parameters of the planetesimal disk. The first issue was addressed in [12], where hydrodynamical simulations were used to support that differential gas-driven migration could have lead the outer planets to get "locked" in a *quadruple resonant configuration*, similar to the Laplacian resonance in the Jovian satellites. While this seemed to "pin down" the initial conditions for the planets, it actually made it harder to solve problem (b), as it required fine-tunning of the disk parameters in order for the instability to occur late.

Problem (b) was actually resolved by [13], where it was demonstrated that velocity stirring, caused by close encounters of small planetesimals with Pluto-sized objects, could lead to *secular energy exchange* between the planets and the distant planetesimal disk. The planets could eventually break-off their mutual resonance – without the need for close encounters with disk

particles – thus becoming unstable. As shown in [13], for realistic values of the disk parameters, the onset of the instability is naturally delayed, so that it could coincide with the onset of the LHB. As the disk becomes depleted, the orbits of the planets become more and more stable.

As shown in [14], the revised initial conditions for the planets lead to a smaller set of "good" solutions for their final orbits; this is a direct consequence of the fact that the instability is more violent in this model (more closely "packed" planets). On the other hand, as also shown in [14], in situ formation of the "cold" Kuiper Belt could be reconciled with the Nice model, at least for a given set of possible planetary evolutions. The same was shown to hold in [15] where (as in [16]) a 5-planet model was considered (an "extra" ice giant, lost during the instability); a model that increases the success rate of Nice-model-like evolutions.

Discussion: Planet migration played a decisive role in shaping our solar system. Nice-model-like evolutions can explain much of the observed dynamical configuration. However, it is clear that as these models become more and more refined, the unstable character of the underlying dynamical processes make it harder and harder to pin down a narrow set of initial conditions that could reproduce all the desired observables, within the framework of a unique model.

Some clues to the course of events that shaped our system may be hidden in the Kuiper Belt, as different models (smooth vs. chaotic) most likely correspond to different collisional evolution histories and/or formation regions for Pluto and the KBOs. This certainly needs to be further explored, in the light of *New Horizons*.

References: [1] Fernandez J. and Ip W.-H. (1984) *Icarus 58*, 109. [2] Malhotra R. (1993) *Nature 365*, 819. [3] Malhotra R. (1995) *Astron. J. 110*, 420. [4] Gomes R. *Icarus 161*, 404. [5] Levison H. and Morbidelli A. (2003) *Nature 426*, 419. [6] Tsiganis K., Gomes R., Morbidelli A. and Levison H.F. (2005) *Nature 435*, 459. [7] Morbidelli A., Levison H.F., Tsiganis K. and Gomes R. (2005) *Nature 435*, 462. [8] Gomes R., Levison H.F., Tsiganis K. and Morbidelli, A. (2005) *Nature 435*, 466. [9] Nesvorny D. and Vokrouhlicky D. (2009) *Astron J 137*, 5003. [10] Nesvorny D., Vokrouhlicky D. and Morbidelli A. (2007) *Astron J. 133*, 1962. [11] Levison H.F., Morbidelli A., VanLaerhoven C., Gomes R. and Tsiganis K. (2008) *Icarus 196*, 258. [12] Morbidelli A., Tsiganis K., Crida A., Levison H.F. And Gomes R. (2007) *Astron J. 134*, 1790. [13] Levison H.F., Morbidelli A., Tsiganis K., Nesvorny D. and Gomes R. (2011) *Astron J 142*, 152. [14] Batygin K, Brown M.E. and Frser W.C. (2011) *Astrophys J. 738*, 13. [15] Batygin K, Brown M.E. And Betts H. (2012) *Astrophys J. 744L*, 3. [16] Nesvorny D (2011) *Astrophys J 742L*, 22.

Atmospheric Escape from the Pluto/Charon Binary System: Kinetic Monte Carlo Simulations

O. J. Tucker[1] and R. E. Johnson[2], [1]University of Michigan, Department of Atmospheric, Oceanic and Space Sciences 2455 Hayward St. Ann Arbor, MI, 48109-2143, [2]University of Virginia, Department of Engineering Physics, 395 McCormick Road Charlottesville, VA 22904-4745

Introduction: Recent hybrid fluid/molecular kinetic models for Pluto's atmosphere (Erwin et al., 2013; Tucker et al. 2012) demonstrate that Pluto's upper atmosphere may be warmer and more extended than previously thought. For such an extended atmosphere we examine the effect of Charon on the molecular escape rate for solar minimum and solar medium conditions. In addition we consider Pluto's primary constituent N_2 as a source of molecules for Charon that can be re-emitted and form a tenuous atmosphere. Including Charon's gravity and orbital motion in the simulations, the atmosphere on the Pluto's Charon facing hemisphere is more strongly bound to the system and becomes more extended than the atmosphere on Pluto's the anti-Charon hemisphere. We calculate a ~10-15% smaller escape rate from Pluto, but the escape from the Pluto/Charon system, is increased by ~1-2%. Much less than 1%, of the flux from Pluto's exobase impinges on Charon, so that it is not a significant sink as compared to escape. However, this impinging flux of molecules, $\sim 10^{25}$ s^{-1}, is a source of a tenuous surface-boundary layer atmosphere on Charon. Such an atmosphere might be detectable during the solar occultation that will occur during the New Horizon encounter. This could provide a direct measure of the transfer of gas between bodies in this binary object.

References: [1] Tucker O. J., Erwin, J. T., Deighan, J. I., Volkov, A. N. and Johnson, R. E. (2012) *Icarus, 217,* 408–415. [2] Erwin, J. T., Tucker O. J., and Johnson, R. E. (2013) *Icarus, accepted*.

A COMPLETE 3D GLOBAL CLIMATE MODEL (GCM) OF THE ATMOSPHERE OF PLUTO

M.Vangvichith (1) and F. Forget (1)
(1) Laboratoire de Météorologie Dynamique LMD, Paris, France, (mvalmd@lmd.jussieu.fr)

Introduction : Pluto has a predominantly tenuous N_2 atmosphere, in which CH_4 and CO are present with no negligible quantities. This atmosphere results from the sublimation equilibrium of these ices at surface temperatures near 40K. During the last twenty years, observations by stellar occultations have shown that the thermal profile is composed of :
-a stratosphere with an important thermal gradient
- just above, an isotherm part with a temperature of 100±20K.
However, there is little information about its low atmosphere.

Pluto currently generates much interest, notably because it is the target of the mission New Horizons. Some 3D models [1] have been built but are not complete. To better understand the Pluto dynamic and its thermal structure, we have developed a complete 3D general circulation model of Pluto's atmosphere.

Description of the 3-D model : The model includes parameterizations (figure 1) of 1) turbulent mixing and convection in the boundary layer, 2) thermal conduction and heat storage in the surface and sub-surface 3) molecular conduction in the upper atmosphere 4) N_2 condensation/sublimation on the surface and in the atmosphere [2] 5) radiative transfer of CH_4 and CO molecules and 6) the CH_4 cycle (sublimation, transport, condensation in the atmosphere and on the surface; see abstract by Forget and Vangvichith, this issue).The dynamical core employs a grid point model composed of 32 longitudes, 24 latitudes and 25 layers distributed from the surface to about 150 km.

Results : The key assumption in Pluto GCM simulations is the initial distribution of surface ices. In our baseline simulation, we have taken the "Modified Grundy and Fink" surface map from [3] which assumes three kind of surfaces (N_2 ice, CH_4 ice, Tholins) and which is derived from observations taken in the 80s and 90s. In fact, because the surface thermal evolution timescale and the atmospheric radiative timescale are very long, we perform simulations starting in 1988 and ending in 2015 (at the periods of the New Horizons flyby) taking into account the seasonal variations of insolation.
Without any ad-hoc tuning, this baseline model of the Pluto climate simulates a realistic atmosphere in comparison with the observations. and allows us to investigate on the atmospheric circulation, to study winds and waves for different years of observations : 2007, 2010 and 2015 (forecast). The thermal profile is consistent with observations [4] and shows the absence of a troposphere (figure 2). The zonal circulation is characterized by retrograde circulation near the surface (probably induced by the nitrogen condensation/sublimation flow) and a super-rotation (somewhat analogous to Titan) between 10 and 80km, with prograde zonal winds of the order of 10m s^{-1}. The diurnal cycle induces thermal tides planetary waves (diurnal and semi-diurnal) which propagate upward. (figure 4). Retrograde winds blow at low altitudes, due to condensation flux. Figure 5 displays a map of winds at 10m.

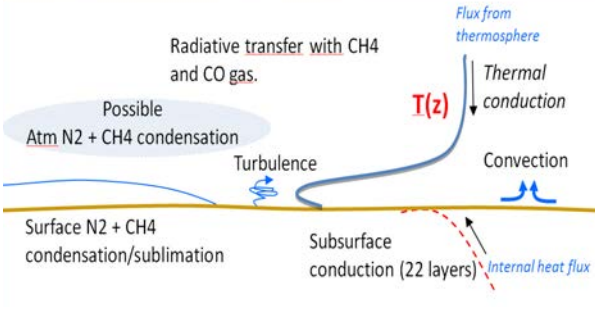

Figure 1 : An illustration of the different physical parameterizations taken into account in the Pluto GCM.

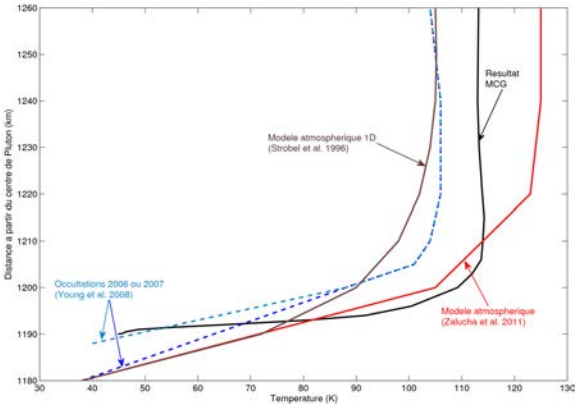

Figure 2 : Comparison of thermal profiles : 1) black solid line : GCM, 2) red solid line : model of Zalucha et al., 3) brown solid line : profile of Strobel et al. [5] and 4) blue line : occultations (2006 and 2007)

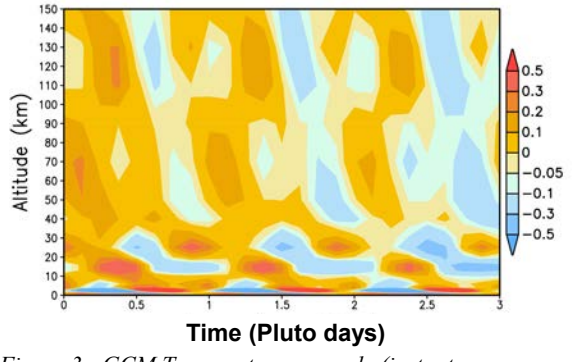

Figure 3 : GCM Temperature anomaly (instantaneous minus diurnal mean, in K) at 0°N O°E in 2007, illustrating the presence of diurnal thermal tides below 100 km and semidiurnal tides above 100 km.

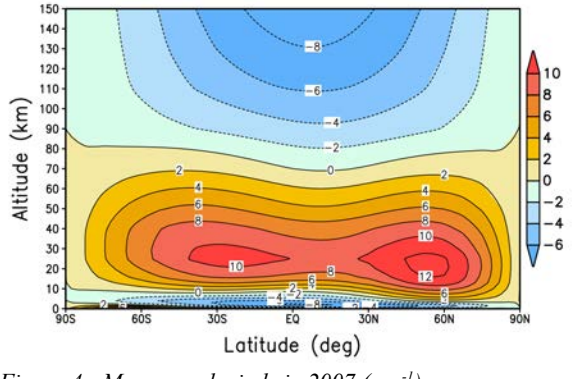

Figure 4 : Mean zonal winds in 2007 (m s^{-1}).

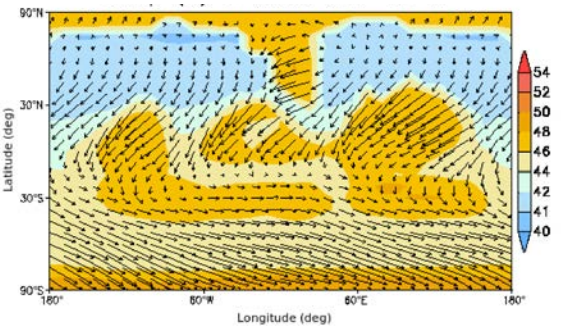

Figure 5 : Map of temperature (K) and wind vectors at 10m in 2007

References :

[1] Zalucha, A., and Michaels,T. : A 3D general circulation model for Pluto and Triton with fixed volatile abundance and simplified surface forcing, Icarus, 223, 819-831, 2013.

[2] Forget, F., Hourdin, F. and Talagrand, O. : CO_2 snowfall on Mars : Simulation with a General Circulation Model, Icarus, 131, 302-316, 1998.

[3] Lellouch, E., Laureijs, R., Schmitt, B., Quirico, E. et al. : Pluto's non-isothermal surface, Icarus, vol. 147, issue 1, pages 220-250, 2000.

[4] Young, E., French, R., Young, L., Ruhland, C., Buie, M., Olkin, C., Regester, J., Shoemaker, K., Blow, G., Broughton, J., Christie, G., Gault, D., Lade, B., and Natusch, T. , Vertical structure in Pluto's atmosphere from the 2006 june 12 stellar occultation, The astronomical journal, 136, 1757-1769, 2008.

[5] Strobel, D., Zhu, X., Summers, M., and Stevens, On the vertical thermal structure of Pluto's atmosphere, Icarus, 120, 266-289, 1996.

NEAR-INFRARED SPECTRA OF PLUTO

A. J. Verbiscer and M. F. Skrutskie, University of Virginia (Astronomy Department P.O. Box 400325 Charlottesville, VA 22904-4325 verbiscer@virginia.edu).

Introduction: We present near-infrared spectra 0.96 – 2.45 μm of Pluto obtained with TripleSpec[1], a facility instrument at the Astrophysical Research Consortium's 3.5-m telescope at Apache Point Observatory in Sunspot, New Mexico. TripleSpec is a cross-dispersed near-infrared spectrograph that provides simultaneous wavelength coverage in five spectral orders at a spectral resolution ($\lambda/\Delta\lambda$) of R=3500.

Observations: Using TripleSpec we acquired spectra of Pluto on 19 July 2010, 6 April 2012, and 22 April 2013 UT. The sub-Earth latitudes on 19 July 2010 was -44^o and the sub-Earth longitude was 157^o. On 6 April 2012, the sub-Earth latitude and longitude were -49^o and 236^o, respectively, and on 22 April 2013, the sub-Earth latitude and longitude were -50^o and 112^o.

Evidence for Seasonal Change: The observing geometry of our 22 April 2013 spectrum most closely matches that of a spectrum of Pluto we obtained [2] using the CorMASS [3] spectrograph while it was a visiting instrument at the 6.5-m Magellan telescope at Las Campanas, Chile, in May 2005. Our CorMASS spectrum was centered over latitude -36^o, longitude 123^o and suggested the presence of pure ethane on Pluto's surface. Although the CorMASS spectrum was acquired at lower spectral resolution (R~300), the close proximity of sub-Earth locations between our spectra obtained in 2005 and 2013 enables comparisons between spectral absorption bands due to the presence of CH_4, CO, and N_2 ice. Differences in these spectral bands may be attributed to composition and/or temperature changes on Pluto's surface in the past eight years.

References: [1] Wilson, J. C. et al. (2004) *SPIE* 5492, 1295-1305. [2] Verbiscer, A. J. et al. (2007) *38th LPSC* Contribution No. 1338, 2318. [3] Wilson, J. C. et al. (2001) *PASP* 113, 227-239.

Karl Wahlberg Jansson
Lund Observatory
kalle@astro.lu.se

The effects of dissipative bouncing collisions in a particle cloud in virial equilibrium

Abstract

In protoplanetary disks around young stars planets form from initially μm-sized dust particles. In the formation process the size of the particles increases with many orders of magnitude: μm dust to km-sized planetesimals to planets with sizes up to $> 10^4$ km. Formation of planets is done in different stages with different governing forces. From planetesimals to planets gravity is the dominant force and planetesimals can be accumulated to form terrestrial planets and giant planet cores. The earliest stages can also be explained by coagulation of dust particles. When small dust particles collide they can stick together via surface forces, van der Waals forces. This process works up to mm-cm-sized particles when particles tend to bounce or fragment rather than stick when they collide. I work on one way to overcome this barrier.

I investigate a scenario where I have a self-gravitating cloud of particles of a certain size that is in virial equilibrium. I place the cloud at some distance from the Sun and assume that the initial size of the cloud is equal to the Hill sphere of the mass of the cloud. In this cloud, as the particles move around, collisions between particles will occur. Next I assume that these collisions are not elastic so some energy is dissipated in each collision. Since the cloud is in virial equilibrium it will therefore get more and more bound and contract for each collision. This is a runaway process and results in the collapse of the cloud into a solid body. If you do an analytic approximation of this collapse time you find that a Pluto mass cloud of cm-sized particles at a Pluto distance from the Sun and assume perfectly inelastic collisions it collapses on a time scale of order years only. However collisions might not be perfectly inelastic and during the collapse the particles start to move faster and faster and at some point the collisions will result in fragmentation instead of bouncing. Nonetheless this is an interesting result which I plan to investigate in computer simulations where I can add an initial size distribution, coagulation and fragmentation to the calculations.

PLUTO'S SMALL SATELLITES

H. A. Weaver[1], [1]JHU Applied Physics Laboratory, Space Department, 11100 Johns Hopkins Road, Laurel, MD 20723-6099, hal.weaver@jhuapl.edu.

Introduction: Four small satellites have been discovered in the Pluto system, highlighting its complexity and challenging theories of its formation and evolution. All the new satellites were discovered using the Hubble Space Telescope (HST). Nix and Hydra were found during deep exposures with the Advanced Camera for Surveys (ACS) in 2005 [1, Fig. 1], P4 (provisional name) was detected using the Wide Field Camera 3 (WFC3) in 2011 [2], and P5 (provisional name) was discovered using WFC3 in 2012 [3, Fig. 2]. Nix and Hydra can now be routinely observed using large ground-based telescopes, but P4 and P5 have only been detected with Hubble. Future observations with the Atacama Large Millimeter Array (ALMA) should be capable of detecting thermal radiation from Nix and Hydra, which will more tightly constrain the albedos and sizes of those satellites. New Horizons will provide resolved imaging of the small satellites and global compositional information.

Dynamical Properties: All the small satellites appear to lie in the Pluto-Charon orbital plane and to be in circular orbits, within the current measurement uncertainties. Remarkably, the small satellites also appear to lie near Mean Motion Resonances (MMRs) with Charon with period ratios of 1:3:4:5:6 for Charon:P5:Nix:P4:Hydra. Dynamical simulations by multiple groups [4,5,6] show that Charon clears satellites and debris in the region ~0.8-2.1 a_0 from Pluto (a_0 is the Pluto-Charon separation), and no new objects have been discovered in that region. Families of stable orbits exist inside Charon's orbit [7], but the proximity to Pluto and Charon makes it very difficult to search for small satellites or debris in that region. We can currently rule out any satellites brighter than Nix or Hydra within Charon's orbit, but P4 or P5 sized objects could easily escape detection there. LORRI on New Horizons is expected to discover objects down to ~7x fainter than P5 in this region.

All the small satellites discovered to date lie well outside Charon's orbit, near the MMRs where the dynamical simulations show that stable orbits are possible. Although many stable orbits exist between Hydra's distance (64,700 km from the barycenter) and the outer edge of the solar tidal stability zone (at ~2 million km), and observations in that region are not strongly affected by scattered light from Pluto and Charon, no satellites down to P5's brightness (V~27) have yet been detected. New Horizons will only provide modest sensitivity improvements in this region.

Physical Properties: There have not yet been any resolved observations of the small satellites, nor have any stellar occultations been detected. Thus, information on the size and shape of the small satellites must be inferred indirectly from photometry and light curves. The latest photometric results [8] indicate significant variability in the measured brightnesses of the small satellites, with *preliminary* values ranging from ±10% for Nix and Hydra to ±25% for P5 and ±40% for P4. These brightness variations are probably indicative of non-spherical body shapes, but there could plausibly be surface albedo variation as well. New Horizons will provide spatially resolved images of Nix and Hydra, possibly with hundreds of pixels across their diameters in the best cases. NH should also provide spatially resolved images of P4 and P5, but those data will be much more limited.

Several authors have attempted to use subtle dynamical effects to constrain the masses of the small satellites [9,10]. In particular, the dynamical stability of P4 suggests that both Nix and Hydra have masses at the lower end of their plausible ranges [10].

Composition: Pluto's small satellites are too faint to be observed spectroscopically from the Earth, but limited color data (e.g., B-V) on Nix and Hydra are consistent with Charon's [11] color, supporting the suggestion that the small satellites may be exchanging material with Charon [12]. New Horizons will test this hypothesis further by obtaining extensive color observations of Charon, Nix, and Hydra, and more limited data on P4 and P5. And infrared spectral mapping of Pluto's satellites with LEISA can investigate the compositional interrelationships even more extensively.

Dust Hazard: The small satellites are pummeled over time by impacts from small Kuiper belt objects passing through the Pluto system. These impacts eject debris that can escape the small satellites but remain bound to the Pluto system, potentially forming dust rings that might pose a hazard to the New Horizons spacecraft as it flies by Pluto at 13.8 km/s. However, these dust rings, if they exist, are probably extremely tenuous ($\tau \approx 10^{-11}$). Furthermore, at the time of the Pluto-Charon orbit plane crossing, the trajectory of the New Horizons spacecraft is being programmed to fly through a region dynamically cleared by Charon, and to stay away from the "debris generators" (i.e., the small satellites), effectively mitigating the impact hazard risk.

References: [1] Weaver, H. A. et al. (2006) *Nature*, *439*, 943-945. [2] Showalter, M. R. et al. (2011) IAUC 9221. [3] Showalter, M. R. et al. (2012) IAUC 9253. [4] Stern, S. A. et al. (1994), *Icarus*, *108*, 234-242. [5] Holman, M. J. and Wiegert, P. A. (1999) *AJ*, *117*, 621-628. [6] Pires dos Santos, P. M. et al. (2011), *MNRAS*, *410*, 273-279. [7] Giuliatti-Winter, S. M. et al. (2013) *MNRAS*, *430*, 1892-1900. [8] Showalter, M. R. (priv. comm.), [9] Tholen, D. J. et al. (2008), *AJ*, *135*, 777-784. [10] Youdin, A. N. et al. (2012), *AJ*, *755:17*. [11] Stern, S. A. et al. (2007), *LPSC*, *#1722*. [12] Stern, S. A. (2009) *Icarus*, *199*, 571-573.

Acknowledgements: The observational results presented here borrow heavily from programs led by Marc Buie and Mark Showalter. Alan Stern either led or motivated many of the observational and dynamical investigations of the Pluto system relevant to this paper.

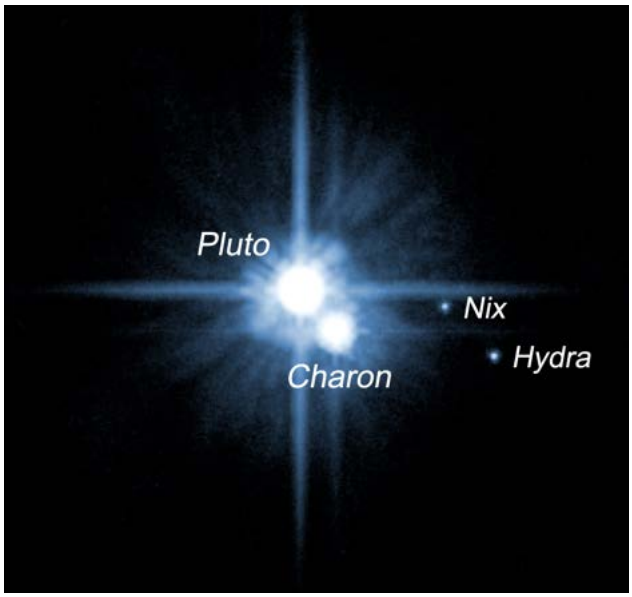

Fig. 1: Deep (1900 s) Hubble ACS/HRC F606W image of the Pluto system taken in February 2006, clearly showing Nix and Hydra. P4 is hidden in Pluto's diffraction spike, and P5 is too faint to be seen.

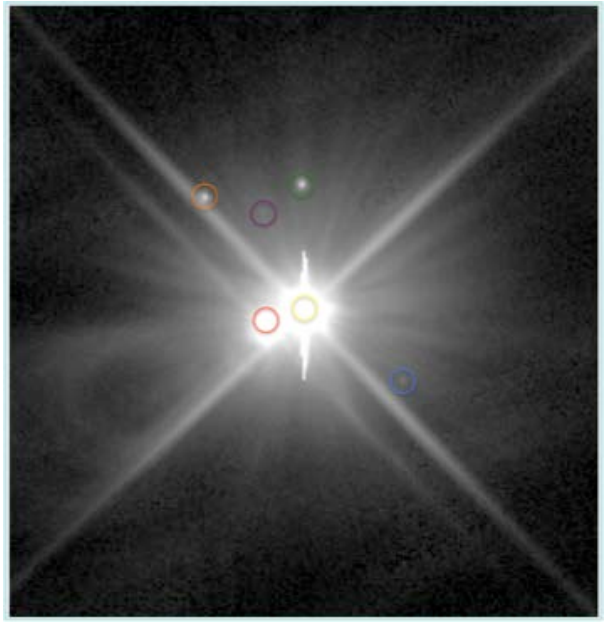

Fig. 2: Deep Hubble WFC3 F350LP image of the Pluto system taken in July 2012, showing Pluto (O), Charon (O), Nix (O), Hydra (O), P4 (O), and P5 (O).

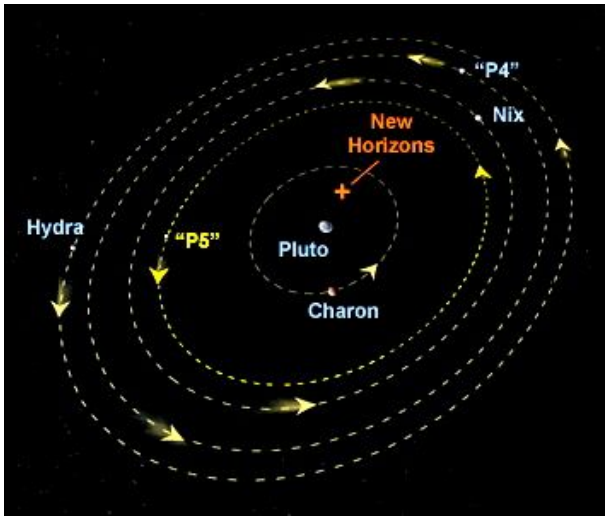

Fig. 3: Cartoon illustrating Pluto's system of satellites as of July 2013.

USING GEOLOGIC MAPPING TO INVESTIGATE THE GEOLOGIC HISTORY OF PLUTO AND ITS SATELLITES.

D. A. Williams[1] and J. M. Moore[2], [1]School of Earth and Space Exploration, Arizona State University, Tempe, AZ 85287-1404 (David.Williams@asu.edu), [2]NASA Ames Research Center, Moffett Field, CA (jeff.moore@nasa.gov).

Introduction: Geologic mapping is an important tool that planetary geologists use to understand the origin and evolution of planetary surfaces. Normally planetary geologic mapping is conducted using data obtained from orbiter missions to produce regional to global-scale geologic maps derived from data sets obtained at the consistent photometric conditions and spatial resolutions afforded by a uniform orbit. However, useful geologic maps have been constructed from images obtained by planetary flybys (e.g., *Mariner 10* at Mercury, *Voyager* & *Galileo* at the Jovian satellites) to understand the evolution of terrestrial planets and outer planet satellites. Thus, it would be entirely appropriate to apply geologic mapping to the upcoming *New Horizons* (NH) images of Pluto and its moons to help derive their geologic histories.

This abstract will discuss the case for applying geologic mapping to the NH Pluto system images to improve our understanding of their surfaces.

Why Geologic Mapping?: The importance of geologic mapping as a tool to understand the evolution of the terrestrial planets and satellites has been discussed by *Carr et al.* [1, 2], *Greeley and Carr* [3], *Wilhelms* [4], *Tanaka et al.* [5], and *Hansen* [6]. The goal of planetary geologic mapping is to place observations of surface features into their stratigraphic context in order to develop generalized geologic timescales that provide a sequence of events for the evolution of planetary surfaces [see 1]. The Earth's geologic timescale was developed by correlating relative ages from extensive field studies with absolute ages obtained from radiometric dating of hand samples. Likewise, the lunar geologic timescale was developed by correlating relative ages from planetary mapping using telescopic and *Lunar Orbiter* photographs with absolute ages obtained from samples returned by the *Apollo* manned landings. For the other planets and satellites, relative stratigraphy and estimates of ages from impact crater populations have proven useful in understanding their geologic evolution. This would be a new exercise for Pluto and its moons, as *New Horizons* will provide the first detailed observations of their surfaces.

The advantage of geologic mapping over photogeology alone is that it reduces the complexity of heterogeneous planetary surfaces into comprehensible proportions, in which discrete material units are defined and characterized based upon specific physical attributes related to the geologic processes that produced them. The distributions of these units are then mapped, along with visible structural features, in order to identify the relative roles of impact cratering, volcanic, tectonic and gradational (i.e., weathering, erosion, and deposition) processes in shaping their surfaces. Application of this technique to the Moon revealed the heterogeneous nature of its surface [see 7], and the return of samples confirmed the complex geologic evolution of the Moon. The stratigraphic techniques developed for early lunar studies [8, 9] are now the basis for the study of other planets and satellites [4, 10].

Planetary geologic mapping has been applied to most terrestrial planets and satellites for which adequate imaging data are available. The nature of planetary surfaces must be interpreted within the context of the internal and external geologic processes that resulted in their present state. The relative roles of these two broad classes of geologic processes (internal or external) can be assessed from stratigraphic studies. In the case of NH at Pluto, the images obtained will reveal the surface for the first time, and enable an initial assessment whether these objects are dominated by internal (cryovolcanism and/or tectonism) or external (impact cratering and gradation) processes. The point is that geologic mapping has aided in the understanding of the processes that produced complex surfaces on the terrestrial planets and outer planet satellites, and that (in general) spectroscopic and geophysical analyses of a planetary body can be investigated far better if the geologic setting of the site is known first. This is a fundamental concept in terrestrial geology, but it is a concept that has found slow acceptance in the exploration of other planets and satellites in the Solar System.

The stratigraphic sequences and photogeological maps of the Moon were developed based upon the pioneering work of *Shoemaker and Hackman* [11]. These maps provided a context for other geological and geophysical studies (e.g., the *Surveyor* program), culminating in the program to map the nearside of the Moon to aid site selection for the manned *Apollo* landings. *Wilhelms* [10] "codified" the techniques developed for geologic mapping of the Moon, which were adapted to Mars in a systematic mapping program using *Mariner 9* images [e.g., 12] and later *Viking* images [e.g., 13]. A similar program was established for the Galilean satellites with *Voyager* data [14]. Since the 1960s, lunar, venusian, and martian mapping programs have focused

for the most part on the production of individual regional quadrangle maps using available orbital imagery involving numerous investigators. However, regional to nearly hemispheric to global geologic maps were produced from flyby imaging of Mercury by *Mariner 10* [9 maps: e.g., 15-17], of the Jovian satellites by *Voyager 1* and later *Galileo* [e.g., 18-20], and most recently for an area of Titan using *Cassini* RADAR flyby data [21]. Given the success of geologic mapping from these previous flyby missions, geologic mapping of flyby images of Pluto and its moons using NH data should be attempted to aid the NH Science Team to understand better the geologic complexities that might appear on their surfaces.

References: [1] Carr, M.H., D.E. Wilhelms, R. Greeley, and J.E. Guest (1976) NASA SP-417, 13-32; [2] Carr, H.R., R.S. Saunders, R.G. Strom, and D.E. Wilhelms (1984) NASA-SP 469, 317 pp.; [3] Greeley, R., and M.H. Carr (1976) NASA SP-417; [4] Wilhelms, D.E. (1990) in *Planetary Mapping*, R. Greeley and R.M. Batson, eds., Cambridge Univ. Press, New York, 208-260; [5] Tanaka, K.L., et al. (1994) *U.S. Geol. Surv. Open File Rep*., 94-438, 66 pp.; [6] Hansen, V.L. (2000) *Earth and Planet. Sci. Lett*., 176: 527-542; [7] Wilhelms, D.E. (1987) U.S. Geol. Surv. Prof. Paper 1348; [8] Shoemaker, E.M., and R.J. Hackman (1962) in *The Moon*, Z. Zopal and K.Z. Mikhailov, eds., Academic, San Diego, CA, 289-300; [9] McCauley, J.F. (1967) in *Mantles of the Earth and Terrestrial Planets*, S.K. Runcorn, ed., Interscience, New York, 431-460; [10] Wilhelms, D.E. (1972) *U.S. Geol. Surv., Interagency Report, Astrogeology*, 55; [11] Shoemaker, E.M., and R.J. Hackman (1962) in *The Moon*, Z. Zopal and K.Z. Mikhailov, ed., Academic, San Diego, CA, 289-300, 1962; [12] Scott, D.H., and M.H. Carr (1978) *USGS Misc. Inv. Series Map I-1083*; [13] Scott, D.H., and K.L. Tanaka (1986) *USGS Misc. Inv. Series Map I-1802-A*; [14] Lucchitta, B.K. (1986) in *The Solid Bodies of the Outer Solar System*, Proc. Conf. Volcano, Italy, ESA SP-242, 27-29; [15] De Hon, R.A., Scott, D.H., Underwood, J.R. (1981) *USGS Misc. Inv. Series Map I-1233*; [16] Spudis, P.D. and Prosser, J.G. (1984) *USGS Misc. Inv. Series Map I-1659*; [17] Strom, R.G., Malin, M.C., Leake, M.A. (1990) *USGS Misc. Inv. Series Map I-2015*; [18] Greeley, R., P.D. Spudis, and J.E. Guest (1988) *U.S. Geol. Surv. Misc. Invest. Series Map I-1949*; [19] Lucchitta, B.K. and Soderblom, L.A. (1982) In *Satellites of Jupiter*, D. Morrison, ed., 521-555, Un. Arizona Press; [20] Bender, K.C., Rice, J.W., Wilhelms, D.E., Greeley, R. (1997) *USGS Misc. Inv. Series Map I-2581*; [21] Williams, D.A., J. Radebaugh, R.M.C. Lopes, and E. Stofan (2011) *Icarus*, *212*, 744-750.

ON THE RELEVANCE OF THE SAILBOAT ISLAND FOR THE NEW HORIZONS MISSION

O. C. Winter, S. M. Giuliatti Winter, E. Vieira Neto, and R. Sfair – Grupo de Dinâmica Orbital & Planetologia – Univ Estadual Paulista – UNESP, Av. Ariberto Pereira da Cunha, 333, Guaratinguetá – SP, 12.516-410 – Brazil. ocwinter@gmail.com

Introduction:

In previous works [1,2] we have studied the location of stable regions in the Pluto-Charon system. We found several stable regions for a sample of test particles located between the orbits of Pluto and Charon. Some of these particles are in orbits around Pluto and some of them in orbits around Charon. One peculiar stable region in the space of the initial orbital elements is located at a = [0.5d, 0.65d] and e =[0.2, 0.9], where *a* and *e* are the initial semi-major axis and eccentricity of the particles, respectively, and d is the the Pluto-Charon distance (Figure 1). This peculiar region (hereafter called sailboat region) is associated to a family of periodic orbits derived from the circular, restricted 3-body problem (Pluto-Charon-particle). More recently [3] we explored the extent of sailboat region by adopting different initial values of the orbital inclination and argument of the pericenter of the particles. Sailboat region is present for I = [0, 90◦], and for two small intervals of ω, ω = [−10◦, 10◦] and ω = (160◦, 200◦). Since the existence and size of this stable regions depend sensitively on the initial values of the orbital inclination and argument of pericenter, the extent is much smaller than the whole space of initial conditions.

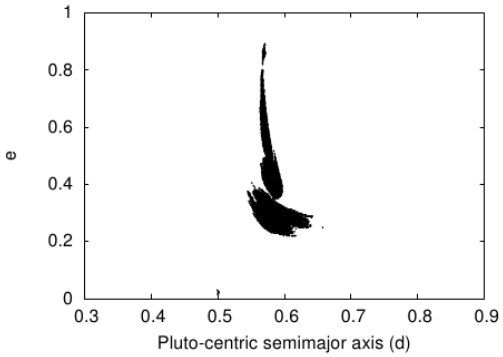

Figure 1. Diagram of initial a versus e. Sailboat region (in black) represents those test particles which remain in orbit around Pluto for the whole timespan of the numerical simulation. The nominal parameters of the particles are: $\omega = 0$, $I = 0$, and $\tau = 0$, where τ is the epoch of the pericentre.

Current work:

In the present work we analyze the relevance of the Sailboat island for the New Horizons mission. First we identified the location and extent of the stable trajectories in physical space around Pluto. They go beyond the trajectory of Charon in a way that Charon never crosses such trajectories. However, we verify that the planned trajectory of the New Horizons spacecraft passes through the region of the Sailboat island trajectories. The existence of particles (small boulders) in such region might result in a collision with the spacecraft, what would be catastrophic for the whole mission. Then, we explore the relative density of probability of having particles in such region compared to well known stable circular trajectories close to Pluto (Figure 2). The preliminary results indicate that the risk may not be negligible, needing further studies.

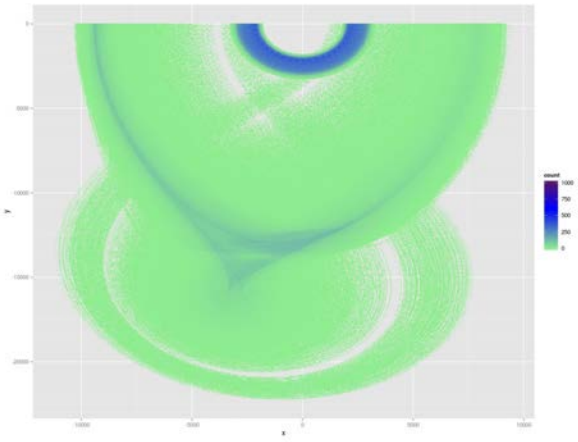

Figure 2. Density of trajectories of the sailboat island.

Therefore, it is reduced the possibility of the New Horizons finding objects in this region during its passage through the Pluto system.

References:

[1] Giuliatti Winter, S.M.; Winter, O.C.; Fernandes Guimarães, A.H.; Silva, M.R. (2010) *MNRAS, 404*, 442-450. [2] Giuliatti Winter, S.M.; Winter, O.C.; Vieira Neto, E.; Sfair, R. (2013a) *MNRAS 430*, 1892-1900. [3] Giuliatti Winter, S.M.; Winter, O.C.; Vieira Neto, E.; Sfair, R. (2013b). A peculiar stable region around Pluto, *MNRAS* (submitted).

Acknowledgment:

This work is supported by FAPESP (proc. 2011/08171-3), and the Federal Brazilian agency CNPq.

USING ORBITAL STABILITY TO CONSTRAIN THE MASSES OF PLUTO'S MINOR MOONS

A. N. Youdin[1] , K. M. Kratter[1] and S. J. Kenyon[2], [1]JILA, University of Colorado (JILA Tower, Boulder, CO 80304), [2]Smithsonian Astrophysical Observatory (60 Garden Street, Cambridge MA 02138).

Introduction: Astrometric measurements of orbital motion in the Pluto system do not yet precisely constrain the masses of the known minor moons: Nix, Hydra, P4 and P5 [1]. The long term orbital stability of the system provides a complimentary method to constrain system masses [2]. Our calculations indicate that the orbital stability of P4 likely requires low masses for Nix and Hydra, below 5×10^{16} kg and 9×10^{16} kg respectively [2]. These constraints lie an order of magnitude below previous constraints from astrometric orbit fitting alone [1]. For a density of 1 g cm^{-3}, our results imply that the albedos of Nix and Hydra are > 0.3. We also find that the 5:1 resonance with Charon can destabilize P4. Combined with current estimates of P4's orbital period [3], we conclude that P4 most likely lies just outside the 5:1 with Charon [2].

Methods: Our main results (above) follow from a an ensemble of few body simulation of the Pluto system in isolation from any external perturbations. Pluto, Charon, Nix and Hydra interact as gravitating point masses, while P4 (and P5 when included) are treated as massless test particles, allowing the simulateous integration of many test orbits. We use the Radau integrator provided with *Swifter* [4], taking care to monitor energy errors. The short period of Charon makes (large numbers of) Gyr calculations impractical. Hence we rely on extrapolation from runs with higher masses of Nix and Hydra (Fig. 1).

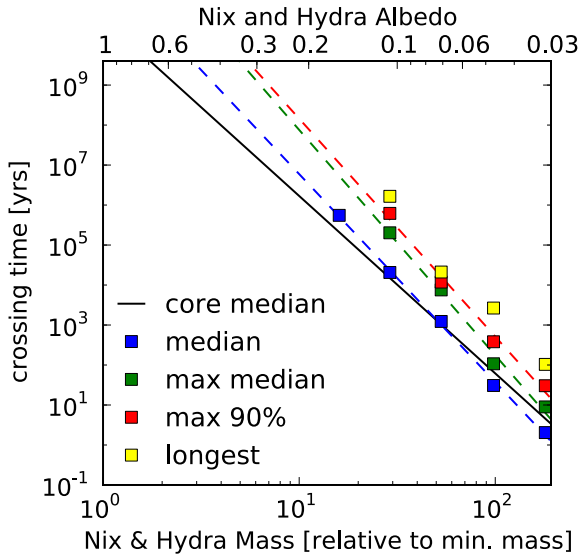

Fig 1: The orbital stability timescale, in years, for P4 to cross the orbit of Nix or Hydra increases as the assumed masses of Nix and Hydra decrease.

Implications: Ongoing observations, especially by *New Horizons* will refine the orbits, albedos and masses of bodies in the Pluto system. Stability calculations should remain a useful tool to refine these parameters and aid in the interpretation of models for the system's intriguing origin [4. 5].

References: [1] Tholen D. J. et al. (2008) *AJ*, *135*, 777. [2] Youdin A. N. et al. (2012) *ApJ*, *755*, 17. [3] Showalter, M. R. (2011) *CBET*, *2769*. [4] http://boulder.swri.edu/swifter [5] Canup R. M. (2011) *AJ*, *143*, 35. [6] Kenyon S. J. and Bromley, B. C. (2013) arXiv:1303:0280

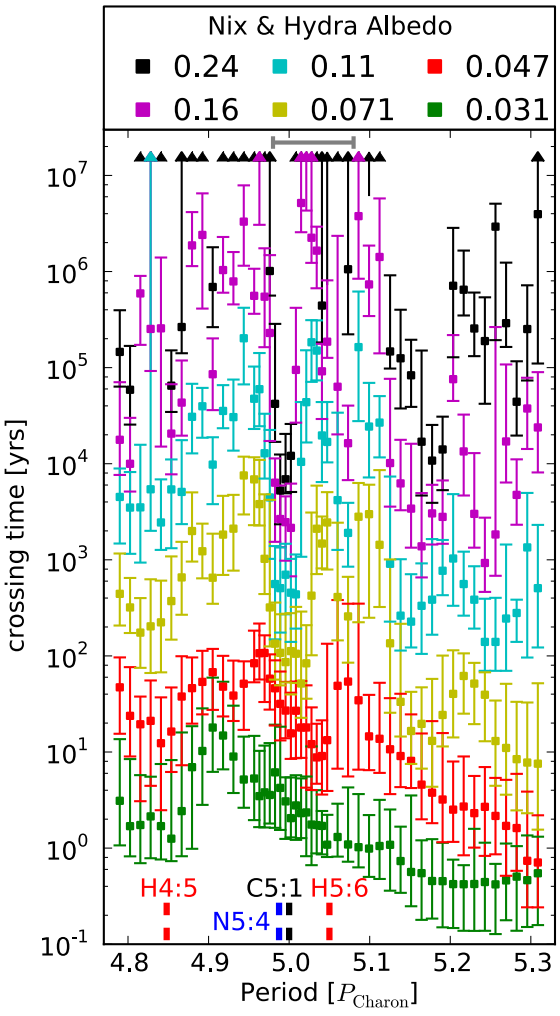

Fig 2: Stabilty time for P4 vs. its orbital period for different choices of the masses of Nix and Hydra (labelled as albedo for an assumed density of 1 g/cm^3).

EVIDENCE FOR RECENT CHANGE IN PLUTO'S HAZE ABUNDANCE.

E. F. Young[1] and E. L. Barth[2], [1]Southwest Research Institute, 1050 Walnut St, Suite 300, Boulder, CO 80301; efy@boulder.swri.edu, [2]Southwest Research Institute, 1050 Walnut St, Suite 300, Boulder, CO 80301; ebarth@boulder.swri.edu.

Introduction: Pluto's 1988 stellar occultation lightcurve showed a discontinuity just below the half-light radius which was attributed to either the onset of a haze layer [1] or to a thermal inversion [2].

Evidence for haze or clouds. Strong evidence for haze in Pluto's lower atmosphere was observed during a 2002 occultation that was observed in wavelength bands ranging from 0.65 to 2.2 μm [3]: the minimum flux during that event increased as a function of wavelength, as one would expect if sub-micron haze particles were present in Pluto's atmosphere (Fig. 1).

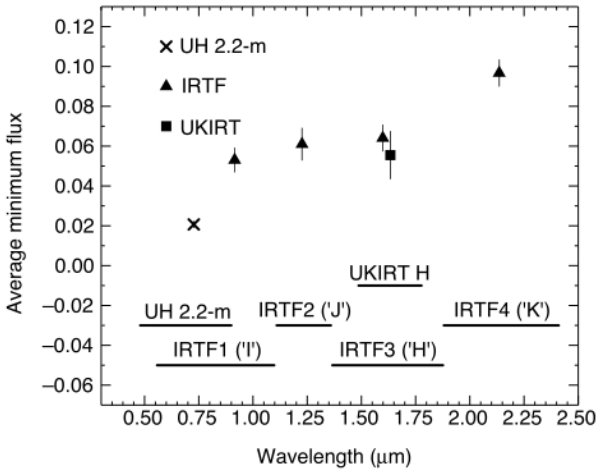

Figure 1. Evidence for wavelength-dependent haze extinction in Pluto's atmosphere [3]. Haze particles would be expected to scatter light more effectively at shorter wavelengths. During a 2002 occultation, the minimum flux levels were correlated with wavelength.

Subsequent modeling of haze production rates in Pluto's atmosphere (scaled from models of haze production on Titan) suggests that no reasonable haze production rate can produce the observed 2002 multi-wavelength lightcurves. Instead, condensed droplets are presented as a solution, with accompanying requirements that there be a troposphere in which the droplets form [4].

The haze disappears. Subsequent occultations that were measured in two wavelengths did *not* show evidence of a wavelength-dependent scatterer. A 2007 event was observed from Mt John Observatory (New Zealand) at 0.51 and 0.76 μm with virtually no color difference (Fig. 2) and a 2011 event was observed from San Pedro Martir Observatory (Mexico) in Johnson I- and K-bands, also showing no color differences (Fig. 3).

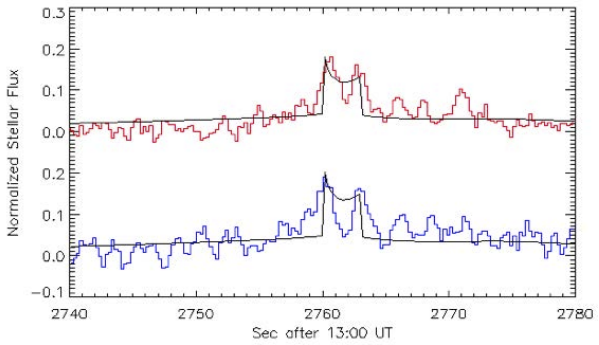

Figure 2. A central-flash occultation observed from Mt John, NZ in 2007 at 0.51 μm (blue) and 0.76 μm shows no evidence of enhanced extinction at the shorter wavelength.

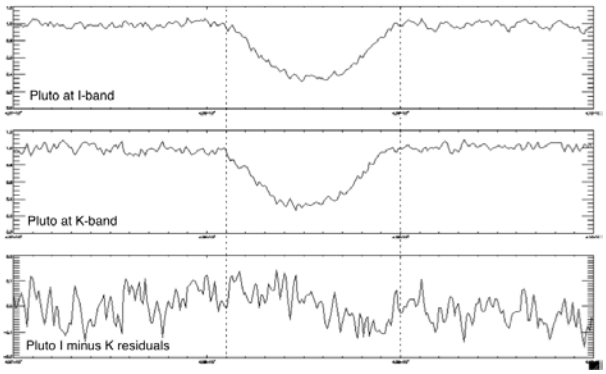

Figure 3. A 2011 lightcurve was simultaneously observed in I- and K-bands from San Pedro Martir (Mexico). The residuals show no evidence of wavelength-dependent extinction.

Constraints from Supersaturated CH_4: Recently a much stronger constraint on haze abundance has become available. The direct detection of gas-phase methane on Pluto [6], combined with temperature profiles derived from Pluto occultation lightcurve obtained in 2006 and later, suggests that methane is supersaturated in Pluto's troposphere [4, 5]. We have run run microphysical models with very modest haze productions and find that even slight supersaturation levels of CH_4 are

incompatible with the presence of haze particles as nucleation sites.

Conclusions: There are now multiple lines of evidence that the wavelength-dependent extinction layer which existed on Pluto in 2002 (and perhaps before) ceased to exist by 2006 and later. Occultations observed in multiple wavelengths in 2007 and 2011 show no evidence of wavelength-dependent extinction. In addition, if Pluto's troposphere is supersaturated in methane (as suggested in [4] and [6]), then we have a very strong constraint limited the production rate of hazes on Pluto.

References: [1] Elliot J. L. et al. (1989) *Icarus, 77*, 148-170. [2] Eshelman, V. R. (1989) *Icarus, 80* 439-443. [3] Elliot J. L. et al. (2003) *Nature, 424*, 165-168. [4] Rannou P. and Durry G. (2009) *JGR., 114*, E11013. [5] Lellouch et al. (2009) *A&A, 495*, L17-L21.

Plans for NASA's *New Horizons* Encounter with the Pluto System

L. A. Young[1]. [1]Southwest Research Institute, Boulder, CO, USA (layoung@boulder.swri.edu).

New Horizons is a NASA mission to explore the Pluto system and the Kuiper Belt. The spacecraft was launched on 19 January 2006 and will begin its encounter studies of Pluto in early 2015, culminating on 14 July 2015 with a close approach just 12,500 km from Pluto. The spacecraft carries panchromatic and color imagers, IR and UV mapping spectrometers, a radio science package, two in situ plasma instruments, and a dust counter.

Planning for the *New Horizons* science operations at Pluto is very advanced [1,2]. Twenty-seven days of the encounter have already been sequenced, spanning 21 days before to 6 days after closest approach. The period nearest closest approach has already been rehearsed on the spacecraft, and a more complete 9-day test is scheduled for execution just weeks before this meeting.

The *New Horizons* encounter meets or exceeds the *Group 1* (required) goals of 0.5 km/pix panchromatic and 1.5-5 km/pix color maps of Pluto and Charon, 10 km/pix composition maps of their surfaces, and various measurements of Pluto's neutral atmosphere (Table 1). It also meets or exceeds all the *Group 2* (highly desired) and *Group 3* (desired) goals specified by NASA or adopted by *New Horizons*, including stereo and high-resolution imaging, imaging and composition mapping of Nix and Hydra, and searching for rings and satellites. One Group 3 goal, the search for magnetic fields, is only addressed indirectly.

I will describe in detail the observations planned for Pluto and its system of satellites. I will cover the start of science operations in January 2012 through the final approach observations the final three weeks (final three Pluto rotations), the intensive 24 hours near closest approach, and the departure measurements. I will summarize the observations for geology, surface composition, atmospheric science, and other disciplines. I will end with a brief description of our downlink and PDS archive plans.

Acknowledgements: The plans presented here reflect a huge amount of work from a dedicated and cohesive Pluto Encounter Planning team. Particular thanks goes to Cathy Olkin, John Spencer, Alan Stern, Jeff Moore, Hal Weaver, Bonnie Buratti, Will Grundy, Randy Gladstone, Maarten Versteeg, Ivan Linscott, Dave Hinson, Matt Hill, Heather Elliot, Fran Baganal, Henry Throop, and Mihaly Horanyi.

References:

[1] Young L. A. et al. (2008) *Space Sci. Rev. 140*, 93.

[2] Young L. A. and Stern, S. A. (2010) *IAU Symposium 263*, 305-311.

Table 1: Summary of key observations of the *New Horizons* encounter with the Pluto system

Target	Panchromatic	Color	Surface composition	Atmosphere
Pluto	0.46 km/pix 0.09 km/pix regional	0.64 km/pix	6.0 km/pix 2.7 km/pix local	Airglow UV solar occultation UV stellar occultation UV stellar appulses Radio occultation
Charon	0.61 km/pixel 0.15 km/pixel regional	1.40 km/pix	8.4 km/pix 4.7 km/pix local	Airglow UV solar occultation Radio occultation
Nix	0.46 km/pix 0.29 km/pix possible	1.98 km/pix	3.6 km/pix	Not applicable
Hydra	1.14 km/pix	4.60 km/pix	14.6 km/pix	Not applicable
P4	3.2 km/pix 2.0 km/pix possible	44 km/pix[a] 8 km/pix possible[b]	24 km/pix[a]	Not applicable
P5	3.2 km/pix	8 km/pix[b]	200 km/pix[c]	Not applicable

[a] Disk-integrated. [b] Possibly disk-integrated. [c] Disk-integrated; probably no useful SNR.

Modeling Pluto's Diurnal and Seasonal 3-Dimensional Volatile Transport with VT3D

L. A. Young[1]. [1]Southwest Research Institute, Boulder, CO, USA (layoung@boulder.swri.edu).

Introduction: Pluto's thin atmosphere transports frosts from areas of high insolation to areas of low insolation. The N_2-rich atmosphere is in equilibrium with the frozen N_2 on the surface; as the N_2-rich volatiles warm up or cool down, the overall atmospheric pressure increases or decreases, perhaps by orders of magnitude over a Pluto year. I have developed a new 3-dimensional volatile transport model, VT3D, that calculates temperatures as a function of latitude, longitude, and depth [1,2].

Model: As in [3,4], energy is balanced locally between (i) insolation, (ii) thermal emission, (iii) conduction, (iv) internal heat flux, and, in areas covered by solid N2, (v) latent heat of sublimation and (vi) specific heat needed to raise the temperature of the volatile slab. Advantages of VT3D are rapid calculation based on an efficient matrix formulation, accurate and stable semi-implicit timesteps, and an initial condition that decreases the time to reach convergence.

Diurnal results: For areas bare of volatiles, thermal behavior is generally described with a thermal parameter related to thermal inertia [4], where large thermal parameters indicate a suppressed temperature variation. I define two additional thermal parameters, related to the specific heat of the volatile slab and the latent heat of sublimation. The temperatures of the surface can be expressed analytically with these three parameters, allowing for physical insight and rapid calculation of temperatures. N_2 is distributed unevenly over Pluto's surface. If the N_2 thermal emission were in instantaneous balance with the globally averaged insolation, then the pressure would vary by a factor of 12. However, thermal inertia of the substrate, specific heat of the volatile slab, and, most importantly, the latent heat of sublimation keeps the surface pressure constant over Pluto's day to within 0.15%.

Seasonal results: The latitudinally averaged seasonal calculations with VT3D are very fast, about 10 seconds per simulation, allowing a large parameter space search. Of 672 cases, only 51 were roughly consistent with stellar occultations. Rough comparison with visible, thermal, and infrared observations narrowed the list of favored models to only 19.

Fourteen of these have Permanent Northern Volatiles (PNV, using rotational North pole; Fig 1, top) or only has a short period when the northern hemisphere is bare of volatiles. These have thermal inertia near that of pure H_2O ice and less than a factor-of-10 variation in Pluto's surface pressure over a Pluto year.

Four of the favored 19 cases have smaller thermal inertia, ~10 J m^{-2} $s^{-1/2}$ K^{-1}, near that derived from its diurnal thermal signature [6]. All four cases with smaller thermal inertia have complete exchange of volatiles between the hemispheres. Three of these predict northern volatiles three decades after equinox, and pressure variation of several orders of magnitude (Fig 1, middle). Only one case predicts a collapse in the atmosphere before the arrival of New Horizons (Fig 1, bottom), with essentially complete collapse before the arrival of New Horizons.

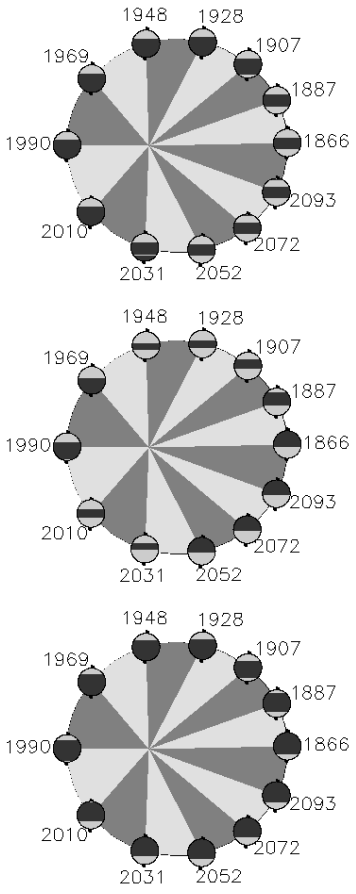

Fig 1. Over views of Pluto's orbit with the latitudinal distribution of frost indicated on the tiny globes. **Top**: Large thermal inertia, showing Permanent Northern Volatiles (PNV). **Middle**: Small thermal inertia, with moderate total N_2 inventory. In this Exchange with Pressure Plateau (EPP) case, pressures stay high for decades after equinox. **Bottom**: Small thermal inertia, with little total N_2 inventory. In this Exchange with Early Collapse (EEC) case, pressures peaks shortly after equinox.

Acknowledgements: This work benefited from many discussions with John Spencer and Candy Hansen, and was supported, in part, by NASA Grants NNG06GF32G and NNX12AG25G.

References:

[1] Young, L. A. (2012). *Icarus 221*, 80-88. [2] Young, L. A. (2013). *AJ 766*, L22. [3] Hansen, C. J. and Paige, D. A. (1996). *Icarus 120*, 247-265. [4] Spencer, J. R. and Moore J. M. (1992). *Icarus 99*, 261-272. [5] Spencer, J. R., et al. (1989). *Icarus 78*, 337-354. [6] Lellouch, E., et al. (2011). *Icarus 214*, 701-716.

PLUTO'S IMPLICATIONS FOR A SNOWBALL TITAN

Y. L. Yung[1], M. L. Wong[1] and G. R. Gladstone[2], [1]California Institute of Technology (Pasadena, CA, 91125; yly@gps.caltech.edu), [2]Southwest Research Institute (San Antonio, TX, 78238)

The recent Cassini-Huygens Mission to the Saturn system provides compelling evidence that the present state of Titan's dense atmosphere is unsustainable over the age of the Solar System [1]. Instead, for most of the time Titan's atmosphere must have been in a collapsed snowball state, characterized by a cold surface and a thin atmosphere, not unlike that of Pluto or Triton [2]. Human observers probably arrive at a privileged time during the third episode of outgassing on Titan [3], thereby gaining a sobering insight into the transience and fragility of the only other dense N_2 atmosphere in the Solar System. Lessons from Titan may prove invaluable as humanity contemplates the destiny of its own atmosphere, which is seriously impacted by anthropogenic forcing [4].

Table 1. Isotopic composition of selected chemical species in the atmosphere of Titan (adapted from [8] and [9]). For comparison, reference values for the terrestrial atmosphere are listed.

Isotope Ratio	*Species*	*Titan Observation*	*Terrestrial Reference*
D/H	H_2	$(1.35 \pm 0.30) \times 10^{-4}$	1.56×10^{-4}
	CH_4	$(1.59 \pm 0.33) \times 10^{-4}$	
	C_2H_2	$(2.09 \pm 0.45) \times 10^{-4}$	
$^{12}C/^{13}C$	CH_4	86.5 ± 8.2	89.4
	C_2H_2	84.8 ± 3.2	
	C_2H_6	89 ± 8	
$^{14}N/^{15}N$	N_2	167.0 ± 0.6	270
	HCN	65 ± 12 76 ± 6	
$^{16}O/^{18}O$	CO	380 ± 60	499
	CO_2	346 ± 110	

We will briefly review how the present Titan atmosphere exists due to a sensitive coupling between photochemistry, radiation and dynamics [5, 6, 7]. This delicate "house of cards" must have collapsed in the past when it ran out of CH_4 or when the sun was dimmer. We will also review the isotopic fractionation data on H-, C-, N- and O-bearing molecules obtained by Cassini-Huygens that support the newly emerging perspective on Titan (see Table 1). The forthcoming New Horizons Mission to Pluto and the Kuiper Belt may allow us to gain insights into the fine balance and the evolutionary history of certain planetary atmospheres.

REFERENCES. [1] Lorenz, R. D., et al. (2008) *Geophys. Res. Lett., 35* (2) L02206. [2] Lorenz, R. D., C. P. McKay and J. I. Lunine. (1997) *Science, 275* (5300), 642-644. [3] Tobie, G., J. I. Lunine and C. Sotin. (2006) *Nature, 440* (7080), 61-64. [4] Yung, Y. L., and W. D. DeMore (1999) *Photochemistry of Planetary Atmospheres*, Oxford University Press. [5] Yung, Y. L., M. Allen, and J. P. Pinto (1984) *Astrophysical Journal Supplement Series, 55* (3), 465-506. [6] Wilson, E. H. and S. K. Atreya (2009). *J. Phys. Chem., 113*, 11221-11226. [7] Krasnopolsky, V. A. (2009). *Icarus, 201*, 226-256. [8] Bézard, B., R. Yelle and C. A. Nixon (2013). To appear as Chapter 6 of book: Titan: Surface, Atmosphere and Magnetosphere, Editors, I. Müller-Wodarg, C. Griffith, E. Lellouch and T. Cravens, Cambridge University Press. In press. [9] Nixon, C. A., *et al.* (2012). *The Astrophysical Journal, 749*, 159.

PREDICTIONS OF RADIO OCCULTATION TEMPERATURE PROFILES FROM A PLUTO GENERAL CIRCULATION MODEL

A. M. Zalucha[1], S. C. R. Rafkin[2], and T. I. Michaels[3], [1]SETI Institute (azalucha@seti.org), [2]Southwest Research Institute (rafkin@boulder.swri.edu), [1]SETI Institute (tmichaels@seti.org).

Introduction: Since its discovery in 1988 [1], Pluto's atmosphere has undergone many subsequent observations via ground based stellar occultation measurements [2–5] and spectroscopic measurements [6]. A number of analysis techniques have been used to derive temperature as a function of altitude (i.e. temperature profiles), including: assuming an idealized model to fit the occultation data to [7]; the inversion method [8], where the light curve flux is integrated downward without any assumption for the shape of the temperature profile (however an upper boundary condition is required, which can lead to significant errors); and performing a parameter sweep by varying parameters of a physically based model and comparing with the data [9]. While these techniques have yielded valuable results regarding Pluto's vertical temperature structure, they are static; in other words, missing the transport of heat by wind. Thus, it is time for a new class of models: general circulation models (GCMs). GCMs operate over the entire globe and over long time scales. They solve the Navier-Stokes equations on a sphere, which simultaneously solves for temperature, 3D velocity, and surface pressure. Here, we use a GCM to predict the temperature profiles that the radio science experment (REX) [10] instrument on New Horizons will observe during the radio occultation experiment. These predictions will be the most physically comprehensive predictions to date.

Model Setup: Our Pluto GCM is based on the Massachusetts Institute of Technology (MIT) GCM. The dynamical core solves the primitive equations of geophysical fluid dynamics in 3D using the finite volume method on an Arakawa C-grid [11]. The model atmosphere is hydrostatic and compressible and may exchange mass with the surface via a source/sink term in the continuity equation. Convective adjustment is performed on the temperature profiles to prevent superadiabatic temperature profiles. The default configuration has neither viscosity nor vertical diffusion, but uses an eighth-order Shapiro filter to remove numerical noise. In the horizontal, a cubed-sphere grid [11] with 32 x 32 points per cube face is used, equivalent to a grid spacing of 2.8° at the equator. Compared to the more common cylindrical projection grid (i.e., a latitude/longitude grid), this type of horizontal grid eliminates singularities at the poles that force meridional winds to zero and removes the requirement for Fourier filtering in the high latitudes (in order to maintain a practical timestep). The vertical grid has 30 levels and uses a terrain-influenced η coordinate [13] based on atmospheric pressure.

Zalucha and Michaels [14] developed a 3D Pluto version of the MIT Pluto GCM. The model top was extended to ~600 km (or several scale heights) and the atmosphere was assumed to be N_2 with trace amounts of CH_4. Planetary constants were adjusted accordingly. The external heating and cooling scheme was modified for CH_4, using the radiative-conductive scheme of [15]. The scheme has the value of capturing the stratospheric temperature inversion, while remaining computationally practical. Subsequent upgrades include an N_2 volatile cycle. We have also adapted the radiative-conductive scheme of [16], which is fully tested at this time but will be included at the time of presentation. The model of [16] includes, among other upgrades, the inclusion of CO, and additional bands of CH_4 heating/cooling.

Simulation Configuration and Results: We have performed a parameter sweep that represents conditions that potentially exist on Pluto. At this time, the predictions should be considered preliminary. For each group of simulations, a simulation was initialized with a global mean surface pressure of 8, 16, and 24 μbar. Then there were two other initial conditions: (1) the surface had no ice on it and (2) the surface had an infinite reservoir of ice. We assumed the albedo of N_2 ice-covered surfaces was 0.72, and surfaces without N_2 ice had an albedo of 0.46 (following [17]). Thus, in total 6 simulations were performed. Furthermore, in all cases we initialized the Pluto GCM to a steady state (no wind), uniform surface pressure, and radiative-conductive equilibrium temperature. All simulations were started on 14 July, 2000, to allow enough spin-up time for the 14 July 2015 New Horizons encounter. The methane mixing ratio was constant with height and fixed at 1% (following [14]) and the surface radius was fixed at 1180 km (following [9]

Figure 1 shows the preliminary predicted temperatures from the REX radio occultation experiment at ingress, while Fig. 2 shows the same but for egress. The Pluto latitudes and longitudes (assuming Pluto's north pole is in the same hemisphere as the ecliptic north pole) for ingress are 15.480° and 164.559°, respectively; for egress they were -14.268° and -16.584°, respectively [18].

Figures 1 and 2 show that there is a small difference between starting with a ice-free vs. ice-covered surface (<5 K), but a much larger difference (as much as 13 K) between the profiles with different initial global mean surface pressures. Although it is difficult to see here, there is little difference between the ingress and egress curves. This behavior is consistent with the prediction of the GCM by [14] that Pluto's atmosphere has very little horizontal variation.

References:

[1] Elliot, J. L., et al. (1989) *Icarus 77*, 148–170. [2] Elliot, J. L., et al. (2003) *Nature 424*, 165–268. [3] Sicardy, B., et al. (2003) *Nature 424*, 168–170. [4] Elliot, J. L. et al. (2007) *Astron J. 134*, 1–13. [5] Person, M. J., et al. (2008). [6] Lellouch, E., et al. (2009) *Astron J. 512*, L8. [7] Elliot, J. L. and Young, L. A. (1992) *Astron J. 103*, 991–1015. [8] Elliot, J. L. et al. (2003) *Astron J. 126*, 1041–1079. [9] Zalucha, A. M. et al. (2011) *Icarus 211*, 804–818. [10] Tyler, G. L. et al. (2008) *Space Science Reviews 140*, 217–259. [11] Marshal J. et al. (1997) *J. Geophys. Res. 102*, 5753–5766. [12] Adcroft A. et al. (2004) *Mon. Wea. Rev. 132*, 2845–2863. [13] Adcroft A. et al. (2004) *Ocean Modelling 7*, 269–284. [14] Zalucha, A. M., and Michaels, T. I. (2013) *Icarus 223*, 819–831. [15] Yelle, R. V. and Lunine J. I. (1989) *Nature 339*, 288–290. [16] Strobel, D. F., et al. (1996) *Icarus 120*, 266–289. [17] Lellouch, E., et al. (2000) *Icarus 147*, 220-250. [18] Hinson, D. P. (2013) personal communication.

Acknowledgments: This work was supported by NASA grant NNX12AI70G and the NASA High End Computing Program.

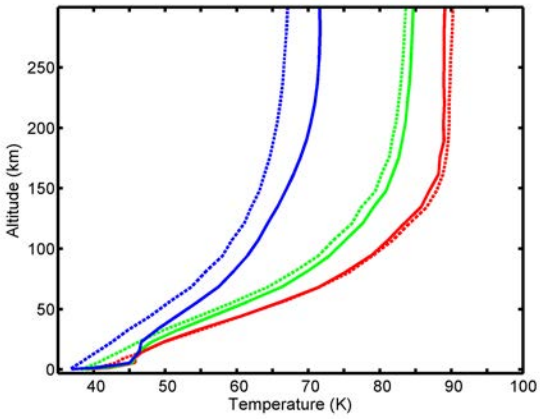

Figure 1: Preliminary temperature profiles predicted to be observed by REX during ingress. The solid lines are for no initial frost on the ground; the dashed lines are for an infinite reservoir of surface N_2 ice. The red color is for the cases with initial global mean surface pressures of 24 μbar, the green for 16 μbar, and the blue for 8 μbar.

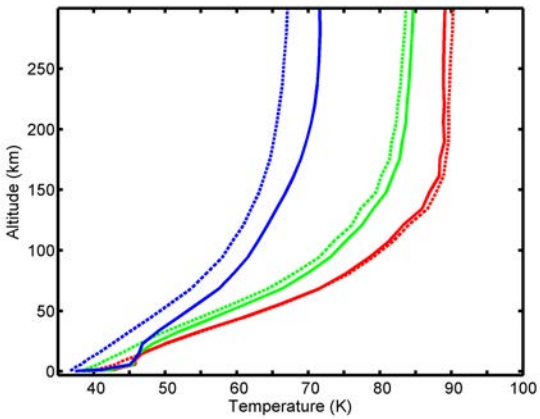

Figure 2: Same as Fig. 1 but for egress.

Plutography: A Meta-analysis of Coordinates on Pluto from Charon's discovery to the Present Day

A. M. Zangari[1], [1]M. I. T. (77 Massachusetts Avenue, Cambridge, MA 02139 azangari@mit.edu).

Abstract:

After the reclassification of Pluto as a dwarf planet in 2006, the International Astronomical Union redefined the north pole of Pluto to be aligned with its angular momentum vector[1]. I will present the results of a survey of more than 800 articles on Pluto written since the discovery of Charon in the late 1970s. While there are eleven possible conventions to describe longitude and latitude, only eight are commonly used in peer-reviewed literature. Though the angular momentum convention was far and away the most popular before the IAU Working Group on Cartographic Coordinates and Rotational Elements adopted it in 2009, to date, no published papers acknowledge this small silver lining from Pluto's demotion. Unfortunately, errors and ambiguities in the literature are fairly common, especially among papers that compare new results directly to previous measurements. Roughly 5% to 10% of all papers that mention longitude or latitude on Pluto contain some sort of error or ambiguity. As all past and future Pluto research will be compared to the results from the upcoming New Horizons Pluto encounter, avoiding comparative errors is of the upmost importance. I will discuss common pitfalls to look out for and recommend best practices for avoiding future confusion.

References:

[1] Archinal, B. A. et al. (2011) *Celestial Mechanics and Dynamical Astronomy, 109*, 101–135.